Digital workflow for the design, construction and management of natural bamboo pole structures

Jose Leonel Mimendi Cruz

A dissertation submitted in partial fulfilment for the degree of

Doctor of Philosophy

Department of Civil, Environmental and Geomatic Engineering

University College London

2021

- Blank -

Declaration

I, Jose Leonel Mimendi Cruz, confirm that the work presented in this thesis is my own. Where information has been derived from other sources, I confirm that this has been indicated in the thesis.

Signed: _____

- Blank -

Abstract

The ever-growing global urbanisation has been lately associated with a negative environmental impact caused by the energy consumption and carbon dioxide emissions that the building industry has been responsible for. To turn the tide, the building industry needs to transition from industrialised, non-renewable materials, to natural, sustainable and renewable ones. Bamboo poles are currently the most promising resource due to their relatively good environmental credentials, in comparison with industrialised materials. However, there are significant technical challenges that have prevented bamboo poles from their formal integration into the building industry. One of the main challenges is associated with the inherent variability of the geometric, physical and mechanical properties and the impact that this produces on the reliability of bamboo structures. This research focuses on the development of a digital workflow that tackles the inherent variability of bamboo poles through the quantification of material properties on every single pole and thus, provides the fundamental basis to ensure structural reliability. Reverse engineering methodologies supported by modern digital technologies, such as 3D scanners and robotic fabrication, were developed to intensively measure the geometric, physical and mechanical properties of a stock of bamboo poles, regardless their species, age or size. These methodologies were then integrated and implemented into a proof-of-concept digital workflow that quantifies the variability and uses the resulting data to design and construct a reciprocal frame bamboo structure. This research sets out the initial steps towards an alternative approach that allows the design and construction of reliable bamboo structures through the management of their digital data, which in turn, will allow bamboo poles to competing with industrialised construction materials.

- Blank -

Impact statement

Currently, one of the most important issues involving every human being on this planet is the decadent state of our environment which has a direct impact on the well-being of future generations. The core of this research contributes towards setting back the overall environmental damage particularly produced by the building industry through the adoption of bamboo poles as a natural and renewable resource, but also, through the incorporation of modern technologies that help to manage these resources. The impact of mobilising a renewable and sustainable resource as a construction material is not just focused on protecting, restoring and promoting sustainable use of resources but it further encourages a sustainable economic growth, the development of resilient industries and human settlements, and the overall wellbeing of entire communities.

The environmental credentials of bamboo poles are significantly better than any current structural element, however, their formal utilisation in the building industry requires the development of a framework that involves the production, distribution, sustainability and technical use of bamboo poles, as well as public policies, codes of practice and institutional bodies that together will ensure the reliability of bamboo buildings. The intensive measuring techniques for bamboo poles, developed and implemented in this thesis, contribute towards this overall framework by providing detailed technical data of bamboo poles, mimicking a semi-industrial quality control procedure, which provides the fundamental basis to ensure the reliability of bamboo structures.

The outputs of this research can have an impact on local and regional economic and sustainable development. For example, the intensive measuring methodologies can potentially be implemented to develop a robust quality control procedure within local production companies of bamboo poles. This, in turn, will push other related disciplines, on a national or international level, to simultaneously develop matching standard processes or public policies that ensure the widespread use of bamboo poles as a product.

From an academic perspective, this research challenges the overall perception that bamboos can only be managed through the use of analogue tools and encourages researchers, especially from regions where bamboo is endemic, to explore modern design and construction approaches that are compatible with this and other organic materials. This research has already served as a platform for institutional collaboration, the outputs of which have been disseminated through international conferences, proceedings, workshops and journal articles. The digital workflow developed through this research has been further implemented to support the reconstruction project of bamboo houses in Lombok, Indonesia - a project that aims to provide for a low-cost and sustainable house demand - in collaboration with Ramboll UK Ltd., as an industrial partner. Likewise, the workflow has been also implemented in an exploratory collaboration project between UCL, Nanjing Forestry University and Zhejiang Daming Renewable Resources Utilisation Co. Ltd. This project focused on improving the quality of social housing in China while reducing non-renewable resource consumption. Both collaboration projects have been supported by the Engineering and Physical Sciences Research Council and the Chinese government.

Acknowledgements

Thank you, God, for all the blessings during this journey.

To my parents that have always been my main guidance and inspiration contributing to the pursuit of my projects and dreams, I thank you because this achievement reflects all your efforts and support. I also thank my sister for her always present encouragement towards my personal development. I am especially grateful to my wife who has accompanied me through my doctoral studies, always comforting me with all her love.

To my supervisor, Dr Rodolfo Lorenzo, who always shared with me his passion for critical thinking through countless academic discussions that contributed to the core of my overall research training, I am truly grateful for that. To my second supervisor Dr Mingzhong Zhang for his academic advice throughout my studies and the people in the bamboo research group at UCL with whom I shared many learning experiences. I am also thankful to Dr Haitao Li who welcomed me at Nanjing Forestry University and supported my research. I would like to recognise the fundamental role of technical staff at UCL CEGE, UCL at Here East and NFU laboratories; research would not exist without you.

To all my colleagues and friends across UCL, especially to every single person I shared office with at GM16! I extend my gratitude to friends who supported me during my fieldworks in Mexico and China.

This work would not have been possible without the sponsorship of the National Council of Science and Technology in Mexico (CONACyT), the Global Challenges Research Fund, the British Council and the Chinese Scholarship Council.

- Blank -

A mis padres, Leonel y Rosalía

Στη γυναίκα μου, Ξανθενία

- Blank -

Table of contents

- Blank -

List of Figures

- Blank -

List of Tables

List of Symbols

A	Cross-sectional area
A_f	Area of vascular bundles (fibres)
A_i	Inner cross-sectional area
A_o	Outer cross-sectional area
b	Width of clear bamboo sample
c	Half of the wall thickness
D	Equivalent diameter of a cross-section
dF_c	Internal compressive force in bending
dF_t	Internal tensile force in bending
Dv	Equivalent diameter reduction rate
e	Distance between the surface of the pole and centroid of the studding bar connection
E_b	Apparent modulus of elasticity in bending
E_c	Compressive elastic modulus
E_{eq}	Equivalent elastic modulus in bending
e_n	Distance from the centroidal axis to the neutral axis of a curved beam
E_t	Tensile elastic modulus
E_{tr}	Transverse elastic modulus
f	Frame rate
f_c	Compressive strength
F_{lin}	Maximum applied bending load within the linear portion of the load-displacement curve
F_m	Maximum applied bending load before failure
f_t	Tensile strength of bamboo fibres
f_{tr}	Circumferential tensile strength
f_v	Shear strength
h	Scanning frame height
I	Second moment of area of a thin circular tube
$I_{1,2}$	Principal moments of inertia (principal directions: *1 & 2*)
I_b	Equivalent moment of inertia
IL	Internode length
I_{rc}	Moment of inertia of a cross-sectional ring
I_y	Moments of inertia of the actual cross-section about *Y* global axis

I_{yz}	Product moment of inertia of the actual cross-section about *Y &Z* global axis
I_z	Moments of inertia of the actual cross-section about *Z* global axis
J	Equivalent polar moment of inertia
K	Equivalent elastic modulus factor
K_{Eb}	Moisture content correction factor for bending test sample
K_{Ec}	Moisture content correction factor for compressive elastic modulus
K_{fc}	Moisture content correction factor for compressive strength
K_{fv}	Moisture content correction factor for shear strength
k_n	Characteristic fractile factor for the 5% characteristic value
L	Length of pole
L_i	Internodal length
L_n	Length from the first to the last node of the scanned pole
L_{rc}	Length of a cross-sectional ring
M	Bending moment acting on a section
m_0	Mass of the clear bamboo specimen fully dried
m_1	Mass of the specimen
M_{cr}	Brazier's ovalising critical moment for unidirectionally reinforced cylindrical tubes
M_{lin}	Maximum applied bending moment within the linear portion of the load-displacement curve
M_m	Maximum applied bending moment before failure
$M_{n+,n-}$	Maximum positive and negative transverse bending moments, respectively
m_x	Mean of the *n* samples tested
n	Number of samples tested
n_f	Number of frames
N_l	Number of scanner frames per unit of length
n_r	Modular ratio
P_{cmax}	Maximum compression load (clear sample test)
P_{vmax}	Maximum shear load (clear sample test)
q	Shear flow in bending
$\bar{R}$	Thin ring average radius
s	Offset distance of studding bar along its circumferential curve assumed as 25 mm

s_x	Standard deviation of the *n* samples tested
t	Equivalent wall thickness of a cross-section
T	Period (seconds per rotation)
t_l	Scanning time per unit of length
t_v	Equivalent thickness reduction rate
V	Shear force in bending
v	Translation speed
V_0	Volume of the clear bamboo specimen fully dried
V_f	Fibre bundle volume fraction
V_n	Applied load on each loading saddle
V_x	Coefficient of variation
w	Scanning frame width
X	Global X-axis
x	Observed value for each specimen
$x_{i,f}$	Coordinate component of the pole's centroidal line in the X-axis for the initial and final nodes, respectively
$x_{j,k}$	Coordinate component of the pole's internodal length in the X-axis for any two consecutive nodes
$X_{k(n)}$	Characteristic value
y	Distance from the centroid of the pole to a position defined by α
$\bar{y}$	Distance from the extreme fibre in tension to pole's neutral axis
Y	Global Y-axis
$y_{i,f}$	Coordinate component of the pole's centroidal line in the Y-axis for the initial and final nodes, respectively
$y_{j,k}$	Coordinate component of the pole's internodal length in the X-axis for any two consecutive nodes
Z	Global Z-axis
$z_{i,f}$	Coordinate component of the pole's centroidal line in the Z-axis for the initial and final nodes, respectively
$z_{j,k}$	Coordinate component of the pole's internodal length in the X-axis for any two consecutive nodes
ε_t	Tensile strain at the section's extreme fibre in bending
ΔD	Differential equivalent diameter between the bottom and a section at a distance ΔL
ΔIL	Differential internode length between the bottom and an internode length at a distance ΔL
ΔL	Length between two sections that define the differential diameter

Δ_{lin}	Maximum mid-span deflection within the linear portion of the load-displacement curve
Δt	Differential equivalent diameter between the bottom and a section at a distance ΔL
Δ_{δ}	Difference in maximum deflection between structural models (%)
Δ_{ε}	Deformation difference between the minimum and maximum stress limit in elastic modulus test
Δ_{σ}	Stress difference between the minimum and maximum stress limit in elastic modulus test
α	Position around the section ($0 \leq \alpha \leq \pi$)
β	Overlapping height
δ	Out-of-straightness of a pole
δ_r	Out-of-straightness ratio
ε	Bending strain
ε'	Bending strain within the section for an isotropic material
ε_t	Maximum tensile bending strain
μ	Overlapping width
ϕ	Top view angle between two RF connecting elements
ν	Poisson's ratio
θ	Position of the neutral axis
θ_o	Direction of the principal moment of inertia
ρ	Dry density
σ	Bending stress within the section
σ'	Bending stress within the section for an isotropic material
σ_b	Local buckling of a thin-walled cylinder
σ_c	Maximum compressive bending stress within the section
σ_t	Maximum tensile bending stress within the section
$\sigma_{ti+,to+}$	Critical inner and outer transverse stresses, respectively
τ	Shear stress within the section
τ'	Shear stress within the section for an isotropic material
τ_{max}	Maximum shear stress within the section
ω	Moisture content
ω_{Eb}	Moisture content of a bending test sample
ω_{Ec}	Moisture content of a compressive strength clear bamboo sample
ω_v	Angular velocity

List of Abbreviations

3D	Three-Dimensional
AEC	Architectural, Engineering and Construction
ASTM	American Society for Testing Materials
BIM	Building Information Modelling
CAD	Computer-Aided Design
CAM	Computer-Aided Manufacturing
CEGE	Civil, Environmental and Geomatic Engineering
CNC	Computer Numerical Control
CO_2	Carbon Dioxide
CoV	Coefficient of Variation
EN	European Standard
FE	Finite Element
LED	Light-Emitting Diode
LiDAR	Light Detection and Ranging
MC	Moisture Content
NFU	Nanjing Forestry University
NURBS	Non-uniform Rational B-Splines
RE	Reverse Engineering
RF	Reciprocal Frame
TCP	Tool Centre Point
UCL	University College London
UNAM	National University of Mexico (Spanish acronym)
ZCB	Zero Carbon Building

- Blank -

1 Introduction

The world's increasing urbanisation is placing an unprecedented burden on natural resources and the environment. By 2017, the construction industry was responsible for the largest global share of energy consumption and carbon dioxide (CO_2) emissions accounting for 36% and 39% respectively [1]. Steel, concrete and aluminium, the three main construction materials, are alone responsible for almost 50% of all industrial CO_2 emissions worldwide with demand expected to double by 2050 [2]. The growing demand, together with the negative environmental impact, are mainly taking place in developing regions where the pace of urbanisation is the highest [3]. Global guidelines and policies have been put in place to reduce the negative impact of the building industry by increasing the efficiency of current material production, construction procedures and building functioning [4]. Nonetheless, a gradual transition from non-renewable, highly industrialised materials to natural, sustainable and renewable ones is a fundamental step to achieve balanced sustainable development.

Bamboo in its natural form (round pole) is one of the most promising sustainable and ready to use structural elements due to the large endemic natural reserves prevalent in the Southern Hemisphere, coincidentally, the region where the majority of developing countries are situated [5]. Studies on bamboo's biological and anatomical properties [6,7] have confirmed their potential as a renewable construction material, reaching heights of up to 30 m in a few months and full maturity in three to five years. With over one-hundred species scattered around the world identified as suitable for construction purposes [8] bamboo is capable of reducing the demand for industrialised building materials, while promoting economic activity in rural regions to reduce the current pressure over urbanised areas [9]. For all their qualities and potential, bamboo poles still need to overcome multiple technical (e.g. material variability, durability or fire performance) and cultural (e.g. preference over

industrial materials) barriers before they become an accepted alternative structural element.

Concrete, steel and aluminium have overshadowed the integration of natural bamboo poles into the industry due to the high-quality assurance achieved over decades of refining the production processes of structural elements manufactured from the former. As a result, the material properties (geometric, physical and mechanical) of these elements are quantifiable, standardised and in agreement with international building standards. This all together brings a relatively high level of confidence over industrialised materials for their acceptance and use in the building industry. The wood industry has also experienced a higher development compared to the bamboo industry. Despite wood being a natural material, the elements that are commonly used for construction purposes pass through semi-industrialised quality control processes, for example, to cut logs down into uniform, prismatic and standard shapes and sizes [10], partially reducing the uncertainties on material properties associated to these organic structural elements and increasing the confidence in their use. Similar semi-industrial processes allowing the formal use of bamboo poles within the building industry are practically non-existent, as design and construction techniques for bamboo structures still depends on empirical knowledge.

In addition, current design and construction procedures were developed during the past century having the aforementioned industrialised and standardised materials in mind, therefore, the transition to renewable and sustainable materials, such as bamboo poles, requires the parallel development of new approaches using state-of-the-art tools that allow exploiting their potential without compromising the future state of our environment. To achieve this, the construction industry must look beyond its traditional processes and the empirical know-how that bamboo construction currently relies on. Digital modelling, robotic fabrication and other advanced tools are revolutionising the built environment and thus, it seems fitting to challenge the common misconception that bamboo poles and these advanced technologies are part of mutually exclusive realms.

1.1 Problem statement and hypothesis

The use of structural elements produced from industrialised materials, such as concrete, steel, aluminium and even timber, have flourished in the architectural, engineering and construction (AEC) industry mainly because of the quality assurance on which their production and subsequent construction processes are based on. Construction using these conventional standard materials would continue unchanged if it was not for the significant negative impact that their production causes in the environment, provoking a need to alternate towards more sustainable options. It has been estimated that construction of bamboo structures (including material production process) has a relatively lower negative environmental impact when compared with conventional materials. Bamboo poles have been used as a construction material for vernacular and traditional architecture since the beginning of the last millennium in regions where the material grows naturally. Further development and applicability of bamboo poles as structural elements in the building industry have been hampered due to the inherent geometric, physical and mechanical variability of their material properties, combined with the limited data of material properties and the lack of quality control for the production of round bamboo poles.

Despite the efforts made to standardise bamboo poles, as it occurred with timber, there still is a lack of robust methodologies to tackle the variability issue, to guarantee the necessary quality assurance of the poles as a product and to ensure the reliability of the structures built with them. This has caused a practically negligible utilisation of bamboo poles in the building industry. Consequently, the overall design and construction processes for bamboo pole structures has remained in the era of manual and analogue tools, driven by empirical knowledge and engineering concepts based on other standard materials.

The underdeveloped condition of bamboo poles as a structural product gives at least the opportunity to change our perception about its organic nature and how to provide the fundamental basis to ensure the reliability of bamboo structures. This thesis postulates that modern digital technologies, such as 3D

geometric acquisition, computational modelling and automated fabrication/assembly, are necessary to revolutionise the way structural systems for bamboo poles are being developed. These digital technologies can offer an opportunity for bamboo poles, as structural elements, to become a sustainable alternative to conventional materials to produce high-quality structures.

1.2 Aim and objectives

The overall aim of this research is to develop a digital workflow that tackles the geometric, physical and mechanical variability of bamboo poles by quantifying the properties of every pole contained in a specific stock, mimicking a semi-industrial quality control procedure applied prior the design and construction of a bamboo structure. To achieve this aim, the following overall research question was formulated:

How can state-of-the-art digital technologies, such as geometric acquisition and automated fabrication, be implemented within a digital workflow to quantify the geometric, physical and mechanical properties of bamboo poles and provide the fundamental basis to ensure the reliability of bamboo structures?

To answer this question, a series of specific research objectives were conceived and therefore, conformed the main body of this doctoral thesis:

- To develop a geometric digitisation procedure for individual bamboo poles based on a reverse engineering approach that captures their irregular and organic shape into digital 3D models and numerical geometric data that describes their unique properties
- To implement the digitisation procedure and gather geometric numerical data of multiple bamboo species to analyse their geometric variability and explore correlation patterns
- To develop a material sampling procedure based on clear bamboo samples using an automated fabrication approach that allows the fabrication of samples from an entire stock of poles

- To determine physical and mechanical properties of different bamboo species and explore characterisation approaches that reduce the variability effects on a specific stock of bamboo poles
- To study the bending behaviour of bamboo poles and determine their elastic properties based on clear bamboo samples
- To integrate the developed material quantification methodologies into a digital workflow for the design, construction and management of bamboo structures through a practical case study

1.3 Outline

This work is divided into seven chapters addressing the research objectives. The following is a description of each chapter:

- Chapter *1* presents an overall introduction to the topic, highlighting the research problem that this thesis is addressing. A general research question, together with the overall aim of this thesis is also presented, which are then translated into specific research objectives. This chapter also includes the organisation of the work and the contributions and publications from the author.
- Chapter *2* presents the relevant literature review of the research topic, covering the use of bamboo poles as construction material, together with their geometric, physical and mechanical properties. It then focuses on the variability of properties associated with the organic nature of bamboo poles and the negative impact this variability produces to implement bamboo poles as a construction material. Finally, this chapter introduces relevant digital technologies and approaches that can potentially close the gap to integrate bamboo poles in the building industry.
- Chapter *3* develops and presents the details of a geometric digitisation procedure of bamboo poles suitable for construction purposes focusing on key aspects that ensure efficiency and quality. The geometric digitisation is validated through its practical implementation on bamboo poles of three different species, under both on-site and laboratory

conditions, whose digital geometric data is then used to analyse their geometric variability and explore geometric correlation patterns.

- Chapter *4* develops and presents the details of a scan-to-fabrication procedure to efficiently extract small clear bamboo samples that enable the quantification of relevant physical and mechanical properties from an entire stock of poles. The scan-to-fabrication is validated through its practical implementation to produce the relevant material testing samples.
- Chapter *5* is an extension of the study of physical and mechanical properties of bamboo poles presented in Chapter *4*. This chapter explores the use of basic material properties obtained through clear bamboo samples, to predict the elastic behaviour of bamboo poles in bending. This contributes to a better understanding of bamboo's structural behaviour. Chapter *5* also presents an experimental programme that analyses the failure behaviour and the influence of transversal stresses when the pole is subjected to bending.
- Chapter *6* presents a case study where the material quantification of geometric, physical and mechanical properties is integrated into a digital workflow for the design and construction of a reciprocal frame bamboo structure. This case study highlights the importance of the adoption of digital technologies to develop acquisition methods that tackle the organic material variability of bamboo poles by generating digital data that describes their properties. This data is further used to drive the design and construction of the reciprocal frame prototype.
- Chapter *7* summarises the outputs of the research in response to the overall research question, including the contribution to how this work supports the integration of bamboo poles as alternative structural elements.

1.4 Contributions and publications

This doctoral thesis contributes to the general research topic to integrate bamboo poles into the building industry as structural elements. Therefore, the collaboration with overseas institutions, located in regions where bamboo is

endemic, was crucial for the successful development of this project. The institutions involved were: the National University of Mexico (UNAM) and the Nanjing Forestry University (NFU) in China, where multiple visits accounted for almost a year of laboratory and fieldwork. The result of the entire collaborative work developed by the author of this thesis has been presented in multiple conference proceedings and journal articles which comprised the core of the present work, distributed as follows:

Chapter 3.

Lorenzo, R., & Mimendi, L. (2019). **Digital workflow for the accurate computation of the geometric properties of bamboo culms for structural applications**. *ACEM2018 and SBMS1*, *275* (1024), 1–11. doi.org/10.1051/matecconf/201927501024

Lorenzo, R., & Mimendi, L. (2020). **Digitisation of bamboo culms for structural applications**. *Journal of Building Engineering*, *29*, 101193. doi.org/10.1016/j.jobe.2020.101193

Lorenzo, R., Mimendi, L., Godina, M., & Li, H. (2020). **Digital analysis of the geometric variability of Guadua, Moso and Oldhamii bamboo**. *Construction and Building Materials*, *236*, 117535. doi.org/10.1016/j.conbuildmat.2019.117535

Chapter 4

Lorenzo, R., Godina, M., Mimendi, L., & Li, H. (2020). **Determination of the physical and mechanical properties of moso, guadua and oldhamii bamboo assisted by robotic fabrication**. *Journal of Wood Science*, *66*(1), 20. doi.org/10.1186/s10086-020-01869-0

Chapter 5

Lorenzo, R., Mimendi, L., Li, H., & Yang, D. (2020). **Bimodulus bending model for bamboo poles**. *Construction and Building Materials*, *262*, 120876. doi.org/10.1016/j.conbuildmat.2020.120876

Lorenzo, R., Mimendi, L., & Li, H. (2019). **Digital analysis of the geometric variability of bamboo poles in bending**. *ACEM 2018 and SBMS1*, *275* (1007), 1–12. doi.org/10.1051/matecconf/201927501007

- Blank-

2 Background

2.1 Bamboo poles as a construction material

Bamboo is the only grass-like material from which the stem or pole, as its shape approximates a circular hollow tube, is used as a primary structural element. The availability of bamboo concentrates in the tropical regions worldwide, however not all the species are suitable for structural purposes. Bamboo is endemic to all continents, yet natural growing in Europe has not been reported [7]. More than 1600 different bamboo species have been already identified, however, this number is likely to increase as gaps still exist in the classification and identification of tropical plants, including bamboo [11]. There are more than 36 million hectares of bamboo forest in the world, which represent around 1% of the total global forested area, being Asia the major contributor with 65% [12]. The diversity of the plant is apparent when looking at the sizes of different species, while some species can be kept in a pot as home decoration, the species that are suitable for construction purposes need the open space of a forest or plantation site to be grown. There are about a hundred species globally distributed that fulfil the basic requirements for structural elements (e.g. diameter above 50 mm), they normally grow in forests and are commonly classified as “woody” bamboo [8]. The abundancy and potential of bamboo poles have therefore been widely exploited for construction purposes.

The history of bamboo construction in Asian countries can be traced back thousands of years, while in South America its use has become popular just over the last millennia. In China, evidence has shown that during the late Neolithic era, bamboo was used by humans to support their shelter development, migrating from trees and caves to small hand-made bamboo houses where other bamboo products such as homeware and working tools were also found [13]. The Asian vernacular architecture is therefore closely associated with bamboo poles and has been the main reference for the development of recent bamboo buildings [14]. The development of houses

and other small structures in South America have been documented only after the arrival of Spanish conquerors, around 500 years ago, being the bahareque - a combination of rammed earth, timber and bamboo frame structures - the most popular construction system for bamboo poles [15]. However, in South America bamboo has been usually referred to as “the poor man’s timber”, therefore bamboo poles did not experience the same utilisation and importance as in Asian countries [5].

Bamboo poles have lately been used to construct modern buildings in different countries around the world, but these technical demonstrations have not been significant for the building industry to divert its main interest on man-made, conventional materials, such as concrete, steel or timber. Currently, there are a number of globally distributed outstanding bamboo buildings that illustrate the high potential of bamboo as a construction material. The type of buildings includes houses, schools, pavilions, footbridges, hotels, warehouses and tollgates, built in countries where bamboo is endemic, such as China, Colombia, Indonesia, Mexico and Japan, but also built in European countries such as Germany and Italy [14]. In Africa, the application of bamboo as a construction material has been aimed at tackling housing demand by providing sustainable and affordable solutions, however, the production of bamboo poles, as well as their implementation for construction are still being discussed [16,17]. The average harvesting of bamboo poles was 150 thousand cubic meters in 2017 [5] from which only six per cent was used in its round nature for different purposes and the rest was used as raw material for post-processed products [18]. In context, the production of bamboo poles helped to provide shelter to approximately 15% of the global population (mostly local communities in developing countries) by 2005 [12]. Although the volume of harvested bamboo poles can be considered higher because its production and use would normally happen in local communities and therefore not reported, raw bamboo is well behind the production of steel (including non-structural purposes), sawn wood and concrete that reported 230 million cubic meters in 2018, 453 million cubic meters in 2016 and 10 billion cubic meters in 2012, respectively [19–21].

The production and utilisation of conventional construction materials are entirely based on industrial processes, posing a significant technical advantage against bamboo poles. Major institutions for concrete and structural steel such as the European Standard (EN) in Europe or the American Society for Testing and Materials (ASTM) in the United States have spent decades developing material specifications and production guidelines, such as EN-206:2013 for structural concrete and EN-10025:2004 or ASTM-A6 for structural steel [22–24], so that the structure built with these materials complies with specific quality standards approved by industry professionals. In the case of timber, the construction industry and research institutions have put extra effort to categorise and grade the species of wood with potential for construction purposes and define uniform shapes, sizes and allowable deviations for its subsequent utilisation [10,25]. The drawback of these industrialised materials is the negative impact that their production and utilisation causes in the environment as the construction industry was responsible for almost 40% of the global carbon dioxide (CO_2) emissions by 2017 [1].

The increase of the global population and the development of urban areas are the principal factors for the rise of CO_2 emissions from the construction industry, particularly in developing countries. For example, the production of steel is responsible for approximately 8% of the global CO_2 emissions in the world where China alone produces about 40% of the global steel [26]. The cement industry produces around 4% of the global CO_2 emissions, again, China is the leading producer country in the world with India following close behind [27]. As the pace of urbanisation is the fastest in developing countries, it is expected that these countries will increase their industrial production and CO_2 emissions in the coming years [28]. However, this pace of development needs adjustment as steel and concrete still depend on the exploitation of non-renewable fossil resources which availability is limited to no more than two hundred years [5]. Wood products appear to have a more promising future as their production generates low carbon footprints in the environment and it is a renewable resource, nonetheless, excessive

agricultural activities and commercial logging have worryingly reduced the forested area in tropical regions [29].

The environmental impact caused by the building industry has come to the attention of research and commercial organisations during the last decades, consequently, the pursuit of alternative sustainable and renewable construction materials begun. Bamboo's environmental credentials place it as one of the most promising options, as far as alternative materials are concerned. For example, the diurnal growing rate of bamboos ranges from 20 to 100 centimetres per day, depending on the species, and can reach heights of up to 30 meters during the first year [7]. Furthermore, bamboo reaches maturity after 3 to 5 years - half the time for softwoods - which in turn means that a well-managed bamboo plantation has the potential to generate negative carbon footprints [9]. Bamboo growing regions are considered strategic to help in the economic development of local communities as bamboo can play an important role towards the Sustainable Development Goal 12: sustainable production and consumption of the United Nations due to its affordable, sustainable and resilient characteristics [30]

As a natural construction material, bamboo is susceptible to rapid decay and insect attack, and its fire resistance properties score lower than those of timber. These challenges require innovative design solutions to manage the bamboo poles' durability and fire resistance characteristics and ensure safe and permanent bamboo buildings. The relatively high water and sugar content during the growing and harvesting period of bamboo poles attract different types of insects and fungi, similar to what is observed in wood products [31]. To protect the bamboo and increase its working life, each pole can be subjected to chemical treatment (e.g. disodium octaborate tetrahydrate) and drying procedures [32]. However, studies assessing the impact of chemical treatment on the bamboo poles' mechanical properties and their potential use (e.g., as biomass) once their working life has ended are scarce. To ensure long-lasting and safe bamboo structures, a holistic durability by design approach is required, where adequate protection, maintenance and

replacement of elements is considered from the very conception of a construction project.

The hollow nature of bamboo poles is a condition affecting their durability as decay and fungal attack spread faster through the section of the pole. Also, water and insects can infiltrate and spread through the hollow pockets of the pole. However, the hollow condition becomes more critical for fire performance. In contrast with timber products, the thickness of bamboo elements is relatively thin, which means that the mass and mechanical capacity will decrease rapidly once the element is ignited [8]. Also, the air contained inside the hollow section of the pole supplies extra oxygen which increases combustion. Research has found that the high concentration of silicate in the external layer of the bamboo surface may offer certain protection against fire, delaying the ignition of a bamboo element when compared with other wood products [14,33]. Nonetheless, the thickness of the silica layer is not significant in comparison with the wall thickness of the pole and can be easily removed through handling during construction. Similar to the durability by design approach, a bamboo structure requires innovative design considerations that protect load-bearing components against fire. To develop such approaches, a digital framework is needed to manage the properties of the bamboo poles involved in a construction project.

In the 1970s a new bamboo product made of laminated bamboo strips was introduced as a potentially sustainable alternative for structural elements, allowing the manipulation of shape, size, physical and mechanical properties, however, this product is still under development to become a regulated standard material. A laminated bamboo structural element is produced by cutting the bamboo pole in strips that are flattened, planned and trimmed before being subjected to preservation and caramelisation processes (Figure *2.1a*) and eventually glued (Figure *2.1b*), heated and pressed to its final shape (Figure *2.1c*). Although laminated bamboo is already industrially produced, mainly in China [12], the processes or quality control measures that regulate its production are still under development [34]. For example, the type of adhesive, proportions and spread rate are not regulated and depends on the

manufacturer criteria for its application [35]. Mechanical and physical standard tests for this product are inexistent and normally tested under adaptations from standards that were developed for other wood laminated products [35]. The basic mechanical properties and characteristic values, which are not usually similar to those of bamboo poles [36], are still under investigation [37–39]. Despite the great potential for producing standard bamboo structural elements, the development of laminated bamboo has not reached the levels required to alternate from steel, aluminium or even wood, to laminated bamboo products. The cause of this is not only related to the limited development conditions for production and material characterisation but also the environmental properties of laminated bamboo.

Figure 2.1. Laminated bamboo structural element process. Images were taken in a factory of bamboo laminated products in Jiangxi, China.

The raw material used to produce laminated bamboo is a natural, fast-growing and sustainable one, but the industrial processes involved in its production have shown a considerable impact on the environment. The overall environmental impact of laminated bamboo is lower than other industrialised materials such as masonry or concrete products [40], however, it contributes notably to the acidification and global warming potential [41]. Also, it is important to consider the impact related to the formaldehyde resin-adhesive used to glue the strips together, that in addition, prevents the recycling of laminated bamboo elements. Moreover, power consumption in the laminating process depends only on fossil fuels, contributing to energy consumption and CO_2 emissions [41]. Any processed or semi-processed bamboo construction material such as laminated bamboo, woven mat panels or flattened bamboo induce a considerably higher negative impact on the environment than natural

bamboo poles [42], leaving the latter, as the most environmental friendly bamboo product.

Production and construction procedures for natural bamboo poles generate lower environmental impact than any other conventional material and its readiness for utilisation locates them at the top of alternative natural and sustainable materials. There is still uncertainty about carbon sequestration from bamboo plantations due to the limited research applied over the different growing regions and species, however, a conservative study suggests that a bamboo plantation can store up to 4.3 tonnes/ha [43] which is comparable with the 3.2 to 10 tonnes/ha range of a tropical forest [44]. Other alternative natural materials such as hemp plant sequestrate less than 1 tonne/ha due to the low amount of biomass that can be produced [45]. Contrary to structural applications based on bamboo poles, the hemp plant is normally used for non-bearing walls and insulation purposes, involving longer production processes before its utilisation [46]. In terms of construction procedures, bamboo's sustainability is considered to be twenty times more favourable than that of wood, metal and masonry products, assuming that the bamboo is locally sourced [47]. The environmental credentials of bamboo fit the current need for alternative construction material, that is renewable, sustainable and abundant, however further knowledge on the physical and mechanical properties also has to be well established before the widespread utilisation of bamboo poles becomes a reality.

2.2 Geometric, physical and mechanical properties of bamboo poles

The main components of a bamboo plant are divided into rhizome, stem and branches. The rhizome remains underground, from which several bamboo shoots (or sprouts) emerge out of the surface. Bamboo shoots continue growing straight-up to become the stem. The branches normally cover two-thirds of the upper part of the stem and will appear soon after the stem's growing period has finished. The part of the plant that is used as a structural element is the stem (branches are removed), its main features are shown in Figure *2.2*. The stem is commonly known as "bamboo pole" because

the cross-section throughout the stem is similar to a circular tube, although solid diaphragms appear at intermittent intervals along its height. These diaphragms will produce circumferential ridges in the outer surface of the bamboo pole known as “nodes” and the portion between nodes is known as “internodes”. These general features are the basic characteristics to identify bamboo poles and can be found throughout different species.

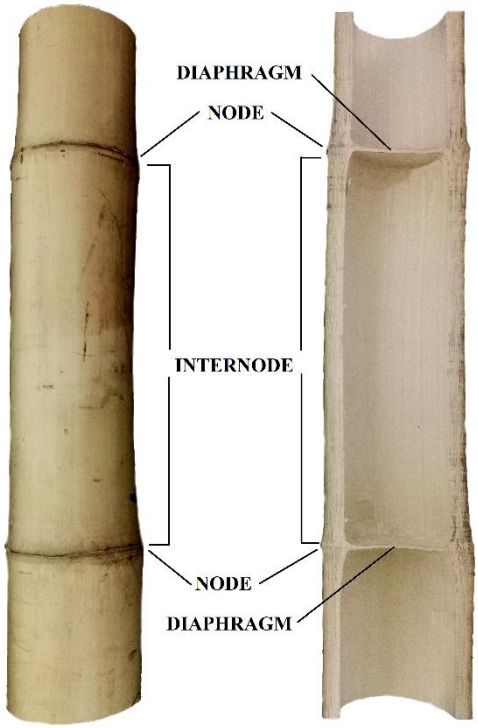

Figure 2.2. Basic geometric features of bamboo poles

The typical single stem of the plant facilitates its use as a natural resource because in that way bamboo grows practically ready for its utilisation [5]. However, when bamboo poles are compared with conventional structural members of similar geometry (e.g. steel or aluminium profiles) there are critical geometric characteristics that increase the complexity of the material: it tapers along its length; has irregular internodal distances; cross-section varies along its axis (shape and thickness); and presents a spatial longitudinal out-of-straightness [48]. Similar to other plants, the cross-section of the pole reduces with height, thus affecting the cross-sectional properties, and as the cross-section reduces the internodal length becomes longer [49]. Out-of-

straightness normally occurs as a spatial variation, and therefore its accurate assessment is complex and usually ignored for structural purposes.

The anatomical structure of bamboo is, in general, simple: longitudinal unidirectional fibres surrounded by a matrix as bounding material. The matrix is composed of parenchyma cells on which vascular bundles are embedded. The vascular bundles are made of fibres (sclerenchyma), vessels and sieves tubes (conducting tissue). The approximate average distribution of matrix/fibres within the cross-section has been measured as 50/40, the remaining ten per cent corresponds to the conducting tissue [7]. The complexity of the material lies in that the internal structure of bamboo is considered functionally graded because the matrix/fibre ratio changes across the wall thickness and along the pole (Figure *2.3*). The matrix/fibre ratio comes from a process that has been subjected to thousands of years of natural optimisation as a response to external physical stimuli from the environment [50]. The fibre content in the outer portion of the wall thickness surpasses sixty per cent but can decrease to ten per cent at the inner part depending on the species [49]. Fibres run along the bamboo pole within the internode, however, the fibre's direction and the anatomical arrangement changes at every node, as the fibres are diverted into the diaphragm (Figure *2.4*)[49].

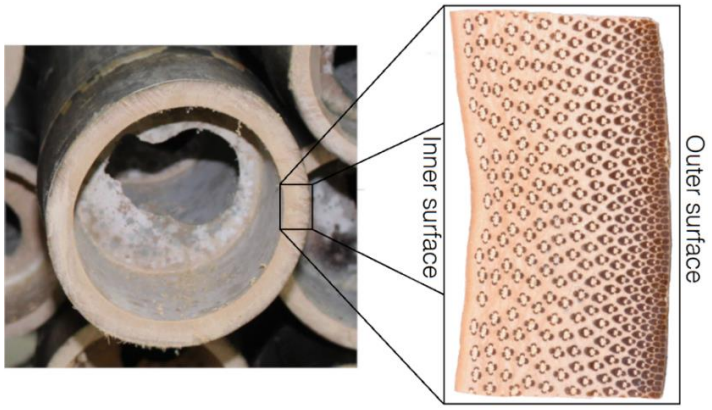

Figure 2.3. Functionally graded fibre distribution in bamboo wall thickness increasing radially from the inner to the outer surface

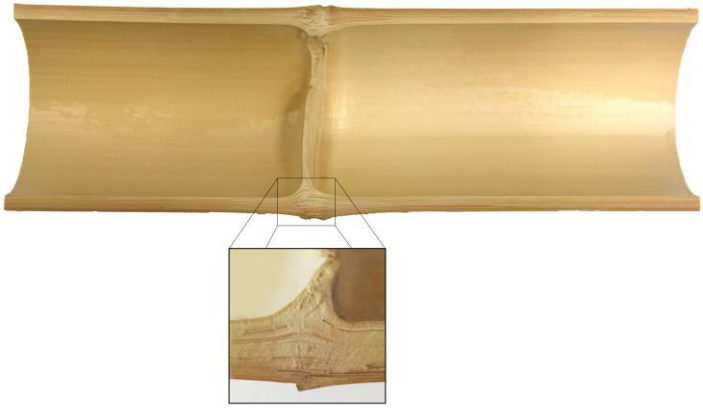

Figure 2.4. Longitudinal section of bamboo pole showing in detail, fibres diverting at the diaphragm

The strength of the material derives from its inner anatomical arrangement so that the properties parallel to the fibres are considerably higher than the ones perpendicular to the fibres. The fibres' tensile strength is around 610 MPa for Moso (Phyllostachys pubescens) bamboo, being this the capacity that is commonly used to compare bamboo with steel, however, the modulus of elasticity is around 46 GPa, approximately 4.5 times lower than steel [49]. On the other hand, the parenchyma properties are estimated to be 12 times lower than those of the bamboo fibres [49]. Therefore, the different mechanical properties will depend on the structural arrangement of matrix/fibres within the cross-section which can be approximated using the rule of mixtures [50]. The rule of mixtures is a weighted mean theory generally accepted to predict the behaviour of composite materials with continuous unidirectional fibres [51]. For tension, compression and bending strength parallel to the fibres the interface matrix/fibre and its functionally graded distribution might play an important role in the general mechanical behaviour of bamboo poles. However, tension and compression strength perpendicular to the fibres as well as shear parallel to the fibres appears to depend purely on the matrix, showing constant properties along the pole and low interface strength with the fibres [52,53].

Similar to timber products, the physical properties of bamboo poles are important for construction purposes and should always be measured and considered. The moisture content is the most important physical property, as it is related to the strength of the material and produces shrinkage and swelling,

similar to what is observed in timber [54]. The changes in moisture content would normally produce splitting effects that can only be controlled by a systematic drying process [55]. If splitting happens, it normally appears along the height of the bamboo poles, as the material lacks circumferential reinforcement, and will easily extend through the entire wall thickness, damaging the integrity of the cross-section and changing the shape from closed to an open one (Figure *2.5*). The dry density of bamboo poles partly depends on the matrix/fibre ratio because the fibre's density is about two to three times higher than the matrix [53], therefore the density across the wall thickness and along the pole can vary. Bamboo poles can be harvested after three to five years when they reach maturity, before this period the nutrients are still being transported to the branches, which means that starch and water content levels are too high for harvesting and can affect the overall durability of the pole [56]. According to Kaminski et al., the durability of bamboo can range between 1 to 30 years, depending on the preservation treatment applied and its location within the structure (outdoors or indoors) [32]. The most common preservation treatment for durability consists of immersion in a borax solution, however other treatments, such as carbonization, smoking, salt-water and water immersion, are also applied depending on different regions around the world [5].

Figure 2.5. Natural splitting appearing along the height of bamboo poles

The mechanical properties of bamboo poles are, to some extent, correlated to physical properties and therefore different correlations have

been explored to estimate the resistance of the material based on physical indicators. According to Chung & Yu [57], axial mechanical properties (compression and bending parallel to the fibres) increase with a decrease of moisture content in the bamboo pole, where they found that the optimal moisture content for Moso and Kaojue (Bambusa pervariabilis) bamboo is around 5%. Axial compression and bending properties have also been found to increase with density, but little variation has been observed when compared to the radial and tangential compression properties [53]. Combination of physical properties such as linear mass has also been correlated with the axial bending properties of Guadua (Guadua angustifolia kunth) [58] and Tali (Gigantochloa apus) bamboo [59] and with the axial compression properties of three Indonesian species [60].

The correlation of physical and mechanical properties can therefore help to estimate mechanical properties, but it is also important to consider the internal anatomical distribution of fibres and their effect. For example, a significant relationship of tensile strength and tensile modulus of elasticity with the fibre content has been reported on Moso bamboo [61]. According to Harries et al. [62], the functionally graded nature of the fibre distribution within the wall thickness improves the effective moment of inertia and radius of gyration between five to twenty per cent. The distribution of the fibres also contributes to the radial increment of the axial properties of bamboo, from the inner to the outer part of the wall thickness, which has been observed in Moso bamboo [53]. These anatomical characteristics have been modelled as orthotropic composite material using the rule of mixtures approach, finding good agreement between theoretical capacity and experimental data of small bamboo coupons extracted from Moso bamboo [53].

Despite the significant correlation found between physical and mechanical properties of samples extracted from some of the most common bamboo species, there exist clear variation of those correlation patterns when different studies focusing on the same species are compared. For example, Dixon & Gibson [53] found that the dry density of Moso bamboo is directly proportional to the vascular bundle volume fraction with a coefficient of

determination equal to 0.80. In a later study, Zhang et al. [63] measured a similar coefficient of determination from a linear regression between these two parameters (0.76), however, the mathematical equations in both studies differed from one another to the point that the dry density estimated from the vascular bundle volume fraction was 25% higher in Zhang et al.'s study when compared to Dixon & Gibson's. The difference suggests that the density of bamboo varies independently of the number of fibres present in a certain area. This idea was then supported by a study [64] where the variation of the fibre density along the height of four different bamboo species (Dendrocalamus pendulus, Dendrocalamus asper, Gigantochloa levis and Gigantochloa scortechinii) varied by ±7% from the average fibre density in every species. It could also be assumed that the dry density of matrix is not constant, as suggested by Dixon & Gibson [53], and therefore it will also be reflected as variability on the bamboo pole's dry density. The relatively high coefficient of determination for dry density and vascular bundle volume fraction found in both studies (≈0.8) [53,63], indicates that properties are indeed related to each other but those relations appear to be valid only for the individual studied cases and cannot be translated to other bamboo poles, even if they belong to the same species. This suggests that to extrapolate correlation results that help to estimate physical or mechanical properties of a whole population (or species), a substantial amount of studies would be necessary to quantify the inherent variability and adjust the numerical models accordingly, bearing in mind that the organic nature of the material may be a challenge to produce accurate predictions. The inherent variability of the geometric, physical and mechanical properties of bamboo poles is, therefore, the main challenge to overcome so that the environmental advantages of bamboo poles can be fully exploited for bamboo's utilisation as a construction material in the building industry.

2.3 Geometric variability

The main technical challenge posed by bamboo's organic nature is the one associated with the inherent variability of the geometric, mechanical and physical properties. Different testing methods to measure the material

properties have been already developed [65–67], but the variation of the properties cannot be yet predicted. Variation of properties happens from species to species, within poles of the same species and even within a single pole. The geometry and anatomy vary from bottom to top and across its section [7,49], which happen not in a random manner but in an unpredictable way, as it depends on the bio-nutrients availability and distribution, as well as on the external stimuli during the growing period of the pole [50]. The mechanical and physical properties of a bamboo pole partly depend on the organic arrangement of the matrix/fibre ratio but also the different properties of each constituent part. Variation in material properties is an inherent characteristic that all structural components possess, however, natural materials lack the production and quality control of manufactured ones, where a significant reduction of variability is accomplished or simply quantified. Consequently, the magnitude of variability in bamboo poles has such an impact that to this day it has been impossible to define a set of characteristic values that closely represent the properties of a specific species. This section describes the current methods proposed across different studies to determine the geometric properties of bamboo and their variation.

Building with bamboo poles is considered, up to this day, to depend on craftsmanship, normally reliant on manual or analogue tools, from which the geometric properties are measured [68]. Diameter, thickness and total length are the most common geometric properties measured from a bamboo pole to use it in a construction process or to perform physical and mechanical tests [66,69]. According to ISO-22157 [66], the diameter and thickness should be taken from the ends of a pole (two diameter and four thickness measurements at each end) to then calculate the mean of each and assign it as the diameter and thickness of the measured pole. This measurement process assumes that the bamboo resembles a circular hollow tube which linearly tapers from bottom to top. Although the measuring method is practical (easily performed on-site and using simple analogue tools) and is supported by research showing a linear variation of diameter and thickness along the length [49,57], more research is making evident that a bamboo pole is not exactly a perfectly

straight, circular hollow and tapered tube. Instead, its cross-section is an organic shape that varies with height, needing more complex measurement tools and geometric assumptions [48,70,71].

With the growing interest in using bamboo poles as an alternative construction material, more geometric studies on different species located around the world have been performed. Part of them has focused on measuring the diameter and thickness of common bamboo species to provide average values that can inform preliminary structural design. For example, Paraskeva et al. [72] collected the first six metres of 88 Kaojue bamboo poles of three to six years of age. After measuring the diameter and thickness of every pole they calculated basic statistical properties, from which the coefficient of variation (CoV) can be extracted (Table *2.1*). The coefficient of variation measures the dispersion of a probability distribution, this is, the higher the coefficient of variation, the greater the level of dispersion around the mean. Paraskeva et al. also collected 36 Moso bamboos with similar characteristics as Kaojue (first six meters from the bottom and age between three and six years), from which the CoV for diameter and thickness were also extracted (Table *2.1*). The variability of geometric properties found in Paraskeva et al.'s study is not just higher than the expected range in current structural elements of any conventional material (e.g. concrete or steel) [73,74], but due to the organic nature of bamboo poles, the variability would tend to increase when a larger amount of samples are measured [75]. For example, results of another study [57], where a higher amount of poles were measured for both Kaojue (364 samples) and Moso bamboo (213 samples) with similar characteristics (six meters long and 3 to 6 years of age), a significant CoV increase of 7% in both species compared to Paraskeva et al.'s results were found (Table *2.1*). For other species, the CoV of diameter and thickness has been found to range between 0.15 to 0.40 [60], which suggest that special attention to the geometric properties should be considered when designing buildings using natural bamboo poles.

	Kaojue			Moso		
	[72]	[57]	Difference	[72]	[57]	Difference
Age (years)	3 - 6		-	3 - 6		-
Length (m)	6		-	6		-
Samples	88	364	-	36	213	-
CoV Diameter	0.08	0.15	0.07	0.09	0.17	0.08
CoV Thickness	0.2	0.26	0.06	0.12	0.18	0.06

Table 2.1. Comparison of the coefficient of variation values for Kaojue and Moso bamboo

The rate of taper is another property that has called the attention of researchers because of the potential implications that this might have for structural and construction purposes [34,62,76]. Several authors have studied the diameter and thickness variation along the height of the pole and have suggested that this variation tends to be linear for both diameter and thickness [49,57,64,71,77]. The main limitation of these studies is the low number of samples that were measured (ranging from one to five), therefore it is difficult to conclude whether the recorded tapering rates are representative of a whole species or region. As an example, diameter and thickness data recorded at every three meters from seven 9-m long poles can be used to compare the different taper ratios found in a Brazilian species Bambusa vulgaris [78]. The taper was measured as the difference of diameter (or thickness) measured over the length, which essentially gives a slope describing the reduction of diameter (or thickness) per unit metre. The reduction rate of diameter and thickness ranged from 0.34 mm to 5.25 and 0.28 mm to 2.05 mm per metre respectively. In terms of average values, tapering rate found in Ribeiro et al.'s study for diameter and thickness was 2.50 mm/m and 1.33 mm/m, respectively, with a relatively high CoV: 0.60 and 0.44, respectively. Wider ranges of tapering rates have been found in four Indonesian species being 1.3 mm/m to 12.7 mm/m the widest range of diameter taper found [79]. A comparison between average reduction rates can be made using the study of Paraskeva et al. [72] and Chung & Yu [57] which focused on Moso and Kaojue species. After measuring diameter and thickness in Moso, Chung & Yu found average rates of 5.0 mm/m and 0.7 mm/m, respectively, whereas Paraskeva et al. reports 7.5 mm/m and 1.0 mm/m. In the case of Kaojue, Chung & Yu reports zero taper in diameter and 0.7 mm/m in thickness, whereas Paraskeva

et al. shows average rates of 2.4 mm/m and 0.8 mm/m respectively. These findings suggest that a linear correlation of diameter and thickness variation over the length of a bamboo pole might exist, however, these studies also show that the rate of that variation changes even among bamboo poles of the same species, increasing the geometric complexity of each bamboo pole.

The use of analogue measuring tools also limits the level of complexity that can be acquired from an organic shape, such as the one found in bamboo poles. It is well known that the shape of bamboo differs from a straight circular tube [80], therefore researchers have developed tools and methodologies to investigate the details of those natural deviations. One study focused on the shape of the cross-sections by measuring four diametrically opposite, perpendicular points, representing the largest and shortest pair of diameters within a cross-section. Using these two measurements, the deviation from circularity (or ovalisation) was estimated and the cross-section idealisation was proposed as an ellipse [70]. Although an ellipse is another idealisation of what in reality a non-regular shape is, it helped to understand that the variation in cross-sectional shape can, for example, affect the estimated bending capacity of the pole when compared with a perfect circular shape.

Another critical variable and relatively complex geometric characteristic is the out-of-straightness. Its importance has been mainly related to the axial capacity of poles but the understanding of its variability and therefore the effects that it can produce are limited. The main reason for this limitation is related to a lack of a robust and effective method to accurately estimate the centroidal axis' spatial deviation of a bamboo pole. Ghavami & Moreira [71] developed an intricate method to measure discrete cross-sections of the external surface of bamboo poles along its height. This method allowed to estimate the organic external surface at different sections along the pole and based on these sections approximate the spatial centroidal axis of the bamboo pole. The method could deliver accurate measurements; however, its procedure was complex and time-consuming (multiple manual measurements at every discrete height along the pole), therefore no further development or application of this method for construction or research purposes has been

recorded in the literature. Instead, a simpler method designed by Richard [81] and based in only two measurements have been used to determine the out-of-straightness of culms for research purposes [59,62]. However, the method measures the out-of-straightness in two arbitrary orthogonal planes, where visual criteria is needed to determine the direction of the maximum deviation and use that subjective direction to define the measuring planes.

The measuring technique developed by Ghavami & Moreira [71], whose schematic diagram is shown in Figure *2.6a*, demonstrates that a single holistic measuring method can be developed to extract accurate information of the bamboo's surface at discrete intervals, where the closer the spacing of the intervals around and along the pole, the more accurate the acquired geometry would be (Figure *2.6a*). When the data collected is put together, the result can describe the general features of bamboo's geometry, such as the length of the pole, change in external diameter along the length (taper) and its out-of-straightness. Furthermore, the points collected describe the three-dimensional non-regular geometry of the pole as a discrete cloud of points which can further support the implementation of bamboo poles into the building industry if the data points are further processed (Figure *2.6b*). Ghavami & Moreira's approach allows to quantify the inherent geometric variability on individual poles, however, the complexity of performing the measurement prevents it from being used as a tool to quantify variability by measuring the geometry of individual poles. This problem was addressed by Lorenzo et al. [82] which proposed the implementation of digital technologies to acquire the three-dimensional (3D) bamboo surface with a much higher level of detail when compared to Ghavami & Moreira's approach but with a simpler and intuitive reverse engineering method supported by 3D scanning equipment. Lorenzo et al. put forward the idea of intensively measuring bamboo poles, approaching a semi-industrial set-up, and effectively managing geometric data to allow its use within the disciplines of the AEC industry. The state of the art and different applications of 3D scanning equipment as a reverse engineering geometric acquisition methodology are discussed later in this chapter.

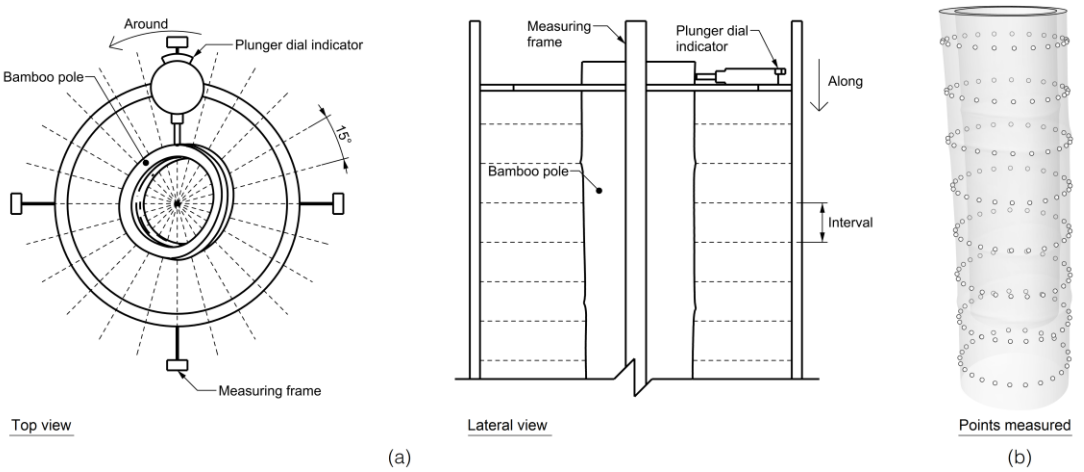

Figure 2.6. Diagram of Ghavami & Moreira's geometric acquisition method for a bamboo pole (a), together with the schematic results of measured points (b)

2.4 Physical and mechanical variability

Unlike any other conventional and industrialised structural material, such as concrete, steel or aluminium, bamboo poles are not produced to a particular specification which can ensure their reliability for construction purposes. The variability in physical and mechanical properties is present in every single structural material, however, an industrial process or systematic sorting of elements can be used to manage the effects of this variability. Concrete is a mixture of aggregates and cement that once is cured it can reach high compression capacities, however, the consistency in the mixture is essential to keep material reliability to an optimal level. Mixtures of concrete produced under industrial conditions, following production specifications and including on-site quality control measures have registered a strength-independent coefficient of variation of 10%, after testing around thirty thousand samples acquired from different producer companies [83]. Tension and compression properties of different types of metals, such as aluminium and steel, have also shown relatively low levels of variability in their properties [84], in fact, the variability has been reducing with the years because more robust processes and quality control measures have been put in place. For example, from the 1960s to 1990s the coefficient of variability of the yield stress in structural steel reduced from 13% to 8% [85]. In the case of timber, researchers have shown that variability for the mechanical properties ranges

from 20% to 40% [86,87], depending on the species, growth condition and grading method. For example, Tsehaye et al. [86] divided two species of timber into three groups depending on their axial stiffness and then compared the tension properties among each group, finding that the CoV dropped to a range of 5% to 15%, proving that a systematic sorting can reduce variability. The following paragraphs describe the current methods to measure the physical and mechanical properties of bamboo poles as well as the variability found in the material and how this issue has been addressed.

The development of physical and mechanical testing methods for bamboo poles has been following a similar path to the approach adopted for the development of testing and grading methods for timber. It is believed that the first comprehensive set of tests carried on wooden structural elements was in the 1700s by Georges Buffon, who tested different large and small samples of wood. Large samples were used to provide engineers with sufficient data for structural integrity and safety, whereas small samples allowed to describe the average material properties of wood species without material imperfections such as knots or splits [88]. The increasing demand for wooden products promoted extensive research projects led by public organisations and universities during the 1800s. By the early 1900s, research efforts were combined in a massive database to create the first standard for the material characterisation of wood elements and were published into the American Society for Testing Materials (ASTM). Since then, ASTM has updated and expanded the methodologies for the characterisation of the physical and mechanical properties of wooden elements for different species and under different conditions, including the utilisation of full-size and small clear wood samples.

In contrast, material characterisation for bamboo poles is just in its infancy. The physical and mechanical properties of bamboo poles have been explored through experimental testing for about a century to use bamboo poles as a construction material [89–91]. Nevertheless, it was not until the beginning of this century that the first international code for the determination of physical and mechanical properties (ISO 2217-1) became available so that

testing conditions and results could be more consistently produced and compared with each other [92]. This code, however, only focused on mechanical testing of full-size samples. Together with ISO 22157-1, a more recent grading standard has been published where basic principles are presented to sort bamboo poles and assign them characteristic values based on visual and non-destructive procedures [34]. A characteristic value is a representative value of a basic variable which is associated with a prescribed probability of not being violated and is determined using statistical data. One of the issues to assign characteristic values to bamboo poles is that there is not enough statistical data for all the bamboo species suitable for construction purposes. Besides, the part that these standards are not considering is that the high magnitude of variability that exists in bamboo poles can punish the characteristic value, reducing its effectiveness as a representative value of physical and mechanical properties.

The mechanical variability can be explored through one of the most common properties of bamboo poles, compression strength parallel to the grain, however, only a few studies have been performed using the same testing method and therefore results can be numerically compared. Table *2.2* shows the results of compression strength for different species, extracted from different sources. The samples on these studies were selected according to ISO 22157-1 and tested following the same procedure (the experimental testing program for [57] was performed before the publication of ISO 22157-1 but the procedure was the same). For the species Kaojue (normally used in the scaffolding industry in Hong Kong), there is a clear difference in the average properties and a considerably large dispersion of results. Similar dispersion was found for Moso (in Hong Kong) and other Indonesian species (Hitam, Tali and Andong) when compressive strength and modulus were investigated. Bending properties have also been explored, however, species being tested by different researchers but following the same method (ISO-22157-1) are not yet available. Table *2.2* shows available experimental results obtained from different species (Kaojue, Guadua and Tali) following the ISO 22157-1 testing procedure. This simple exercise highlights the problematic

which is twofold: i) lack of a robust and extensive database containing statistical values from different sources focusing on the same species; and ii) high mechanical variability can exist even between bamboo poles of the same species. Having these two issues suggests that testing and reporting basic statistical values obtained from a limited source of poles within a species is not sufficient to understand and manage the effects of natural variability. Instead, alternative methods are needed to tackle the variability of the material so that physical and mechanical properties are quantified to ensure the material reliability of bamboo poles.

		Specie	Samples	Mean	Std Dev	CoV
Compression strength (N/mm^2)						
	[57]	Kaojue	136	69	12	17%
	[93]	Kaojue	4	55	8	15%
	[72]	Kaojue	37	45	9	21%
	[57]	Moso	41	75	18	24%
	[93]	Moso	4	56	8	14%
	[60]	Hitam	100	45	9	20%
	[60]	Tali	102	45	7	17%
	[60]	Andong	108	38	9	24%
Compressive modulus (N/mm^2)						
	[57]	Kaojue	100	9300	2900	31%
	[60]	Kaojue	37	1988	-	-
	[57]	Moso	41	7800	1900	24%
Bending strength (N/mm^2)						
	[57]	Kaojue	53	82	17	21%
	[58]	Guadua	121	78	17	22%
	[59]	Tali	62	70	13	18%
Bending modulus (N/mm^2)						
	[60]	Kaojue	-	12104	-	-
	[58]	Guadua	168	17204	3005	17%
	[59]	Tali	62	13309	4221	32%
Density (kg/m^3)						
	[57]	Kaojue	364	709	87	12%
	[60]	Kaojue	50	674	98	15%
	[59]	Tali	62	565	100	18%
	[60]	Tali	102	670	80	12%
	[57]	Moso	213	794	108	14%
	[60]	Hitam	100	620	100	16%
	[60]	Andong	108	600	90	15%

Table 2.2. Physical and mechanical properties comparison for different species

An alternative is the visual and mechanical sorting of round bamboo poles based on observation of physical characteristics and non-destructive measurements [34]. Visual sorting looks at defects on the bamboo's surface, such as splits, and discards the bamboo that does not comply with the proposed criteria. However, some defects can develop during the working life

of the pole, which questions the implementation of these measures. As for the non-destructive measurements, the diameter, taper, ovality and out-of-straightness criteria suggest that only bamboo poles within a specified range that approaches the shape of a regular tube can be assigned with a specific grade. However, as shown in Section *2.3*, the inherent geometric variability considerably limits the implementation of a sorting method based on narrow geometric criteria because the material stock would reduce from an entire population of poles produced in a plantation site to just a portion of the most regular shaped poles (the exact proportion remains unknown until an extensive investigation on a specific plantation takes place). This approach would support the use of bamboo poles into the building industry but will be contradictory of a sustainable material as high amount of waste from the out-of-range poles can be generated. Another non-destructive measurement to be used as a sorting index is the dry density. Although the variability of dry density for different species has shown low values compared to the mechanical properties (a characteristic also observed in timber), researchers have found significant differences in average values when studying the same species, for example in Tali bamboo (Table *2.2*). Moreover, different studies [58–60] have made evident that density has low correlation coefficients with mechanical properties. Combining multiple non-destructive measurements, such as diameter and density, to sort bamboo poles according to their mechanical properties has been proposed and implemented in a couple of bamboo species [58–60], however, this approach has to be expanded to include a wider range of visual and non-destructive mechanical sorting characteristics, which means a large amount of destructive full-size testing has to be performed [34]. Visual and mechanical sorting are still being developed as a long-term project as it intends to gradually create a classification of bamboos depending on the unique variable and measurable characteristics of bamboos harvested in a specific region, however, the urgent need for alternative sustainable materials puts critical questions on how to acquire sufficient data in the near future and calibrate the sorting procedures to cover this need.

A more compatible alternative can be based on the assumption that the answer to controlling variability is not found by narrowing the criteria to select bamboo poles, where sorting criteria discard potentially useful elements, but rather by intensively measuring and managing the physical and mechanical properties of individual poles, without any initial sorting criteria, therefore increasing material utilisation and assigning properties to a bamboo pole according to its individual capacity. Lorenzo et al. [82] proposed a methodology to extract and test clear bamboo samples (small samples free of imperfections) from individual bamboos without damaging their integrity. In a similar analogy to that proposed to measure geometric properties, clear samples are obtained from every bamboo pole harvested in a plantation area, as a quality control process applied by the producer. This process automatically reduces the variability as the properties measured from a bamboo pole are not being related to an entire species or bamboos grown in a specific region but are only used to assess the capacity of that same pole. A drawback from this approach is the low quantity of samples on which the physical and mechanical properties of a single-pole can be based on. Lorenzo et al. suggest that intensive measurement can support the immediate implementation of bamboo poles as a construction material, supported by efficient management of digital data containing physical and mechanical properties, while at the same time, it builds up a robust database of physical and mechanical properties which will support the long-term objective to understand, sort and characterise bamboo material according to its inherent variability [34]. Sampling and testing can be performed following an official Chinese standard for the determination of physical and mechanical properties of bamboo used in the construction industry that employs clear bamboo samples and small-scale testing machines [65]. This is an advantage that can allow non-destructive mechanical testing by extracting small samples from the ends of a pole. At the same time, physical and mechanical property data, such as moisture content, dry density, volume fraction, compression, tension and shear strength, among others, can be combined in a comprehensive database with the general characteristics of the pole, such as age, region, harvesting

date or treatment, and even include the relevant geometric information. The main challenge, however, lies in the development of a practical fabrication procedure of the clear bamboo samples to enable fast and efficient production. Digitally assisted fabrication techniques are being discussed later in this chapter as a potential solution to intensively produce the necessary samples to test bamboo while adjusting those fabrication methods to the organic shape of each bamboo pole to ensure material efficiency and keep the required sample sizes within tolerances.

2.5 Variability effect on design values

The scope of this work does not cover the development of a method to determine characteristic or design values for a bamboo pole, however, this section intends to provide a wider view on the effects of high variability on the physical and mechanical properties and the importance to quantify and manage it accordingly. It is well known that the average nominal values extracted from material testing are not directly used in a structural design procedure. Instead, a design value is derived from the assessment of characteristic values which is then divided by a partial or safety factor [94]. The point of interest in this section is to understand how a characteristic value is obtained and how the variability of the property measured directly affects the design value. To obtain a characteristic value, the following should be taken into account: i) the scatter of test data; ii) statistical uncertainty associated with the number of tests; and iii) prior statistical knowledge (if available). These three aspects are summarized in the following equation [94]:

$$X_{k(n)} = m_X\{1 - k_n V_X\} \quad (2.1)$$

where $X_{k(n)}$ is the characteristic value, n is the number of samples, m_X is the mean of measured results, k_n is the fractile factor of the five per cent characteristic value and V_X is the coefficient of variation. Therefore, the variation of physical and mechanical properties is directly proportional to the characteristic value, and thus to the ultimate design value. Although there might be different methods to estimate characteristic values [69,95,96], they are all affected by the dispersion of the measured property. That is the reason why measures to manage the inherent geometric, physical and mechanical

variability are needed to increase the reliability of structures made of bamboo poles. Assigning a characteristic value (associated with a prescribed probability of not being violated) of a specific property to an entire bamboo species following Eq. *2.1*, means that the specific property of any bamboo pole belonging to that species is equal or higher than the characteristic value. If the property has high variability, like the ones found in bamboo (Table *2.2*), it would mean that the characteristic value drops significantly in comparison with the mean value of the property. As a result, the assigned characteristic value can be over-conservative because a significant portion of bamboo poles from that species would have higher values. An example can be illustrated by examining a study [57] where characteristic values were determined for the compression and bending strength of Kaojue and Moso bamboo with moisture content in the range of five to twenty per cent. In average, the characteristic value was 65% of the mean (Table *2.3*). This is a clear effect of high variability magnitudes. In the supposed case that the CoV measured was in the order of ten per cent, the characteristic value compared to the mean would have been about 85%. Individual and non-destructive measuring, as proposed by Lorenzo et al. [82], can therefore help to measure the wide range of variability found in a specific stock of poles, and therefore, manage the variability to estimate more representative structural design values.

	Sample	$\mathbf{m_x}$	**Std Dev**	$\mathbf{V_x}$	$\mathbf{X_{k(n)}}$	$\mathbf{X_{k(n)}/m_x}$
Kaojue						
Compression strength (N/mm^2)	136	69	12	17%	48	70%
Bending strength (N/mm^2)	53	82	17	21%	54	66%
Moso						
Compression strength (N/mm^2)	41	75	18	24%	46	61%
Bending strength (N/mm^2)	32	88	19	22%	56	64%

Table 2.3. Determination of characteristic value and its corresponding reduction compared to the mean. Data were taken from [57]

Safety factors for structural materials were introduced by the end of the 19th century to define allowable strength values for cast iron. Factors were based on experimental testing but mostly on experience and good engineering practice to ensure structural safety. Over the years, the safety factors were reduced from a value of five to values lower than two due to the advances in

material production and quality control but also pushed down by political and economic reasons, such as World War II [97]. The safety factor for bamboo poles ranges between 1.5 and 2, depending on different criteria, obtained through previous experience and experimental observations [57,72,96,98]. The international standard ISO 22156 [69] suggests that the ultimate design value for bamboo poles is about 1/7 of the measured mean, for a standard deviation of approximately 15% of the mean. In summary, the inherent geometric, physical and mechanical variability is directly related to the design values and therefore to the overall structural efficiency of any building made out of bamboo poles. Uncertainties can only be managed by quantifying the variation of the properties of a structural element and use that information to improve the overall design procedure. The present work aims to implement individual quantification methods that help acquire relevant data from bamboo poles and therefore support the development of alternative design workflows.

2.6 Reverse engineering methodologies for digital geometric acquisition

Engineering is the science responsible for designing, constructing, manufacturing and maintaining products, systems or structures. There are currently two ways of doing engineering, one is the conventional or forward engineering which starts defining concepts on a high level to then systematically bring it down to the physical application of the system [99]. The second way of doing engineering is when a specific project, system or structure is the starting point and a process of measuring, analysing and testing is applied to reconstruct a mirror image of that project, system or structure or else to retrieve the past events that led to that product, system or structure, this process is called Reverse Engineering (RE) [100]. Today, RE is widely applied in the industry of aerospace, automotive, electronics, medical devices, sports equipment, clothes accessories, among others, this is, it can be applied to every single man-made product. Also, different methodologies of RE have been applied for forensic and criminology sciences, as well as to determine the causes of physical, biological and chemical phenomena. The objective of reverse engineering is to recover the blueprints or details of any

unknown physical object or event and use those details to perform a physical or theoretical analysis of that object. Furthermore, during the digital era, RE has also started to be used to unveil source codes of software or computational systems so that they could be not just replicated but improved.

There are currently hundreds of applications of RE, from mechanical pieces to the reconstruction of human bones, but the main interest of this section will focus on applications for the building industry and its potential implementation for bamboo poles. One of the disciplines that apply RE processes is the automotive industry where, for example, the geometry of the full body of a car can be digitally acquired, processed and then brought back to reality to build a scaled replica of the car [101]. RE is also used to design medical devices such as bone implants, to characterize pharmaceutical drugs of unknown formulas, to list genes and proteins that affect cellular behaviour and to disassemble or decompile codes of software [99]. For the building industry, it has become an important method to assess the structural integrity or functioning of a building from which no information is available. The acquisition of the geometric information is always the first step in the process, commonly performed with digital devices such as three-dimensional scanners. Then the information is analysed and matched with the as-built knowledge of materials and construction methodologies employed on that building to produce a digital reconstruction of the building, which includes semantic information attached to the geometry such as the name of the component, material, age, among others [102]. The reconstruction of a digital three-dimensional model is the main outcome of RE in the building industry, especially when working with heritage buildings because the geometric model can be used to produce, for example, numerical models to determine the capacity or response of a building under seismic conditions, and therefore retrofit the existing building accordingly [103]. Furthermore, RE methodologies can also be employed to determine the cause of failure or malfunctioning of specific structural elements.

A three-dimensional (3D) model is a virtual representation of an object's geometry. The model can be manually built in a Computer-Aided Design (CAD)

software if the geometry of the object is known. For uniform, manufactured objects, the determination of their geometry is a straightforward process. Columns and beams in civil engineering or shafts and bearings in mechanical engineering are a good example of uniform objects. The virtual reconstruction of non-uniform, natural objects, however, is considerably more intricate and complex because of their irregular geometry. For centuries, manual measurements have been the only way to acquire the geometry of objects, nevertheless, their accuracy has been questionable when applied on complex objects. Non-intrusive methods have been developed to acquire the geometry of complex objects [104], but only in the last two decades, with the emergence of digital technology, new imaging methods have been developed to acquire and build digital models of practically any physical object. The main methodologies involve the use of photographs [105,106], video-recording [107], laser sensors [108,109] and LED light projections [110,111].

Photogrammetry is a methodology normally used to acquire 3D geometry for objects that can be represented by line-based structures, especially if the object has a distinct texture. However, methodologies that are increasing in popularity, mainly because of their practicality and affordability, are based on laser and structured-light 3D scanners, which are more useful when irregular objects like sculptures, reliefs or archaeological sites are involved [112]. Nevertheless, it has been proved [113,114] that a combination of both methods (photogrammetry and 3D scanner) can also be applied into large (e.g. buildings) and small (e.g. coins) objects to acquire both, high accuracy representations of a non-uniform object and their real colour. Currently, there exist a wide range of 3D structured-light scanners that can be applied for RE processes to acquire geometry and colour of large and small objects as a 3D point cloud. A point cloud is a set of points, normally acquired by 3D scanners, that describe the outer surface of the scanned object [115]. Point clouds are recorded as text files containing the 3D coordinates of the acquired points based on an arbitrary origin. Additionally, to the coordinate information, point clouds can also store red, green and blue colour information, but this can vary from one equipment to another. The point cloud represents

very basic information, especially for 3D visualisation, therefore a process commonly known as surface reconstruction is needed to convert the points into a triangulated polygon-mesh [116]. A polygon-mesh file of a bamboo pole would be the 3D digital representation of the physical bamboo pole, acquired with RE methodologies. This digital model can help to detect major defects in the bamboo, as well as facilitate the exploration of aesthetics and architectural effects due to the high accuracy and texture quality [82]. It is important to mention, however, that this type of files might possess unnecessary information for other purposes, and therefore, a bamboo polygon-mesh file can be simplified to extract the principal geometric characteristics relevant for design and engineering applications, such as structural analysis or building information modelling (BIM).

Processing and simplification of digitally acquired geometries have been addressed by studies that focused on the potential of converting point cloud or mesh models into files that can be applied into different applications such as BIM [117], through the implementation of point-cloud segmentation [118], or for structural engineering applications, through voxel-based [119] or boundary-representation models [120]. Different simplification methodologies have been already applied in specific case-studies, such as retrofitting heritage buildings [121] or as-built structural analyses of complex space structures [122] by adapting NURBS curves to the original meshed geometry. Non-Uniform Rational B-Splines (NURBS) [123] curves and surfaces have been developed for many years to address the challenge of modelling complex objects [124]. This technique has been successfully applied to model natural and artificial objects using point clouds or 3D polygon-mesh models as input data, converting into a lightweight, high-accuracy 3D model. NURBS can easily represent free-form shapes and offer a common mathematical form already widely used in the industry. The object can be organized in cross-sectional data (along an arbitrary axis) and NURBS curves are fitted to each cross-section approximating the object's surface [125]. Another similar approach applied by some researchers [126,127] was a RE reconstruction process using boundary representation surfaces [128] which can be defined

by combining a collection of NURBS curves. Key NURBS curves can be extracted from the polygon-mesh model of a bamboo pole to convert them into a more practical surface model [82], in this way, the elements extracted can form the basis of a finite element discretisation that takes into account the geometric variation along the bamboo pole. These geometric variations were described by Janssen [48] and can form the basis to define a methodology required to accurately extract the geometric properties of individual bamboo poles.

The digitisation of bamboo poles for construction purposes was first proposed and developed within the BIM Bamboo project at UCL as a proof of concept [82,129]. As such, the aim was to acquire the outer surface of a bamboo pole, together with its texture, using a structured light 3D scanner to create a digital model of the physical bamboo which could be further used for the design, construction and maintenance of bamboo structures. Different approaches for the scanning method were developed as trials which included the manipulation of scanning equipment with a robotic arm (Figure *2.7*) and a bespoke scanning frame (Figure *2.8*).

Figure 2.7. Scanning of a bamboo pole driven by a robotic arm, taken from [82]

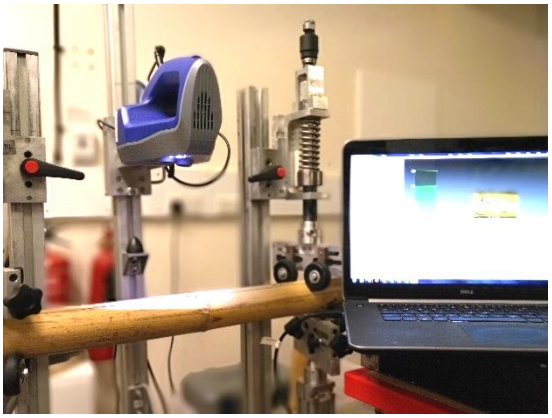

Figure 2.8. Scanning frame holding the 3D scanner while bamboo is fed through

At this preliminary stage of the digitisation workflow, the entire outer surface of a bamboo pole, together with its texture, could be acquired to produce the digital model of a physical pole, as shown in Figure *2.9*. The wall thickness of the bamboo pole was not acquired during the scanning process nor the method was optimised to intensively quantify the geometry of multiple bamboo poles for their subsequent utilisation in a construction project. These first trials, however, are essential to further develop a more efficient reverse engineering method to efficiently quantify the geometric properties of bamboo poles.

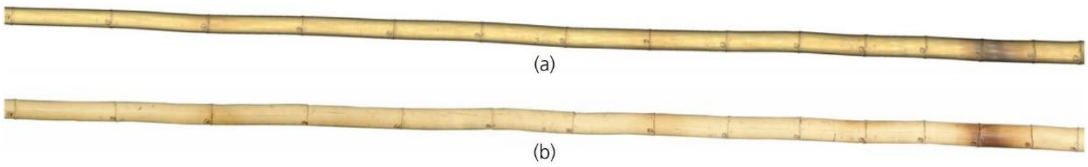

Figure 2.9. Images of a physical (a) and digitally scanned (b) bamboo pole, taken from [82]

2.7 Digitally assisted fabrication

It is well known that fabrication processes went through a considerable change during the industrial revolution, where machines started to replace manual labour resulting in lower production cost and higher volumes of product, in what is called today mass-production. Nevertheless, to produce an object, even with machines, it is necessary to design and produce physical drawings and instructions with the relevant details that allow the fabrication of the object. Digital fabrication refers to the direct fabrication of an object from a 2D/3D digital model, this is, without the use of printed drawings and/or

instructions for fabrication. The technological and digital revolutions made its appearance in the development of digital fabrication with the introduction of two major computational advances: Computer-Aided Design (CAD) and Computer-Aided Manufacturing (CAM) software.

As described in Section *2.6*, CAD software allows the creation of 3D geometric digital models. Subsequently, CAD became the basis of more complex computational tools such as finite element, dynamic and kinematic analysis, as well as simulation of geometric characteristics such as texture [130]. CAM systems also use CAD as a starting point; however, the main objective of CAM is to generate the digital code required to drive machines for the production of a specific object [131]. Such technology was mainly developed for the mass-production of objects within industrial processes, however, other disciplines such as biomedical and dentistry have found digitally assisted fabrication as a suitable alternative procedure [132,133]. Cultural heritage is another discipline where digital technologies applied for fabrication purposes are helping the preservation of different artworks. An example is a case study where the geometry of two Roman statues was acquired and then the corresponding moulds to cast the replicas of each statue were manufactured using a 7-axis robotic arm adapted with a milling machine [134].

Robotic arms have recently become more popular for fabrication purposes than, for example, computer numerical control (CNC) machines due to the flexibility (large range of motion), lower cost (compared to complex assembly/fabrication machines), minimal installation disruption (the same robotic arm is installed regardless the activity to perform) and the large working volume (especially when extra axes are added) [135]. Researchers have taken into consideration that compared to a conventional CNC machine, the static stiffness of an industrial robot is relatively lower which causes deflections of the cutting tool and subsequently higher inaccuracies, therefore, robotic milling is commonly suggested for tasks with reduced cutting forces or on relatively soft materials (e.g. plastics, foam, wood) [136]. The advantages of milling with a robotic arm have been reflected in different disciplines during

the last two decades for the development of highly efficient fabrication procedures. For example, in the biomechanical industry, robotic milling has been used to produce custom-made bone implants where a perfect fit between joining parts is essential [137]. Just in the last few years, robotic milling has made its appearance in the construction and assembly of timber structures, where it is expected to evolve onto an entirely new way of construction [138,139]. The operation of cutting-edge tools involves a higher level of complexity and requires a semi-industrial set-up for the proper performance of fabrication tasks (e.g. a laboratory or a workshop). However, the fabrication task can potentially be automated to the point that only minimum supervision is needed while maximising material utilisation, fabrication efficiency and quality [139].

Individual fabrication of small samples extracted from bamboo poles, as proposed by Lorenzo et al. [82], can receive great benefits from a digitally assisted fabrication process. If a 3D model representing the geometry of a bamboo pole is created through digital 3D scanning, then that same model can be used to create the necessary CAM instructions, adapted for the unique organic shape of each pole, for a robotic arm equipped with a milling machine to fabricate the clear bamboo samples to the highest accuracy and in the most efficient way [82]. A similar scan-to-fabrication approach has been already developed [140], where a stock of trunks and branches of different trees were individually 3D scanned to not only design a wood barn chip with them but also to generate the necessary digital toolpaths for a robotic arm to machine bespoke interlocking connections for each element.

The importance of acquiring digital geometric information of bamboo poles as structural elements is not only useful to machine small testing samples but also to help in the fabrication or assembly of components within a bamboo structure. At the beginning of the 21st century, researchers, architects and engineers started to recognise that digital fabrication can bring an opportunity to reintegrate the AEC disciplines by the joint development of fabrication processes such as 2D, subtractive, additive and forming fabrication as well as new structural assembly procedures driven by CAD and CAM

systems [141]. Since then, new methodologies and the exploration of alternative and more adaptable materials that enhance the benefits of new fabrication technologies took place among the different disciplines of the AEC industry. Nevertheless, timber has remained the preferred material for researchers to experiment with and create fabrication procedures supported by CNC machines or robots, which assist during the production and assembly processes [142,143]. For example, a method was proposed to assemble thin, free-form shell structures made of timber [144]. The construction of scaled-down models of Tepavcevic et al.'s project was highly dependent on digital information, first to generate 2D CAM fabrication commands for a CNC cutting machine, which created flat triangular timber panels, and second, to create an automatic tagging system for the individual identification of panels to assemble the shell structure according to the CAD model. These developments in digital fabrication have shifted the industrial mass-production into a mass-customisation of unique structural components/connections enabled through the direct link between CAD and CAM production [130].

Further development within CAD software has been its combination with parametric design tools that support the digital design and mass-customisation production of non-standardised structural components. Parametric design refers to the use of relations and constraints to define geometric shapes, which once defined, they can be modified if the parameters assigned in the relationship are changed [145]. For example, a line can be created if the origin, direction and length (parameters) are defined, however, these parameters can change at any stage of the design and therefore the geometry of the line changes. A constraint is defined when, for example, a line has to be parallel to another or tangent to a specific curve, in this case, the line will change according to the parameters of the line (e.g. length or direction), as long as the constraint is satisfied. The design task is now focusing on the creation of design relationships, rather than geometric design, that when applied to CAD/CAM software allows the user to find optimal design and fabrication solutions by varying the initial parameters of a specific geometry. Researchers have already started to use parametric design to

tackle bamboo material variability and jointing challenges by encoding the properties and develop freeform shape optimisation relationships [146]. The constraints of the parametric design process for Wang et al.'s study were a multi-angle connection and a multi-length constraint that limited the type of bamboo (based on its variational properties) that could be used in the structure. This project highlights the essence of parametric design and its applicability for non-standard or non-conventional materials such as bamboo poles. Finally, another example of parametric design in combination with digital fabrication was developed to design tailored joints for bamboo structures, followed by their fabrication using additive fabrication methodologies [147]. As yet, the applicability of digital fabrication into bamboo structures, and any other material, is seen as a promising alternative, nonetheless, the AEC industry requires a higher level of robustness through the overall design and fabrication process, thus it is highly important to give continuity to these projects and increase the development and adaptation of digital fabrication for non-conventional materials.

2.8 Design and construction approach using bamboo poles

The basic objective of structural design is to provide the details of a structure, such as dimensions, arrangement, types of elements and connections, that are capable to carry certain loads without collapsing or incurring into unaccepted deflections [148]. The current structural design paradigm can be described as a top-down approach, where the process starts with a conceptual planning phase, followed by a preliminary and general structural design which is gradually refined until a detailed design of specific sections or components of the structure is performed [149]. For example, Mora et al. [150] illustrates a top-down structural design procedure, where a main independent structural volume is first defined in a process denominated as massing (Figure *2.7*). The structural volumes can be subsequently refined into subsystems (foundation, horizontal, vertical and lateral), from which general assemblies are proposed as a supporting structure. Finally, structural elements and connections are assigned, the detailed structural analysis and

design of these elements take place, and mathematical or physical proof is produced to show that the structure will be capable of maintaining its integrity during its expected life. This current approach has been devised having industrialised construction materials in mind so that the design procedure can be more easily standardised, always depending on the complexity of the structure.

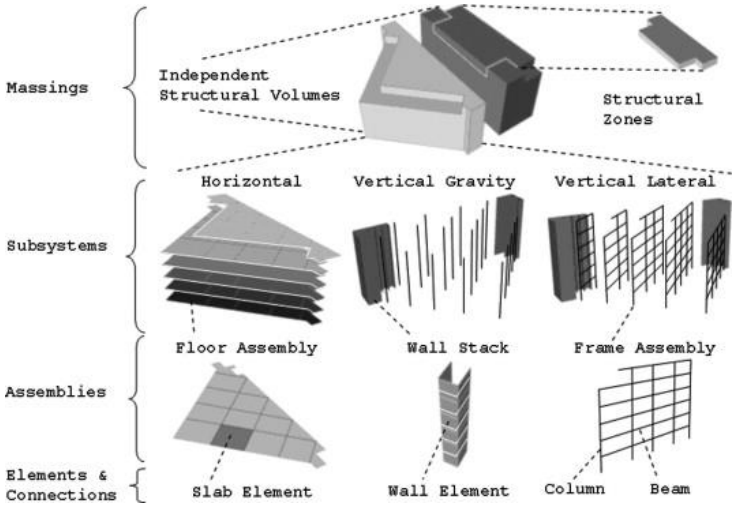

Figure 2.10. The top-down structural design process, extracted from [150]

To implement bamboo elements into a top-down design approach, the material has to be sorted into different structural classifications depending on their individual use, such as column, rafter, beam or bracing, so that adequate designation of different assembly categories can be performed according to the general properties of the material. The main problem, as outlined in Sections *2.2-2.4*, is that the material has inherent geometric, physical and mechanical variability, which are yet not fully addressed by the current visual grading or characterisation methods and therefore that kind of classification has not been achieved. The general solution to this problem has been to adopt existing typical structures and replace the conventional structural elements (steel or wood) with pieces of bamboo poles, using bamboo's available data to perform structural design [72,151]. This becomes more critical when complex structural systems such as active bending are adopted as a structural system for bamboo poles [152]. Active bending is a technique that creates curved geometries by mechanically bending straight uniform elements within

their elastic limit [153], however, evidence in this work of a structural design approach considering the organic nature of bamboo poles was not observed.

Instead of adopting typical structural systems that were designed having different materials in mind, the approach should look at the individual geometric, mechanical and physical characteristics of bamboo poles and use that information to create structural systems according to the characteristics of each element. This process is known as bottom-up design, where the specific details of every single element that can potentially form part of a structure are first defined, together with its compatibility or matching capabilities with other elements (connections). The individual elements are then linked together or put in the right place to form sub-systems that subsequently fill in the structural volume [154]. This process follows the analogy of a bunch of interlocking bricks, from which only the dimensions and linking capabilities are known (Figure *2.8a*). The bricks can then be linked together to build the desired shape of the structure that would cover the visual, environmental or functional needs; however, the individual characteristics of every brick can change the arrangement of sub-systems and multiple structural volume solutions can be achieved (Figure *2.8b*). Architects have been already working with bottom-up design approaches, where the design follows an organic path that results in optimal shapes, however, these methods are commonly known as an evolutionary or generative design [155,156]. Researchers have started to develop alternative design approaches using bottom-up paradigms supported by the implementation of new digital technologies to build bamboo structures [146,157], however, the digitisation of bamboo poles and its corresponding database can offer the necessary support for bamboo designers as the acquired information would improve the overall quality and reliability of the structure [82].

Figure 2.11. Interlocking bricks (a) extracted from [158], from which multiple structural volume solutions can be achieved following a bottom-up design approach (b), extracted from [159]

A bottom-up design approach for bamboo poles would mean that a secondary issue is generated: an appropriate procedure between the different design and fabrication platforms is needed to manage the data that describes the properties for each bamboo element. Management of datasets is not new within the AEC industry since the collection and analysis of data have been already applied to different purposes such as identifying causes of construction delays; structural damage detection; stiffness reduction on structures; structural health monitoring; among others. The main challenge is the identification of the relevant data that allows performing design, construction and maintenance of a bamboo structure according to the bamboo poles involved in the process. Manging the acquired information in a digital environment would therefore be the main advantage of an intensive measuring procedure. Furthermore, it is expected that collection and management of data related to structural elements together with parametric design can support: resource and waste optimisation; development of the generative design; BIM implementation; and augmented reality [160]. In the particular case of bamboo structures, the efficient management of data can support an innovative and robust structural design, following a bottom-up approach, which can subsequently be used to complement a digitally assisted construction procedure and the further management of the structure.

The process on which a structural system is assembled has to receive as much attention as the structural design. The construction procedure is important because the integrity of the structure can be compromised during its assembly process due to the loads (gravitational or accidental) and the assembly of future components in the system [161]. An excellent example of digitally assisted construction procedure is the Arch_Tec_Lab building for the Institute of Technology in Architecture at ETH Zurich which has a 2300 square-metre roof with more than fifty thousand unique timber elements that were assembled using robotic-aided processes [138]. The designers highlighted that the construction procedure had constant digital guidance as the unique pieces were manufactured right before putting them in place and therefore a simultaneous design and construction procedure relying on large digital data was needed.

The great majority of bamboo structures have been built following a combination of traditional methods (mainly for connections) and assembly procedures derived from typical structural systems, focusing on self-construction for local communities. These bamboo structures are considered so simple that no structural stability or geometry checks are appointed during the different steps of the assembly process [68,162]. For example, trusses or frames are normally assembled on the floor and subsequently fixed into their final position within the structure (Figure *2.9a*). Then, braces and beams are used to stiffen the frames or connect trusses, perpendicular to their plane, forming the main structural skeleton. Finally, secondary or non-structural elements are positioned in the structure (Figure *2.9b*). For more complex bamboo structures, such as domes, pavilions, membrane roof or hyperbolic paraboloid systems, where the capabilities of the material can be explored, the construction procedure requires advanced instructions to be deployed, however, the details of the construction sequence are commonly not presented [14]. The ZCB bamboo pavilion, built in Hong Kong, is one of the few projects that focused on the procedure for the design and management of digitised construction data from which a bespoke assembly process for the structure was produced [163]. The drawback from Crolla's project was that the

bamboo poles were simply idealised as straight cylindrical tubes with average properties, which is a practical assumption for a preliminary design (top-down) but not enough for detailing procedures where the individual properties of each element are needed.

(a) (b)

Figure 2.12. Bamboo pole structural frame being assembled on the floor (a), followed by the subsequent structural skeleton of a house (b)

One alternative to implementing the digitisation of bamboo poles in combination with a bottom-up design approach is modular systems. Modular construction is a technique where a variety of structural (or non-structural) components or modules are separately fabricated, normally off-site, to then be assembled in a specific and efficient way [164]. One of the main advantages of modular structures (for concrete and steel) has been the reduction of construction time of about 30% to 50% [165]. However, more emphasis is now placed to improve the manufacturing of components, increase the structural reliability, reduce on-site labour and also to reduce material waste [164]. Some researchers have tried to combine the advantages of modular construction with the sustainable benefits of bamboo poles. The developed modular systems for bamboo poles have been composed of small easily built modules that facilitate the addition of more similar modules in a fabrication process that gradually can build up, for example, a house. Among the different projects of bamboo modular construction, the truss system presented by [151,166,167] agree with the basic modular system requirements: i) short bamboo elements that facilitate construction; ii) single jointing system repeated throughout the structure; iii) possible off-site fabrication; and iv) production can be subjected to quality checks [164].

Another similar proposal allows free-form structures by defining a basic, small, self-contained subsystem in the shape of a three-dimensional cubic wireframe (Figure *2.10*), similar to the interlocking bricks system, that once completed, the structural system acts as a unit [168]. With an appropriate design approach that digitally manages the data of individual bamboo elements, modular construction can help to ensure the overall quality of the structure in terms of geometry, structural reliability and behaviour of connections, including the maintenance or replacement of a module/element that has reached its serviceability limit [169]

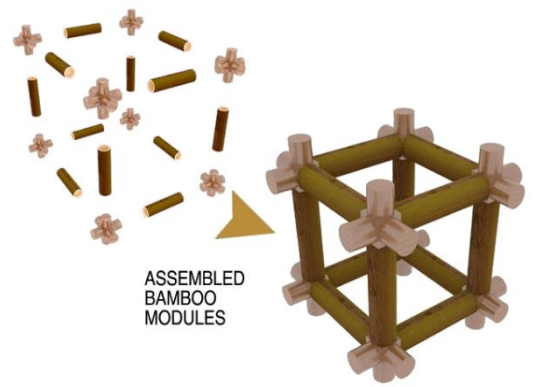

Figure 2.13. Image showing example of a 3D modular system, extracted from [168]

2.9 Summary

This chapter has discussed the several environmental advantages that bamboo poles have over industrialised conventional construction materials such as concrete, steel, aluminium or even wood. The most important environmental advantages are that bamboo is a fast-growing grass which can be harvested in 3 to 5 years and its production can create a positive environmental impact. Bamboo has been used for centuries as a construction material but mainly in local communities of developing countries, providing shelter to approximately 15% of the global population. During the last decades, bamboo's popularity has grown significantly due to the constant environmental damage that the production and utilisation of conventional construction materials have caused. However, there are still technical challenges, such as material variability, durability and fire resistance, that hamper bamboo's implementation into the construction industry, therefore, its utilisation, when compared to conventional materials, is practically negligible.

The focus of this chapter was to outline one of the main technical challenges for bamboo poles: the inherent geometric, physical and mechanical variability. Although durability and fire resistance are also important challenges, this research will first focus on developing a digital workflow for the design, construction and management of bamboo structures driven by the individual data of bamboo poles. This workflow will then be the backbone to allow new exploratory design approaches on which durability and fire resistance of a bamboo structure can be properly managed. The variability of material properties is present in every construction material, however, industrial production, quality control, extensive testing and systematic sorting are techniques that help to manage the variability. These techniques have been developed and implemented on conventional construction materials, but unfortunately bamboo is not one of those. As a result, it has been found that there is a considerable lack of information regarding the properties of about one-hundred bamboo species which are suitable for construction purposes and therefore their properties and range of variability is unknown. Variability has also been a challenge for standardisation and grading methods which suggest that bamboo is not compatible with approaches that were developed for other materials and therefore an alternative approach is needed.

An alternative conceptual approach to individually quantify the geometric, physical and mechanical properties of bamboo and therefore tackle the variability issue was introduced. This concept relies entirely on the intensive measuring and managing of the relevant properties for construction purposes of a stock of bamboo poles so that they can be implemented as a construction material. To develop an individual quantification procedure, reverse engineering techniques for the geometric acquisition of poles and fabrication of testing samples were introduced, showing examples of how new digital technologies can support an intensive measuring method. These techniques are explored, developed and implemented for quantifying the properties of bamboo poles and produce a digital database that provides the fundamental basis of structural reliability during the design and construction stages.

3 Geometric digitisation of bamboo poles

3.1 Overview

This chapter focuses on the development of a digitisation workflow to address the inherent geometric variability found in bamboo poles. Section *2.3* described the different geometric properties commonly measured from a bamboo pole, highlighting the challenges to accurately measure them. This practical challenge of measuring the irregular shape, in combination with the high magnitudes of geometric variation (Section *2.4*), produces a significant impact for the design and construction of bamboo structures, therefore, a concept to intensively acquire the geometry of every individual pole belonging to a specific stock of poles has been proposed to effectively quantify and manage the geometric variability [82]. The accurate geometric acquisition of irregular objects through reverse engineering procedures together with its subsequent conversion into three-dimensional (3D) models have helped multiple engineering disciplines to adopt workflows where analysis and design of products are performed in a digital environment. 3D scanning is a powerful tool to effectively and accurately acquire the geometry of practically any object (Section *2.6*), including bamboo poles, however, the acquisition methodology itself and the further digital processing of the geometric information acquired, relevant for structural purposes, has not been yet defined. This Chapter is divided into two main sections focusing in the following research objectives: i) develop a digitisation workflow based on 3D scanning technology that successfully and efficiently acquires, processes, quantifies and stores in a digital environment, the geometric properties of individual bamboo poles; and ii) analyse the geometric variability, as a practical research implementation of the digitised geometric data.

The section focusing on the digitisation workflow presents the details of a reverse engineering method to individually measure the geometry of bamboo poles before their utilisation in the design and construction of bamboo structures. The novelty of the workflow lies on the development of an efficient

non-contact reverse engineering method to intensively acquire the three-dimensional geometry of bamboo poles regardless their species, colour, texture or age, and translate this information into practical 3D models. Furthermore, numerical data is extracted from each digitised 3D model to build a robust digital database containing relevant geometric information for structural applications. The developed digitisation workflow is tested on three different bamboo species and the resulting data is validated through a direct comparison of dimensions measured from the physical and digital poles. The practical implementation of the digitised data consisted of a study to analyse the geometric variation in bamboo poles based on the numerical geometric data acquired from 235 bamboo poles from three different species. The study analyses the variability of different geometric properties but also searches for potential correlation between them.

3.2 Geometric digitisation workflow

Previous bamboo scanning trials within the BIM Bamboo project were essential to set the key aspects on which the present work focused to further develop a bespoke scanning procedure and are herein defined as: i) a scanning method applicable to any bamboo with potential for structural use, regardless its species, shape, colour or age; ii) the acquisition of the entire outer surface, including the wall thickness at each end of the pole and a portion of its inner surface; iii) the optimisation of the scanning time; iv) a simple set-up with potential to be implemented on-site but also at an industrial level; and v) an efficient acquisition of point cloud data to optimise file size and subsequent post-processing.

3.2.1 Scanning subject and scanner parameters

Structured-light 3D scanners have recently been growing in popularity because of their high-accuracy on the surface acquisition, efficiency (no need for tracking references) and affordability in comparison with other geometric acquisition equipment such as photogrammetry, light detection and ranging (LiDAR) systems or laser trackers. Structured-light scanners are subdivided by its source of light projection, laser or LED light, which have a very similar performance, however, their application depends on the characteristics of the

scanning subject and the desired data to acquire [170]. For this work, the scanning subject is a bamboo pole, which can be described as a cylindrical slender element with a relatively small depth-to-span ratio. The internodal surface is smooth and relatively reflective with only minimal distinctive texture or clear geometric features which is detrimental for 3D scanning processes. On the contrary, the area around the bamboo nodes exhibits characteristic growth scars in the form of circumferential ridges and other imperfections (e.g. branch stubs) that provide the required texture and geometric features that facilitate the 3D scanning process. The range of diameter for structural bamboo can vary from 50 to 200 mm [8], and although the length could reach more than 30 m, the height of culms is normally divided into manageable sizes for transportation purposes (e.g. 4 m). The wall thickness of the pole should also be acquired during the scanning workflow and its dimension normally ranges from 4 to 30 mm.

Based on the scanning subject's qualitative and quantitative description, two hand-held scanners, Space Spider and Eva, from Artec 3D [171], were the scanning equipment in consideration due to their balance between sub-millimetric accuracy, portability, texture acquisition and cost, to further develop the scanning method focusing on the aforementioned key aspects. Both devices are based on structured light sensor technology and their technical specifications are summarised in Table *3.1*. Majority of the characteristics of these two scanners are similar except for the accuracy, scanning range and the frame rate. A frame is a collection of points and texture data captured within the scanning range, which is comparable with the frames taken by a video-camera. The equipment to operate both scanners consisted of a laptop Dell XPS 15 equipped with an Intel i7-6700HQ CPU @ 2.66 GHz, 16 GB of installed memory and a dedicated video card Nvidia GTX GeForce 960m with 4 GB of memory. The interface to control the scanners was their proprietary software Artec Studio 12 [171].

Technical Specifications	Space Spider	Eva
Scanner type	Handheld	Handheld
3D point accuracy, up to (mm)	0.05	0.1
3D resolution, up to (mm)	0.1	0.5
3D accuracy over distance, up to (% over one meter)	0.03	0.03
Scanning range (m)	0.2 - 0.3	0.4 - 1.0
Linear field of view, (H×W @ closest range in mm)	90 × 70	214 × 148
Linear field of view, (H×W @ furthest range in mm)	180 × 140	536 × 371
Angular field of view, (H×W)	30° × 21°	30° × 21°
Ability to capture texture	Yes	Yes
Texture resolution (MP)	1.3	1.3
Colours (bpp)	24	24
Frame rate for real-time fusion, up to (fps)	7.5 fps	16 fps
Exposure time (s)	0.0002	0.0002
Data acquisition speed, up to (million points/s)	1	2
3D light source	Blue LED	White LED
2D light source	White LED	White LED

Table 3.1. Comparison of Artec Eva and Space Spider scanner specifications

The scanning acquisition process of hand-held devices is based on surface smart-tracking, which means that the scanner uses the data points of a frame previously taken to keep track of the object and its relative movement against the scanner while acquiring a new frame. This allows the scanner to be moved around and/or along the object's surface, similar to a spray-painting motion, while the object itself can also be translated or rotated. The Space Spider and Eva scanners operated through their proprietary software Artec Studio 12, can scan an object's geometry in a single or multiple scanning sessions. A scanning session is a collection of frames acquired and grouped during a single recording session, similar to a clip recorded with a video camera, which can be paused and resumed multiple times. Multiple sessions are recommended when the entire scanning of an object cannot be performed due to occlusions or limitations of movement. Furthermore, multiple sessions are also automatically created by the software when the smart-tracking is lost for a short period while scanning. The drawback of multiple sessions is that an additional aligning procedure between the sessions is required. Therefore, a single scanning session was prioritised to acquire the entire geometry of a bamboo pole and optimise the geometric acquisition procedure.

The optimisation of the scanning method also depends on the frame rate at which the scanner is acquiring the geometry of a bamboo pole and the speed of motion of the scanner and/or the bamboo. The motion is defined by the scanning path which is the relative movement of the scanner against the bamboo, or vice versa. The scanning path was defined through a series of trials using both scanners and five pieces of air-dried Moso bamboo (Phyllostachys pubescens), with a range of length between 2 and 4 m, diameters of 65 to 85 mm and thickness of 6 to 10 mm. By combining different motion patterns with the trial poles, it was found that the best scanning path to acquire the geometry was by a simultaneous rotation and translation of the bamboo around and along its length while keeping the scanner in a static position. This motion ensured that the full surface was scanned without leaving gaps on the surface or losing the smart-track through a helicoidal pattern that provided longitudinal and circumferential overlapping of individual frames as shown in Figure *3.1*.

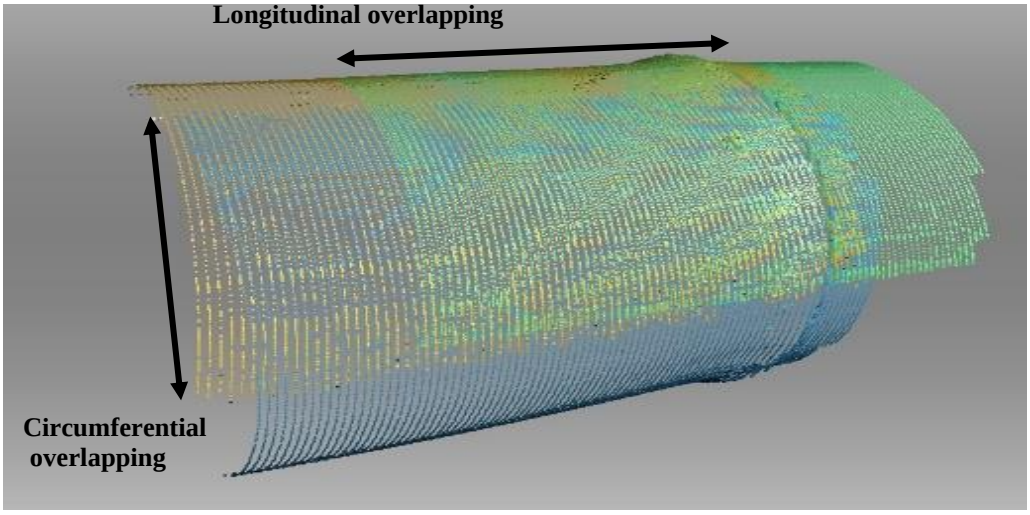

Figure 3.1. Circumferential and longitudinal overlapping of frames after the first (yellow) and last (green) frames taken following a helicoidal scanning pattern

During the trials, the distance between the scanner and the bamboo pole was kept at mid-range, which was 250 mm for the Space Spider and 700 mm for the Eva. At mid-range, the field of view for Space Spider and Eva were 135 x 105 mm and 365 x 260 mm (height and width), respectively. The trials also showed that the speed at which the bamboo was rotated should be kept to a

maximum of three seconds per revolution regardless the size of the pole, otherwise loss of track will occur. Artec 3D does not specify the percentage of overlapping needed between current and previous frames to ensure a smooth scanning session that prevents loss of track or surface gaps. This is because the equipment has been designed to scan any kind of surface within the entire scanning range, therefore, overlapping of frames would depend on individual cases. Although some authors consider that 15 to 30% of overlapping is sufficient to keep track and avoid surface gaps [172], it was found through an assessment of successful scanning trials, this is, scanning the full geometry of a bamboo without losing track, that the minimum overlapping needed between adjacent frames was 75%, both circumferential and longitudinal (Figure *3.1*).

The relatively high overlapping percentage is partly related to the reduction of the effective scanned height of each acquired frame due to the circular shape of the pole (Figure *3.2*). Therefore, the height, *h*, of the captured frame was conservatively assumed to be half the pole's diameter, *D*, as shown in Figures *3.2* and *3.3*, along with the sequence of frames captured during a full revolution and the corresponding translation of the pole. Figure *3.3* also shows that the critical circumferential overlap *(βh)* is the one that occurs between sequential frames while the critical longitudinal overlap *(μw)* takes place between the first (frame 1) and last frame (frame n) within one full revolution.

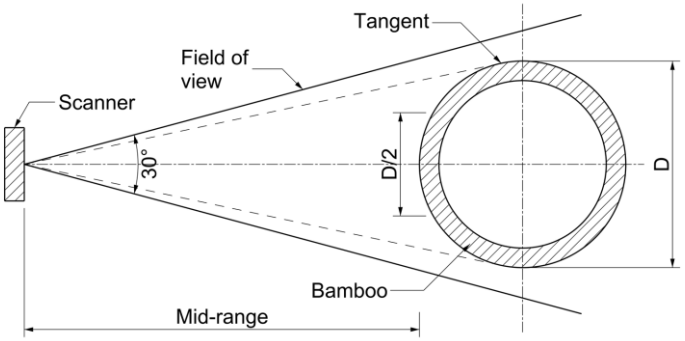

Figure 3.2. Scanner's field of view

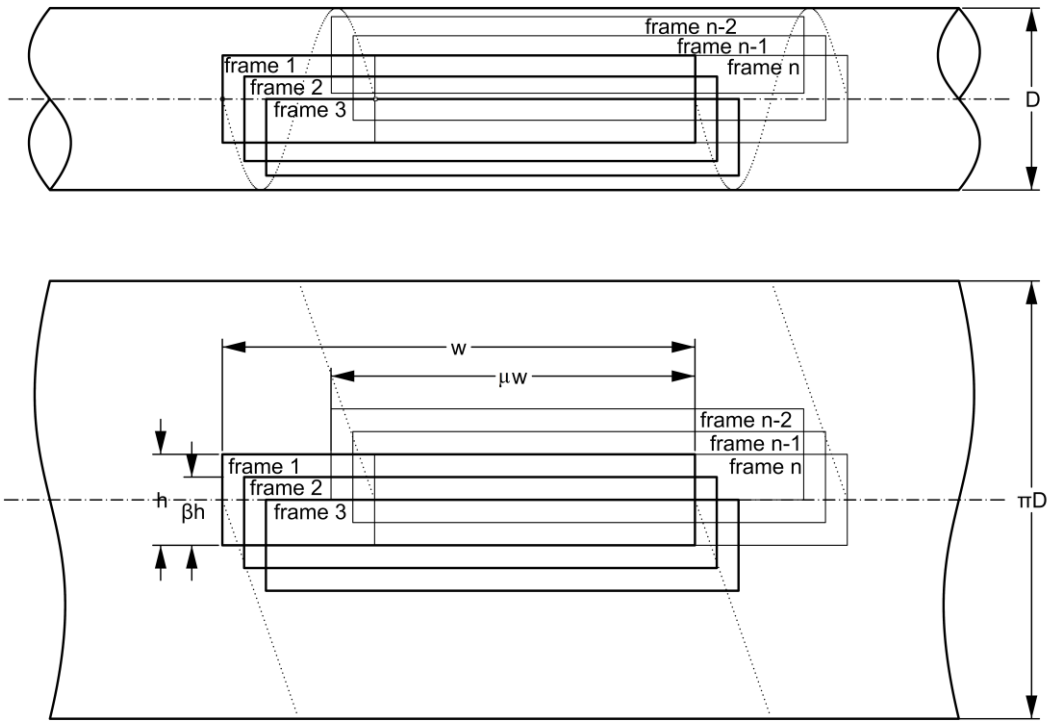

Figure 3.3. A sequence of scanned frames per revolution on the idealised cylindrical pole and developed surface

Based on these considerations, the following scanning parameters can be drawn. The total number of captured frames per revolution is:

$$n_f = \frac{\pi D}{(1-\beta)h} = \frac{2\pi}{(1-0.75)} = 8\pi\ frames/rev \quad (3.1)$$

Considering a period, *T*, of three seconds per revolution, the angular velocity of the pole is:

$$\omega_v = \frac{2\pi}{T} = \frac{2}{3}\pi\ rad/s \quad (3.2)$$

leading to a scanner frame rate of:

$$f = \frac{n_f \omega_v}{2\pi} = \frac{8\pi}{3} \cong 8fps \quad (3.3)$$

Finally, the pole's translation speed (mm/s) is defined by:

$$v = \frac{(1-\mu)w}{2\pi/\omega_v} \quad (3.4)$$

and the scanning time per unit of length is therefore defined by:

$$t_l = \frac{L}{v} \quad (3.5)$$

where *L*, is a unit of length (mm). The number of scanned frames per unit of length is:

$$N_l = ft \quad (3.6)$$

Table *3.2* shows the theoretical scanning parameters for each of the scanners that ensure the entire acquisition of the pole without losing track or surface gaps. These scanning parameters are independent of the pole's diameter, length, species, colour or age and can deviate approximately ±10% from their theoretical values without affecting the digitisation of a pole. The Space Spider has higher accuracy than Eva but when put in the context of the building industry's working tolerances [173], both scanners were accurate enough. For example, the working tolerances for timber structures ranges between ±5 to ±10 mm and the cross-section of an element is measured to a tolerance of one millimetre. The accuracy of both scanners is sub-millimetric, therefore both scanners were acceptable. The fixed period *(T)* of three seconds per revolution, which ensures the necessary longitudinal and circumferential overlapping, meant that the frame rate was the same for both scanners, therefore this characteristic did not differentiate between them. However, the wider field of view and larger scanning range played an important role to reduce the scanning time per metre for the Eva scanner (Table *3.2*). Besides, the larger scanning range was more compatible with the unpredictable geometric variability of bamboo poles which can allow the successful scanning of a pole when the shape of the pole significantly differs from a straight hollow tube. Consequently, the number of frames acquired by the Eva scanner was much lower than Space Spider, reducing the point cloud file size and any subsequent post-processing related to it. As a result, the Artec Eva scanner was selected as the best option for an intensive geometric acquisition procedure.

Parameter	Space Spider	Eva
Captured frames per revolution	8π	8π
Angular velocity (rad/s)	2π/3	2π/3
Frame rate (fps)	8	8
Width (mm)	105	260
Translation speed (mm/s)	8	20
Scanning time (s/m)	125	50
Number of frames (f/m)	1000	400

Table 3.2. Estimation of scanning parameters based on Artec Eva and Space Spider 3D scanner

3.2.2 Scanning workflow

During the proof-of-concept stage of the BIM Bamboo project [82], a bespoke scanning frame was proposed to perform the geometric acquisition as shown in Figure *2.8*. The scanning frame consisted of an aluminium frame that held the bamboo at a comfortable height for its simultaneous rotation and translation. The frame was equipped with a system of two adjustable springs with rollers attached to them to control the movement of the pole and counter react with a push-pull against the unbalanced weight of the bamboo as it is being scanned. The scanner was located in between the spring's system, ensuring that only the bamboo pole was within the scanner's field of view.

Multiple scanning trials of the five Moso bamboos were performed using the scanning frame to evaluate the potential of the setup and workflow to be implemented in an intensive geometric acquisition task. The main disadvantage observed during trials of the scanning frame was that the geometric acquisition only covered a portion of the pole, leaving about 250 mm from each end without scanning and preventing the scanner to acquire the wall thickness. This was because the bamboo had to be in contact with both spring systems which provided support to it. Besides, the scanner was fixed on its position between the springs and manual manipulation of the scanner to acquire the missing geometry was not considered an appropriate approach. During the operation of the scanning frame, the simultaneous movement was performed as smoothly as possible, in agreement with the estimated parameters (Table *3.2*). However, the pressure of each spring system on the bamboo's body made hard to produce the movement which was translated in a continuous loss of track, either by rotating at an unstable

speed rate or by shaking the whole scanning frame while producing the motion. In average, the smart-tracking was lost at least once every two scanning sessions. In addition, it was found that one in every ten successful scanning operations (entire outer surface acquired in a single session) the acquired frames were not overlapped in some parts of the surface, therefore, gaps were present.

The issues found on the scanning frame had a great negative impact on four of the five key aspects set to develop the scanning method, therefore the entire scanning workflow and setup previously developed were modified. By exploring different options, a much simpler scanning setup, considering the Artec Eva scanning parameters, was proposed. A schematic representation is shown in Figure *3.4*, where four equally distributed V-head pipe stands equipped with ball heads, support the bamboo while it's being simultaneously rotated and translated about its longitudinal axis. The scanner sits on a camera dolly, 700 mm away from the bamboo and approximately perpendicular to the pole's longitudinal direction. The scanner remains stationary as the pole is scanned in a helical pattern that ensures the longitudinal and circumferential overlap of individual frames. At the start and finish of the helical motion, when the ends of the pole are in the scanner's line of sight, the pole is held in position rotating it about its longitudinal axis for one full revolution after panning the scanner 45° around a semi-circular path to capture the inner surface at each end of the pole.

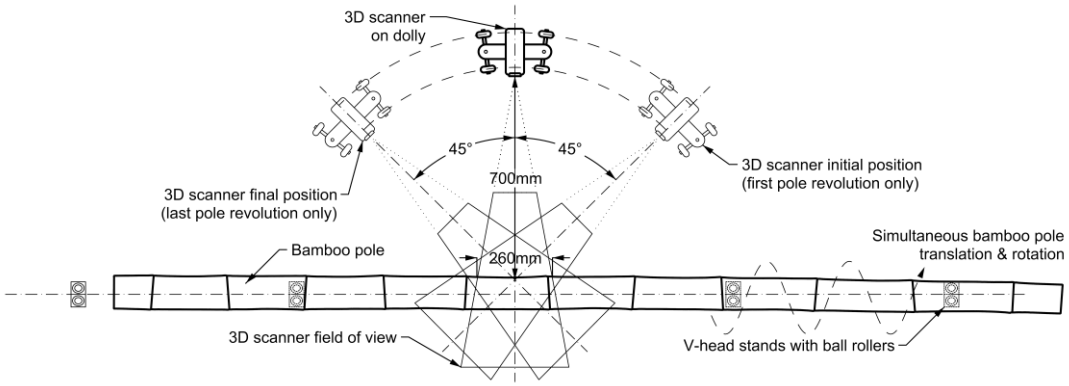

Figure 3.4. Schematic plan view representation of scanning set-up

The wall thickness and a portion of the inner surface of the pole can be directly acquired from the ends of the pole by ensuring that these end sections lie within the central portion of the internodal region to guarantee an unrestricted view without interference from the nodal diaphragms as shown in Figure *3.5*. A couple of M5 socket head button screws were used as permanent reference markers between the physical poles and its scanned digital model. Each screw head was coated with a white liquid chalk marker before their insertion into predrilled holes to facilitate their identification by the scanner (Figure *3.5*). The screws were located at the last internode of each end of the pole, approximately one diameter away from the last node, which was denominated as sacrificial internode. For identification purposes, a pair of screws were installed at the bottom of the pole and a single screw at the top.

Figure 3.5. End section of bamboo pole and scanning reference markers

Scanning trials were again performed to ensure that the smooth and continuous scan of the outer surface and wall thickness of each pole in one single session was achieved. The new scanning setup and procedure prevented from leaving surface gaps and losing track, and it also improved the efficiency to acquire the point cloud which benefits its subsequent post-processing [174].

3.2.3 Point cloud post-processing

A sample of the scanned raw data acquired during trials is shown in Figure *3.6* for a portion of a scanned bamboo pole. This raw data was subsequently processed with the proprietary algorithms contained in Artec Studio 12 to obtain a registered point cloud followed by a 3D polygon-mesh reconstruction. Point cloud post-processing was performed in a workstation Dell Precision T5810 with an Intel Xeon E5-1620v3 CPU @ 3.5 GHz, 32 GB of memory and a dedicated video card Nvidia Quadro K2200 with 4 GB of memory. Firstly, the point cloud is processed through the *Fine Registration* algorithm which aligns the captured frames based on both geometry and texture information. This is the default configuration for Artec Eva as this scanner can acquire both geometry and texture. Within this algorithm there is a secondary Loop Closure process to register frames not necessarily captured in series, compensating for cumulative errors and highly recommended for hand-held devices. Secondly, the *Global Registration* algorithm converts all acquired points contained in every frame to a single coordinate system by matching the position of surface pairs, also using geometry and texture information. Thirdly, an *Outlier Removal* algorithm removes all small surfaces (noise) not connected to the main surface of the scanned body. This process is based on a statistical algorithm that calculates the mean distances between each surface point and its neighbouring points. Distances greater than an interval of the standard-deviation multiplier (Artec defines this as 2 mm for noisy surfaces acquired with Artec Eva) define the outliers which are removed from the model. The *Outlier Removal* resolution should be the same as that in the subsequent *Fusion* algorithm that generates a polygon-mesh. The “fast” version of the *Fusion* algorithm is recommended by the manufacturer for Artec Eva scans. This algorithm triangulates the acquired point cloud within an average point to point distance or resolution. The scanning setup was designed so that only the bamboo pole is within the scanning range and therefore the acquired surfaces within the trials presented a relatively low surface noise. Therefore, the resolution for both outlier removal and fusion algorithms was defined as 0.5 mm according to the resolution of the Eva

scanner (see Table *3.1*). The polygon mesh is then processed with a *Mesh Simplification* algorithm which reduces the size of the polygon mesh optimising the model to a predetermined accuracy or maximum deviation from the original mesh. An accuracy of 1 mm was adopted for this study as a suitable compromise between accuracy and computing capacity requirements. Finally, the *Texturing* algorithm applies colour information to the polygon mesh for which a 512x512 resolution (the minimum option available) was adopted to ensure a polygon-mesh with texture but maintain a manageable file size. A summary of the post-processing algorithms and parameters adopted are listed in Table *3.3* and the final polygon-mesh model of a typical bamboo pole is shown in Figure *3.7*.

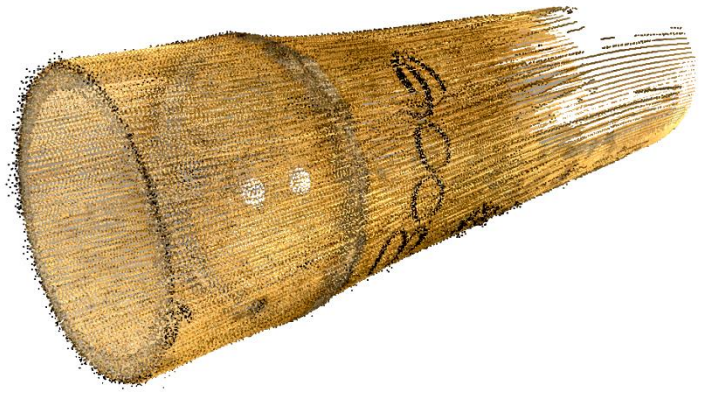

Figure 3.6. Scanned raw data of the end-section of a bamboo pole

Algorithm	Function	Parameters
Fine registration	Alignment of captured frames	Registration algorithm: Geometry and Texture Loop closure: On
Global registration	Optimisation of frame positions	Registration algorithm: Geometry and Texture
Outlier removal	Elimination of outliers and noise	Std Dev mul_threshold: 2 Resolution: 0.5 mm
Fusion (Fast)	Creation of polygonal 3D model	Resolution: 0.5 mm
Mesh simplification	Reduction of the number of polygons	Accuracy: 1mm
Texture	Projection of textures onto mesh	Texturing for: Export Enable texture normalization: On
Export	Export polygon mesh	Mesh format: obj Texture format: png

Table 3.3. Post-processing algorithms and parameters in Artec Studio 12

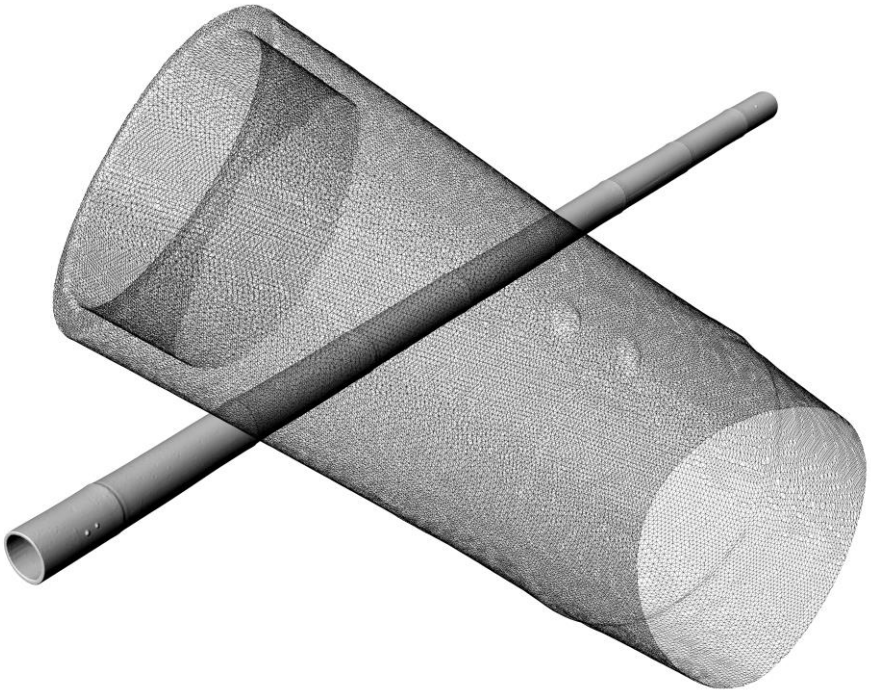

Figure 3.7. Rendered polygon-mesh model of a bamboo pole and a detail of its end section

The resulting polygon-mesh file size for a bamboo pole with a length of up to 4 m is around 50 MB (75 MB with texture) and its final digital representation is shown in Figure *3.8*. In comparison with the digital model obtained using the scanning frame (Figure 2.9), the wall thickness and a portion of the inner surface using the proposed setup were successfully acquired. The use of a bamboo polygon-mesh for any design application could be impractical due to its large file size and lack of explicit geometric information. This polygon-mesh was therefore adopted as the basis to develop a much lighter NURBS-surface model and a numerical database of geometric properties extracted from it.

Figure 3.8. Texturized polygon-mesh model of a scanned bamboo pole

3.2.4 Non-Uniform Rational B-Splines model and numerical database

A bespoke Rhino.Python [175] script was developed to create a NURBS-surface model, much smaller in file size and more flexible for computational manipulation than the polygon-mesh. This script uses the large function library in Rhino3D [176] to generate a NURBS-surface and discretise, extract and calculate all the relevant geometric properties of the poles.

The processing of the polygon-mesh starts with the identification of the position of all bamboo nodal diaphragms (nodes) and reference markers (i.e. M5 socket screws) through the analysis of the angle between the normal vector of the polygon-mesh faces in the model. Neighbouring polygon-mesh faces form a relatively flat bamboo surface within an internodal region and therefore the angle between their normal vectors is close to zero. On the contrary, there is a well-defined angle between the mesh faces around both the characteristic circumferential nodal ridges on the bamboo surface and the raised and well-defined reference markers. The angle between the normal vectors of these polygon-mesh faces ranges from approximately 10° to 20° for the adopted mesh density (Table *3.3*) and thus it is possible to isolate them from the rest of the mesh. Figure *3.9a* shows a render of a section of a typical polygon-mesh model together with the extracted vertices of the mesh faces defining the nodal regions and the reference markers. Rectangular planes fit through these mesh vertices define the nodal planes of the pole while the position of each reference marker is determined by the centroidal point of the corresponding mesh vertices as shown in Figure *3.9b*.

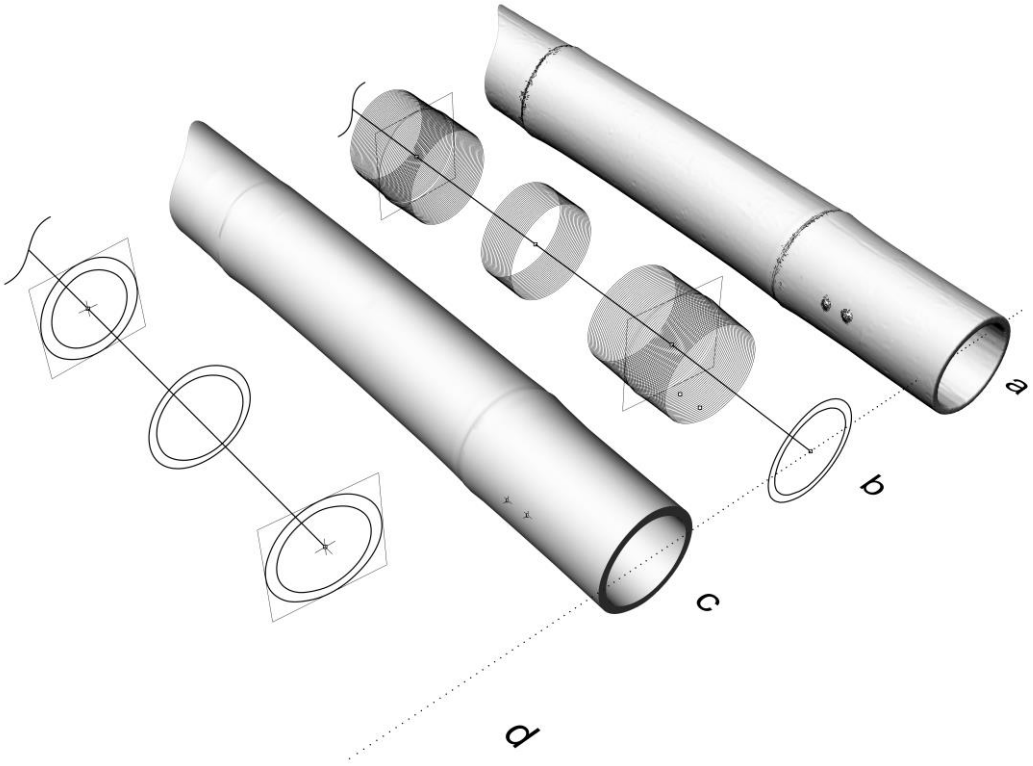

Figure 3.9. Development of a NURBS-model of a bamboo pole and its structural discretisation

Sections are also extracted from the mesh at both ends of the poles and include both the outer and inner bamboo mesh surfaces captured at the start and end of the scanning process. Figure *3.9b* shows the cross-sections extracted from the polygon mesh at the bottom end of the pole, together with the nodal cross-sections of the external bamboo surface obtained from the intersection between the rectangular nodal planes and the mesh. The centroids of these nodal sections and those of the external sections at the pole ends are used to define the centroidal axes of the external surface of the model shown in Figure *3.9b*. Further sections parallel to the nodal planes and perpendicular to this centroidal axes are extracted from the mesh at the nodes and internodes respectively. To capture all relevant pole features, these sections are spaced 2 mm apart and extend over a variable distance, which depends on the internode length, and are centred on the nodes and middle of the internodes as shown in Figure *3.9b*. These sections are highly irregular and therefore modelled as Non-uniform rational B-splines (NURBS) whose shapes are determined by a series of control points [123]. The number of

control points of each extracted NURBS section was explored through multiple processing trials and was limited to 20 as this significantly reduces the complexity of the model without affecting its accuracy. A surface is subsequently fit through all the external NURBS to create the bamboo exterior. Previous studies [49,71,72] have suggested a linear variation in the wall thickness of individual bamboo poles along their length. Based on these, It was assumed that the two inner cross-sections acquired at the ends of the pole were sufficient to produce a linearly interpolated surface, therefore, a second surface is fit through the two internal cross-sections at the ends of the pole following its centroidal axis, which defines the surface's edge, and tapers from one cross-section to the other as shown in Figure *3.9b*. These external and internal surfaces constitute the final NURBS-surface model of the bamboo pole shown in Figure *3.9c* including the bottom and top reference markers represented by the centroid of the M5 socket screws on the bamboo's surface.

The file size of the final NURBS-model for a bamboo pole of up to 4 m is approximately 1 MB (compared to a mesh file size of 50 MB) and the distance between its outer surface and the corresponding vertices of the original mesh is approximately 0.1 mm in average and 0.2 mm of standard deviation (Rhino3D analysis).

The final stage of the post-processing involves extracting all relevant geometric properties from this NURBS-model to build a suitable geometric database of each pole to support the subsequent modelling of a bamboo structure. The growth pattern of bamboo [7,177] produces a series of relatively straight and prismatic internodes with significant changes of direction occurring at the nodes where they join adjacent internodes. This anatomic feature was the basis to propose a structural discretisation of bamboo poles from the first to the last scanned node, in which the overall geometry of a pole is defined by the centroids of its nodal sections while the geometric properties of the cross-section at the centre of each internode are assigned to that entire internode (Figure *3.9d*). The data contained the numerical geometric properties of each pole in-between the first and last nodes. The cross-sections at the nodes of the pole are found intersecting the rectangular nodal planes in

Figure *3.9b* and both the internal and external NURBS surfaces (Figure *3.9c*). These cross-sections conservatively ignore the solid internal diaphragms that divide adjacent internodes and so the centroid corresponding to the cross-section of the hollow tube can define the true centroidal axis of the pole. The internodal sections (at the centre of the internode) are normal to this centroidal axis as shown in Figure *3.9d*. A typical internodal section and its corresponding equivalent circular tube are shown in Figure *3.10* together with the position of the arbitrary centroidal axes *Y & Z* as well as the section principal axes *1 & 2* and their orientation angle, θ_o. The properties of each internodal section considering both an equivalent circular tube and its actual asymmetric geometry are calculated as follows:

Cross-sectional area (mm^2),

$$A = A_o - A_i \tag{3.7}$$

equivalent outer diameter (mm),

$$D = \sqrt{\frac{4A_o}{\pi}} \tag{3.8}$$

equivalent thickness (mm),

$$t = \frac{D - \sqrt{D^2 - \frac{4A}{\pi}}}{2} \tag{3.9}$$

equivalent moment of inertia (mm^4),

$$I_b = \frac{\pi}{64}[D^4 - (D - 2t)^4] \tag{3.10}$$

equivalent polar moment of inertia (mm^4),

$$J = \frac{\pi}{64}[D^4 - (D - 2t)^4] \tag{3.11}$$

principal moments of inertia (mm^4),

$$I_{1,2} = \frac{1}{2}\left[\left(I_y + I_z\right) \pm \sqrt{\left(I_z - I_y\right)^2 + 4I_{yz}^2}\right] \tag{3.12}$$

and direction of principal moments of inertia (°),

$$\theta_o = \frac{1}{2} tan^{-1}\left(\frac{2I_{yz}}{I_z - I_y}\right) \tag{3.13}$$

where: A_o & A_i are the cross-sectional areas of the outer and inner pole surfaces respectively and I_y, I_z & I_{yz} are the moments of inertia and product moment of inertia of the actual internodal cross-section. These five properties are calculated directly from the NURBS-model using the relevant Rhino3D function library. The properties of an equivalent circular tube [66] can be very powerful aids during the preliminary stages of a project, but the formal design, analysis and fabrication of bamboo structures require the use of the actual geometric properties of the poles to ensure their reliability and quality. The processing time required to obtain the NURBS-model and all relevant geometric properties of a pole with a maximum length of 4 m was approximately three minutes. This processing time can be further improved if full automation within the script is developed, however, this activity was not within the scope of the work.

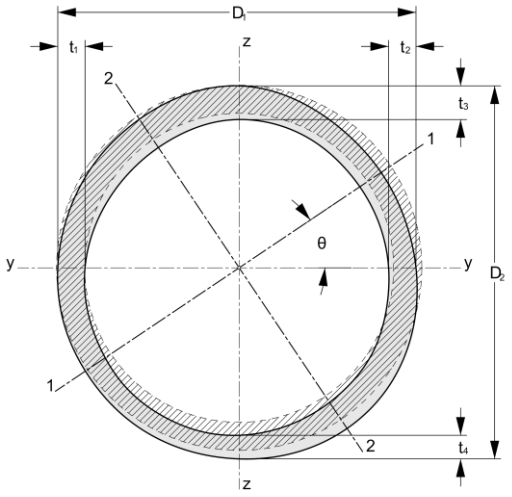

Figure 3.10. Cross-section of bamboo and equivalent circular tube idealisation

3.2.5 Digitisation of bamboo poles

The scanning trials were significantly helpful to define the fundamental relationships (Eq. *3.1 - 3.6*) of the scanning methodology and main parameters for the point cloud post-processing, as well as to develop the bespoke script to simplify the polygon-mesh into a NURBS-model. However, the entire digitisation workflow aims to intensively quantify the geometry of multiple bamboo poles and produce their corresponding digital model for their subsequent utilisation in design, construction and maintenance of bamboo

structures. Therefore, a digitisation programme for bamboo poles of three different species, Guadua angustifolia kunth (Guadua), Phyllostachys pubescens (Moso) and Bambusa oldhamii (Oldhamii), was proposed.

The developed scanning method was first implemented in regions where the bamboo is endemic because it offered the opportunity of first-hand material exploration and the chance to document the product history of bamboo poles as a ready-to-use material so that the scanning workflow could be implemented at the right stage of the bamboo pole production process. The product history of bamboo poles refers to the process to which the bamboo is subjected, from the harvesting up to the point when the bamboo pole is ready for its commercial distribution. The places where the scanning workflow was tested and from which the bamboo poles were obtained were Nanjing, China and Mexico City, Mexico (Figure *3.11*).

a) b)

Figure 3.11 Plantation site in China (a) and Mexico (b)

The selection of poles was similar in both Jiangsu and Veracruz which mainly depended on the empirical knowledge of the harvesting team and informal guidelines [68,178]. The technique consisted of felling the bamboo at breast-height to avoid complex arrangement of the nodes and initial deformations that appear in the area closest to the ground. Figure *3.12* shows the harvesting process in China and Figure *3.13* shows the typical deformation at the part of the plant closest to the ground. From breast-height until the height where branches start to appear, the stem is considered suitable for construction purposes. Nevertheless, this selection criteria represents a

relatively high volume of material waste and there is no scientific basis to reject the area below breast-height and the branched area on the top of the plant. Based on the aforementioned, a wider selection of the plant was requested in both plantation sites so that the bamboo was cut close to the ground to reduce the exclusion of certain sections (Figure *3.12*), unless the diameter was smaller than 50 mm. Figure *3.14* shows the bamboo supplied in China (Figure *3.14a*) and Mexico (Figure *3.14b*).

Figure 3.12. Bamboo harvesting process in China

Figure 3.13. Typical initial deformation that occurs under breast-height

a) b)

Figure 3.14. Bamboo poles supplied in China (a) and Mexico (b)

The bamboo species procured from Jiangsu was Moso, which is the main produced species in China whereas the Mexican one was Oldhamii, a native species of Mexico. Table *3.4* shows the general characteristics of the bamboos subjected to the scanning workflow for both locations. In China, the bamboo was transported from the warehouse in Jiangsu province to the NFU, in the city of Nanjing. In Mexico, the bamboo was transported from the state of Veracruz to the Architecture campus of the National University of Mexico (UNAM) in Mexico City.

Species	**Origin**	**Number of samples**	**Age** (years)	**Length** (m)
Phyllostachys pubescens (Moso)	Jiangsu, P.R. China	84	3 - 4	2.2 - 4.0
Bambusa oldhamii (Oldhamii)	Veracruz, Mexico	121	3 - 5	1.2 - 4.2
Guadua angustifolia kunth (Guadua)	Valle del Cauca, Colombia	30	2 - 5	2.2 - 3.2

Table 3.4. General properties of bamboos scanned during on-site testing

In both locations, the bamboo poles were first sorted by length and assigned with a specific coded label for identification purposes. Then, each end of the poles was cut at the first mid-internode to allow an unrestricted view of the wall thickness and finally, the corresponding reference marks were put at their respective location. The last step prior scanning was to label the poles and quickly clean the bamboo, brushing away any dust or scrap material attached to the surface that could cause noise during the geometric

acquisition (Figure *3.15a* in China and Figure *3.15b* in Mexico). The bamboo poles were systematically scanned following the developed scanning method (Section *3.2.2*), and after every scanning session, the acquired frames were checked to confirm that the full geometry, including the wall thickness and a portion of the inner surface at each end, was complete. The length of the poles ranged from approximately 1.2 m to 4.2 m with an average length of 2.8 m for both species. A total of 84 and 121 bamboos were scanned in China and Mexico, respectively. In both locations, the scanning process was performed with a rate of 10 to 15 bamboo poles per day.

a) b)

Figure 3.15. Sorted bamboo ready for the geometric digitisation process in China (a) and Mexico (b)

The third species could not be scanned on-site, but instead, Guadua bamboo poles were acquired and scanned at UCL, their general properties are described in Table *3.4*. The treatment of these poles consisted of submersion in boric acid and air-drying. The selection process for the material is unknown, however, the bamboo poles had the main characteristics for construction purposes described by Kaminski et al. [8] and the poles belonged to the bottom part of the plant. The bamboo poles were sorted, cut and labelled accordingly (Figure *3.16*), the scanning setup was prepared (Figure *3.17*) and the geometric acquisition took place (Figure *3.18*). All thirty bamboos were successfully scanned in two days.

Figure 3.16 Guadua bamboo ready to be scanned in UCL at Here East

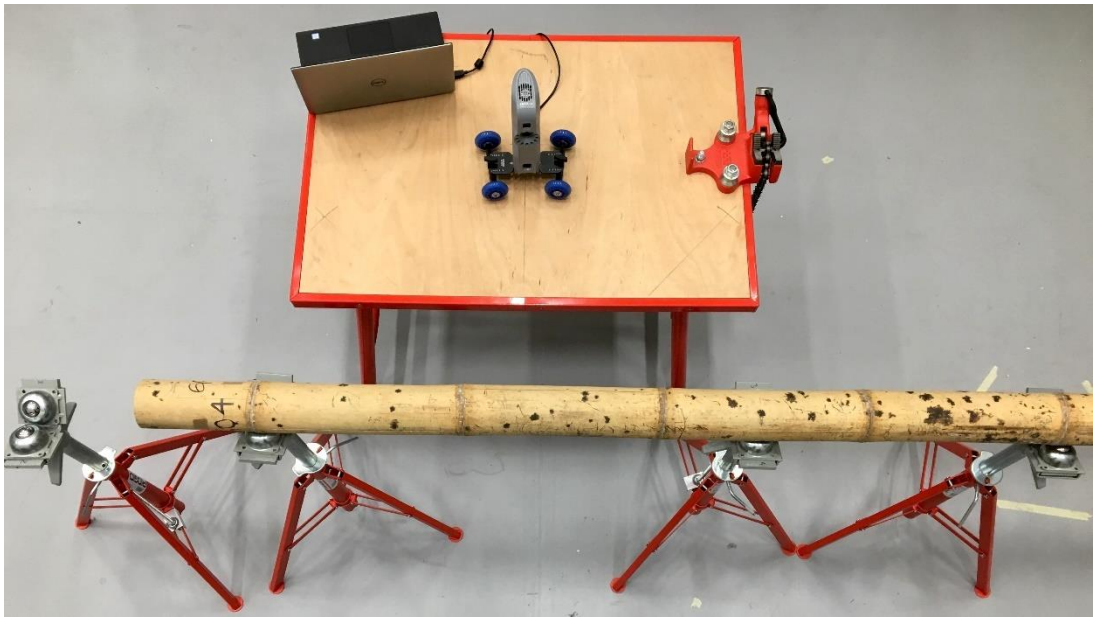

Figure 3.17. Scanning set-up prior implementation of scanning workflow (top view)

Figure 3.18. Scanning procedure on a Guadua bamboo pole

3.2.6 Results

A sample of one NURBS-model per species is shown in Figure *3.19*. The digitisation workflow was summarised in a standard operating procedure as an internal standard for digitising bamboo poles in projects within the UCL bamboo research group. The digital outcomes of the digitisation procedure as well as the numerical data are shown for a short bamboo pole in Appendix *A.1*.

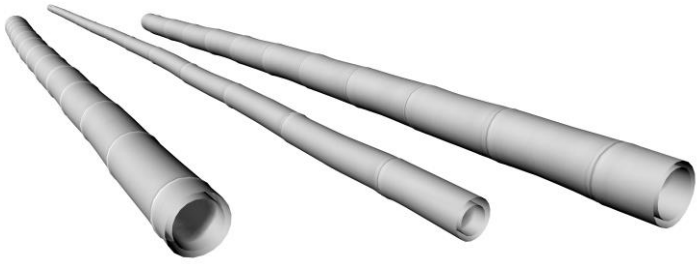

Figure 3.19. From left, NURBS-model of a Moso, Oldhamii and Guadua bamboos

Artec Studio 12 displays the elapsed time after scanning, processing and saving the geometric data. The time of approximately 10% of the digitised poles from the three different species was manually recorded after a scanning, processing or saving activity was performed. Figure *3.20* shows the relationship of the pole length against the recorded scanning time and total frames acquired. The estimated scanning time and the number of frames obtained from Table *3.2* is also plotted as a reference. The point cloud processing time was compared against the frame number, finding, as expected, that processing time increases with the frame number, however,

there was no clear correlation between them (Figure *3.21*). Saving the Artec Studio 12 project is also related to the number of frames acquired (Figure *3.21*), but similar to the case of the point cloud processing, no clear correlation was present. This data, however, was useful to estimate that a bamboo pole with a length of up to 4 m (~1600 frames) can be scanned and processed in approximately 15 min (including NURBS-model) following the digitisation workflow developed in this section. However, additional activities related to the preparation of the set-up and bamboo poles (cutting, marking, labelling and cleaning) add an average of 10 min per bamboo giving a conservative estimate of 15 bamboo poles digitised per day.

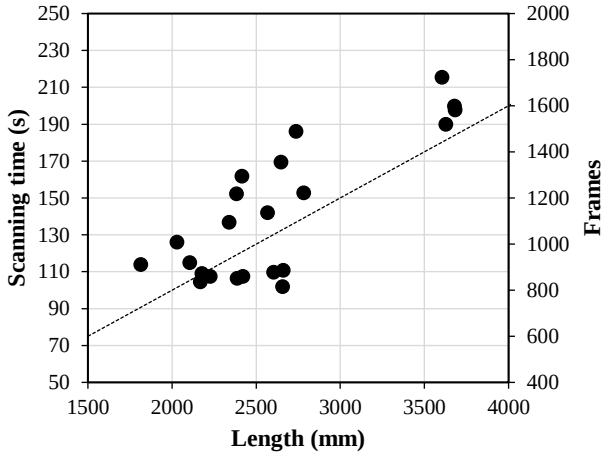

Figure 3.20. Relationship of scanned length (*L*) with the scanning time (t_l) and frame number (N_l). The dotted line represents the theoretical estimation of the scanner parameters

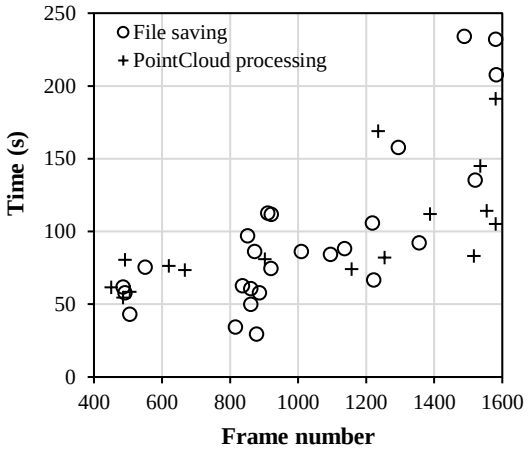

Figure 3.21. Relationship between frame number and file saving, as well as with point cloud processing time (proprietary algorithm by Artec Studio 12)

3.2.7 Validation

The developed digitisation workflow for bamboo poles was validated through the digitisation of 235 individual poles from three different species and with a combined length of approximately 500 m. The basic dimensions of approximately 15% of the scanned poles were hand-measured, following ISO 22157-1 [92], and included diameter, thickness and length. Measurements were taken from ends of the pole and at mid-length after cutting each pole. Two diameters, D_1 and D_2, and four thicknesses, t_1, t_2, t_3 and t_4, were measured on each cross-section with a Vernier calliper as shown in Figure *3.10*, to then estimate the average diameter and thickness of the section [92]. The diameter and thickness of the corresponding digital cross-section were calculated as shown in Eq. *3.9* and *3.10.* Finally, dimensions were compared using the reference markers (Figures *3.5* and *3.9c*) to locate each cross-section's precise position. The length of the poles was measured as the distance between these reference markers at both ends of the pole.

The average relative difference (accuracy) in the measurements of diameter and thickness between the physical poles of the three species and their digital models was approximately 0.65 mm (0.5%) and 0.44 mm (3.9%) respectively (Table *3.5*). An average correlation factor, R^2, of 0.92 was obtained from linear regression analyses of the average section thicknesses physically measured at the ends and middle of each pole. This high correlation factor confirms the suitability of linearly interpolating the captured cross-sections at the ends of the poles to model the internal surface of the bamboo wall. Also, the pole lengths extracted from the digital models were within 1/1000th of the measured length on the physical poles (Table *3.5*). The accuracy achieved in the scanning process is in line with the general requirements for reverse engineering in buildings [179]. Also, compared to a manual measurement process, a similar but more consistent level of accuracy can be achieved through the digitisation of bamboo poles and it is estimated that a complete digital model of a bamboo pole can be generated in the time that would take a skilled operator to collect the basic measurements of only a few discrete sections along the pole.

Geometric parameter	Samples compared	Accuracy (mm)		Accuracy (%)	
		Mean	Std Dev	Mean	Std Dev
Diameter	105	0.65	0.78	0.5	0.6
Thickness	105	0.44	0.42	3.9	3.0
Length	45	3.05	2.47	0.08	0.03

Table 3.5. Summary of accuracy measurement for diameter, thickness and length

3.3 Analysis of geometric variability

The objective of this section is to analyse the geometric variability of three different bamboo species whose data was acquired through the implementation of the digitisation workflow, developed in Section *3.2,* on 235 bamboo poles of three different species (Guadua, Moso and Oldhamii). The output of this workflow was a numerical database that describes the discrete geometry of individual bamboo poles and was therefore used to examine the variability of bamboo poles and identify any potential correlation pattern within each species.

In addition to the numerical database of geometric properties acquired in Section *3.2.4*, the centroid coordinates of the cross-sections at the nodes were used to calculate the following:

Length, from first to last node (mm),

$$L_n = \sqrt{\left[\left(x_f - x_i\right)^2 + \left(y_f - y_i\right)^2 + \left(z_f - z_i\right)^2\right]} \quad (3.14)$$

and internodal length (mm),

$$L_i = \sqrt{\left[\left(x_j - x_k\right)^2 + \left(y_j - y_k\right)^2 + \left(z_j - z_k\right)^2\right]} \quad (3.15)$$

where *x, y & z* are the coordinate components of the centroid, sub-indexes *i & f*, are the initial and final node and *j & k* are any two consecutive nodes. Also, the variation of the equivalent diameter and thickness along the length of the pole was computed as:

Equivalent diameter reduction rate (mm/m),

$$D_v = \frac{\Delta \mathrm{D}}{\Delta \mathrm{L}} \quad (3.16)$$

and equivalent thickness reduction rate (mm/m),

$$t_v = \frac{\Delta \mathrm{t}}{\Delta \mathrm{L}} \quad (3.17)$$

where ΔD & Δt are the difference in diameter and thickness between the bottom section of each pole and a section at a distance ΔL measured towards the top end of the pole.

A fundamental geometric property not covered in [66] is the out-of-straightness of the poles which can have significant implications on the structural behaviour [71] and buildability of bamboo structures [62]. The complexity of manually measuring out-of-straightness is evident from the methods developed by Ghavami & Moreira [71] and Richard [81] as bamboo poles are highly irregular without any clear reference features. This irregularity is illustrated in Figure *3.22* which shows the longitudinal cross-section of a digital model of a doubly curved 3.2 m long bamboo pole and its centroidal axis, against a reference horizontal line (dashed).

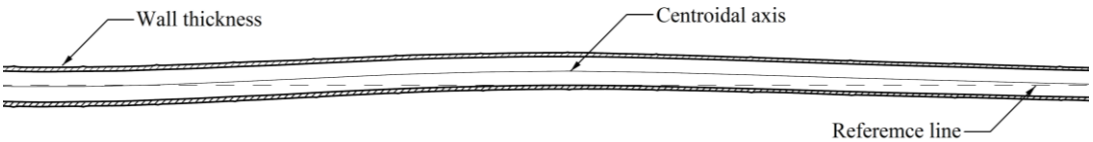

Figure 3.22. Longitudinal cross-section of a bamboo pole with double curvature

The out-of-straightness was digitally measured following the recommended methods in [34]. As such, the out-of-straightness was calculated as the maximum perpendicular distance between the centroidal axis of the digitised bamboo pole (Figure *3.9d*) and a straight line joining the centroid of the cross-sections at each end and it is here presented as a ratio (δ_r) of the total length (L) to the out-of-straightness (δ):

Out-of-straightness ratio (mm/mm),

$$\delta_r = \frac{L}{\delta} \qquad (3.18)$$

3.3.1 Basic geometric properties

In total, 250, 961 and 650 digital measurements of diameter, thickness and internodal length were extracted for Guadua, Moso and Oldhamii bamboo, respectively, while 30, 84 and 121 out-of-straightness were measured on each species. Figure *3.23* shows an example of a typical bamboo NURBS-model and its corresponding geometric properties extracted from it.

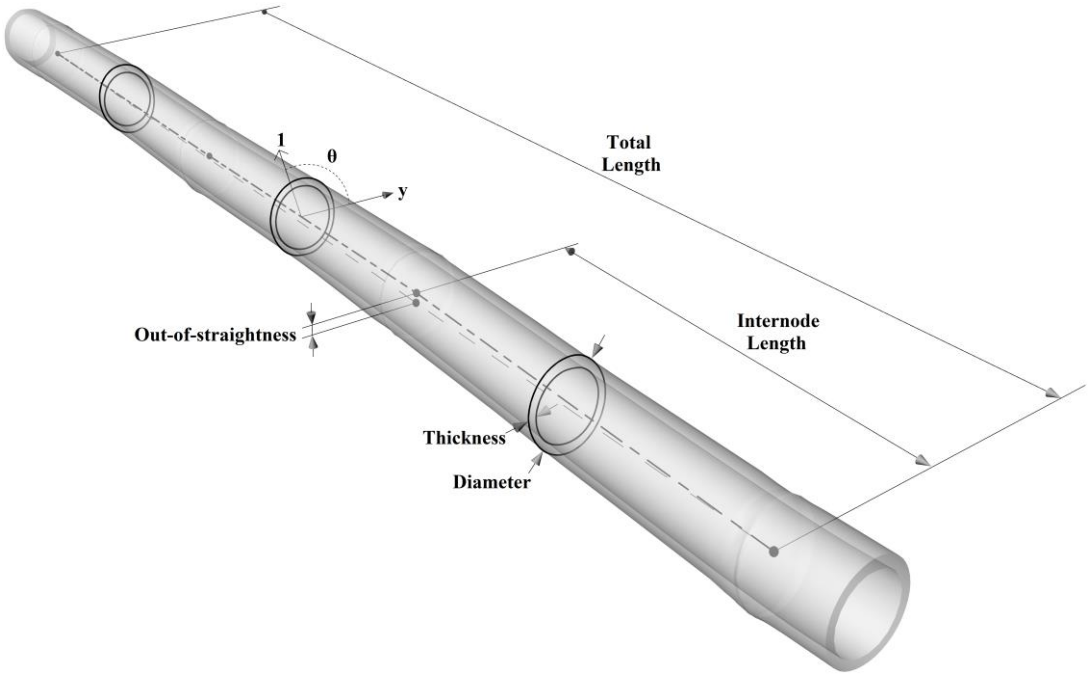

Figure 3.23. Typical NURBS-model of a digitised bamboo pole and the basic geometric properties extracted from it

The basic geometric data of diameter, thickness, internode length and the out-of-straightness ratio was first sorted and presented by species to evaluate the dispersion of the data. Statistical values (mean, standard deviation, coefficient of variation, minimum and maximum) of these basic properties were calculated and a summary of results is shown in Figure *3.24* and Table *3.6*.

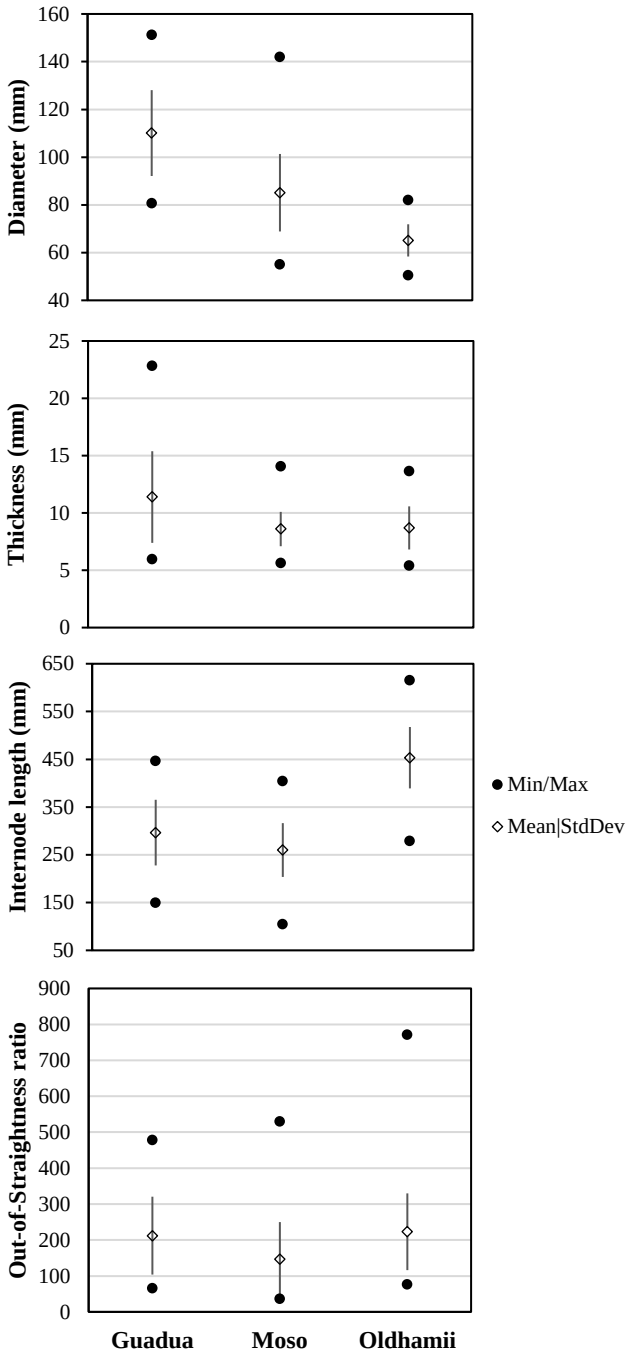

Figure 3.24. Mean, standard deviation and extreme values of basic geometric properties

	Min	Max	Mean	Std Dev	CoV
Diameter (mm)					
Guadua	81	151	110	18	0.16
Moso	55	142	85	16	0.19
Oldhamii	50	82	65	7	0.11
Thickness (mm)					
Guadua	5.9	22.8	11.4	4	0.35
Moso	5.6	14	8.6	1.5	0.17
Oldhamii	5.4	13.6	8.7	1.9	0.22
Internodal length (mm)					
Guadua	149	446	296	69	0.23
Moso	104	404	260	56	0.22
Oldhamii	279	615	453	64	0.14
Out-of- straightness (mm/mm)					
Guadua	66	478	212	108	0.51
Moso	37	529	147	103	0.70
Oldhamii	76	771	223	107	0.48
% Difference I_1/I					
Guadua	0	14	4	3	-
Moso	0	26	5	3	-
Oldhamii	0	17	5	3	-
% Difference I_2/I					
Guadua	0	16	5	3	-
Moso	0	29	5	3	-
Oldhamii	0	20	6	3	-
Inertia reduction (% per m)					
Guadua	6	28	15	5	-
Moso	10	32	20	4	-
Oldhamii	1	40	15	6	-
θ variation (°)					
Guadua	0	180	77	65	-
Moso	0	180	77	70	-
Oldhamii	0	180	78	61	-
Diameter variation (mm per m)					
Guadua	-3.9	7.7	3.0	2.1	0.70
Moso	-4.7	17.6	7.1	2.2	0.31
Oldhamii	-5.0	8.6	1.3	2.2	1.69
Thickness variation (mm per m)					
Guadua	0	6.2	1.0	1.3	1.30
Moso	0	1.2	0.4	0.3	0.75
Oldhamii	0	3.5	0.9	0.6	0.67

Table 3.6. Summary of geometric properties

The measured range of diameter for Guadua and Moso were relatively high compared to Oldhamii, which presented more consistent equivalent diameter values for the measured poles. Coefficient of variation for diameter and thickness were relatively similar for the three species and in line with previous studies [57,58]. Guadua presents the largest range in thickness but with an average value similar to those of Moso and Oldhamii. Oldhamii presented the largest average internodal length in comparison with Guadua

and Moso. The out-of-straightness ratio showed the most variable results among the studied species (CoV around 0.50) with Oldhamii being on average the straightest pole and Moso the species with the highest out-of-straightness.

Out-of-straightness is a relatively complex property to measure as the deviation of the centroidal line occurs in a 3D space and can present a double curvature (Figure *3.22*). Bamboo NURBS-models are particularly useful to enable the accurate and systematic measurement of the out-of-straightness for each pole which is a fundamental property, for example, to determine their load carrying capacity [62,71,180]. The out-of-straightness ratio *(δ_r)* is an index commonly used to define the compression capacity for column elements and has been proposed as a grading parameter for bamboo columns [71,181]. Table *3.7* shows a summary of the limits that have been proposed for different bamboo species and timber. As expected, the limits for bamboo allow a larger deformation than for timber but the values for bamboo vary substantially from one species to another, highlighting the impact of geometric variability and the importance to quantify it. Comparing the results in Table *3.6* with the limit ratios in Table *3.7*, it was found that 80% of the Guadua and 40% of Moso bamboo would be rejected for construction purposes (no limit has been proposed for Oldhamii). This result suggests that out-of-straightness should be assessed on an individual basis according to the final use of the bamboo pole within a structure by simply quantifying the magnitude of out-of-straightness and the impact that it would cause in the structure. This becomes more evident by considering that bamboo poles are organic structural elements that, similar to other construction materials, are cut to any length according to the building requirements. Therefore, the out-of-straightness of the final, cut-to-size, structural pole is a more relevant structural parameter than that of harvested poles which are cut to arbitrary lengths. Figure *3.25* shows an example where a shorter length within a harvested pole *(L_b)* produces a more critical out-of-straightness ratio than the original harvested length *(L_a)*. Associating an out-of-straightness *(δ_r)* value to a harvested pole is therefore not appropriate for any grading or selection process, as suggested

by ISO-19624 [34], so that each structural element should be assessed depending on its final length.

Limit ratio (δ_r)	Specie	Source
150	Dendrocalamus giganteus	[71]
200 or 0.15D	Bambusa pervariabilis (Kaojue)	[181]
100 or 0.15D	Phyllostachys pubescens (Moso)	[181]
300	Guadua angustifolia kunth (Guadua)	[96]
50	-	[180]
150	-	[34]
300	Sawn timber	[25]

Table 3.7. Out-of-straightness limit ratio (δ_r) for bamboo poles and timber

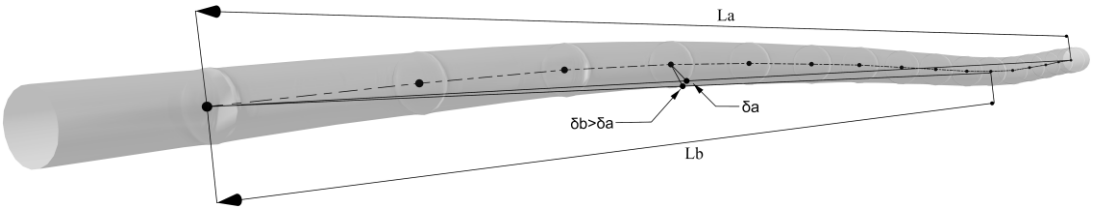

Figure 3.25. Spatial out-of-straightness of a bamboo culm

3.3.2 Cross-section properties

As displayed in Figure *3.10*, the actual cross-section properties of the bamboo differed to those of an equivalent circular tube because of the bamboo's organic nature. Figure *3.26* and Table *3.6* show the percentage difference between the moment of inertia of an equivalent circular tube *(I_b)*, taken as a benchmark, and the principal major *(I_1)* and minor *(I_2)* moments of inertia of the actual cross-section. Figure *3.27* shows the cumulative frequency distribution related to the percentage difference between I_b, as a benchmark, and I_1 & I_2. This figure illustrates the percentage of bamboo poles (vertical axis) whose actual moment of inertia *(I_1 or I_2)* differs from the equivalent inertia *(I_b)* by no more than a given percentage difference (horizontal axis). In average, actual cross-section properties differed 5% from the equivalent properties, however, the percentage of culms having an equivalent cross-section deviating 5% or more from the actual property was 35%, 42% and 45% for Guadua, Moso and Oldhamii respectively. This deviation of cross-sectional properties is directly related to the irregularity of the actual tubular shape. Furthermore, Figure *3.10* also shows that the principal axes orientation angle *(θ_o)* of the cross-sections along a bamboo pole

differ from an arbitrarily defined set of global axes *Y-Z* assigned automatically to the NURBS-model during its processing. Mean, standard deviation and extreme values for the absolute range of angle variation per bamboo pole with respect of the arbitrary set of axes are shown in Figure *3.28* and Table *3.6*. This result indicates that the local angles of principal moments do not coincide with each other along the bamboo pole and can indeed occur at any direction around the bamboo's centroidal axis with relatively high and unpredictable dispersion.

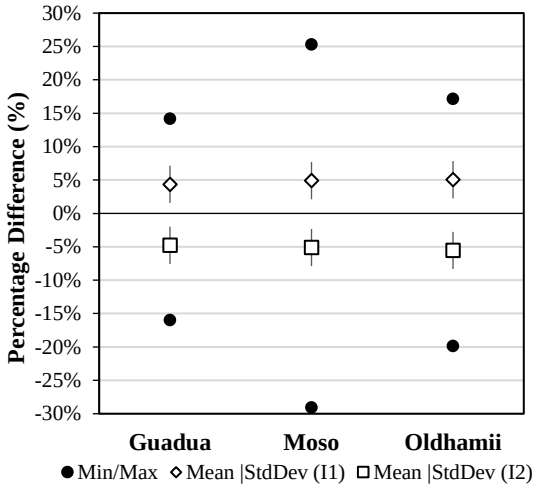

Figure 3.26. Percentage difference between the actual major (I_1) and minor (I_2) principal moment of inertia and the moment of inertia of an equivalent circular tube (I)

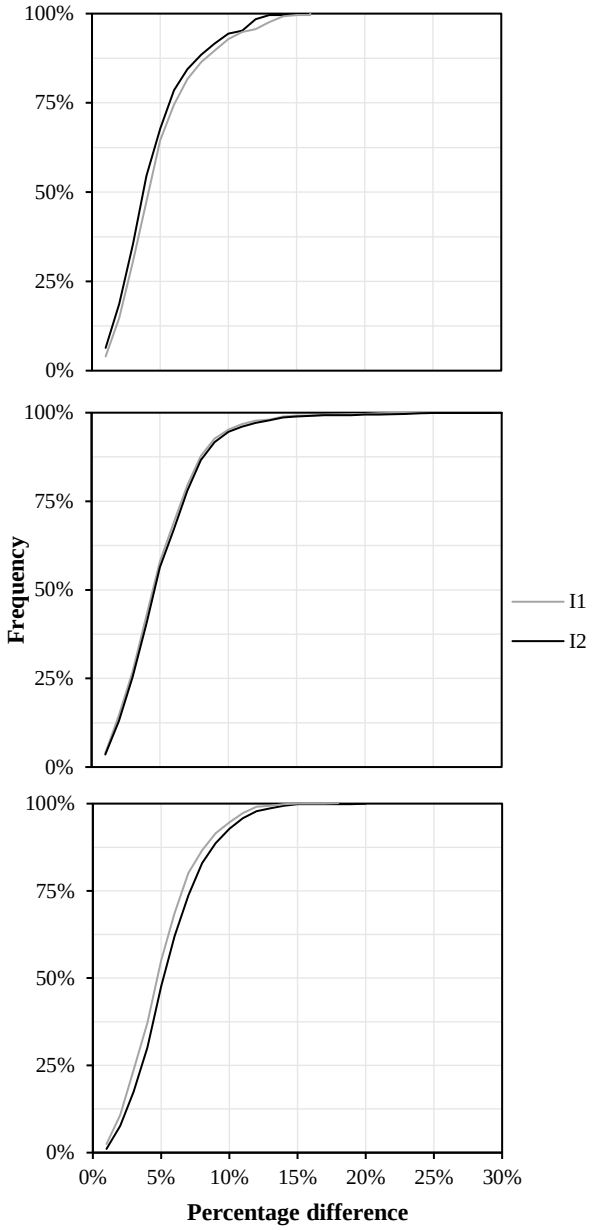

Figure 3.27. Cumulative frequency distribution for the difference between equivalent inertia (*I*) and its corresponding major (I_1) and minor (I_2) principal inertia of the measured cross-sections

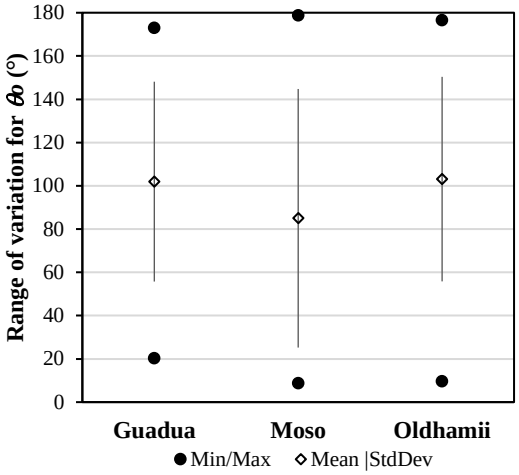

Figure 3.28. Mean, standard deviation and extreme values for the absolute range of variation of the direction of principal moment of inertia θ_b

The reduction of equivalent inertia *(I_b)* per unit meter along the bamboo pole was also analysed and is presented in Figure *3.29* and Table *3.6*. The average reduction values were, 15% for Guadua and Oldhamii and 20% for Moso. Studies have shown that this geometric characteristic can have negative effects in the design of bamboo structures [62,76], however, the reduction of inertia should be assessed on an individual basis due to the wide range and dispersion of the results. The change in section properties is in part related to the irregular shape of the discrete cross-sections extracted along the pole but mainly is due to the typical taper of the pole towards the top of the plant. Results of the variation of diameter and thickness along the pole are shown in Figures *3.30* and *3.31* and Table *3.6*. These results show that the reduction rate for both dimensions are highly variable and therefore, a single reduction rate would not be suitable for an entire species. Results also suggest that diameter and thickness might have different reduction rates within the same pole. However, authors have shown that, for example, the variation of diameter along the length of the pole approximates a linear regression [49,57,64,71,77]. To test this assumption, the diameter was plotted against the length of every pole to individually assess the slope of the taper and its coefficient of determination for linear regression. It was found that for Guadua, Moso and Oldhamii, the average coefficient of determination (R^2) was 0.87, 0.98 and 0.79, respectively. The same analysis could not be

performed for the thickness along the pole as the inner surface of the NURBS-model was initially modelled following a linear assumption.

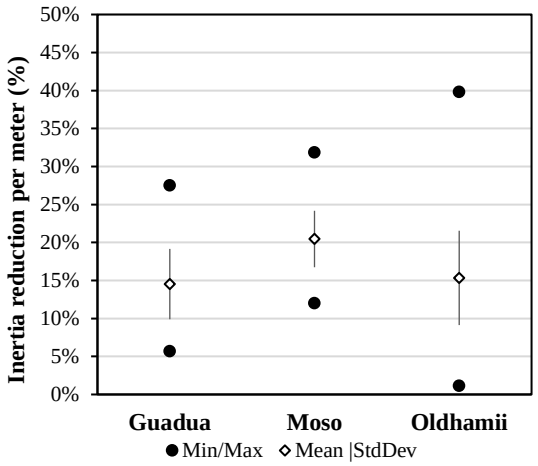

Figure 3.29. Mean, standard deviation and extreme values of inertia reduction per meter (%) measured from the bottom end of the pole

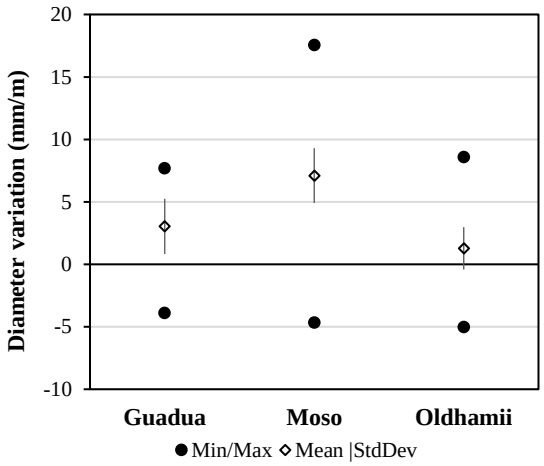

Figure 3.30. Diameter variation per meter

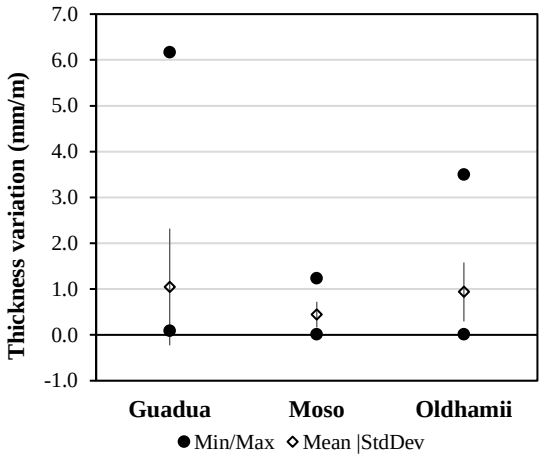

Figure 3.31. Thickness variation per meter

3.3.3 Correlation analysis

The correlation plots between all measured basic geometric properties (diameter, thickness and internode length) and their correlation along the length of the pole are shown in Appendix *A.2*. The Pearson's correlation coefficient [182], together with the coefficient of determination (R^2) of linear regression, were used to measure the statistical correlation between i) equivalent thickness *(t)* and diameter *(D)*; ii) differential diameter *(∆D),* in comparison to the bottom, to its corresponding length *(∆L);* iii) differential thickness *(∆t),* in comparison to the bottom, to its corresponding length *(∆L*); iv) differential internode length *(∆IL),* in comparison to the bottom, to its corresponding length; v) equivalent diameter (*D*) to internode length (*IL*); and vi) equivalent thickness (*t*) to internode length (*IL*). These results are shown in Table *3.8*. The coefficients of correlation obtained indicated that only the correlation between diameter and length of Moso was relatively strong (Pearson= 0.93, R^2= 0.86), which is in agreement with previous findings [62]. However, this result is far from conclusive as Moso is only one of the many potential species suitable for construction and results from this work can only be related to Moso bamboo with similar characteristics.

Correlation	**Pearson**			**Linear regression (R^2)**		
	Guadua	Moso	Oldhamii	Guadua	Moso	Oldhamii
Thickness to diameter	0.76	0.83	0.34	0.57	0.69	0.11
Differential diameter to length	0.75	0.93	0.60	0.57	0.86	0.36
Differential thickness to length	0.08	0.22	0.71	0.01	0.05	0.51
Differential internode length to length	0.28	0.54	0.33	0.07	0.30	0.11
Diameter to internode length	0.28	0.20	0.62	0.08	0.04	0.03
Thickness to internode length	0.66	0.03	0.41	0.44	0.01	0.17

Table 3.8. Pearson's correlation and linear regression results (R^2)

Common statistical methods to find correlation patterns are based on the assumption that the data follows a normal distribution, therefore the acquired database of basic geometric properties of bamboo poles was also tested for

departure from normality, according to [183], applying the directional test for skewness and kurtosis. Table *3.9* contains the results of directional test analysis, showing that the geometric data acquired departed from normality in the majority of the cases. This is a considerable obstacle to implement common correlation tools to test, for example, the precision, bias or variance of sets of data, that can be useful to develop models that describe the variability of the basic geometric properties of bamboo poles.

	Skewness		**Kurtosis**	
	Value	Limit	Value	Limit
Guadua	0.62	0.25	2.44	2.55
Diameter	0.00	0.25	0.00	2.55
Thickness	0.96	0.25	3.12	2.55
Internode length	-0.18	0.25	2.36	2.55
Out-of-straightness	0.66	0.66	2.53	1.98
Moso				
Diameter	0.65	0.13	2.95	2.76
Thickness	0.74	0.13	3.33	2.76
Internode length	-0.16	0.13	2.51	2.76
Out-of-straightness	1.84	0.6	6.25	2.35
Oldhamii				
Diameter	0.51	0.16	2.55	2.71
Thickness	0.41	0.16	2.37	2.71
Internode length	-0.11	0.16	2.49	2.71
Out-of-straightness	1.56	0.35	7.64	2.4

Table 3.9. Departure from normality test for the basic geometric properties

3.4 Discussion

The digitisation of bamboo poles addressed in this Chapter was carried beyond the isolated topic of scanning an object; it explored the possibilities of acquiring the geometric data of a bamboo pole in the most efficient manner so that the workflow could be implemented consistently. This workflow was developed based on the concept of quantifying the inherent geometric variability of a bamboo pole, opposed to forcibly eliminating it, by 3D scanning and producing digital models and numerical databases of the relevant geometric properties of individual bamboo poles. The scanning approach was developed according to specific key aspects derived from a previous work related to the geometric acquisition of bamboo poles. The focus of these aspects was to develop a scanning method applicable to any bamboo pole

with potential for construction purposes, acquiring their entire geometry (including wall thickness) efficiently and using a basic set-up that could be further implemented in an industrial environment. The scanning method presented in Section *3.2* successfully met all these fundamental requirements through the performance of scanning trials that helped to establish fundamental theoretical parameters that ensured the correct geometric acquisition of bamboo poles. The scanning trials were also used to explore the different point cloud post-processing steps contained in the software Artec Studio 12 and define the most relevant parameters to produce a polygon-mesh. An important contribution for the digitisation workflow was the development of a semi-automatic reverse engineering method to further convert the polygon-mesh file into a lightweight and more practical NURBS-model, which closely follows the organic geometry of the pole by extracting NURBS curves from the polygon-mesh and fitting free form surfaces through those curves. The bamboo NURBS-model is suitable for its implementation in multiple areas of the AEC industry where digital data plays an important role, for example, in design, material selection, robotic fabrication and rapid prototyping, assembly and maintenance of structures. Besides, relevant geometric properties of the bamboo pole NURBS-model, fundamental to produce structural models, were extracted and stored as a text database. The database contains both the equivalent properties of the pole, which could be used during the preliminary stage of a project, but more importantly, it also includes the data of the irregular section properties, discretised between nodes.

The scanning workflow was tested through the acquisition and processing of 235 bamboo poles from three different species, Moso, Oldhamii and Guadua, demonstrating the workflow's adaptability to the different characteristics found across species such as colour, size, length and texture. The accuracy of the final bamboo NURBS-model was validated through the direct comparison of physical and digital dimensions on approximately 15% of the scanned poles presenting a sub-millimetric accuracy for both diameter and thickness, comparable with the tolerance limit recommended for timber

elements. The digitisation process already improves the acquisition of geometric properties commonly performed with manual tools but its potential to be implemented in an industrial environment opens the opportunity to be considered as a quality control process, enhancing the added value for this sustainable construction material.

Having a geometric database containing the detailed description of bamboo poles was essential to conduct an analysis of the geometric variability and the exploration of correlation patterns on a relatively large stock of bamboo poles. The geometric analysis showed a high coefficient of variation values for basic properties such as diameter, thickness and internode length, in agreement with variability results found in previous studies, but also more complex properties such as out-of-straightness and diameter and thickness reduction showed the same significant variation between poles of the same species. This variation prevents from defining average properties that describe, for example, the reduction rate of diameter for an entire species as it was proved that this rate varies significantly from one pole to the other. As expected, the comparison between equivalent and principal moments of inertia showed that the organic shape of a bamboo departs from a perfectly circular shape, however, the significance of this study lies on the demonstration that the real shape of the cross-section can be accurately quantified. Besides, the high variation in the different properties appears to reduce the possibility to find strong correlation patterns. It was expected that with a relatively large number of scanned poles belonging to the same species and harvested in the same region, the dispersion of data for the correlated properties would be smaller. In fact, it was found that the data of the different geometric properties analysed not only showed a high dispersion but also departed from normality, which suggests that alternative statistical analysis (for data that do not follows a normal distribution) might be needed to improve the general understanding of geometric variability in bamboo poles, however, it can be simply deducted that geometry varies unpredictably due to its organic nature.

3.5 Summary

This chapter focused on the development of a reverse engineering method based on 3D scanning and computational geometric processing to successfully and efficiently acquire, quantify and store the geometric properties of individual bamboo poles within a digital environment. The details of the scanning methodology such as equipment, setup and basic parameters that ensure the correct and efficient acquisition of the geometry were presented. The geometric digitisation workflow included the further processing of raw data (polygon-mesh) obtained from the 3D scanner and converted it into a lightweight and more practical (for design and construction purposes) NURBS-model. This polygon-mesh to NURBS process is an important contribution to support the formal incorporation of natural bamboo poles into the AEC industry and, therefore, align bamboo poles with current digital design tools. The digitisation workflow was validated through its direct implementation on 235 bamboo poles belonging to three different species (Guadua, Moso and Oldhamii), accounting for almost 500 linear meters. The accuracy of the NURBS-model was evaluated through the direct comparison of physical and digital dimensions finding good agreement with similar ranges used in the industry. Furthermore, the digitisation process, within an industrial environment, has the potential to be applied as an alternative quality control measure for bamboo producers.

A practical research implementation of the geometric numerical data was performed to conduct a variability analysis of the 235 digitised poles, being this the first study that included a high number of bamboo samples with measurements taken at multiple discrete sections of each pole. Basic geometric properties such as diameter, thickness and relative length, were used to explore correlation patterns between them. This practical exercise not only demonstrated the potential of acquiring the geometric information of a stock of bamboo poles in a digital environment but also served to confirm the high variation magnitudes found within the different basic geometric properties and the low coefficient of correlation that exist between them. The chapter's contribution on the overall objective of the present research is to offer a

solution towards the individual quantification of the inherent geometric variability of bamboo poles and the subsequent implementation of digitised geometric data into modern design, construction and management of high-quality structures that incorporate this sustainable and renewable resource.

4 Quantification of physical and mechanical properties of bamboo poles

4.1 Overview

The physical and mechanical variability in bamboo poles is an innate characteristic caused by the organic nature of the material, it is independent of the species, age or region from which the bamboo is harvested and it is partly responsible for the practically negligible formal utilisation of the material in the building industry. Since the very first experimental procedures to measure the physical and mechanical properties of bamboo poles, researchers have mostly focused on developing testing methods and reporting the values of material properties found, without addressing the impact that the variability of properties produces in the structural design values. As shown in Sections *2.4* and *2.5* the high and diverse magnitudes of the coefficient of variation (CoV) found within a single species of bamboo, in comparison with conventional construction materials, produces a negative effect in the estimation of characteristic values which in turn diminish the reliability and efficiency of a structure built with bamboo poles. In this context, the current international standards for the determination of physical and mechanical properties and the structural design of bamboo structures, ISO 22157 and ISO 22156 respectively [66,69], suggest that when physical and mechanical characteristic values of a stock of poles are needed, destructive experimental tests are required from a representative portion (at least ten pieces) of the stock. This approach is statistically valid, however, the selection of a representative portion of poles is a subjective task that plays an essential part to determine characteristic values and no further guidance on how to select the representative portion is given. Besides, selecting a portion of the material stock to perform tests and determine the stock's properties is an approach that was conceived having manufactured materials in mind, such as concrete, steel or aluminium, which are produced following specific quality control measures. In the case of bamboo poles, the combination of factors

associated with the high variability in the physical and mechanical properties shows the incompatibility of a single characteristic value to represent a stock of bamboo poles, instead, the concept of non-destructive and intensive testing of the entire stock of poles, as proposed by [82] and introduced in Section *2.4*, can allow the quantification and managing of the physical and mechanical variability contained within the stock and mitigate its ultimate impact on the design values of bamboo poles.

The size of samples and testing methods suggested by ISO 22157 would not be compatible with an intensive and non-destructive testing procedure as it is based on full-size samples, this is, specimens are tested considering the entire cross-section of the pole, which requires a relatively high volume of material to be extracted from each pole. In addition, the irregular geometry of the samples (diameter and thickness taper, as well as out-of-straightness) is arbitrarily assumed as a straight hollow cylinder which induces an unknown level of uncertainty in the physical and mechanical properties measured, derived from the inherent geometric variability (Chapter *3*). This research adopted an individual testing method based on manufactured clear bamboo specimens for two reasons: i) clear specimens are consistent in shape and size and have been widely applied in the timber industry for more than a hundred years as a quick and systematic approach to help characterise, grade and adjust material properties of multiple timber species harvested in different regions, to study growing conditions and to compare material properties between different species [88,184]; and ii) because the anatomical arrangement of bamboos is significantly simpler than that of wood, meaning that material imperfections, such as knots, checks and cross-grain, are not present in bamboo, therefore, material properties can be more easily related to the full bamboo pole [82]. Sampling and testing procedures were based on JG/T-199 [65] as the most recent and comprehensive testing standard for small bamboo samples. The Chinese JG/T-199 standard was originally developed to characterise bamboo material properties for their implementation in glue-laminated bamboo products, however, it was considered that the key material properties needed to perform the structural

design of bamboo poles could be determined using the methods proposed in this standard. Thus, the fabrication and testing of mechanical properties included compression strength *(f_c)*, compression modulus *(E_c)* and shear strength *(f_v)*. In addition, moisture content *(ω)*, density *(ρ)* and the vascular bundle volume fraction *(V_f)*- a property not included in JG/T-199- were also measured from the fabricated samples. Tensile tests were not considered due to their complex practical testing but also because members in tension within a structure are likely to fail at the connection before the material reaches its ultimate tensile capacity [185,186]. The bending properties of the pole are not within the scope of JG/T-199 and therefore not included in the intensive testing of clear bamboo samples, however, the estimation of bending properties and the corresponding distribution of axial stresses and strains within the cross-section are addressed in Chapter *5*.

The practical challenge for the intensive testing of material properties is the actual production of small clear samples from an organic and irregular material such as bamboo poles. The fabrication of connections or structural bamboo components is commonly performed using conventional manual tools (handsaws, knives, jigsaws or bandsaws) [68,186], however, the process is labour-intensive, time-consuming and requires highly skilled personnel [187]. As mentioned in Section *2.7,* the fabrication of small samples can be developed as a bespoke semi-automated procedure based on 3D scanning data combined with robotic milling procedures that can be adapted to the bamboo's irregular and unique shape and produce testing samples within the required tolerances.

The objective of this Chapter was therefore divided into two parts: i) Section *4.2* focuses on the development of a scan-to-fabrication procedure based on 3D scanning and robotic milling that allows the efficient and accurate extraction of clear bamboo samples according to the required shape and sizes specified in JG/T-199; and ii) Section *4.3* analyses the material properties of stocks of poles of three different species to determine and compare characteristic values per specie and per pole, as well as to explore a systematic sorting approach aimed to reduce the variability effects in structural

design values. The species from which clear samples were produced and tested were Phyllostachys pubescens (Moso), Guadua angustifolia kunth (Guadua) and Bambusa Oldhamii (Oldhamii).

4.2 Development of a scan-to-fabrication method for clear bamboo samples

4.2.1 Sampling principle

The required dimensions and tolerances for the compression strength (f_c), compression modulus (E_c) and shear strength (f_v) of clear bamboo samples were taken from JG/T-199 [65]. The concept of extracting and testing samples from every single bamboo pole contained in a stock of poles requires to keep intact the integrity of each pole as much as possible so that the material from which samples are extracted can be later used in a construction project. At the same time, repeated specimens for each mechanical property are desirable to increase the validity of the testing results obtained from each pole. During the development of the geometric digitisation procedure presented in Chapter *3*, a length of up to four meters per pole was proposed as a practical length to handle and transport the bamboo elements. Before the digitisation procedure, each end of the pole was cut within the central portion of the last internode, as shown in Figure *3.5*, to allow a clear view of the cross-section. These internodes of the pole were denominated as sacrificial, as they were pre-drilled to insert the scanning references. To create a continuous workflow for the quantification of bamboo properties, it was proposed that samples could be taken from these internodes at each end of the pole. Considering that the digitisation workflow could be applied on bamboo poles of at least 50 mm in diameter (Section *3.2.1*), it was proposed that two diametrically opposite clear samples for each property are extracted from each end of a pole to ensure a consistent number of samples across different sizes of poles. Figure *4.1* shows an example of the arrangement of clear samples within one end of the pole, as well as their corresponding dimensions and tolerances. In total, four samples for each mechanical property are extracted, which sums up twelve clear bamboo samples per bamboo pole of up to four meters in length.

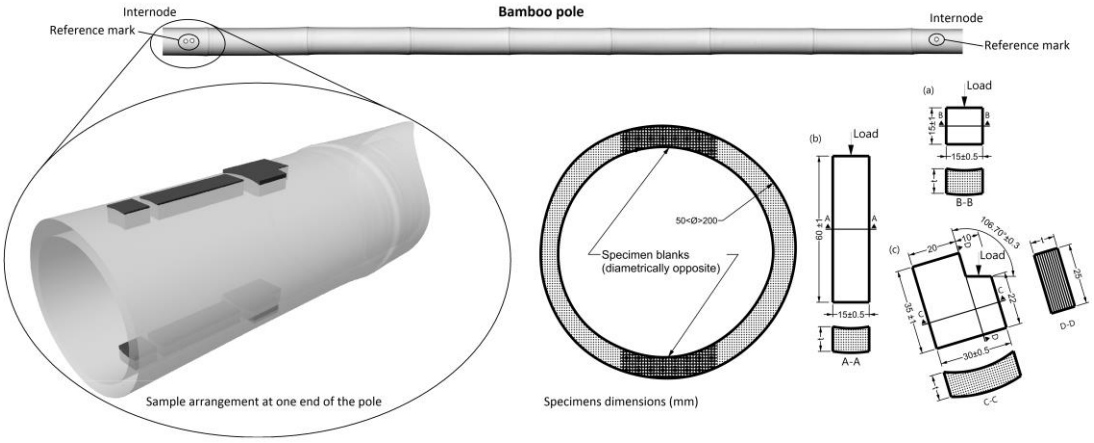

Figure 4.1. Sampling approach for individual bamboo poles where two diametrically opposite samples are extracted from each end per property: a) Compressive strength, b) compressive elastic modulus and c) shear strength samples.

4.2.2 Equipment and milling parameters

An important factor to obtain accurate results from a machining procedure is the proper clamping of the workpiece, therefore, a workbench equipped with an adjustable chain-vice was used to secure the irregular tubular shape of the internode to be machined. Although the quantification of physical and mechanical properties is proposed as a continuation of the geometric digitisation workflow, the ends of the pole from which samples were to be fabricated had to be re-scanned to correlate the position and orientation of the clamped internode with respect to the robot and the fabrication tools attached to it. An entry-level and low-budget Structure Sensor by Occipital [188] was used to acquire the geometry of the internode. The 3D scanner has a scanning range of 0.3 m to 3.5 m, with a linear field of view of 0.6 m x 0.96 m and 7.0 m x 11.2 m at the closest and farthest range respectively. The accuracy resolution of the scanner is 0.5 mm at a range of 0.5 m and 40 mm at 3.5 m. The scanner acquires only the geometry of an object (no texture or colour) at a rate of 30 fps. The scanner was operated through Occipital's proprietary software Skanect [188] installed in a laptop Dell XPS 15 equipped with an Intel i7-6700HQ CPU @ 2.66 GHz, 16 GB of installed memory and a dedicated video card Nvidia GTX GeForce 960m with 4 GB of memory. After a scanning session, Skanect will automatically create a polygon-mesh 3D

model of the acquired geometry, with a resolution of up to 0.5 mm, depending on the scanning range.

The process of subtract manufacturing or machining is a relatively complex task when the workpiece to fabricate has to comply with strict and relatively small tolerance ranges (e.g. microns). For example, the piston of an engine or a valve housing for a hydraulic system has to be fabricated with precise and accurate dimensions to ensure the safe and correct functioning of each piece within their corresponding systems. Multiple parameters affect the precision and accuracy of a machining process, such as machining operations, tool wear, tool forces and vibrations. There is a large quantity of scientific research behind the state-of-the-art of machining processes that address these parameters [189], however, the machining process of what is considered a relatively low accuracy object (e.g. sub-millimetric), such as clear bamboo samples, can be easily performed with basic introductory training, rules of thumb and manufacturer's recommendations [190]. Within the multiple machining operations, milling is one of the most versatile because it allows the removal of material by a relative motion of both the cutting tool and the workpiece [191]. Industrial robots are machines which derived from a different demand in the manufacturing industry, yet, their versatility and capacity to perform specific and repetitive tasks have made them popular for milling operations. The recent advances in technology and computational systems resulted in the development of multi-task robots that can be equipped with a wide range of tools and recognition sensors granting them the capacity to perform different tasks while adjusting their movement according to their environment [192]. Multitasking is the main advantage of modern robotic arms and the reason to be selected as the main equipment for the scan-to-fabrication procedure to effectively extract clear bamboo specimens.

The robotic arm used for the development of the scan-to-fabrication procedure was a KUKA Agilus KR 10 R1100 [193] operated through the Grasshopper [194] plugin KUKA|PRC [195]. With six degrees of freedom (Figure *4.2a*), KUKA Agilus KR10 offers a high flexibility advantage for milling purposes over irregular geometries, such as bamboo poles, as it can adjust

the position and orientation of the milling tool according to the unique geometric features of each sacrificial internode. This robot is equipped with a flange located at the sixth axis, on which high precision tapped holes are available to attach additional tools to the robot (Figure *4.2b*). The milling spindle was a Kress 1050 FME-1 with a range of speed of 5000 to 25000 rpm and a collet that supports shanks of maximum 8 mm. The scanner and the milling tool were mounted at the flange of the robotic arm using a custom-made bracket which holds both scanning and milling spindle at the same time.

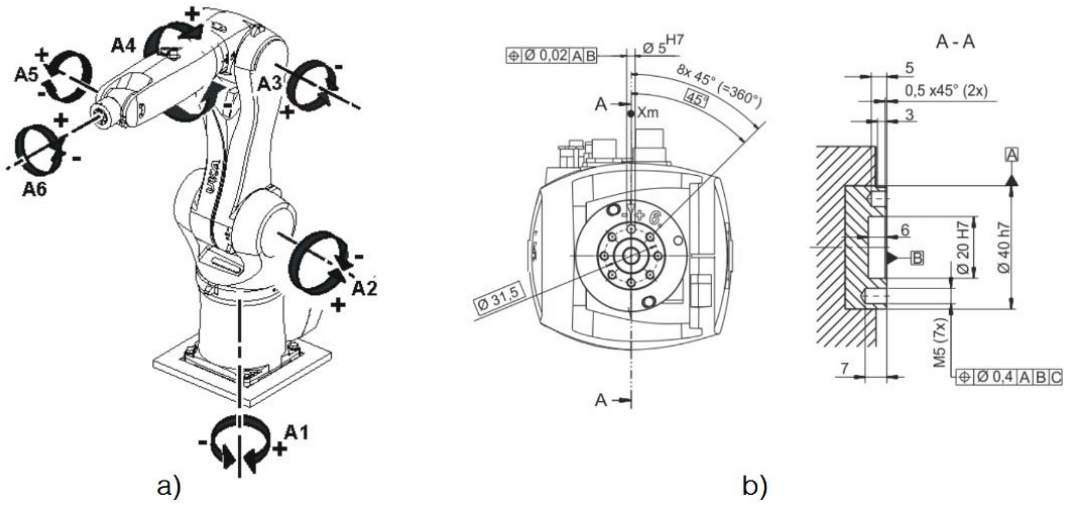

Figure 4.2. KUKA Agilus KR10 6-axis configuration (a) and diagram of the flange and tapped holes on which tools are attached to the robotic arm (b) [196]

KUKA|PRC converts geometric information generated within a CAD software (Rhino3D/Grasshopper) into a coded robotic toolpath. A robotic toolpath is defined by a set of coordinates and orientations to which the tool centre point (TCP) is moved to in a specific order following a specific robotic motion (point-to-point, linear, circular or spline motion) [197]. The TCP is originally located at the centre of the flange of any KUKA robot (Figure *4.2b*), however, when installing a tool, the TCP can be repositioned depending on the tool and the user's criteria as shown in Figure *4.3a* [192]. The calibration of a TCP is a standard procedure included in the operation manual of the KR10 [197], and its corresponding coordinates and orientation are defined relative to the flange of the robot (Figure *4.3b*). Once calibrated, every TCP is associated with a tool number so that different TCPs can be identified when

multiple working tools are attached. Therefore, KUKA|PRC requires the TCP number together with its coordinates and orientations to adjust the robotic toolpath accordingly.

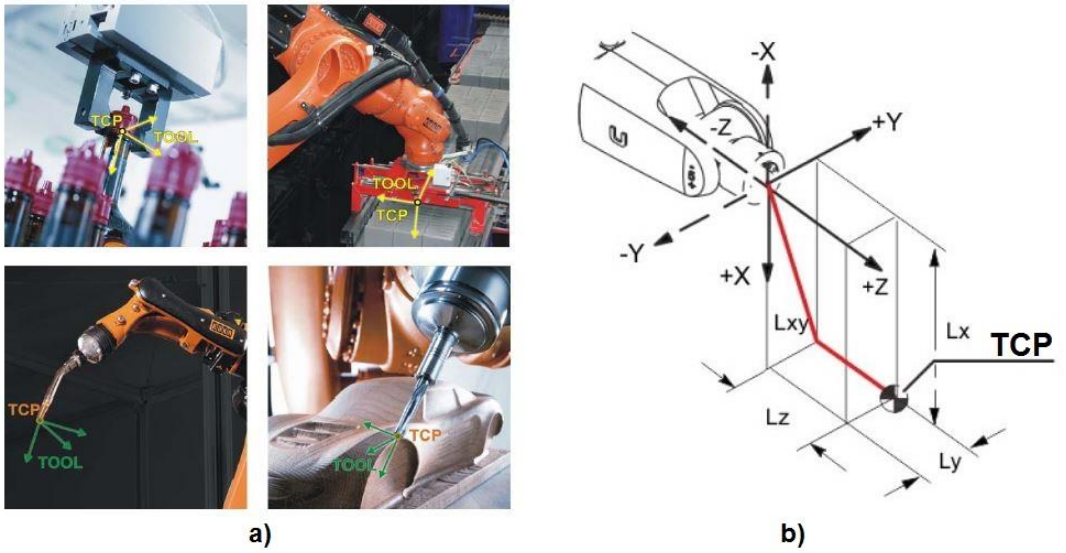

Figure 4.3. Examples of different tool centre point (TCP) depending on the tool attached (a) and definition of local TCP coordinate system referenced to the flange of the robot (b) [197]

Before performing any milling machining procedure, a couple of milling parameters had to be defined. These parameters included: i) tool diameter; ii) tool type; iii) feed of the tool and speed of the spindle; and iv) depth of cut. Due to time and budget constraints of this project, together with the limited scope towards machining efficiency, these parameters were experimentally defined with the support of technical staff at CEGE and UCL at Here East laboratories. Based on previous experience from the technical staff, the tool diameter chosen for the milling procedure was 6 mm. Feed, speed and depth of cut were estimated according to conventional formulas [198] and the manufacturers' recommendations. Although the bamboo material can be similar to a softwood, the performance of the type of cutter can vary significantly depending on the tool's material and the workpiece to be machined, therefore physical tests were performed to define an appropriate type of cutter. Three types of cutting tools were initially considered: i) 3-flute HSS end mill; ii) 3-flute carbide cutter; and iii) 3-flute HSS coarse-pitch ripper. To test the cutting efficiency of the tool, three characteristics where

qualitatively checked: cutting noise, burning of material/tool and surface quality. The test consisted of a slot milling operation following a rectangular shape with the same dimensions and orientations as the compressive elastic modulus sample (Figure *4.1*). The test was repeated for the three cutters, adopting a depth of cut of three millimetres for all of them. The motion of the robot together with the spindle attached to it were manually controlled during the tests. The HSS end mill cutter performed generally well when cutting across the fibres but the material and the cutter got burnt when cutting along the fibres. To amend this behaviour, either the speed or feed had to be reduced by at least 25% of the estimated values. Moreover, when moving along the fibres, these were not properly cut and were left hanging from the slotted wall. The carbide cutter was extremely noisy when cutting both along and across the fibres, which indicated that both feed and speed had to be iteratively modified to find an optimal configuration. Besides, small jumps in the path were observed, which created uneven surfaces on the slotted walls. Uneven surfaces can affect the testing of the samples, especially for surfaces that are loaded. The best result was obtained with the coarse-pitch ripper. It produced a clean cut in both directions and with a relatively low noise level in comparison with the two previous cutters. Table *4.1* shows a summary of the milling parameters adopted.

Parameter	**Specification**
Milling spindle	Kress 1050 FME-1
Material	Bamboo
Tool	3-flute HSS 6mm coarse-pitch ripper
Speed	20000 rpm
Feed	3600 mm/min
Depth of cut	3 mm
Type of movement	Linear

Table 4.1 Milling parameters for robotic fabrication

4.2.3 Scan-to-fabrication method

Figure *4.4* shows the local axes for the robot, its flange and the 3D scanner, together with the location of each TCP. For consistency within all operations (scanning, CAD and CAM), the robot origin and corresponding set of axes were defined as global. Figure *4.5* shows the diagram of the bespoke

bracket which was designed so that both TCPs of the spindle and scanner were contained within the local *X-Z* plane of the flange (Figure *4.3b*). The TCP numerical coordinates of the spindle were assigned according to the dimensions shown in Figure *4.5*, with the option to be parametrically adjusted within Grasshopper/KUKA|PRC according to the length of the cutting tool (manually measured before a milling procedure).

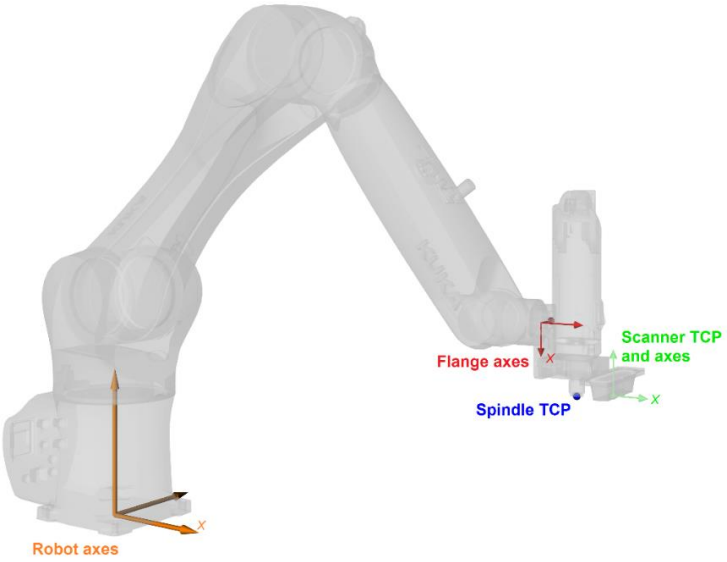

Figure 4.4. Diagram of the different set of axes within the scan-to-fabrication environment

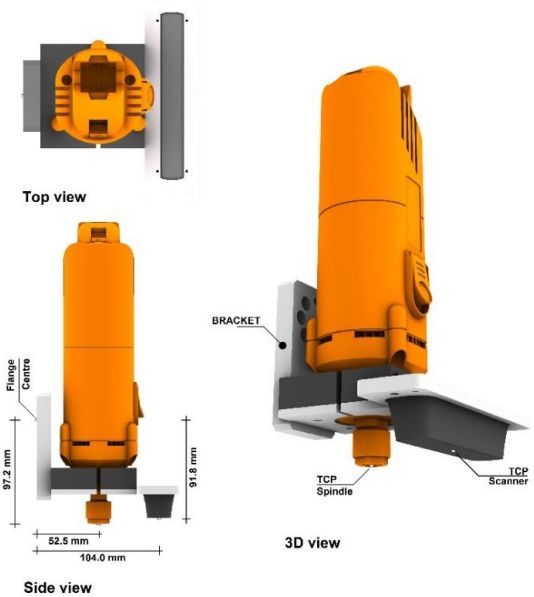

Figure 4.5. Diagram of the bespoke bracket to hold the milling spindle and 3D scanner, together with the numerical coordinates of their TCPs

The scanner's TCP was initially assumed to be on the external surface of the sensor (Figure *4.5*) but was then calibrated through an experimental iterative procedure to find the scanner's true local origin. The true origin of the scanner is used by the Skanect software to define the reference coordinate system for the entire geometry being acquired; therefore, the true origin and its corresponding orientation is the link between the position of the bamboo being scanned and the robotic arm. Although the manufacturer of the scanner provides a detailed 3D model of the sensor, it does not specify where the true origin is located.

The following procedure was used to find the true origin and calibrate the TCP of the scanner: i) a piece of bamboo was scanned using the sensor, driven by the robot. Prior the scanning, five reference targets were put on the surface of the pole, which physical coordinates with respect to the global axes were known; ii) the resulting polygon-mesh of the scanner was then imported into Rhino3D [176]; iii) the entire acquired geometry was transformed into the global set of axes; and iv) the digital coordinates of the reference targets were extracted and compared with the physical ones. The average difference between the physical and digital coordinates was subtracted from the assumed scanner's TCP to adjust its position. The process was repeated until the difference between coordinates was under one millilitre. This threshold was considered acceptable as the scanner's minimum resolution is in the same range. Table *4.2* shows the numerical procedure of the iterative calibration of the scanner's TCP and the adjusted numerical coordinates adopted after three iterations.

Physical coord.	Point	Global (mm) X	Y	Z		Local (mm) x	y	z
	1	620.0	50.1	220.0	Assumed	91.8	0.0	104
	2	620.0	0.0	282.2				
	3	620.0	-	220.0				
	4	570.0	0.0	284.8				
	5	670.0	0.0	280.7				
First iteration								
Digital coord. (mm)	1	611.9	30.3	226.1	Adjusted	81.3	-17.4	108.1
	2	609.9	-	285.2				
	3	606.8	-	224.9				
	4	559.6	-	288.0				
	5	659.6	-	283.9				
Avg. difference		-10.5	-	4.1				
Second iteration								
Digital coord. (mm)	1	622.6	47.4	223.7	Adjusted	92.9	0.1	108.5
	2	621.8	1.7	286.6				
	3	617.7	-	225.5				
	4	571.6	1.6	289.3				
	5	671.7	0.8	285.4				
Avg. difference		1.1	0.1	4.5				
Third iteration								
Digital coord. (mm)		621.3	47.9	220.9	**Adjusted**	**91.3**	**-1.0**	**104.9**
		620.4	0.3	282.8				
		616.0	-	221.1				
		569.6	0.1	286.0				
		670.3	-0.9	281.3				
Avg. difference		**-0.5**	**-1.0**	**0.9**				

Table 4.2. Iterative adjustment to calibrate the scanner's TCP

Figure *4.6* is a diagram showing the proposed scanning setup and procedure for the scan-to-fabrication method where the robot performs a circular motion to go around the bamboo pole with a radius of 500 mm centred approximately at the centroid of the pole being scanned. The scanner's sensor is always oriented towards the centre of the circular path, ensuring that the entire external surface of the pole is scanned. The speed at which the scanner is moved by the robot is 50 mm/s. Due to the large scanning range of the equipment (0.3 m to 3.5 m), a bounding box was defined within the Skanect software to reduce unnecessary surrounding geometric data so that only the bamboo and a small portion of its clamping system (for tracking and reference

purposes) were scanned. The position and orientation of the box were defined according to the manufacturers' specifications [199] and its corresponding dimensions are shown in Figure *4.6*. Scanning trials were performed (during and after the scanner's TCP calibration) to confirm the suitability of the scanning procedure for its further implementation within the scan-to-fabrication method.

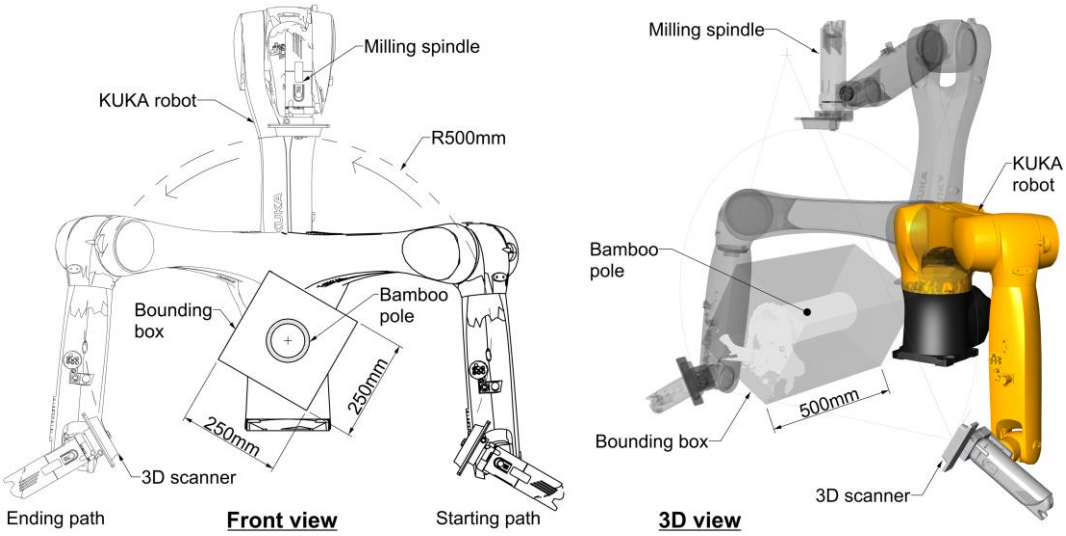

Figure 4.6. Scanning set-up for the fabrication of samples

Once the portion of the pole is successfully scanned, the raw polygon-mesh is subsequently imported into Rhino3D where a bespoke Rhino.Python [200] script was developed to first transform the local orientation of the scanned geometry into the global one (using the calibrated scanner's TCP) and then the polygon-mesh is converted into a NURBS surface [123] by extracting multiple NURBS curves (20 control points) along the internode from which samples can be fabricated and spaced 2 mm from each other. This portion of the internode is assigned manually depending on the available length, diameter and any imperfection present on each internode. Also, to avoid interference with any existing diaphragm the NURBS surface was created at least 25 mm away from the node. The NURBS surface process is similar to the one developed for the digitisation of bamboo poles presented in Chapter *3,* but skips the reconstruction of the inner surface as the wall thickness is not acquired during the scanning procedure and is therefore measured by hand.

The centroidal axis of the tube together with its surface becomes the input of a Grasshopper algorithm that generates the geometry of the clear bamboo specimens on the bamboo's surface, adjusting to the organic and individual geometry of each pole. The input of the user is required to parametrically arrange the position of the specimens depending on the internode's length, diameter and imperfections. The geometric information together with the milling parameters are then combined with the software KUKA|prc to generate the corresponding toolpath, as shown in Figure *4.7*. Finally, a virtual fabrication path is created by KUKA|PRC and is digitally reviewed by the user to assess any possible clashes between the robot, the spindle, the bamboo and its clamping system, before sending the execution command to the robot. Figure *4.8* shows the final result of specimens fabricated using the scan-to-fabrication procedure. A couple of holding tabs per specimen were left to avoid damaging it while finishing off the slot milling. These holding tabs were simply removed with a chisel to obtain the clear bamboo specimen.

Figure 4.7. Robotic toolpath generation with KUKA|PRC [195]

Figure 4.8. Robotically fabricated small clear bamboo samples

4.2.4 Validation and results

The scan-to-fabrication process was validated through its practical implementation to fabricate samples from 30 Guadua bamboo poles harvested in Valle del Cauca, Colombia. Each specimen was measured after fabrication using a Vernier calliper with an accuracy of 0.01 mm. Measurements (length, width and angle) were then compared with the allowed tolerances. Pictures of the fabrication procedure are shown in Figure *4.9*.

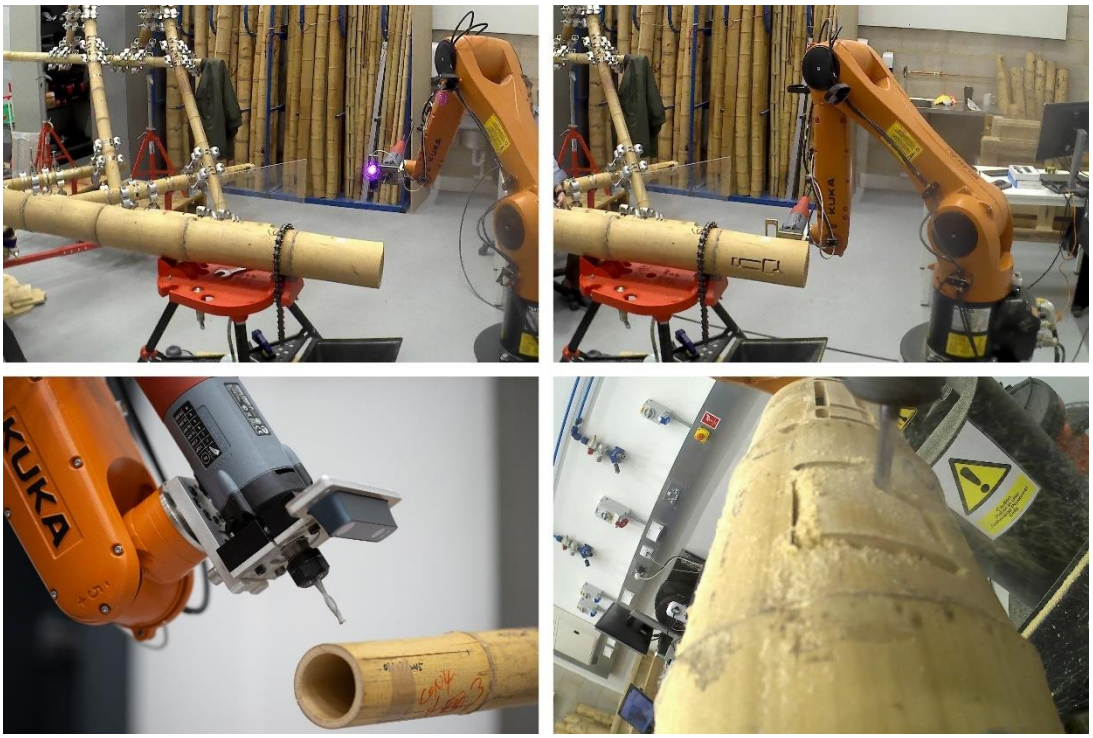

Figure 4.9. Scan-to-fabrication procedure

A total of 81 out of 120 specimens for each type of sample (f_c, E_c & f_v) were produced due to existing imperfections (such as cracks) in the portion of

poles available. The accuracy obtained in the samples was ±0.1 mm and ±0.3 mm in width and length respectively. The accuracy obtained in the angled plane for the shear sample was ±0.09°. The coefficient of variation for all the measured dimensions was under 2%. These results confirm the accuracy and also the precision to which small clear samples can be fabricated. In addition, the semi-automated procedure to extract twelve samples per pole (four samples for each of the three mechanical properties) took between 45-60 min. It is estimated that a fully automated fabrication method can produce the required clear bamboo samples in 25-30 min.

4.3 Determination of physical and mechanical properties

This section describes the material testing methodology based on clear bamboo samples to measure the moisture content *(ω)*, density *(ρ)*, vascular bundle volume fraction *(vf)*, compression strength *(f_c)* and elastic modulus *(E_c)* parallel to the fibres as well as shear strength *(f_v)* parallel to the fibres of bamboo poles from three different species. The results are first analysed per species, determining basic statistics and a single characteristic value per property, per species, following the standard method in BS EN 1990:2002 [94]. Then the characteristic value per property, per bamboo pole, is estimated and compared with the characteristic value per species to assess the advantages and disadvantages of each case. Besides, a sorting approach aimed to balance the factors that affect the characteristic value and based on the measured properties of the stock of poles is proposed. This sorting is aimed at reducing the impact of the natural variability in the design values of bamboo poles for structural purposes based on the individually quantified properties.

4.3.1 Equipment, material and methods

Three different bamboo species from China, Colombia and Mexico were chosen for this study as detailed in Table *4.3*. The Guadua samples were produced during the practical validation of the scan-to-fabrication procedure presented in Section *4.2*. Oldhamii and Moso clear specimens were produced in Mexico and China, respectively, using the conventional manual fabrication tools available in those places (e.g. handsaws or bandsaws) and in line with the fabrication standards shown in Figure *4.1* [65]. The total number of tested

specimens per physical and mechanical property were 80, 81 and 137 for Moso, Guadua and Oldhamii respectively. All fabricated specimens were kept at a constant temperature of 20°C ± 2°C and relative humidity of 65% ± 5% for 14 days prior testing, according to the requirements in JG/T-199.

Species	Origin	Age	Treatment	No of poles	Specimens
Phyllostachys pubescens (Moso)	Jiangsu, P.R. China	3 to 4	Carbonisation /Env. chamber	20	80
Guadua angustifolia kunth	Valle del Cauca, Colombia	2 to 5	Leaching/Air-dried	30	81
Bambusa oldhamii (Oldhamii)	Veracruz, Mexico	3 to 5	Leaching/Air-dried	37	137

Table 4.3. General description of Moso, Guadua and Oldhamii bamboos

The mechanical testing machine used in this study was an electro-mechanical, single-column Instron 3345 with a maximum capacity of 5 kN. Compressive strength samples requiring a higher load were tested on a 300 kN Controls UNIFLEX universal frame. The testing accessories consisted of compression platens with integral spherical seats, an Instron 2630 clip-on strain gauge extensometer for the compressive elastic modulus tests and a bespoke testing jig for the shear strength tests (Figure *4.10*), according to [65]. The robotic fabrication toolpath for the shear sample and the holding piece restraining the top of the shear sample in the corresponding testing jig were designed to accommodate the internal radiused corner produced by the milling operation to maintain the position of the sample's critical shear plane (Section D-D in Figure *4.1*) as shown in Figure *4.11*. Images to quantify the volume fraction contained in the wall thickness of the compression strength specimens were taken with a Nikon D7200 camera equipped with an AF-S DX Micro NIKKOR 85 mm f/3.5G ED VR lens.

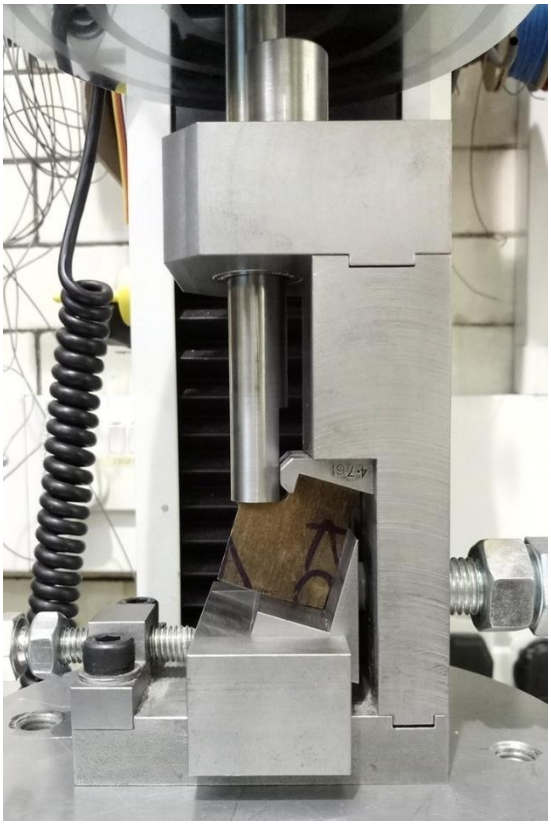

Figure 4.10. Testing jig for shear strength samples according to JG/T-199 [65]

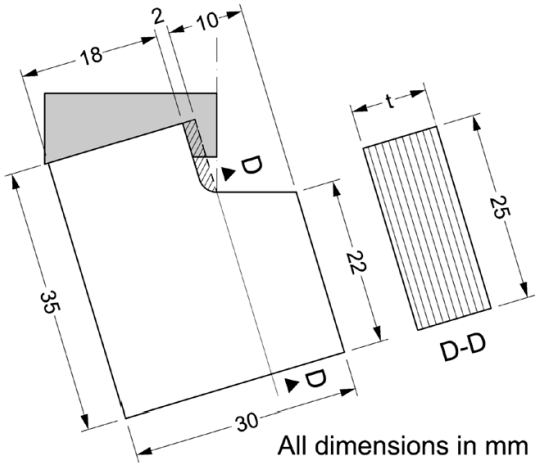

Figure 4.11. Details of the robotically fabricated shear specimen and matching jig holding piece

Experimental testing and calculations for the mechanical properties were performed according to the standard JG/T-199. All the samples were tested per batch of species in consecutive order. The moisture content was calculated from all specimens right after every test. The specimen was weighed to an accuracy of 0.001 g, then the specimen was taken to an oven

and dried for at least eight hours at a constant temperature of 103 °C ± 2 °C. Subsequently, the weight of the oven-dried specimen was also recorded with the same accuracy. The moisture content value was obtained as:

$$\omega = 100\left(\frac{m_1 - m_0}{m_0}\right) \quad (4.1)$$

where m_1 is the mass of the specimen tested (g); and m_0 is the mass of the specimen when fully oven-dried (g). The moisture content at the moment of test allows to further adjust each of the mechanical properties to a reference moisture content of 12% and therefore, results of different specimens can be compared to each other.

The procedure to test the compressive strength specimen included the capturing of an image for the vascular bundle volume fraction prior testing. To take the image, the cross-section of the specimen was lightly sanded with 600/1200 grit silicon carbide sanding paper. The original coloured images were post-processed into binary images from which the area of fibres was calculated using a bespoke Matlab script [201] developed by other researchers within the UCL BIM Bamboo group [129]. This script converts the original RGB image into a greyscale intensity image (Matlab function: rgb2gray) and filters any significant noise from it (Matlab function: imgaussfilt, 0.1 standard deviation). The script then calculates, based on the greyscale image histogram, the threshold value of pixel intensity (Matlab function: graythresh) that differentiates fibre bundles and matrix. This value is subsequently used to generate the final binary image (Matlab function: imbinarize) from which pixel areas for fibre bundles and matrix are quantified. The volume fraction calculated neglects the contribution from the small hollow conducting vessels clustered around fibre bundles as they constitute less than approximately 8% of the total cross-sectional area [7]. After the picture was taken, the dimensions of the specimen were recorded (width, length and thickness) prior to the compression test. The load was applied parallel to the fibres at a rate of 80 MPa/min until failure, recording the rupture load with a minimum accuracy of 10 N. Figure *4.12* shows the compression strength testing set-up and its typical failure, showing how the fibres buckle once the

capacity of the matrix is reached. After testing, the specimen's moisture content was taken following the corresponding procedure. The compressive strength parallel to the fibre, f_c (MPa), at 12% moisture content was calculated as:

$$f_c = K_{f_c} \frac{P_{cmax}}{bt} \quad (4.2)$$

where P_{cmax} is the maximum compression load (N); b & t are the specimen width and thickness (mm); and K_{fc} is the correction factor for the effect of moisture content given by:

$$K_{f_c} = \frac{1}{0.79+1.5e^{-0.16\omega}} \quad (4.3)$$

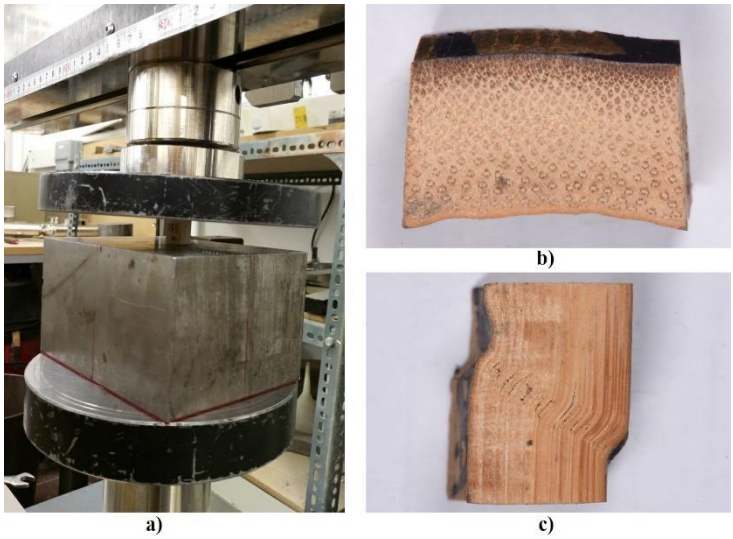

Figure 4.12. Compressive strength testing set-up (a), together with top (a) and side (b) images of the typical failure

The procedure to test the elastic modulus specimen consisted of measuring the required dimensions (width at three positions, length and thickness), to then fix the strain gauge extensometer on one of the cut planar surfaces parallel to the fibres prior placing the specimen in the testing machine. Figure *4.13* shows the testing set-up for elastic modulus specimen. The loading procedure consisted on a cyclic loading and unloading between the stress limits of 5 MPa and 20 MPa (considered by JG/T-199 as a portion of the elastic range), at a loading rate of 13 MPa/min for six cycles. Deformation difference at the limit stress was recorded on every cycle. After the test, the

moisture content and dry density were measured. The dry density, ρ (kg/m^3), was calculated as:

$$\rho = 10E^{06}\left(\frac{m_0}{V_0}\right) \quad (4.4)$$

where m_0 and V_0 are the mass (gr) and volume (mm^3) of the fully oven-dried specimen. The elastic modulus parallel to the fibre, E_c (MPa), at 12% moisture content was then calculated as:

$$E_c = K_{E_c}\frac{\Delta\sigma}{\Delta\epsilon} \quad (4.5)$$

where Δ_σ is the stress difference between the minimum (5 MPa) and maximum (20 MPa) stress limits (MPa); Δ_ε is the deformation difference measured at the stress limits; and K_{Ec} is the correction factor for the effect of moisture content given by:

$$K_{E_c} = \frac{1}{0.89+0.36e^{-0.1w}} \quad (4.6)$$

Figure 4.13. Compressive elastic modulus test set-up including clip-on strain gauge

The dimensions of the shear strength specimen (width, length, length of shear plane and thickness) were first taken and then the specimen was placed

on the testing jig as shown in Figure *4.10*. The load was applied through the loading piston on the angled surface of the specimen at a constant rate of 10 MPa/min until rupture. The ultimate shear load was recorded and the broken piece of the specimen was taken to measure the corresponding moisture content. Figure *4.14* shows the shear plane failure of a sample. The shear strength parallel to the fibre, f_v (MPa), at 12% moisture content was calculated as:

$$f_v = K_{f_v} \frac{P_{vmax}}{25t} \quad (4.7)$$

where P_{vmax} is the ultimate shear load (N); t is the thickness of critical shear section (mm) (Section D-D in Figure *4.11*); and K_{fv} is the correction factor for the effect of moisture content given by:

$$K_{f_v} = \frac{1}{0.67+0.77e^{-0.07w}} \quad (4.8)$$

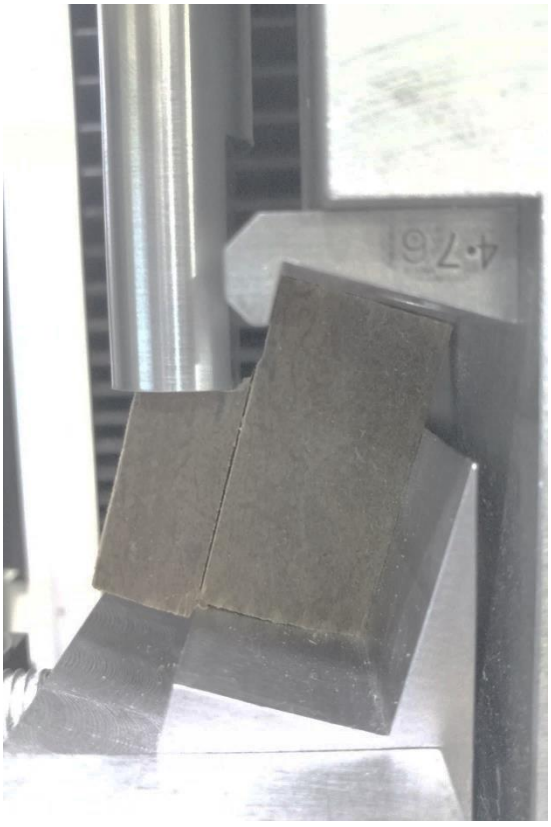

Figure 4.14. Failure plane of the shear strength test

Characteristic values for density, compressive strength, elastic modulus and shear strength were determined for each species according to Annex D: Design Assisted by Testing in BS EN 1990:2002 [94]:

$$X_{k(n)} = m_x\{1 - k_n V_x\}$$ (§ 2.5 Eq. 2.1)

where: $X_{k(n)}$ is the characteristic value; n is the number of test results; m_x is the mean of the n specimens results; k_n the characteristic fractile factor for the 5% characteristic value (Table D1 of [94]) and V_x the coefficient of variation. The coefficient of variation, V_x, was taken from JG/T-199, if available, and also calculated from BS EN 1990:2002 for comparison:

$$V_X = \frac{s_X}{m_X}$$ (4.9)

where s_x is the value of the standard deviation given by:

$$s_X^2 = \frac{1}{n-1}\sum(x_i - m_X)^2$$ (4.10)

and x is the observed value for each specimen.

4.3.2 Test results

Figure *4.15* shows the mean and standard deviation, together with the corresponding characteristic value of dry density for each of the species measured. Similarly, Figure *4.16* shows the results of compression strength for Moso, Guadua and Oldhamii.

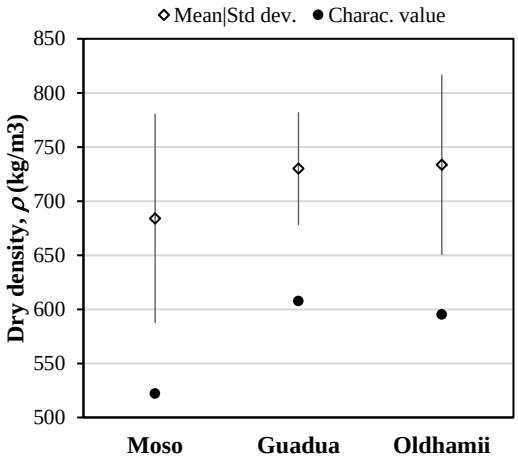

Figure 4.15. Mean, standard deviation and characteristic value for density

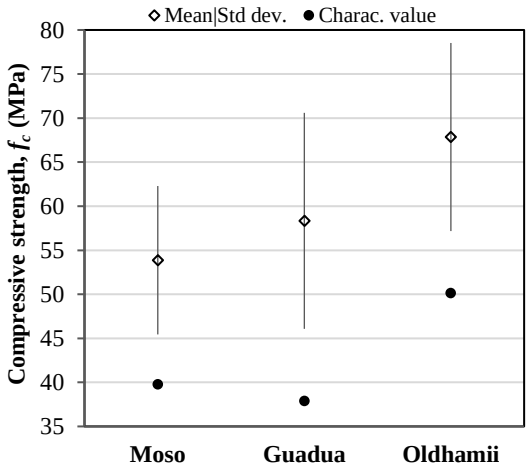

Figure 4.16. Mean, standard deviation and characteristic value for compressive strength

A typical experimental stress-strain curve in Figure *4.17* shows how the elastic behaviour of the sample stabilises after the first three loading and unloading cycles as specified in JG/T-199. According to this standard, the average deformation difference from the last three loading cycles was used to calculate the elastic modulus, E_c, of each specimen (Eq. *4.4*). Figure *4.18* shows the mean, standard deviation and characteristic value of elastic modulus for each species. Similarly, Figure *4.19* shows the testing results of shear strength for Moso, Guadua and Oldhamii.

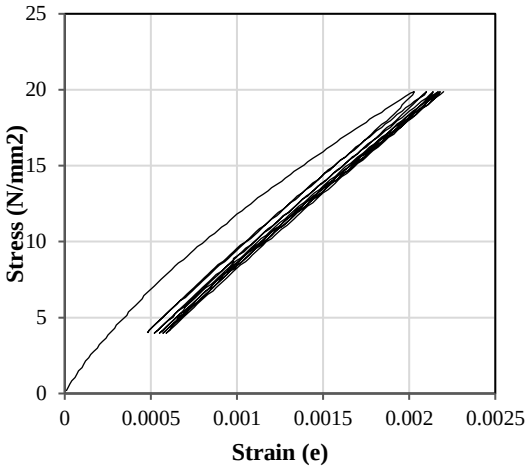

Figure 4.17. Typical experimental stress-strain curve for elastic modulus test

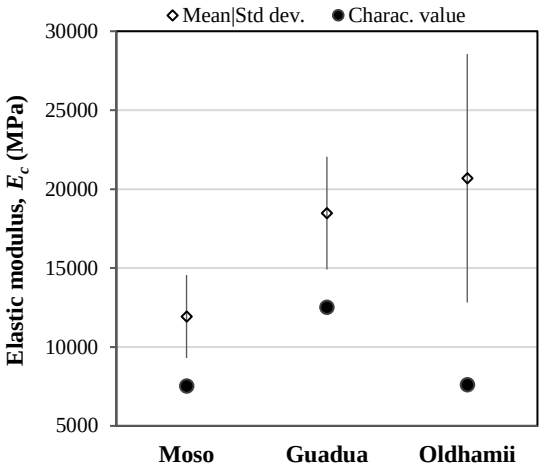

Figure 4.18. Mean, standard deviation and characteristic value for elastic modulus

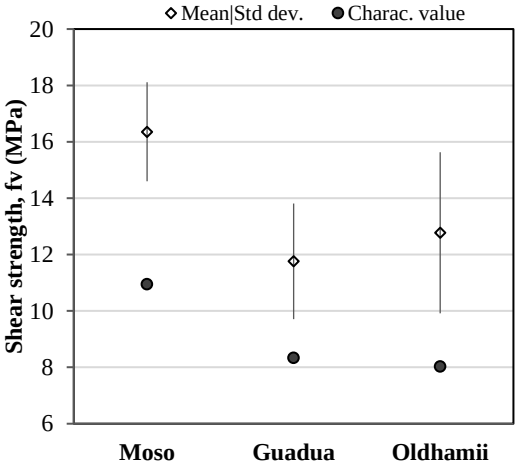

Figure 4.19. Mean, standard deviation and characteristic value for shear strength

Typical wall thickness images for each species are shown in Figure *4.20*, together with their corresponding post-processed binary images, showing the variability in fibre content and their distribution pattern among different species. Statistical results of mean and standard deviation are shown in Figure *4.21* for each species. A summary of the statistical results and characteristic values for each species is shown in Table *4.4*.

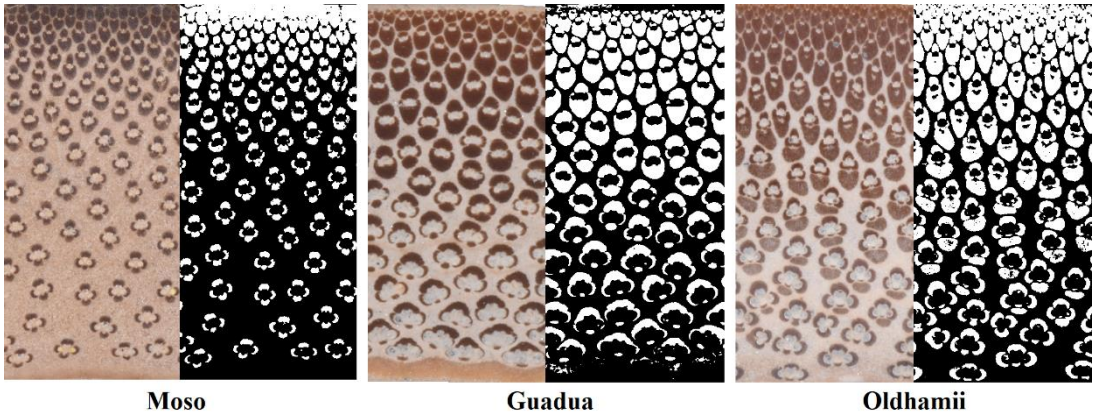

Figure 4.20. Digital image of the bamboo wall and corresponding binary post-processed image

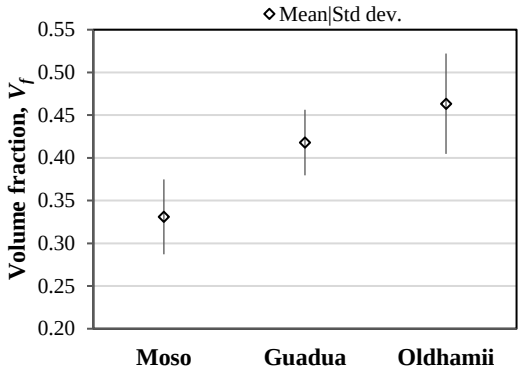

Figure 4.21. Mean and standard deviation for the volume fraction

	Mean	Std Dev	JG/T-199		BS EN 1990		$X_{k(n)}$[a]	$X_{k(n)}$/mean
			V_x(%)	k_n	V_x(%)	k_n		(%)
Moso								
Density (kg/m^3)	684	97	10	1.66	14	1.67	522	76
Comp. strength (MPa)	54	8	13	1.66	16	1.67	40	74
Elastic modulus (MPa)	11930	2628	-	-	22	1.67	7529	63
Shear strength (MPa)	16	2	20	1.66	11	1.67	11	67
Volume fraction	0.33	0.04	-	-	-	-	-	-
Guadua								
Density (kg/m^3)	730	52	10	1.66	10	1.67	608	83
Comp. strength (MPa)	58	12	13	1.66	21	1.67	38	65
Elastic modulus (MPa)	18480	3570	-	-	19	1.67	12502	68
Shear strength (MPa)	12	2	20	1.66	18	1.67	8	71
Volume fraction	0.42	0.04	-	-	-	-	-	-
Oldhamii								
Density (kg/m^3)	734	83	10	1.65	11	1.66	595	81
Comp. strength (MPa)	68	11	13	1.65	16	1.66	50	74
Elastic modulus (MPa)	20683	7868	-	-	38	1.66	7604	37
Shear strength (MPa)	13	3	20	1.65	22	1.66	8	63
Volume fraction	0.46	0.06	-	-	-	-	-	-

Note: V_X: coefficient of variation, k_n: characteristic fractile factor

[a]Based on the governing values of V_X & k_n (i.e. largest $V_X k_n$ product)

Table 4.4. Summary of testing results for each physical and mechanical property

Table *4.5* compares the coefficient of variation (CoV) estimated according to Bs EN 1990:2002 for each physical and mechanical property per species with the average and range of CoV obtained when analysed per bamboo pole (only for poles where four specimens were tested). This table shows that on average, estimating CoV per pole gives a lower value than when considered for the entire species, however, the range found shows that for some poles the measured properties were highly dispersed. The effect of the coefficient of variation found in every pole and the low number of samples (four) on the characteristic value estimated for every pole is shown in Figures *4.22, 4.23* and *4.24,* taking the compressive elastic modulus as an example, where the average of characteristic value over the mean was 50%, 49% and 26% for Moso, Guadua and Oldhamii, in comparison with the 63%, 68% and 37% obtained when analysed per species (Table *4.4*). This means that although the CoV is in average lower when analysed per pole, it is not sufficient to reduce the impact of variability (and the relatively low number of samples) on the design values. In the case of Oldhamii, the CoV relatively high, thus some characteristic values became zero or negative (Figure *4.24*)

	Coefficient of Variation	
	Per	Per pole (range)
Moso		
fc	0.16	0.10 (0.03-0.21)
Ec	0.22	0.19 (0.05-0.35)
fv	0.11	0.08 (0.02-0.2)
Density	0.14	0.10 (0.02-0.32)
Volume fraction	0.13	0.12 (0.04-0.22)
Guadua		
fc	0.21	0.19 (0.05-0.38)
Ec	0.19	0.18 (0.06-0.34)
fv	0.17	0.11 (0.02-0.27)
Density	0.10	0.03 (0.01-0.09)
Volume fraction	0.10	0.06 (0.01-0.12)
Oldhamii		
fc	0.16	0.11 (0.01-0.28)
Ec	0.38	0.32 (0.04-0.59)
fv	0.22	0.15 (0.03-0.41)
Density	0.11	0.07 (0.01-0.15)
Volume fraction	0.13	0.10 (0.02-0.30)

Table 4.5. Coefficient of variation measured on every material property per species, per pole (mean and range) and per bottom or top end (mean and range)

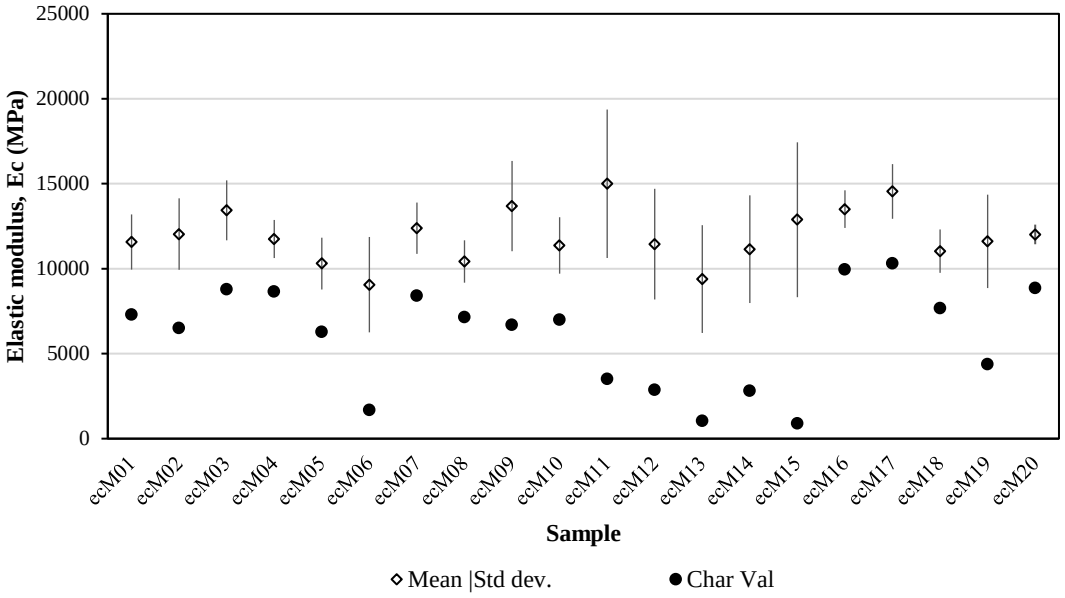

Figure 4.22. Characteristic value of the compressive elastic modulus of Moso estimated per pole

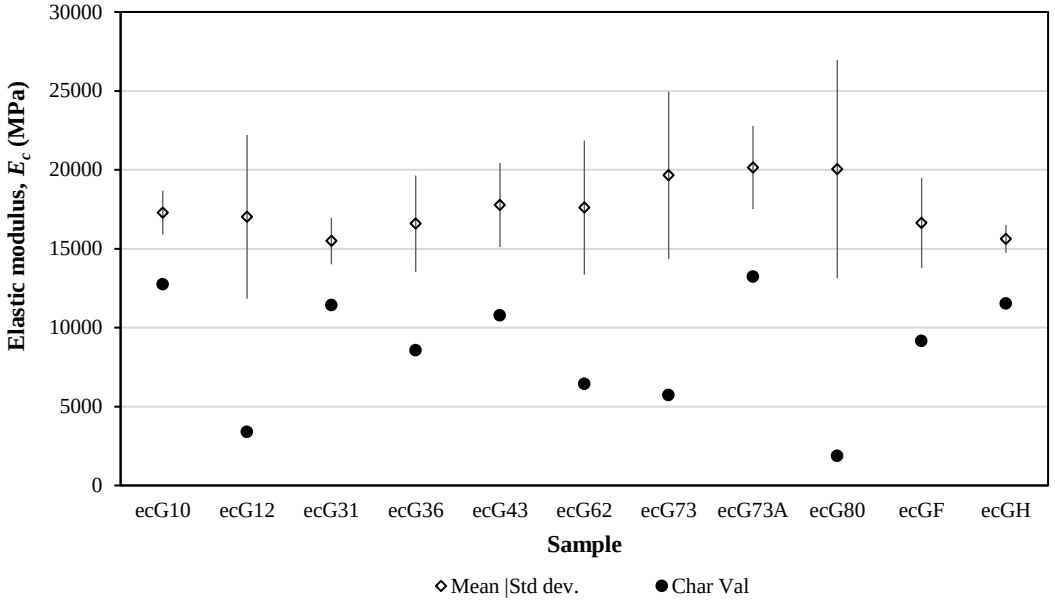

Figure 4.23. Characteristic value of the compressive elastic modulus of Guadua estimated per pole

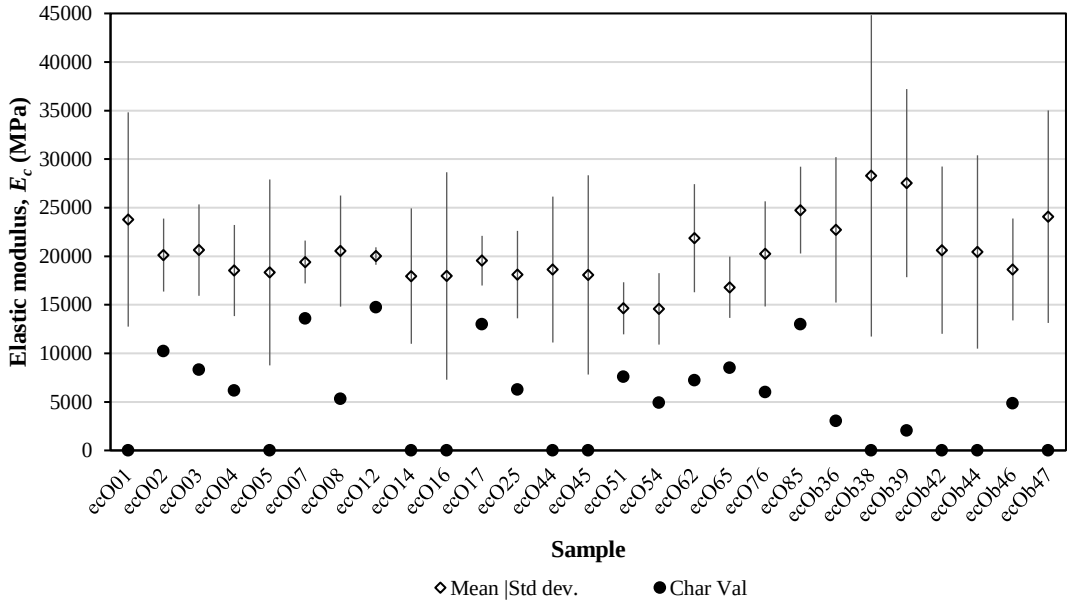

Figure 4.24. Characteristic value of the compressive elastic modulus of Oldhamii estimated per pole

The effect of the number of samples is due to the factor 1-K_nV_x (Eq. *2.1*) which directly correlates the number of samples (n) and the CoV (V_x) obtained from those samples with the characteristic value (Figure *4.25*). On one hand, a large dataset of measured properties (e.g. per species) increases the K_n factor but also the CoV (Table *4.5*). On the other hand, a low number of

measured properties (e.g. per pole) reduces the K_n factor as well as the CoV but not sufficiently. Therefore, to improve the ratio of characteristic value over the mean obtained per species (Table *4.4*), a systematic sorting of data based on average values per bamboo pole is proposed to create small groups containing approximately 30 samples (Figure *4.25*), this is, approximately eight bamboo poles so that the factor (1-K_nV_x) is more balanced. The number of samples was taken from Figure *4.25*, which by taking *n*=30 the factor (1-K_nV_x) gives values considerably close as to when having an infinite number of samples. Table *4.6* shows that creating small groups of the elastic modulus within each species considerably improves the ratio of characteristic value over mean. Moreover, if the stock of bamboos was composed by multiple species, it could be possible to combine the entire database and re-group the bamboo poles and their respective samples regardless their species, which makes the sorting procedure more efficient. Table *4.7* shows an example of sorting and grouping the elastic modulus combining the three studied species.

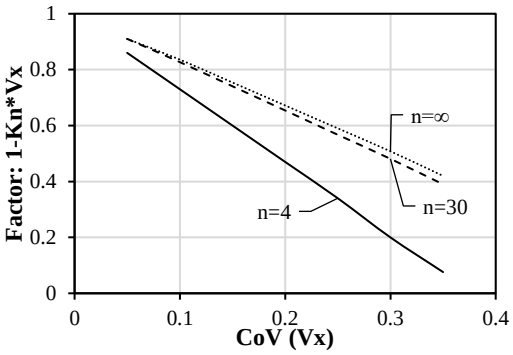

Figure 4.25. Correlation of CoV (Vx) and the number of samples (n) as a proportional factor (1-K_nV_x) for the estimation of the characteristic value

		Range (MPa)	k_n	V_x (%)	$1-K_nV_x$	Mean (MPa)	Std Dev (MPa)	$X_{k(Kn)}$ (MPa)	$X_{k(Kn)}$/mean (%)
Moso	Species	9000 - 15000	1.67	22	0.63	11930	2628	7529	63
	Group 1	9000 - 11700	1.71	18	0.70	11015	1958	7668	70
	Group 2	11700 - 15000	1.71	17	0.71	12959	2223	9163	71
Guadua	Species	15000 - 24500	1.67	19	0.68	18480	3570	12502	68
	Group 1	15000 - 17800	1.71	15	0.75	16745	2493	12488	75
	Group 2	17800 - 24500	1.70	14	0.76	20396	2912	15434	76
Oldhamii	Species	12500 - 31000	1.66	38	0.37	20683	7868	7604	37
	Group 1	12500 - 18000	1.72	28	0.53	15525	4272	8180	53
	Group 2	18000 - 19800	1.72	27	0.54	18771	5046	10069	54
	Group 3	19800 - 21500	1.72	25	0.57	20373	5035	11703	57
	Group 4	21500 - 31000	1.72	30	0.48	25545	7749	12239	48

Table 4.6. Sorting bamboo poles according to their species and average elastic modulus. Characteristic values are then estimated based on those groups which contain approximately eight poles

		Range (MPa)	k_n	V_x (%)	$1-K_nV_x$	Mean (MPa)	Std Dev (MPa)	$X_{k(Kn)}$ (MPa)	$X_{k(Kn)}$/mean (%)
All species	Group 1	9500 - 11200	1.72	17	0.71	11000	1856	7798	71
	Group 2	11200 - 13000	1.72	15	0.73	11912	1836	8746	73
	Group 3	13000 - 15000	1.72	18	0.69	14184	2509	9858	69
	Group 4	15000 - 17000	1.72	20	0.66	16180	3230	10618	66
	Group 5	17000 - 18400	1.72	26	0.56	17731	4579	9846	56
	Group 6	18400 - 19600	1.72	20	0.65	18916	3829	12323	65
	Group 7	19600 - 20300	1.72	16	0.73	20017	3178	14553	73
	Group 8	20300 - 22800	1.72	25	0.58	21389	5240	12391	58
	Group 9	22800 - 31000	1.72	29	0.50	26059	7506	13115	50

Table 4.7. Sorting bamboo poles according to their average elastic modulus as a multiple species stock. Characteristic values are then estimated based on those groups which contain approximately eight poles

The average compressive elastic modulus per pole was used to sort the poles and create groups, however, this does not mean that the same sorting and grouping applies when other properties are analysed. This would depend on whether the physical and mechanical properties are linearly correlated to each other. To test this assumption, Figures *4.26* and *4.27* show individual density and volume fraction values plotted against their corresponding mechanical properties *($f_{c,}$ E_c & f_v)* for each species, whereas Figure *4.28* shows mean density and volume fraction values plotted against their corresponding mean mechanical properties *($f_{c,}$ E_c & f_v)*. The Pearson correlation coefficients [182]comparing the properties of every specimen are shown in Table *4.8*, together with the corresponding correlation coefficients considering the mean values of the properties per species (Table *4.4*). Results show very week correlation when the physical and mechanical properties are individually correlated, which suggest that the sorting and grouping here proposed has to be performed for every physical or mechanical property. Correlation between individual mechanical properties ($f_{c,}$ E_c & f_v) as well as between physical properties *(ρ & V_f)* for Moso, Guadua and Oldhamii also showed low correlation values (<0.30).

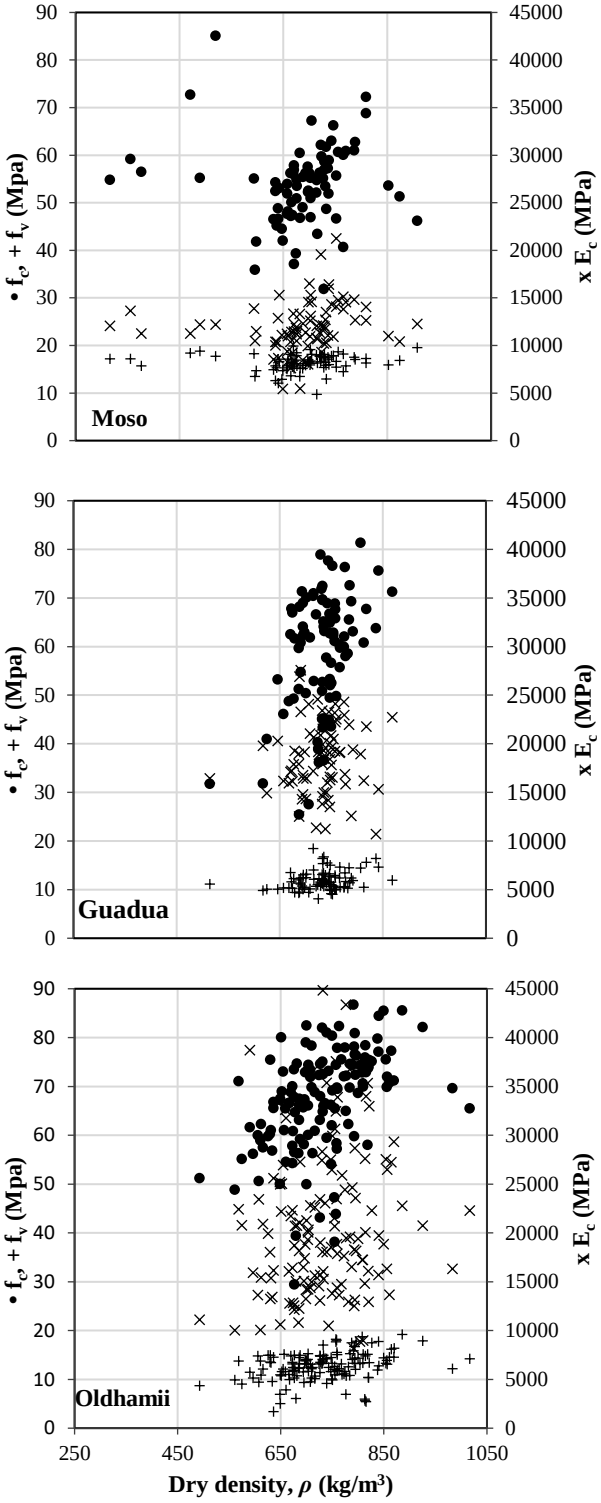

Figure 4.26. Correlation between density and mechanical properties

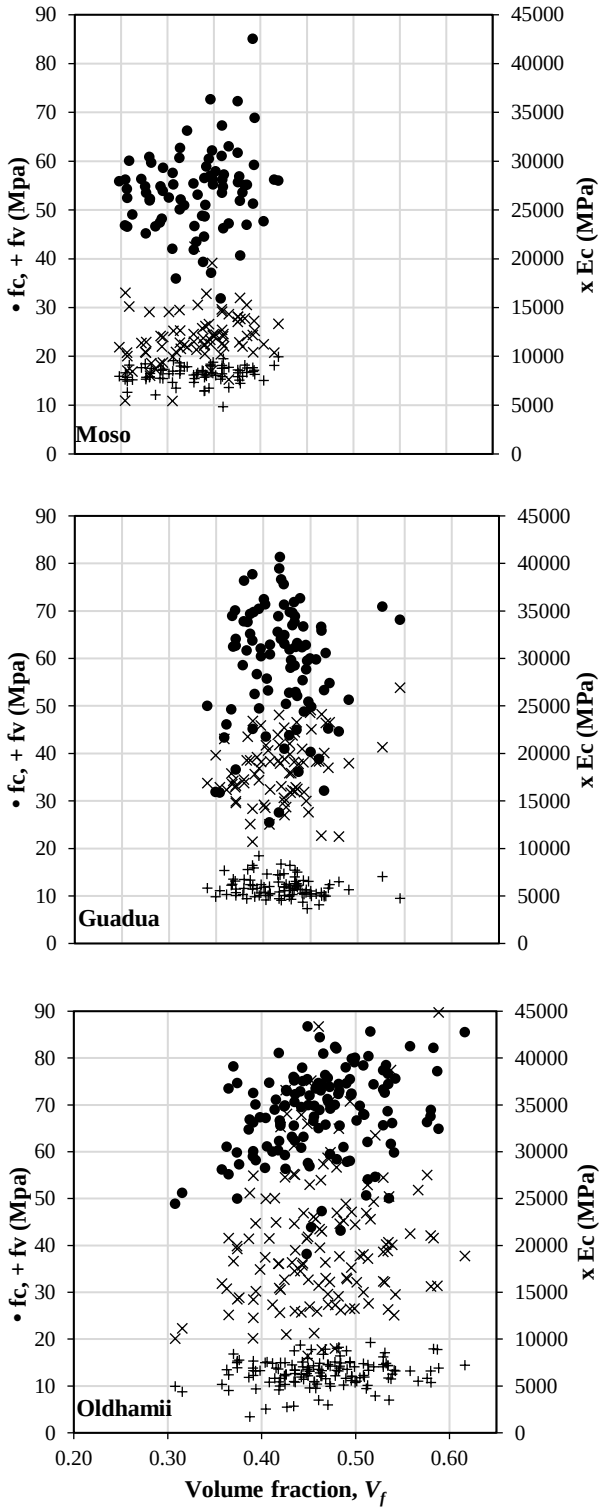

Figure 4.27. Correlation between volume fraction and mechanical properties

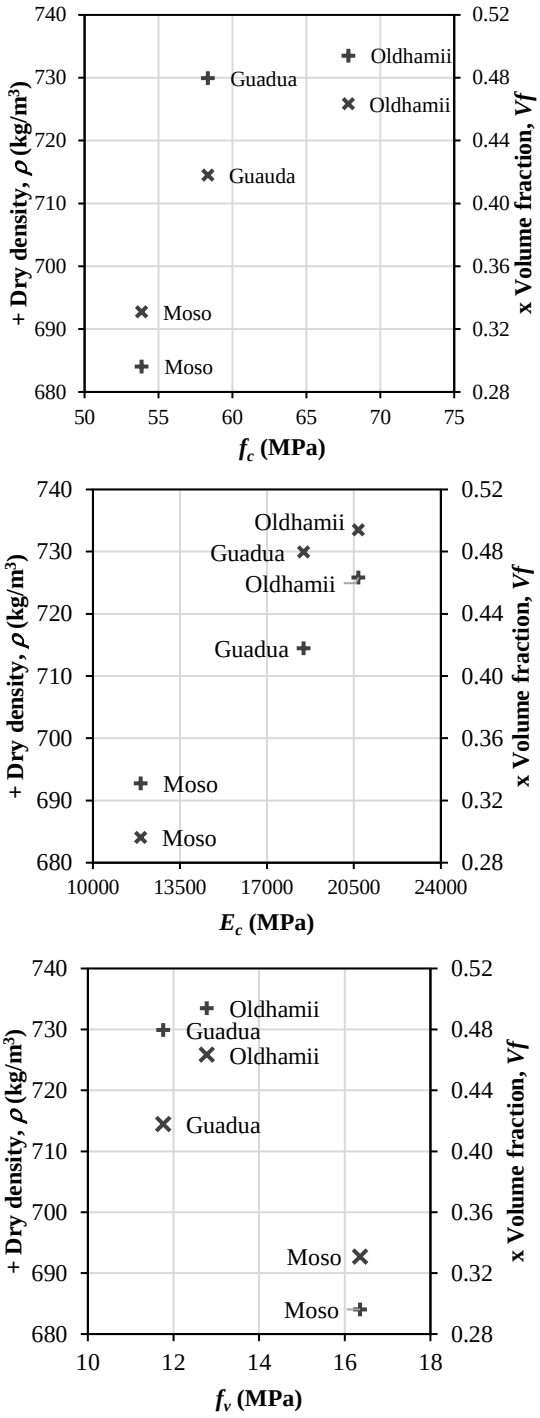

Figure 4.28. Correlation between mean values of mechanical properties with density and volume fraction

	Density	Vol. fraction
Compressive strength		
Moso	-0.019	0.175
Guadua	0.17	0.305
Oldhamii	0.063	0.168
All species[a]	0.787	0.927
Elastic modulus		
Moso	0.427	0.005
Guadua	0.065	0.281
Oldhamii	0.276	-0.076
All species[a]	0.984	0.995
Shear strength		
Moso	0.462	0.323
Guadua	0.162	0.178
Oldhamii	0.333	0.175
All species[a]	-0.962	-0.85

[a]Based on the mean values for each species (Table *4.4*)

Table 4.8. Pearson's correlation coefficients for both individual and mean values

The characteristic values (Tables *4.4*, *4.6* and *4.7*) and correlation coefficients (Table *4.8*) calculated assume that all experimental data follows a normal distribution. This normal distribution hypothesis was tested according to ISO 5479:1997 [183] for a significance level of 0.05 and the results of directional tests for both skewness and kurtosis are summarised in Table *4.9*.

	Skewness		Kurtosis	
	Value	Limit[a]	Value	Limit[a]
Moso				
Density	1.48	0.43	7.18	2.08
Compressive strength	0.41		4.87	
Elastic modulus	0.54		4.79	
Shear strength	0.95		4.77	
Guadua				
Density	0.62	0.43	5.99	2.08
Compressive strength	0.63		2.89	
Elastic modulus	0.15		2.74	
Shear strength	0.8		3.58	
Oldhamii				
Density	0.24	0.34	3.68	2.27
Compressive strength	0.55		4.09	
Elastic modulus	1.17		4.69	
Shear strength	0.49		3.79	

[a]Based on a 0.05 significance level

Table 4.9. Normal distribution directional test results

4.4 Discussion

This chapter presents the development of a semi-automated scan-to-fabrication method to intensively produce clear samples for the material testing of physical and mechanical properties of bamboo poles by extracting specimens from an entire stock of poles involved in a specific construction project. The fabrication method derives from an official Chinese standard (JG/T-199) and is performed through the adaptation of modern, and increasingly affordable, 3D scanning and robotic fabrication technologies. The sampling method of four specimens (two diametrically opposite sampler at each end) per individual pole was conceived as a continuation of the digitisation workflow presented in Chapter *3* and adjusted to extract a consisted number of samples across different bamboo poles while preserving their integrity. The scan-to-fabrication method required the configuration of scanning and robotic equipment to acquire and fabricate clear specimens regardless of the irregularity of individual poles. Details of the setup and milling parameters were given accordingly so that this method can be further implemented for industrial or academic purposes.

The scan-to-fabrication method was validated through its practical implementation on 30 Guadua poles, where samples were fabricated within the tolerances required by the standard. The only dimension that was slightly out of tolerance was the angled plane for the shear sample. According to JG/T-199, the angle should be 106.7° with a tolerance of ±0.3°. This was considered a tight tolerance for a relatively soft material compared to the ±1.0° standard permissible deviation of angular dimensions for relatively hard materials (e.g. steel) within a fine tolerance class [202]. It can be argued that the tolerance proposed by the Chinese code is relatively out-of-context when compared with the tolerances proposed for other dimensions (e.g. width or length), however, separate research would be needed to assess and adjust the tolerances proposed by JG/T-199, if needed.

The fabrication procedure can be potentially extrapolated to any other fabrication needs, for example, connections or structural components, driven by digital modelling and design while exploiting the multi-task and versatility

of a robotic arm. Pushing fabrication processes for bamboo poles into digital technologies would help to integrate bamboo poles and their entire production, structural design, assembly and building management into modern platforms (e.g. BIM) that are already being developed within the building industry.

The fabricated samples E_c, f_c and f_v were subsequently subjected to testing. The samples for compression and shear parallel to the fibres were tested until failure. Figures *4.12* and *4.14* show the typical failure observed in compression and shear samples, respectively. Before failure developed in the compression samples, both matrix and fibres acted as a composite material. However, as the matrix is squeezed, the lateral support for the fibres is reduced which produces a buckling failure of the fibres [203]. As shown in Figure *4.12b*, the typical compressive failure is shown as a shear band at 45°, similar to what has been observed in previous studies [63]. In the case of the shear test, the failure mechanism was developed through the shearing of the matrix alone as the load path does not mobilise the fibres. As shown in Figure *4.14* a clean-cut parallel to the fibres was observed, in agreement with previous experimental observations [204,205].

The bamboo procured for this study was representative of the commercially available material in three global regions with very different levels of industrial development reflected in distinct local plantation management practices and treatment methods (Table *4.3*). The physical and mechanical properties of all three studied species (Table *4.4*) were within the range of values for Moso and Guadua found in previous studies [15,53,57,93,98,206,207], noting that equivalent information for Oldhamii was not found in the literature. All three species showed a relatively large difference between the mean and characteristic values (Table *4.4*) similar to what has been found in the literature. . The difference between mean and characteristic values varied 65% in average, with a range of 37% to 83% depending on the property and species.

The variability range between the different species can be related to the different treatment methods as they are likely to modify the internal physical structure of bamboo to varying degrees which in turn can affect its mechanical

properties as shown by Daud et al. [205] for leaching and by Yongqian et al. [208] for carbonisation treatments. Additional comparison studies beyond the scope of this work are therefore required to study the effect of these complex factors on the properties of bamboo which further justifies the need to adopt a single and consistent testing standard for clear bamboo specimens. Moreover, all specimens in this study were extracted from the bottom part of the harvested bamboo poles and so this variability is expected to increase if samples are taken from other parts of the culms due to the change in the anatomical arrangement of the material along the length of bamboos [49].

The approach of testing all bamboo poles contained in a stock was combined with a systematic sorting based on average properties per bamboo pole, limiting the groups to a minimum of approximately eight poles (or 30 clear bamboo samples), and therefore, use these groups to manage the physical and mechanical variability and reduce its impact on design values. The compressive elastic modulus was taken as an example to group the bamboo poles within their species from which characteristic values were estimated (Table *4.6*). Results showed that creating smaller groups effectively reduces the impact of material variability in the characteristic value of each group by at least 7% when compared to the ratio obtained per species. The range of average compressive elastic modulus for Oldhamii was relatively high in comparison with Moso and Guadua (Table 4.6). This explains the high coefficient of variation obtained per species (0.38) and even per group (0.25 - 0.30). Table *4.7* shows the sorting and grouping of baboo poles regardless their species. This was aimed at distributing the Oldhamii poles among the Moso and Guadua ones, and therefore, reduce the characteristic value over the mean across the groups. In average the characteristic value was further reduce by 2%, except for groups 8 and 9, which were majorly comprised by the Oldhamii poles. The results showed that intensive measuring combined with the sorting and grouping of the material sharing a relatively small range of properties between them can significantly help to manage the variability of physical and mechanical properties and improve the further estimation of design values within a stock of poles. It should be noted that the sorting and

grouping of the poles was based on one single property, the compressive elastic modulus, and therefore, the same sorting and grouping procedure should be repeated for the other physical and mechanical properties. This is due to the lack of correlation found between the different physical and mechanical properties.

The Pearson correlation coefficients for all individual samples did not show any significant correlation between density or volume fraction and any of the mechanical properties studied (Table *4.8*). As shown in Figures *4.26* and *4.27*, the data for each property/species are clustered in a specific region of the graph without showing any potential pattern. This further indicates that neither density nor volume fraction would be suitable parameters to adopt as the basis for a potential grading or sorting system that systematically manages the variability issues. On the contrary, the corresponding correlation coefficients considering only the mean values of these properties for each species show a relatively strong correlation (Figure *4.28* and Table *4.8*). This correlation agrees with the established notion that compressive strength and stiffness increase for denser species with higher fibre content as both matrix and fibres are likely to be mobilised to act as a composite element to resist axial effects. It also suggests that shear strength reduces for denser species with higher fibre content as the matrix constitutes the main resisting component (due to the orientation of the fibres) and its density is 2–3 times lower than that of the fibres [53]. This, however, is a broad assumption taken from average values of only three species and limited samples. Therefore, it does not offer a solution to predict or estimate the inherent variability of a species and might suggest that systematic testing of more specimens and species are needed to improve the general understanding of material properties.

Directional tests to assess the normality of the experimental results showed that, apart from the skewness of the compressive strength in Moso, elastic modulus in Guadua and density in Oldhamii, all other data deviated from a normal distribution to varying degrees (Table *4.9*). No previous knowledge exists on the probability distributions of the physical and

mechanical properties of bamboo and so it is not possible to draw any definite conclusions on the significance of this deviation based only on the relatively limited results of this study. The results presented in this Chapter have been, nonetheless, calculated based on the assumption of a normal distribution to provide an initial benchmark for further studies to assess the suitability of this and other probability distribution models subject to the future availability of comprehensive and consistent experimental datasets for these and other species.

4.5 Summary

This chapter focused on the problems that the inherent physical and mechanical variability of bamboo poles causes for their implementation as construction material within the building industry. The limited information about material properties from different species of bamboo poles suitable for construction purposes, together with the high material variability found in the literature were the main reasons to develop an intensive testing methodology based on small clear specimens to measure material properties and quantify the variability contained within a designated stock of bamboo poles. This method deviates from a standard procedure of performing a destructive test on a representative sample of a stock of bamboo poles considered for a construction project to determine a single characteristic value for each material property. In contrast, the individual testing method measures every bamboo pole involved in a construction project to quantify the material variability and implements a systematic sorting of the material, proposing a range of characteristic values depending on the group to which the poles belong.

The main practical challenge of testing the entire stock of poles was the fabrication of the samples which is directly related to the efficiency of the testing procedure. A semi-automated scan-to-fabrication method was developed and implemented, allowing the efficient and accurate extraction of samples through a digital-driven procedure that adapts to the unique geometric characteristics of each pole. With the current flow towards digital management and automated construction processes, the scan-to-fabrication

method presents a high potential and compatibility within the future digital processes of the building industry, not only for sample fabrication but also for structural bamboo components. The semi-automated procedure presented in this Chapter can also be tied-up with the geometric digitisation presented in Chapter *3* to become an integral workflow to effectively quantify the properties of individual bamboo poles and store the geometric, physical and mechanical properties in a single and robust database.

Test results were analysed both per species and on an individual basis to assess the suitability and the benefits of an individual testing method. However, it was found that due to the low number of samples extracted from each pole the characterisation of individual poles was not beneficial in comparison with the characterisation per species. Therefore, the intensive testing procedure implemented on the entire stock of poles was combined with a sorting approach to manage the variability of the physical and mechanical properties. It was found that creating small groups of bamboo poles balance the factors involved in the determination of characteristic values, which in turn can produce an improvement of structural design values for bamboo poles.

The individual testing methodology here proposed to measure physical and mechanical properties is a suitable approach for the immediate implementation of bamboo poles as a ready to use and sustainable construction material and tackles the inherent variability associated with a specific stock of poles. Future research and, more importantly, bamboo producers, can adopt this method as a quality control procedure for bamboo poles involved in a construction project, and at the same time, support the further development of a robust understanding of material variability, based on clear bamboo samples, to inform the development of future design guidelines for bamboo as a construction material.

- Blank -

5 Behaviour of bamboo poles in bending

5.1 Overview

Chapters *3* and *4* presented different digital workflow approaches for the intensive quantification and further management of geometric, physical and mechanical properties of a stock of bamboo poles to be implemented for structural purposes. As part of the workflow, this Chapter focuses on the bamboo's bending properties and behaviour. Bamboo poles can undergo relatively large deformations in bending, reaching deflections between three to nine per cent of the span before failure [57,78], whereas structural timber beams, for example, are limited to deflections under one per cent of the span [25]. This suggests that only a portion of the bending capacity of bamboo poles can be effectively used for structural applications and that portion would potentially lie within the elastic range of the material.

The elastic bending modulus of bamboo poles depends on the interaction between their constituent parts, matrix and fibres, which mechanical properties and proportion normally differ between poles [49,61,209]. Previous research has focused on the study of the tensile and compressive behaviour of bamboo and its constituent elements based on much simpler small clear bamboo experimental tests and have confirmed the significantly different tensile and compressive elastic properties of the material [49,53,61,63]. Structural materials with different elastic modulus in compression and tension are denominated bimodulus materials and were first introduced by Timoshenko [210]. This theory was later applied to modern fibre-reinforced composites with their constituent materials having different elastic moduli [211–213]. Although bamboo poles have been already identified as a natural fibre-reinforced material [49,53], the elastic bending modulus is still estimated considering bamboo as isotropic [214].

The bending capacity of bamboo poles is currently estimated following the Euler-Bernoulli linear elastic theory [215]. Some studies, experimental and analytical, have used this theory to estimate the bamboo's structural

behaviour (e.g. deformation) and ultimate strength (e.g. stresses) [57–59,76,78,177,205], all of them following the international standard for the determination of physical and mechanical properties of bamboo poles [66]. The typical pure-bending failure mechanism is associated with the exceedance of tension or compression strength at mid-span of the beam, however, in several bending experiments a splitting failure mechanism has been observed [57,58,216], but there has been no clear definition on what is the critical state of stresses that originates them.

As an organic material, bamboo poles are sensitive to the variation of humidity in their surrounding environment, causing the contraction and expansion of the cross-section and thus the appearance of cracks on the bamboo's surface. Surface cracks always appear along the height of the pole, and they propagates in the same direction. This effect might be related to the unidirectional fibre reinforcement that is found in bamboo poles [6]. In contrast with timber elements where a solid section with longitudinal and tangential reinforcement can reduce crack propagation, the hollow section of bamboos and common thin-walled characteristic makes the surface cracking critical as there is less material to avoid the propagation of a crack. The structural behaviour of a bamboo pole with an open-section has not yet been studied based on the assumption that cracked or damaged bamboos are discarded for construction purposes [66]. Besides, drying techniques have been developed to reduce surface cracking of bamboo poles [55]. Nevertheless, there are no further studies that confirm the complete mitigation of cracking phenomena in bamboo poles, meaning that cracks can appear at any point in the bamboo's working life and its mechanical behaviour will correspond to that of an open cross-section element. A common practical solution for surface cracking in bamboo construction is to tangentially reinforce the bamboo poles with steel bands close to the connections to prevent cracking and its propagation [186], but there have been no studies that assess the effectiveness of this practical measure in the bending behaviour.

This Chapter focuses in the following research objectives related to the study of bamboo poles in bending: i) develop a material model for bamboo

poles to estimate the bending elastic modulus and predict the strain and stress distribution of a section considering the bimodulus characteristic of the material based on test results of small clear samples; ii) understand the bending failure mechanism through the comparison of closed formed linear equations and experimental observations; iii) investigate the bending structural behaviour of open and reinforced cross-sections of bamboo poles through experimental tests; and iv) investigate the isolated effect of geometric variability (diameter and thickness taper and out-of-straightness) of bamboo poles subjected to bending through the implementation of their digital geometric data. The results obtained from these objectives will form part of the digital workflow providing the relevant bending properties and structural behaviour to support the design, construction and management of natural bamboo pole structures.

5.2 Analytical elastic model for bamboo poles in bending

The current international standard for bamboo construction ISO 22157:2019 [66] specifies the adoption of full-size experimental testing to determine the elastic bending properties of bamboo poles. These full-size bending tests are usually difficult to implement due to the high amount of material, space and testing machine size required, and their corresponding results formulation is based on standard bending theory that neglects the composite nature of the material. Consequently, the estimation of the elastic modulus, as well as the stresses and strains developed in a cross-section, are not representative, which diminish the potential to quantify the structural reliability of bamboo structures. This section focuses on the development of an analytical bending model considering the fundamental principles of unidirectional composite materials which is based on simple experimental compression tests of small clear bamboo samples and basic imaging processing to determine the volume fraction of fibres. This analytical model is validated through full-scale, experimental four-point bending tests on Moso (Phyllostachys pubescens) bamboo poles.

5.2.1 Analytical model

Bamboo is a natural composite material and so the contribution of its constituents, matrix and fibres, to resist tensile and compressive stresses will vary as a function of their relative stiffnesses under each of these stresses. The tensile stiffness of bamboo fibres is a couple of magnitudes higher than the comparatively flexible matrix [49] and therefore this model neglects the contribution of the matrix to the tensile stiffness of bamboo in bending. On the contrary, a contribution from both fibres and matrix acting compositely is considered for the compressive stiffness of the poles. As such, the proposed bimodulus bending model is based on the use of the elastic modulus of fibres for the tensile region of the cross-section and the combined elastic modulus of both matrix and fibres for the compression region. The cross-sectional fibre content is assumed constant and equal to the average value across the bamboo wall as the effect of the fibre gradient is considered negligible for thin poles with a diameter-thickness ratio greater than eight [48,62]. Therefore, the effect of the fibre gradient on thick poles is beyond the scope of this work. The bamboo's variable geometry was simplified and assumed to be a uniform circular thin-walled tube, following the idealisation adopted in ISO 22157 [66]. The model is based on a linear-elastic material and follows the principles of the Euler-Bernoulli beam theory [217].

Figure *5.1* shows a bamboo cross-section idealised as a thin ring of average radius, $\bar{R}$, and thickness, *t*, together with its linear strain and stress distribution in bending. The bilinear stress distribution assumes two different elastic moduli namely, E_c, in compression (matrix and fibres) and E_t, in tension (fibres only). The distance, $\bar{y}$, from the extreme fibre in tension to the neutral axis defined in terms of the angle θ and shown in Figure *5.1*, is given by:

$$\bar{y} = \bar{R}(1 - \cos\theta) \tag{5.1}$$

From compatibility of deformations and Eq. *5.1*, the strain, ε, within the section is defined by:

$$\varepsilon = \frac{\varepsilon_t}{\bar{y}} y = \frac{\varepsilon_t}{\bar{R}(1-\cos\theta)} y \tag{5.2}$$

where ε_t is the tensile strain at the section's extreme fibre and y, expressed as a function of the angles θ and α shown in Figure *5.1*, is given by:

$$y = \bar{R}(\cos\alpha - \cos\theta);\ 0 \le \alpha \le \pi \tag{5.3}$$

Substituting Eq. *5.3* in Eq. *5.2* gives:

$$\varepsilon = \varepsilon_t \frac{\cos\alpha - \cos\theta}{1 - \cos\theta};\ 0 \le \alpha \le \pi \tag{5.4}$$

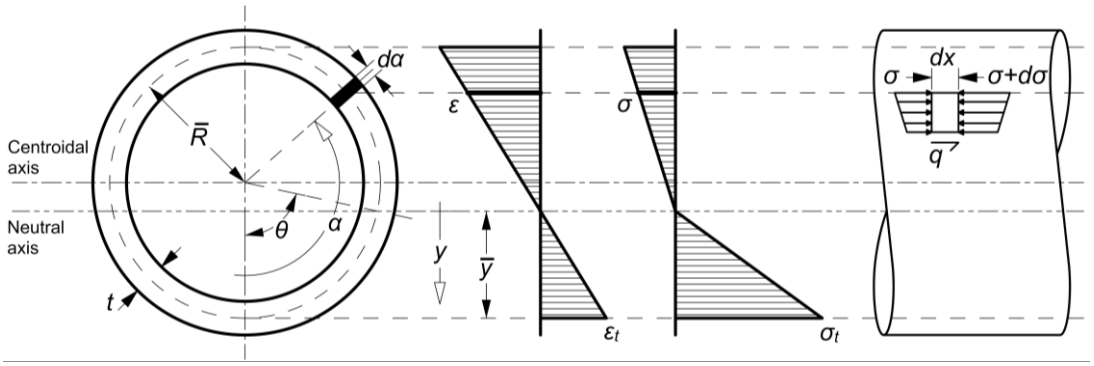

Figure 5.1 Bamboo cross-section and corresponding strain and stress distribution in bending

From Hooke's law [217], the tensile and compressive forces, dF_t and dF_c, acting on an infinitesimal sector of the tube are:

$$dF_t = E_t \varepsilon\, dA \tag{5.5}$$

$$dF_c = E_c \varepsilon\, dA \tag{5.6}$$

where:

$$dA = \begin{cases} t\bar{R}V_f\, d\alpha;\ 0 \le \alpha \le \theta \\ t\bar{R}\, d\alpha;\ \theta < \alpha \le \pi \end{cases} \tag{5.7}$$

The volume fraction, V_f, of the cross-section is defined as the ratio between the area of fibres, A_f, and its total area, A:

$$V_f = \frac{A_f}{A} \tag{5.8}$$

Defining the modular ratio, n_r, as:

$$n_r = \frac{E_c}{E_t} \tag{5.9}$$

and integrating Eq. *5.5* and *5.6* lead to the total tensile and compressive forces, F_t and F_c, acting on the section:

$$F_t = \frac{E_t \varepsilon_t V_f t \bar{R}}{1-\cos\theta}\left[2\int_0^{\theta}(\cos\alpha - \cos\theta)\, d\alpha\right]$$

$$= 2E_t \varepsilon_t V_f t \bar{R}\,\frac{\sin\theta - \theta\cos\theta}{1-\cos\theta} \quad (5.10)$$

$$F_c = \frac{n_r E_t \varepsilon_t t \bar{R}}{1-\cos\theta}\left[2\int_{\theta}^{\pi}(\cos\alpha - \cos\theta)\, d\alpha\right]$$

$$= 2n_r E_t \varepsilon_t t \bar{R}\,\frac{(\theta-\pi)\cos\theta - \sin\theta}{1-\cos\theta} \quad (5.11)$$

From equilibrium:

$$F_t + F_c = 0 \quad (5.12)$$

and substituting Eq. *5.10* and *5.11* in *5.12* leads to:

$$\left(V_f - n_r\right)(\tan\theta - \theta) - n_r\pi = 0 \quad (5.13)$$

which defines the position of the neutral axis (i.e. angle θ) as a function of both the volume fraction, V_f, and modular ratio, n_r, of the section.

The bending moment acting on the section is calculated from the product of the tensile and compressive forces in Eq. *5.5* and *5.6* and their corresponding distances to the centroidal axis:

$$M = 2\int_0^{\theta}(\bar{R}\cos\alpha)\, dF_t + 2\int_{\theta}^{\pi}(\bar{R}\cos\alpha)\, dF_c =$$

$$= \frac{2t\bar{R}^2 E_t \varepsilon_t}{1-\cos\theta} *$$

$$\left[V_f\int_0^{\theta}(\cos^2\alpha - \cos\alpha\cos\theta)\, d\alpha + n_r\int_{\theta}^{\pi}(\cos^2\alpha - \cos\alpha\cos\theta)\, d\alpha\right] \quad (5.14)$$

From bending theory [217]:

$$\frac{M}{E_{eq} I} = \frac{\varepsilon_t}{\bar{y}} \quad (5.15)$$

where *I* is the second moment of area of a thin circular tube:

$$I = \pi t \bar{R}^3 \quad (5.16)$$

and so, substituting Eq. *5.14* and *5.16* into *5.15*, the equivalent modulus of the bamboo pole, E_{eq}, can be defined as:

$$E_{eq} = \frac{2E_t}{\pi} *$$

$$\left[V_f\int_0^{\theta}(\cos^2\alpha - \cos\alpha\cos\theta)\, d\alpha + n_r\int_{\theta}^{\pi}(\cos^2\alpha - \cos\alpha\cos\theta)\, d\alpha\right] \quad (5.17)$$

Integrating and simplifying Eq. *5.17* leads to:

$$E_{eq} = KE_t \tag{5.18}$$

where *K* is a factor introduced for convenience:

$$K = \frac{1}{\pi}\left[\left(n - V_f\right)\frac{\sin 2\theta}{2} + \left(V_f - n\right)\theta + n_r\pi\right] \tag{5.19}$$

and the bending moment (Eq. *5.14*) is simplified as:

$$M = \frac{I}{\bar{y}}E_{eq}\varepsilon_t \tag{5.20}$$

The bending stresses, σ, within the section are defined by:

$$\sigma = \begin{cases} E_t\varepsilon = E_t\varepsilon_t\frac{\cos\alpha - \cos\theta}{1-\cos\theta};\ 0 \le \alpha \le \theta \\ E_c\varepsilon = n_rE_t\varepsilon_t\frac{\cos\alpha - \cos\theta}{1-\cos\theta};\ \theta < \alpha \le \pi \end{cases} \tag{5.21}$$

Rearranging Eq. *5.20*:

$$E_t\varepsilon_t = \frac{M\bar{y}}{IK} \tag{5.22}$$

and substituting Eq. *5.22* in *5.21* gives the general expression for the bending stress distribution within the section:

$$\sigma = \begin{cases} \frac{My}{IK} = \frac{M\bar{R}}{IK}(\cos\alpha - \cos\theta);\ 0 \le \alpha \le \theta \\ \frac{n_rMy}{IK} = \frac{nM\bar{R}}{IK}(\cos\alpha - \cos\theta);\ \theta < \alpha \le \pi \end{cases} \tag{5.23}$$

Also, from an equilibrium of horizontal forces in Figure *5.1*:

$$\int \sigma\, dA + q\, dx - \int(\sigma + d\sigma)\, dA = 0 \tag{5.24}$$

and thus, the shear flow, *q*, is defined by:

$$q = \int \frac{d\sigma}{dx}dA \tag{5.25}$$

Substituting Eq. *5.7* and *5.23* in *5.25*:

$$q = \begin{cases} \frac{dM/dx}{IK}\int_0^{\alpha}\bar{R}(\cos\alpha - \cos\theta)V_ft\bar{R}\, d\alpha\ ;\ 0 \le \alpha \le \theta \\ \frac{n_rdM/dx}{IK}\int_{\alpha}^{\pi}\bar{R}(\cos\alpha - \cos\theta)t\bar{R}\, d\alpha\ ;\ \theta < \alpha \le \pi \end{cases} \tag{5.26}$$

and knowing that the shear force, *V*, is defined as [217]:

$$V = \frac{dM}{dx} \tag{5.27}$$

leads to:

$$q = \begin{cases} V\frac{V_f t\bar{R}^2}{IK}(\sin\alpha - \alpha\cos\theta);\ 0 \le \alpha \le \theta \\ V\frac{n_r t\bar{R}^2}{IK}[(\alpha-\pi)\cos\theta - \sin\alpha];\ \theta < \alpha \le \pi \end{cases} \quad (5.28)$$

and to the expression for the shear stresses, τ, within the section:

$$\tau = \frac{q}{t} \quad (5.29)$$

To estimate the elastic modulus of a bamboo pole considering its fundamental composite condition, Eq. *5.18* can be used. This equation requires only two parameters: modular ratio, n_r, and volume fraction of the section, V_f. When both modular ratio and volume fraction are equal to one, the stresses and strains are equal to the ones estimated for an isotropic standard material. Eq. *5.4, 5.23* and *5.29* can predict the strain and stresses distribution in the cross-section of a bamboo pole if the bending moment is given.

5.2.2 Experimental programme

The proposed analytical bending model for bamboo poles was calibrated against the results of a series of experimental four-point bending tests on twenty Moso (Phyllostachys pubescens) bamboo poles (the material description of these samples correspond to the twenty Moso bamboo poles described, tested and analysed in Section *4.3* and presented in Table *4.3*), comparing the apparent modulus of elasticity in bending, E_b, obtained from these tests with the equivalent modulus of elasticity, E_{eq}, calculated from Eq. *5.18*. The bending test setup for the apparent modulus of elasticity followed the general requirements in [66], and the set-up, as well as the testing procedure, is shown in Figures *5.2* and *5.3*. The setup consisted of a hydraulic servo-controlled actuator Popwil MAS-300 with a maximum capacity of 300 kN and a stroke length of 500 mm (Figure *5.2*). Vertical displacement was measured at the mid-span (Figure 5.2) using a displacement measurement laser sensor Sick OD-Precision with a maximum range of 400 mm and an accuracy of 0.4 mm. The load and displacement data were gathered with a multi-channel data logger TML TDS-530 at a rate of 1 Hz. Figure 5.3 shows the typical set-up of the bending test before the load is applied through a pair of 37.5 mm wooden saddles. The load was applied at a rate of 0.5 mm/s until

failure. Based on a clear span, L, of three metres for all poles (approximately 30 diameters), E_b was calculated as [66]:

$$E_b = \frac{23F_{lin}L^3}{1296I_b\Delta_{lin}} \quad (5.30)$$

where F_{lin} and Δ_{lin} are the maximum applied load (N) and the corresponding mid-span deflection (mm) within the linear range of the load-displacement curve determined based on a least-squares regression with a coefficient of determination (R^2) of 0.99. The second moment of area, I_b (mm^4), is given by Eq. *3.9* in Section *3.2.4*. The moisture content of each pole, ω_{Eb}, was measured according to [66].

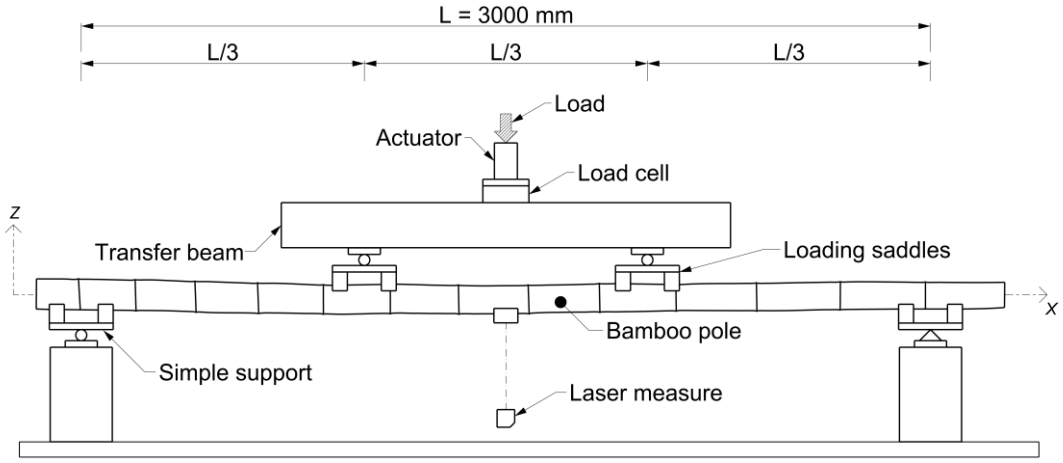

Figure 5.2. Four-point bending test set-up [66]

Figure 5.3. Four-point bending test

To obtain the required parameters to calculate the equivalent modulus of elasticity E_{eq} (modular ratio and volume fraction), small clear bamboo specimens were taken from the ends of the poles before conducting the four-

point bending tests (the clear samples correspond to those presented in Section *4.3.1*). In that way, the procedure to estimate the equivalent modulus of elasticity in bending can be derived from much simpler testing procedures and becomes part of the intensive digital workflow to measure the mechanical properties of bamboo poles.

The compressive elastic modulus, E_c, was determined based on the Chinese industry-standard JG/T-199 [65] and the sampling procedure presented in Section *4.3.1*. Accordingly, two diametrically opposite small clear samples, 60 mm long × 15 mm wide × wall thickness, were extracted from the sacrificial internodes at each end of the bamboo poles (Section *4.2.1,* Figure *4.1*). The value of E_c for each pole was calculated as the average value of all samples extracted from each pole adjusted to the moisture content of the source pole at the time of the four-point bending test to allow a direct comparison such that [65]:

$$E_{\mathrm{c}} = \frac{1}{n_s}\sum \frac{K_{E\mathrm{c}}}{K_{E_b}}\frac{\Delta_\sigma}{\Delta_\varepsilon} \quad (5.31)$$

where n_s is the number of samples (four); Δ_σ is the stress difference between the minimum (5 MPa) and maximum (20 MPa) stress limits [65] and Δ_ε is the corresponding deformation difference measured at these stress limits. K_{Ec} and K_{Eb} are the correction factors for the effect of moisture content given by [65]:

$$K_{E_{\mathrm{c}}} = \frac{1}{0.89+0.36e^{-0.1w_{E_c}}} \quad (\S\ 4.3.1\ \text{Eq. } 4.6)$$

$$K_{E_{\mathrm{b}}} = \frac{1}{0.89+0.36e^{-0.1w_{E_b}}} \quad (5.32)$$

and w_{E_c} and w_{E_b} are the moisture contents at the time of testing of the small clear sample and the full-size pole tested in bending, respectively.

The volume fraction of the poles, defined in Eq. *5.8*, was calculated based on the digital processing of images taken from cross-sections of four small compression strength specimen blanks adjacent to the E_c samples (Section *4.3.1*). These specimens were lightly sanded with 600/1200 grit silicon carbide sanding paper before capturing their image with a Nikon D7200 camera equipped with an AF-S DX Micro NIKKOR 85 mm f/3.5G ED VR lens. The area of fibres was calculated using a bespoke Matlab script (developed

by others within the UCL BIM Bamboo group), which follows the procedure described in Section *4.3.1*.

The tensile elastic modulus, E_t, was inferred from the four-point bending tests results of a control sample of two poles (*eM019* and *eM020*) instrumented with five axial strain gauges at the mid-span section, with a sensitive grid of 10 mm x 3 mm (length x width) in a quarter-bridge configuration and a resistance of 120 Ω. These strain gauges were installed on the front face of the poles ($0 \leq \alpha \geq 180°$ in Figure *5.1*) at equal (45°) intervals. The position of the neutral axis was calculated from the intersection, *a*, of a best-fit line obtained from a stress-strain plot, and so, the angle θ (Figure *5.1*) can be obtained from:

$$\cos\theta = \frac{-a}{\bar{R}} \tag{5.33}$$

Knowing the value of θ, the tensile elastic modulus can be calculated from Eq. *5.9* and *5.13* as:

$$E_t = \frac{E_c(\theta - \tan\theta - \pi)}{V_f(\theta - \tan\theta)} \tag{5.34}$$

To compare the measured values of strain from the test, theoretical strain distributions for poles *eM019* and *eM020* were obtained from Eq. *5.2* based on the maximum tensile strain ε_t (Figure *5.1*) calculated from Eq. *5.22* as:

$$\varepsilon_t = \frac{M_{lin}\bar{y}}{IKE_t} \tag{5.35}$$

where M_{lin} is the maximum bending moment within the linear portion of the load-displacement curve given by:

$$M_{lin} = \frac{F_{lin}L}{6} \tag{5.36}$$

5.2.3 Results

Figure *5.4* shows a typical load-displacement diagram, where the values of F_{lin} and Δ_{lin} are found based on a least-square regression. Figure *5.5* shows a typical stress-strain plot of the compressive elastic modulus and the required loading/unloading cycles. The original digital image of the wall thickness of a

sample, together with its corresponding post-processed binary one, from which the volume fraction is estimated, is shown in Figure *5.6*.

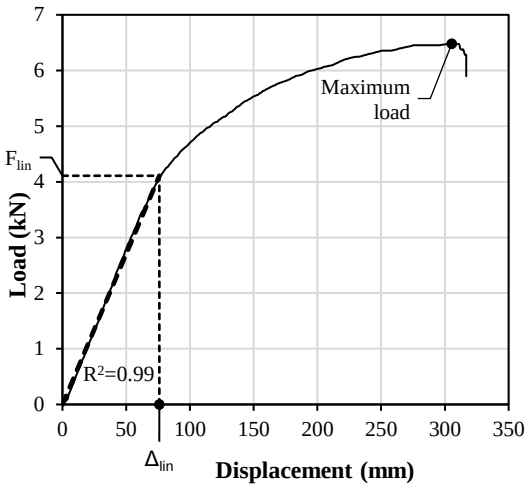

Figure 5.4. Typical load-displacement diagram and assumed linear range (pole eM003)

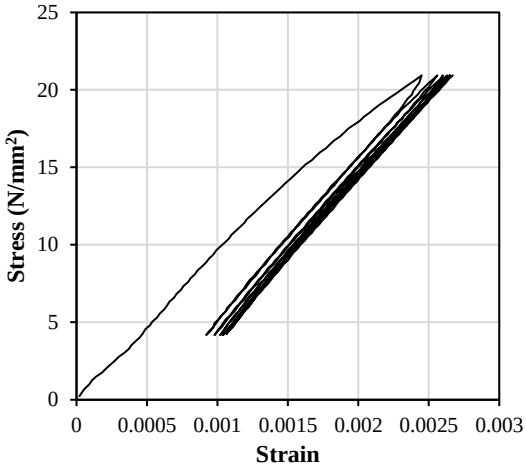

Figure 5.5. Typical stress-strain curve of a small clear bamboo sample (pole eM005)

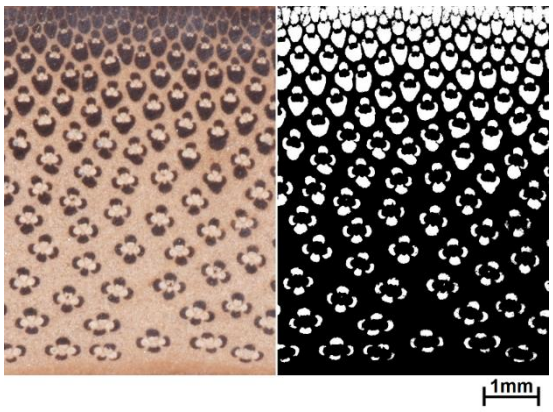

Figure 5.6. Digital image of the bamboo wall and its corresponding binary image (pole eM003)

The longitudinal strains measured for both poles at the maximum force within the linear range, F_{lin}, are shown in Figures *5.7* and *5.8*, displaying the expected linear distribution and shift of the neutral axis towards the tension region of the cross-section. The values of E_t obtained for poles *eM019* and *eM020* using Eq. *5.33* were 46,440 N/mm^2 and 45,740 N/mm^2 respectively. These values are in very good agreement with the elastic modulus of fibres of 46,000 N/mm^2 obtained by Amada et al. [49] applying the rules of mixtures for composites to the experimental results of tensile tests on thin bamboo slices. Based on these findings, a constant value for E_t of 46000 N/mm^2 was assumed for the estimation of the equivalent modulus of elasticity in bending (E_{eq}). Numerical results of E_{eq} are shown in Figure *5.9* and Table *5.1* including a comparison with E_b and E_c. Figures *5.7* and *5.8* also show the theoretical strain distribution for each control pole (*eM019* and *eM020*) calculated from the analytical model.

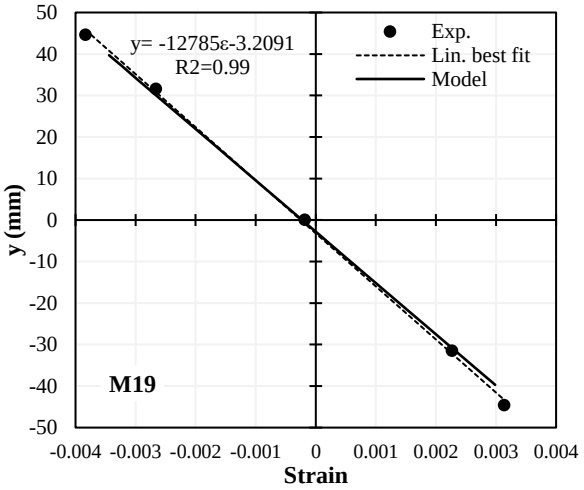

Figure 5.7. Analytical and experimental longitudinal strain distribution (pole eM019)

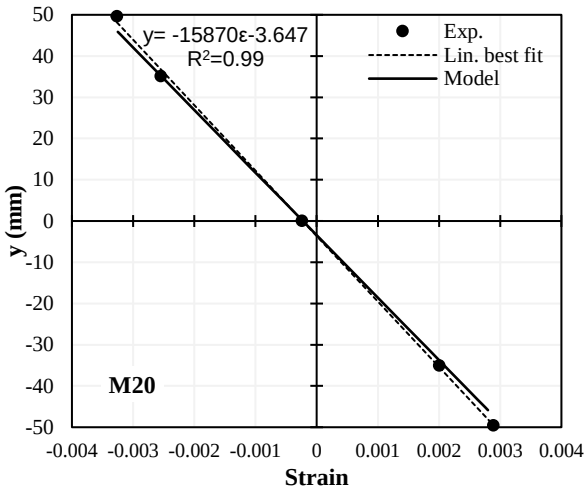

Figure 5.8. Analytical and experimental longitudinal strain distribution (pole eM020)

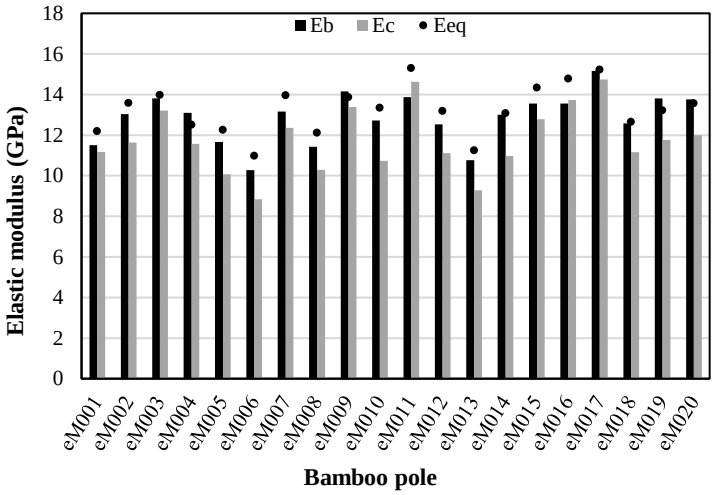

Figure 5.9. Analytical and experimental elastic moduli

Pole	D (mm)	t (mm)	w_{Eb} (%)	E_b (MPa)	E_c (MPa)	vf	E_{eq} (MPa)
eM001	95.1	8.8	15.7	11512	11169	0.29	12198
eM002	94.6	8.5	15.5	13026	11633	0.35	13591
eM003	90.4	9.0	13.5	13807	13205	0.32	13984
eM004	84.3	9.8	13.4	13098	11567	0.30	12511
eM005	92.9	7.3	14.1	11664	10072	0.33	12256
eM006	90.4	8.4	14.4	10280	8835	0.31	10983
eM007	95.0	7.6	12.1	13167	12354	0.35	13964
eM008	88.4	8.0	13.1	11431	10288	0.32	12118
eM009	88.4	8.6	14.2	14159	13374	0.31	13865
eM010	82.2	6.4	18.9	12722	10735	0.37	13343
eM011	95.3	6.8	14.4	13875	14627	0.35	15301
eM012	83.5	9.0	15.0	12528	11104	0.35	13195
eM013	94.5	8.4	13.0	10758	9275	0.31	11259
eM014	95.0	7.1	13.5	12998	10963	0.35	13083
eM015	87.0	7.8	12.6	13551	12775	0.35	14337
eM016	99.2	6.7	10.5	13551	13727	0.35	14788
eM017	96.3	7.6	10.7	15163	14735	0.34	15233
eM018	91.2	9.2	10.8	12579	11162	0.32	12655
eM019	89.2	9.8	10.8	13806	11757	0.33	13227
eM020	99.2	7.5	12.0	13754	11996	0.34	13565

Table 5.1. Summary of analytical and experimental results

There is good agreement between the analytical and experimental modulus of elasticity with an average difference of 4.5% providing a suitable level of confidence in the proposed model to quantify the cross-sectional bending strain and stress distribution in bamboo poles in bending. It is also interesting to note that these results show an average difference of 9.5% between E_{eq} and the compressive elastic modulus of the small clear samples, E_c, which could be a useful parameter to adopt in preliminary conceptual designs subject to confirmation by further studies. By way of illustration, Figure *5.10* shows the results of the bimodulus model applied to one of the control poles (*eM020*) to predict the theoretical strain and stress distributions under the experimental four-point bending test from Eq. *5.2, 5.23, 5.29* and *5.35*. For comparison, this figure also includes the strain, ε', as well as the normal, σ', and shear, τ', stress distributions calculated from standard bending theory for isotropic material given by [218]:

$$\varepsilon' = \frac{\sigma'}{E_{eq}} \tag{5.37}$$

$$\sigma' = \frac{M\bar{R}\cos\alpha}{I} \quad (5.38)$$

$$\tau' = \frac{V\sin\alpha}{\pi t\bar{R}} \quad (5.39)$$

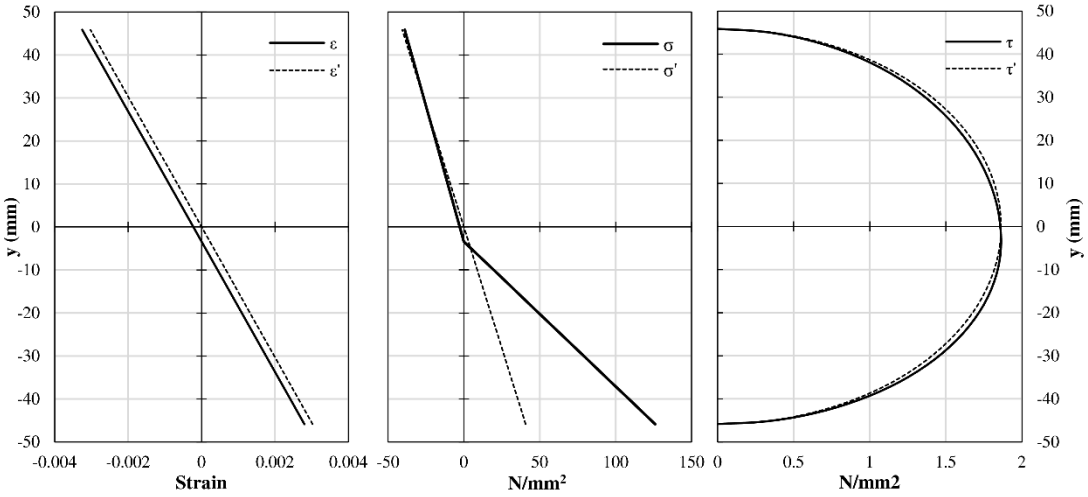

Figure 5.10. Theoretical strain and stress distributions from bimodulus model and standard bending theory (pole eM020)

The strains calculated from the proposed model show a linear distribution with the expected shift of the neutral axis towards the tension region of the cross-section. This shift in the neutral axis position and the significantly higher normal tensile stresses predicted by the bilinear model contribute to achieving a more accurate representation of the overall cross-sectional bending stress distribution in bamboo poles compared to that based on standard bending theory.

5.3 Failure mechanism of bamboo poles in bending

The combination of theoretical analysis and experimental observations have been essential to helping describe the failure mechanism of bamboo poles in bending. For example, Vaessen & Janssen [216] performed several four-point bending tests to determine the minimum clear span that leads to pure bending behaviour and subsequent failure. During their experiment, apart from the typical pure-bending failure associated with direct (compression and tension) stresses, a splitting failure, mainly originating at the load application, was also recorded. This failure has been associated with the longitudinal shear that develops along the bamboo and is maximum at the cross-section's neutral axis [81,187], however, the shear effect is dismissed

as long as the minimum clear span is ensured. In another study [58], splitting and crushing failures, originating at the loading points, were also recorded, even though the minimum length for a pure bending behaviour as suggested by [214,216] was followed. These failures were described as local kink or crushing of the section and were associated with the tensile stresses in the circumferential direction, however, no further investigation of the mechanism that originated them was performed.

Apart from the potential longitudinal shear and circumferential stresses, there are two types of structural instability in bending for the particular case of cylindrical thin tubes that can cause failure but have not been yet considered in the relevant testing and design standards [69,214]: i) ovalisation and ii) local buckling. The ovalisation instability was first studied by Brazier [219] and consists of the transversal and inextensible ovalising deformation of an originally straight circular tube when subjected to pure bending leading to a critical limiting moment where the tube can no longer support loads. After this point the section becomes unstable and a kink is formed. This theory was further developed into more accurate numerical solutions [220], however, simple closed-form equations have proved to give valid results when compared to experimental values [221]. Studies suggest that the ovalisation effect becomes more critical for composite materials, such as bamboo poles, as they have different mechanical properties along and across their length [222–224]. These studies have also presented closed-form equations that depend on the anisotropy ratio, which is the ratio of axial to transversal elastic modulus and strength [223,225], reducing the limiting ovalising moment. Local buckling refers to the buckling of the wall thickness due to compression stresses and can be assessed by setting the compressive stress at the extreme fibre equal to the stress corresponding to classical buckling of a tube loaded uniformly in axial compression [221]. For unidirectionally reinforced materials, the anisotropy ratio also plays an important role in the ultimate buckling capacity of thin-walled cylindrical tubes [226].

This section investigates the different stress and instability state of bamboo poles when subjected to four-point bending and assesses the

significance of these to produce a failure mechanism. The data for this analysis was taken from the four-point bending tests of Moso (Phyllostachys pubescens) bamboo poles performed in Section *5.2*. Subsequently, the results of the stress and instability analysis are contrasted with the corresponding failure mechanism observed in each sample during the experimental tests.

Bamboo poles are herein considered as straight, cylindrical and hollow thin-walled tubes, with length (*L*), diameter (*D*) and thickness (*t*) following [214]. In conformity with Section *5.2*, the bamboo poles are assumed as a linear elastic unidirectional composite material with fibres running along the length of the pole. The poles are subjected to four-point bending, as shown in Figure *5.2*, where the maximum applied bending moment (M_m; N-mm) can be estimated by [66]:

$$M_m = \frac{F_m L}{6} \tag{5.40}$$

where F_m is the maximum applied load before failure (N) and *L* is the length (mm). As shown in Section *5.2.1*, the maximum compressive (σ_c) and tensile (σ_t) stresses are estimated by Eq. *5.23* for $\alpha = 0$ and $\alpha = \pi$ respectively, and the maximum shear stress (τ_{max}) is estimated by Eq. *5.29* when $\alpha = \theta$.

The local buckling capacity of a thin-walled cylindrical composite tube can be estimated as [226]:

$$\sigma_b = \frac{\sqrt{E_b E_{tr}}\, t}{\bar{R}\sqrt{3}\sqrt{1-\sqrt{\nu^2 \frac{E_{tr}}{E_b}}}} \tag{5.41}$$

where $\bar{R}$ is the average radius (mm) of the cross-section (as shown in Section *5.2.1*), E_b is the apparent elastic modulus of elasticity (N/mm^2) given by Eq. *5.30* in Section *5.2.2*, ν is the Poisson's ratio defined as 0.3 as an average value found between different sources [162,227,228] and E_{tr} is the transverse elastic modulus (N/mm^2).

The Brazier's ovalising critical moment for unidirectionally reinforced cylindrical tubes is defined by [223]:

$$M_{cr} = \frac{2\sqrt{2}}{9}\,\pi \bar{R} t^2 \sqrt{E_b E_{tr}} \tag{5.42}$$

The circumferential stresses in a tube subjected to four-point bending are developed through the concentration of load applied at each loading point and can be idealised as shown in Figure *5.11*, where the critical positive and negative moments - acting at the cross-section of a ring with a length (L_{rc}) equal to the length of the loading saddle - are calculated as follows [218]:

$$M_{n+} = \frac{3V_n\bar{R}}{4\pi} \tag{5.43}$$

$$M_{n-} = -\frac{1.2815V_n\bar{R}}{4\,\pi} \tag{5.44}$$

where V_n is the applied load (N) by each loading saddle and M_{n+} & M_{n-} are the maximum positive and negative bending moments (N-mm) acting in an axis perpendicular to the plane of the ring located at the neutral axis of the curved beam's cross-section in flexure (NA_{cb} in Figure *5.11*). These moments create transverse tension and compression stresses which are only carried by the matrix as fibres are oriented along the pole. According to the literature, the compression strength of the matrix is a couple of magnitudes higher than the tension one [15], therefore, the circumferential tension stresses (N/mm^2) are critical at the inner and outer side of the wall thickness (σ_{ti+} and σ_{to-}, respectively) and are given by [218]:

$$\sigma_{ti+} = \frac{M_{n+}\,c}{I_{rc}}\left[\frac{c}{3e}\,\frac{1-\frac{e_n}{c}}{\frac{\bar{R}}{c}-1}\right] \tag{5.45}$$

$$\sigma_{to-} = \frac{M_{n-}\,c}{I_{rc}}\left[\frac{c}{3e}\,\frac{1+\frac{e_n}{c}}{\frac{\bar{R}}{c}+1}\right] \tag{5.46}$$

$$I_{rc} = \frac{L_{rc}t^3}{12} \tag{5.47}$$

$$e_n = \bar{R} - \frac{2\,c}{\ln\frac{\frac{\bar{R}}{c}+1}{\frac{\bar{R}}{c}-1}} \tag{5.48}$$

where c is half the wall thickness (mm), I_{rc} is the moment of inertia of the ring's cross-section (mm^4) and e_n is the distance (mm) from the centroidal axis to the neutral axis of the curved beam measured toward the centre of curvature (see Figure *5.11*).

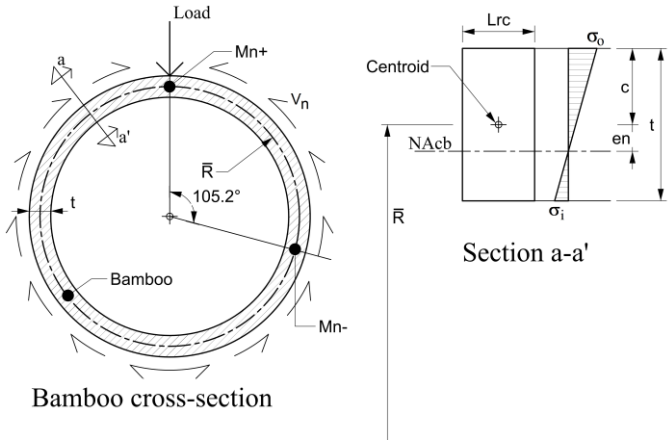

Figure 5.11. Diagram of circumferential moments and stresses acting on a ring of length L_{rc}.

Table *5.2* shows the basic experimental data collected from the twenty Moso (Phyllostachys pubescens) bamboo poles tested in Section *5.2.2*, together with the compressive and shear strength of the same twenty poles measured through the experimental testing of clear bamboo samples presented in Section *4.3.1*, which were extracted before the bending tests. All samples were classified as thin-walled according to the limits suggested by [48,62]. The ultimate moment for pole *eM018* is not shown in Table *5.2* as the pole came of the supports during the test without failing. The length of the loading saddle (two at each loading point as shown in Figure *5.2*) for these tests was 37.5 mm spaced at 75 mm. The nominal strength of Moso bamboo fibres (f_t) can be taken as 600 N/mm^2, according to previous experiments performed by Amada et al. [49]. The transverse elastic modulus (E_{tr}), was adopted as 1685 N/mm^2 which is the average modulus obtained through experimental tests of Moso bamboo rings loaded in the transverse direction [229]. Circumferential tensile strength (f_{tr}) of Moso bamboo was taken as 7.6 MPa, according to numerical estimations based on experimental tests [230].

Pole	***D*** (mm)	***t*** (mm)	M_m (kN-mm)	f_c (N/mm^2)	f_v (N/mm^2)
eM001	95.1	8.8	3.2	55.6	15.2
eM002	94.6	8.5	2.6	53.9	17.1
eM003	90.4	9.0	3.2	62.3	17.0
eM004	84.3	9.8	2.6	54.2	17.4
eM005	92.9	7.3	2.0	48.6	16.6
eM006	90.4	8.4	2.2	45.0	13.8
eM007	95.0	7.6	2.4	51.0	17.1
eM008	88.4	8.0	1.7	42.2	13.3
eM009	88.4	8.6	2.8	54.1	17.5
eM010	82.2	6.4	0.9	48.5	15.0
eM011	95.3	6.8	2.4	52.7	17.7
eM012	83.5	9.0	2.2	52.7	17.2
eM013	94.5	8.4	2.4	48.2	15.9
eM014	95.0	7.1	2.7	48.9	15.4
eM015	87.0	7.8	2.1	56.6	16.4
eM016	99.2	6.7	3.0	58.6	17.3
eM017	96.3	7.6	3.8	65.0	16.9
eM018	91.2	9.2	-	53.8	15.8
eM019	89.2	9.8	3.0	55.6	16.9
eM020	99.2	7.5	3.3	69.8	17.6

Table 5.2. Experimental data collected from poles eM001 to eM020

Figure *5.12* shows the stress-displacement diagram for each of the twenty samples tested. These test results were used to map the range at which bending curves occurred, forming a benchmark envelope defined by the upper and lower stress-displacement curves (*eM017* and *eM010*) meeting at the maximum recorded displacement (of pole *eM003*) using straight lines and so, containing all stress-displacement curves within the perimeter formed. The purpose of the envelope is to compare further experimental tests of Moso bamboo poles within this Chapter.

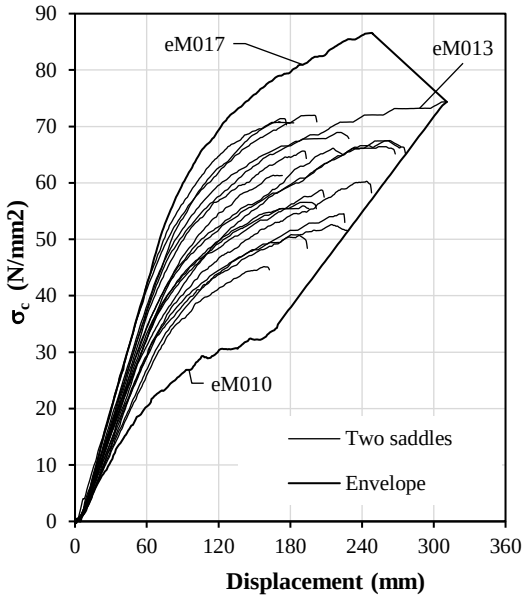

Figure 5.12. Stress-displacement diagram for twenty samples. These results were used to create a benchmark envelope

During the experimental tests, three types of failure mechanism were observed: i) local kink under the saddle; ii) four longitudinal splits (top, bottom and sides of the cross-section); and iii) a combination of the previous two with one of them being more dominant. Even though the minimum length recommended for four-point tests was followed [66], not a single one of the failure mechanism could be related to the typical bending failure of beams through direct (compression or tension) stresses within the middle span. This coincides with similar experimental results [58] where only one per cent of the samples had a clear typical bending failure in the tension region due to direct stresses (the rest being associated with shear, kink, circumferential tension or crushing).

The local kink was a failure where deformation of the top of the cross-section occurred under one of the loading saddles, preceded by cracking sounds, and its development could be appreciated with the naked eye (saddle slowly digging into the bamboo forming a kink). Sample e*M010* is an example (Figure *5.13*) where only a local kink deformation is visible without showing any other additional damage. The longitudinal split failure was brittle, preceded by cracking sounds starting at the second half of the test, but occurring too fast so that the failure could only be captured with a video

camera. The length of the split was at least one metre, centred from the loading saddle where the failure originated. Sample *eM017* is an example of longitudinal split failure (Figure *5.14*) where a longitudinal crack is visible a fraction of a second before failure. From these twenty samples, four samples presented local kink, seven samples presented split failure, eight were a combination of both, with six dominated by local kink and two by splitting, and one sample (*eM018*) came off the supports without experiencing failure. Figure *5.15* shows the combination failure dominated by a local kink under the loading saddle with the additional longitudinal split. Although samples failing by longitudinal split registered the highest stresses and samples failing by local kink the lowest (e.g. samples *eM017* and *eM010* respectively), there was no clear threshold for either stresses or deflections to form groups according to the type of failure. Similarly, there was no correlation observed between the type of failure and the diameter-to-thickness ratio, which might be related to all poles being classified as thin-walled tubes.

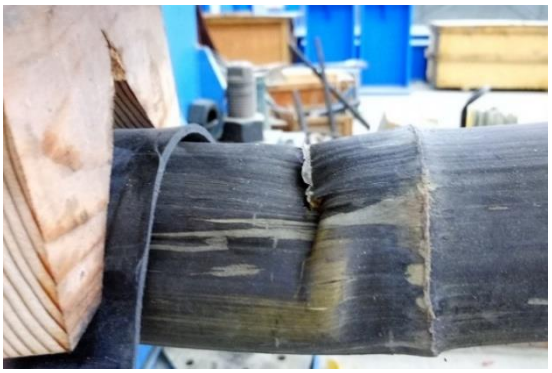

Figure 5.13. Sample eM010 loaded with short saddles, showing local kink failure

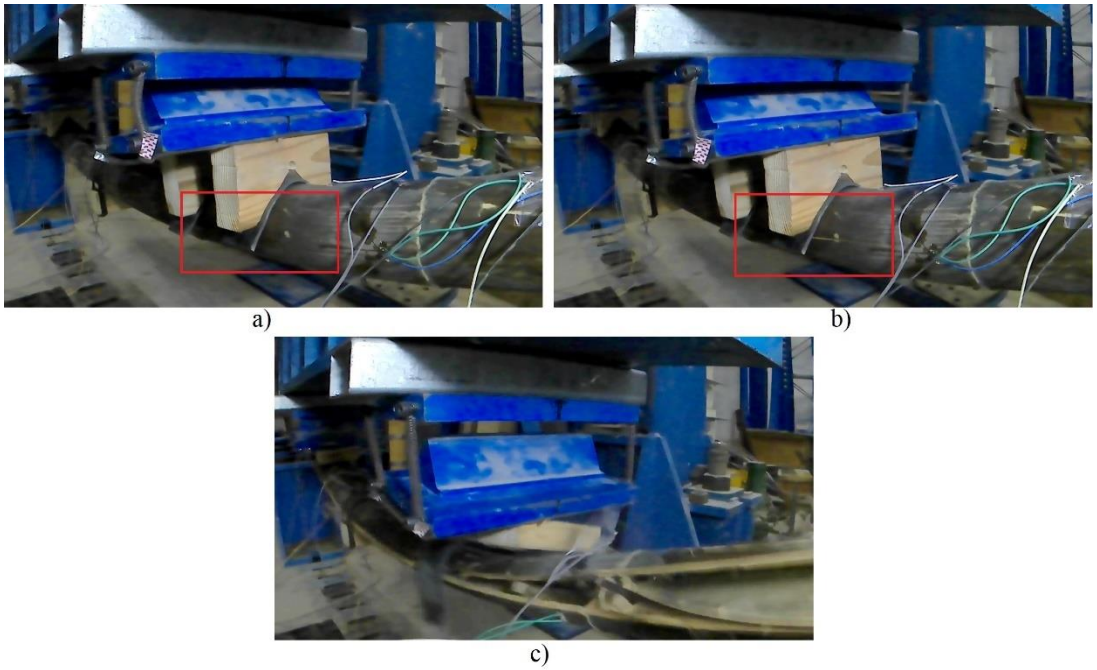

Figure 5.14. Sample eM017 loaded with short saddles, showing longitudinal split before (a), during (b) and after (c) failure

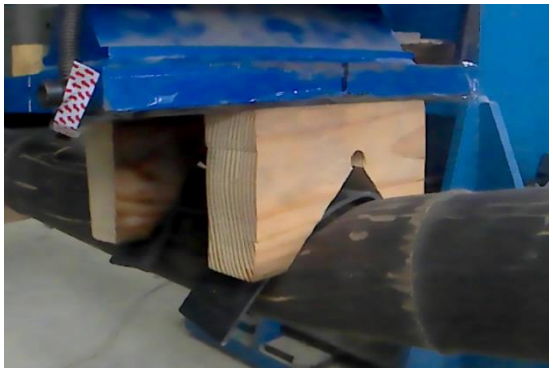

Figure 5.15. Sample eM013 loaded with short saddles, showing a combined failure dominated by local kink under loading saddle, but also developing the typical longitudinal splitting

Table *5.3* shows the numerical results for the maximum stresses and stability limits in the longitudinal and circumferential direction of the Moso bamboo poles subjected to four-point bending loaded with short saddles. Values for *eM018* were not included as the pole did not fail. It is noticeable that direct tension and shear stresses were about a third of the strength of the material and therefore no failure mechanism could be expected from these states of stresses. Local buckling and ovalisation were also excluded as a potential reason for failure because critical values were ten and five times higher than the compressive stress and ultimate moment, respectively,

however, as these values depend on the individual anisotropy ratio of each pole (unknown in this case), stability checks should not be avoided.

Pole	σ_c (N/mm^2)	σ_t (N/mm^2)	τ_{max} (N/mm^2)	σ'_b (N/mm^2)	M_{cr} (kN-m)	σ_{ti+} (N/mm^2)	σ_{to-} (N/mm^2)
eM001	59.7	218.9	5.3	553	14.6	27.1	10.1
eM002	49.2	157.8	4.5	565	14.4	23.5	8.8
eM003	66.4	214.8	5.5	652	15.8	24.6	9.1
eM004	59.0	212.0	4.5	751	16.4	15.9	5.7
eM005	43.9	153.6	4.0	466	10.1	24.0	9.2
eM006	46.8	180.7	4.2	523	11.8	20.1	7.5
eM007	50.3	159.2	4.6	502	11.8	27.5	10.4
eM008	39.7	142.4	3.4	535	11.1	16.5	6.2
eM009	64.9	213.2	5.3	644	14.3	23.5	8.7
eM010	30.2	96.1	2.5	478	7.1	13.2	5.0
eM011	57.0	169.2	5.1	454	9.8	34.9	13.5
eM012	51.8	170.1	4.1	682	13.8	15.4	5.6
eM013	45.3	172.4	4.2	513	12.8	22.1	8.3
eM014	58.0	191.7	5.4	460	10.1	35.4	13.6
eM015	52.0	160.6	4.3	572	11.3	20.9	7.8
eM016	65.2	198.2	6.2	424	9.9	46.5	18.0
eM017	79.4	237.6	7.1	526	12.7	44.1	16.8
eM018	58.7	-	-	-	-	-	-
eM019	58.8	197.0	4.9	781	19.6	19.5	7.1
eM020	63.2	205.9	6.1	488	12.5	40.5	15.5

Table 5.3. Numerical results for the stress and stability analysis for poles loaded with short saddles

The maximum compression stress for each pole (σ_c) was about ±10% of its corresponding average compressive strength (f_c), however, no failure or damage was observed in the compression region of the poles during the experiments. This can be explained by the fact that σ_c and f_c are both estimated following certain assumptions (e.g. geometric) meaning that surpassing the nominal strength by a minimum percentage does not justify the failure. Besides, the lack of a compression failure during the tests, the relatively high circumferential tensile stresses (Table *5.3*) in comparison with the average strength (Table *5.2*) and the non-linear behaviour of the stress-displacement curves (Figure *5.12*) starting at approximately 60% of the maximum load [66] suggest that the calculation of direct stresses at the maximum load might be misleading. The reason is that the non-linearity of the stress-displacement bending curves (Figure *5.12*) could not be related to the

non-linearity of the material. Analysing experimental stress-displacement curves of tension [61] and compression [53] material tests, it was found that the linear behaviour accounted for approximately 95% and 85% of the maximum stress (for tension and compression, respectively), therefore, it is unlikely that the non-linearity in bending observed at approximately 60% of the stress is caused by the material. This, in turn, suggests that damage of the tube could start at an early stage of the test, potentially induced by circumferential tension stresses (which explains the cracking sounds), producing a loss in bending stiffness (non-linearity) and a change in the internal load path of the tube.

By looking at the values of circumferential tensile stresses σ_{ti+} (Table *5.3*), this is, the inner circumferential stresses developed at the location of the maximum positive moments (M_{n+}) as shown in Figure *5.11*, it was found that the stresses of each bamboo at 60% of the maximum bending load had already surpassed the average circumferential strength of the bamboo, according to [230]. This suggest that internal cracks had developed in that region, and those cracks were therefore responsible for the observed loss in stiffness but did not produce the failure of the element. It is likely that failure occurred once σ_{to-} (outer tensile stress developed at the location of the maximum negative moment M_{n-} as shown in Figure 5.11) reached a critical state, however, how the final mode of failure (local kink or splitting) was reached could not be yet explained. The potential of crack development due to circumferential stresses also suggests that the estimation of the compressive strength (σ_c) is not necessarily applicable and that alternative load paths through the cross-section are likely due to the damage inflicted in the tube. Therefore, a local kink under the loading saddle or the four longitudinal splits are failure mechanisms originating from the same source (circumferential tensile strength) only affected by the localised effect of a relatively short loading saddle.

To prove this hypothesis, an extra set of four-point bending tests were performed. Five Moso bamboo poles (the number of samples was reduced due to time constraints) holding the same general characteristics of the

benchmark were prepared and subjected to the bending test following the same procedure and setup (Figure *5.2*), with the only variation that a single loading saddle of 300 mm replaced the two 37.2 mm ones, expecting to see a reduction of the local kink under the saddle. Table *5.4* shows the experimental data collected from the five extra bending tests using long loading saddles. To measure both compressive and shear strength (Table *5.4*), as well as compressive elastic modulus and volume fraction to estimate direct and shear stresses, small clear samples were extracted from the five poles before the four-point bending tests, following the sampling and testing methodology presented in Chapter *4*.

Pole	D (mm)	t (mm)	M_m (kN-mm)	E_b (Mpa)	f_c (N/mm^2)	f_v (N/mm^2)
eM103	95.7	9.7	3.0	11040	49.9	19.4
eM105	89.0	7.8	2.0	10500	45.2	16.7
eM108	99.0	9.0	3.7	12444	63.4	20.3
eM109	89.4	9.0	3.0	12653	63.7	20.8
eM110	92.6	7.4	1.5	9696	51.7	16.9

Table 5.4. Experimental data collected from poles loaded with a single 300 mm saddle

Figure *5.16* shows the stress-displacement diagram for each of the five samples tested with a single 300 mm saddle at the loading points. Comparing these curves with the benchmark envelope shows that the stress-displacement behaviour of these five samples is within the same range (linear elastic up to approximately 60% of ultimate load). However, samples only failed with the sudden four longitudinal splits (type ii) as shown in Figure *5.17*, also preceded by cracking sounds, and therefore showing a piece of evidence that the increase in saddle length reduces the local kink effect but circumferential stresses are still likely to produce a failure mechanism.

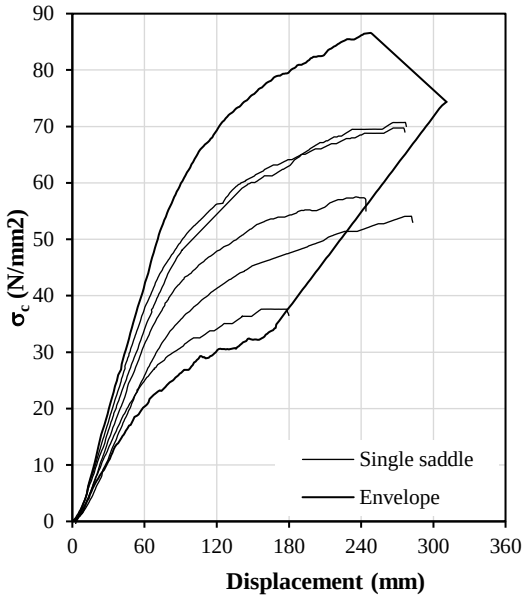

Figure 5.16. Stress-displacement diagram for five samples loaded with long saddles (300 mm). The benchmark range is also displayed.

Figure 5.17. Sample eM107 loaded with single saddle displaying the typical longitudinal split failure

The numerical analysis of maximum stresses in the five poles loaded with a single 300 mm saddle (Table *5.5*) shows identical results than those of the benchmark, with the only difference that circumferential stresses (σ_{ti+} and σ_{to-}) are proportionally lower with respect of the length of the saddle however still within the range of the material strength. These results in combination with the experimental observations confirm that the bending failure of bamboo poles is governed by the circumferential capacity of the material.

Pole	σ_c (N/mm^2)	σ_t (N/mm^2)	τ_{max} (N/mm^2)	σ_b (N/mm^2)	M_{cr} (kN-m)	σ_{ti} (N/mm^2)	σ_{to-} (N/mm^2)
eM103	50.8	229.8	4.5	601	17.4	7.0	2.6
eM105	48.1	217.7	4.1	494	10.1	6.9	2.6
eM108	60.9	207.5	5.8	559	16.4	10.5	3.9
eM109	65.2	244.2	5.3	630	14.7	7.7	2.8
eM110	32.2	145.1	3.0	433	9.3	5.8	2.2

Table 5.5. Numerical results for the stress and stability analysis for poles loaded with long saddles

5.4 Bending behaviour of open and reinforced bamboo cross-sections

Section *5.3* helps to better understand the failure mechanism in bamboo poles in bending and the influence of local effects such as loading saddles, however, the analysis only applies for bamboo poles with closed cross-sections. Because of the organic nature of bamboo poles, it is also essential to investigate the behaviour and failure mechanism for poles with open cross-section, open-reinforced cross-section and closed-reinforced cross-section. This section aims to investigate bamboo poles with these characteristics when subjected to bending through a short experimental testing programme.

A total of twenty Moso bamboo samples were tested (Table *5.6*) from which the first group of five samples were bamboo poles with open cross-sections (prefix "*eM2*"), the following two groups were made of five open-section samples reinforced with steel bands spaced at approximately one (prefix "*eM3*") and three (prefix "eM4") diameters respectively, and the last group of five poles were closed-section samples reinforced with steel bands at approximately one diameter (prefix "*eM5*"). The artificial crack was manually produced within the central span, where bending stresses are maximum, and approximately a diameter away from the end of each loading saddle to avoid interference with the load concentration (Figure *5.18*). The crack was produced with an angle grinder equipped with a 100 mm wood blade giving a final crack width of approximately 2 mm, which is compared with natural surface cracks on bamboo poles. The bending setup and procedure were the same as previous (Section *5.2.2*), using single 300 mm loading saddles to avoid local effects.

Pole	D (mm)	t (mm)	M_m (kN-mm)	E_b (N/mm^2)	σ (N/mm^2)
eM216	106.8	12.3	3961	10161	51.0
eM222	102.5	10.9	3031	11127	46.5
eM224	96.6	10.9	2638	10116	46.4
eM229	96.8	11.0	2405	11513	42.0
eM233	95.8	10.7	2588	10614	47.1
eM318	98.0	9.8	3280	11690	60.0
eM325	107.6	10.7	3909	11268	54.3
eM330	87.3	10.3	2786	12353	64.7
eM331	90.4	8.2	3470	14208	86.7
eM332	90.9	8.3	1810	10164	44.3
eM427	91.4	10.7	2249	10842	45.8
eM428	87.0	9.3	2639	14964	65.9
eM434	83.7	7.1	1614	11992	53.7
eM435	89.1	9.5	1805	10895	42.1
eM421	92.6	7.9	1892	11336	46.2
eM512	99.9	10.6	3082	8865	51.3
eM513	85.6	8.6	2244	11097	61.7
eM517	95.0	8.4	2880	12570	63.2
eM520	96.4	9.0	2152	8321	43.5
eM521	98.5	11.7	3619	9918	58.1

Table 5.6. Experimental data collected from poles tested with open ("*eM2*"), reinforced ("*eM3*" and "*eM4*") and closed-reinforced ("*eM5*") cross-section

Figure 5.18. Artificial crack within the central span, a diameter away from the loading saddles and oriented towards the top of the cross-section

As the crack is relatively small compared to the diameter, the increment on the direct stresses regardless of the orientation of the crack was not considered significant. Therefore, direct stresses can be approximated using the geometric properties of a closed-section. A similar assumption can be made for the shear stress, except when the crack is oriented at the neutral axis. At this orientation, the crack is located exactly at the position where shear

stresses are maximum, this means that the maximum shear stress will concentrate at the opposite side of the crack, doubling its magnitude, however, shear stresses would still be lower than the strength of the material. Similar to "*C"* sections, the shear centre is moved away from the cross-section's centroid and therefore torsional forces are produced, nonetheless, the effect of torsion was not considered in this study for two reasons: i) the setup for the test does not offer proper rotational restriction for the bamboo, as it only depends on friction [92]; and ii) the test was not instrumented to measure rotational movement or torsional strain.

With these considerations, it is estimated that bending behaviour and failure mechanism of open sections oriented at any point around the cross-section would be practically the same as a closed-section. The only concern is the local buckling capacity which might become critical when the crack is oriented at the top of the cross-section (compression region) as seen in other open-section structural elements subjected to pure bending [231]. Based on these assumptions, the crack of the five open-section samples (*Open*) was oriented towards the compression region.

Time constraints did not allow to extract small clear samples to measure the compressive elastic modulus and volume fraction of these batch of samples, besides, Section *5.3* shows that direct and shear stresses are not critical, therefore, direct stresses were estimated using the standard formula for bending (Eq. *5.38*). The basic experimental data acquired from the four-point bending tests are shown in Table *5.6*.

The stress-deflection diagram for the open-section samples is shown in Figure *5.19*. These samples displayed very different behaviour compared to the closed-section samples. The modulus of elasticity presented similar average results to those found in closed-section samples (Section *5.3*), as shown in Figure *5.20* and Table *5.6*, but the typical non-linear portion of the curves was significantly reduced (Figure *5.19*), although within the benchmark envelope. The average magnitude of direct stresses and maximum displacement were relatively lower compared with closed-section samples (Figure *5.20* and Table *5.6*).

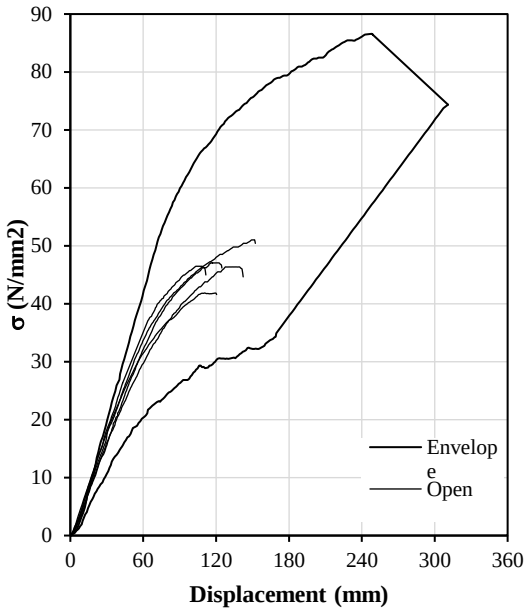

Figure 5.19. Stress-displacement diagram for five open-section samples. The benchmark range is also displayed

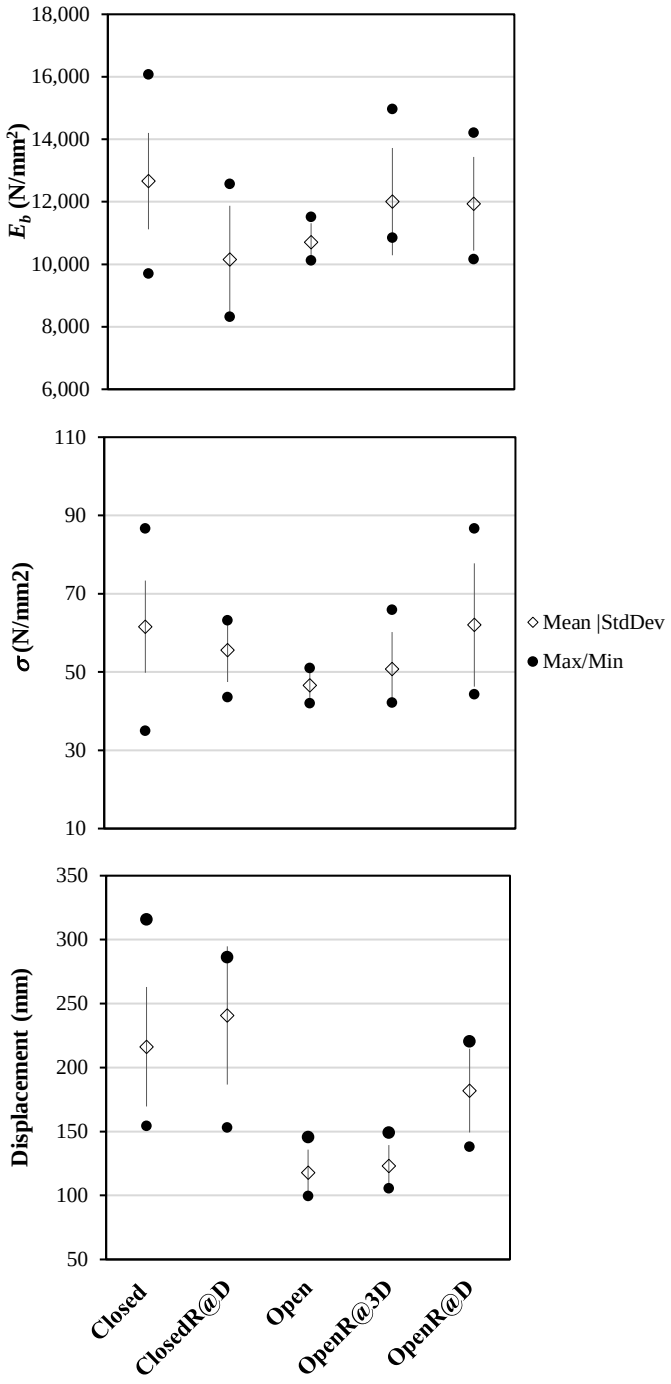

Figure 5.20. Mean, standard deviation and range obtained for apparent modulus of elasticity, direct stress and maximum displacement for the different testing configurations.

The failure mechanism of open-section samples was also different: all samples experienced an outward local buckling failure acting on the open ends of the cross-section occurring at any point within the central span. This

failure mechanism is similar to that observed in *U* and Ω profiles [231] with the difference that the buckling waves did not coincide on each side of the open section as shown in Figure *5.21*. It was also noted that the diaphragm did not have any apparent influence to prevent the buckling mechanism as in some samples the amplitude of the buckling wave was located exactly at the node (Figure *5.22*). This can be related with the low strength capacity of the diaphragms [49] and the fact that diaphragms were perforated prior the preservation treatment, as is the case for many other similar treatment procedures [32,68].

Figure 5.21. Sample eM233 showing typical outward buckling at the open ends of the cross-section. Note that the amplitude of the buckling wave at each side of the crack did not coincide.

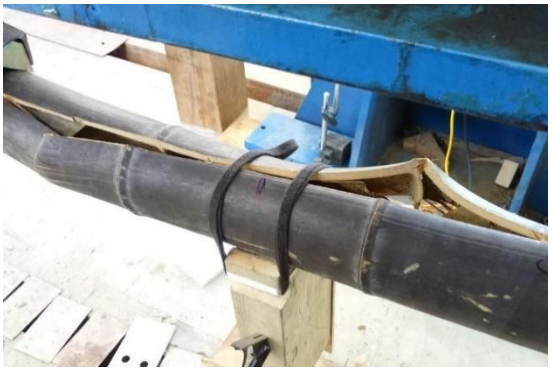

Figure 5.22. Sample eM222 displaying outward buckling failure at the node.

The next two five-group of samples were the ones reinforced with steel bands at approximately one (*OpenR@D*) and three diameters (*OpenR@3D*), the latter being the average distance between nodes and therefore the bands were located at the centre of each internode. The cracks of all the open-reinforced sections were oriented towards the compression region.

The stress-deflection diagrams for the open reinforced samples with steel bands spaced at every one and three diameters are shown in Figure *5.23* and *5.24*, respectively. The apparent modulus of elasticity (E_b) of the two groups of samples was again similar to those obtained for closed-section ones (Table *5.6* and Figure *5.20*). In terms of stresses and deflections, there was a slight increment in average values compared to open-section samples towards values found in closed-section ones (Figure *5.20*). The closer the spacing between steel bands, the more similar was the bending behaviour to a closed-section (Figure *5.23*, *5.24* and *5.20*).

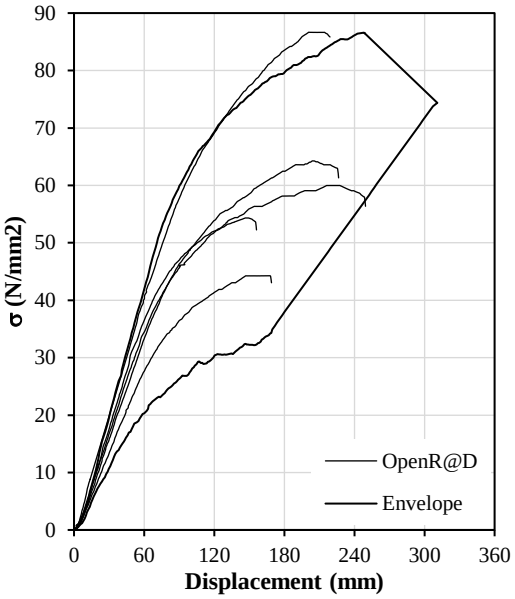

Figure 5.23. Stress-displacement diagram for five open-section samples reinforced at every *D*. The benchmark range is also displayed

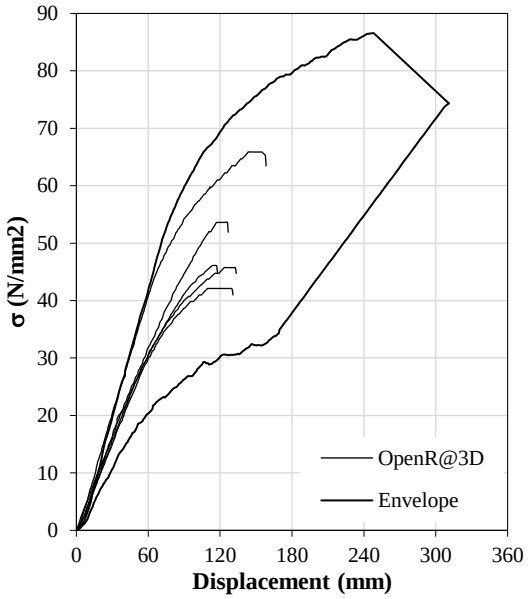

Figure 5.24. Stress-displacement diagram for five open-section samples reinforced at every *3*D*. The benchmark range is also displayed

The failure mechanism for open section samples reinforced at every diameter started with a visible outward local buckling of the open ends, which was well contained between two neighbouring bands (Figure *5.25*). The outward local buckling deformation continued increasing within neighbouring bands until local buckling failure occurred (Figure *5.26*). This type of failure suggests that the bands provided discrete closed cross-sections along the central span together with a tangential reinforcement which prevented the complete development of outward buckling as observed in open-section samples but not sufficiently to prevent a local buckling failure. It also suggests that, if bands were spaced closer than one diameter, the pole with a crack would eventually behave as a closed reinforced bamboo pole and reduce the likelihood of local outward buckling. No effects were observed at the location of the loading/support saddles.

Figure 5.25. Sample eM318 showing initial outward buckling deformation in-between bands of an open reinforced section (OpenR@D).

Figure 5.26. Sample eM325 displaying the typical local kink failure mechanism at the steel band, where the top of the cross-section and the band flattened out (OpenR@D).

In the case of open-sections reinforced with steel bands at every three diameters, the failure was the same as the one observed in open-section samples. This effect was because the spacing between bands was similar to the buckling wavelength, therefore, the amplitude of the wave was simply moved between two neighbouring bands producing an outward buckling failure (Figure *5.27*).

Figure 5.27. Sample eM434 showing typical outward buckling failure in-between bands of an open reinforced section (OpenR@3D)

The effect of tangential reinforcement was also studied by testing closed-section samples with steel bands spaced at every diameter (ClosedR@D) from which stress-deflection diagrams were obtained and showed in Figure *5.28*. The curves were plotted together with the benchmark envelope obtained from the closed-section samples. No clear difference was found either in modulus of elasticity, direct stress, or maximum displacement (Figure *5.20* and Table *5.6*) and the behaviour was relatively contained between the benchmark envelope (Figure *5.28*). The failure mechanism in all five samples was the same: local kink; however, for these samples, the kink occurred right at the location of the steel band, which was located centimetres away from the loading saddle. This is an interesting behaviour because the failure of closed-section samples (local kink or splitting) always occurred under the loading saddle. Longitudinal cracks were also visible; however, they were contained in between the neighbouring bands were the failure occurred (Figure *5.29*). This behaviour suggests that circumferential tension stresses due to the loading saddles were confined by the tangential reinforcement, however, this caused an increment in radial compressive forces exerted by the band, increasing the likelihood of producing a local kink.

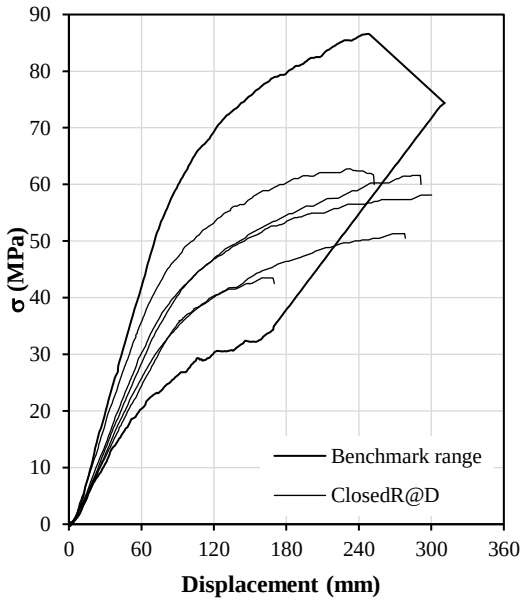

Figure 5.28. Stress-displacement diagram for five closed-section samples reinforced at every *D*. The benchmark range is also displayed

Figure 5.29. Sample eM517 displaying the typical local kink failure for closed-reinforced samples located right at the steel band and away from the loading saddle

5.5 Geometric effects on bamboo poles subjected to bending

The digitisation workflow allows the acquisition of fundamental geometric data from bamboo poles that can be subsequently implemented in structural analysis. This study implements the geometric numerical data to investigate the structural effects caused by the geometric imperfections, inherent of any bamboo pole when the bamboo is subjected to bending moment. The effects of the irregular geometric properties are assessed in terms of the maximum displacement and the distribution of shear forces and bending moments in the local direction of the pole's cross-section. Five Moso (Phyllostachys pubescens) bamboo poles were selected during the four-point bending test programme performed in this Chapter and were subjected to the digitisation workflow presented in Section *3.2*. The scanned poles were *eM103, eM105, eM108, eM109* and *eM110* (Table *5.4*) which general description was presented in Section *4.3* (Table *4.3*). The geometric variations (diameter and thickness taper as well as out-of-straightness) were gradually incorporated to a one-dimensional finite element (FE) model in different iterations, where the result of each iteration was compared against a benchmark model for each corresponding pole containing only average geometric properties as suggested by bamboo design standards [69]. The required modulus of elasticity of each pole to conduct FE analysis was obtained from the apparent modulus of elasticity (E_b) presented in Table *5.4*.

5.5.1 Finite element modelling of digitised bamboo poles

The numerical geometric data obtained from the digitisation workflow was processed through the Rhino3D plugin GeometryGym [232] to gradually incorporate the geometric imperfections of each bamboo pole and further exported to the structural analysis software GSA [233]. The FE models incorporated the geometric imperfections in four stages: i) Model A (Figure *5.30A*), was the benchmark assuming a straight cylindrical hollow tube according to [67,92]; ii) Model B (Figure *5.30B*), was discretised as straight uniform cylindrical tube between nodes and the corresponding equivalent section properties of the internode were assigned to each discrete element; iii) Model C (Figure *5.30C*), was a straight discretised tube with actual irregular cross-section properties; and iv) Model D (Figure *5.30D*), incorporated the spatial deviation of the centroidal line in a discretised tube with actual cross-section properties.

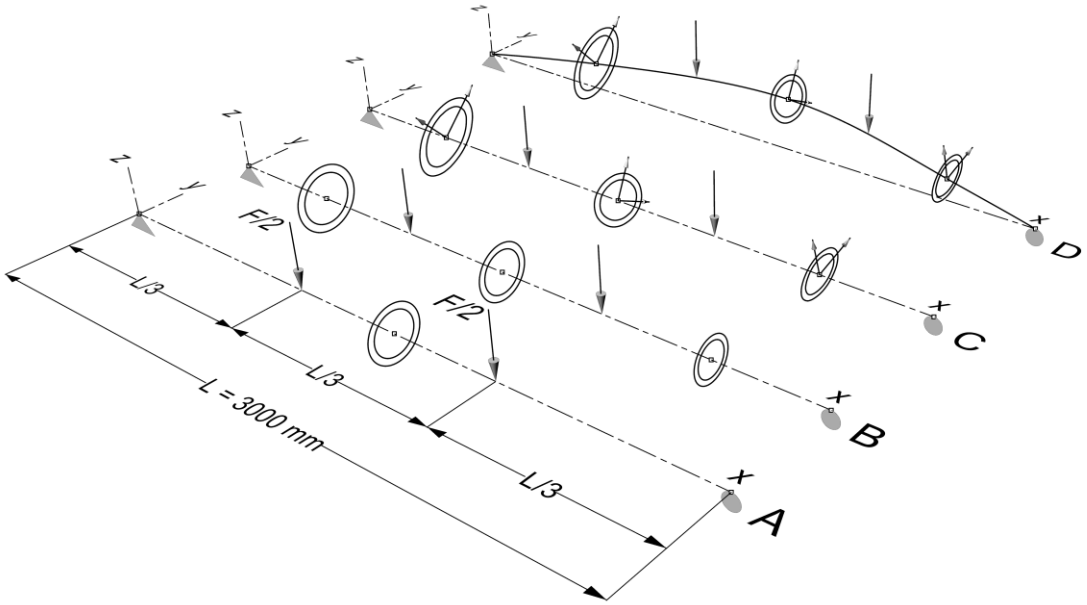

Figure 5.30. Diagram of the structural FE models A, B, C & D, incorporating geometric imperfections in four stages. (Not to scale)

The calculation of the section properties for equivalent and actual cross-sections for each model was performed according to the equations shown in Section *3.2.4*. The modulus of elasticity for each model was assigned according to the results obtained from the bending tests performed on the physical poles (E_b) in Section *5.3*. To assess the geometric effects in isolation,

the material for these five samples was treated as isotropic and a static linear-elastic analysis was performed. The support system consisted of a simply supported beam (Figure *5.30*) without rotational out-of-plane restraints to capture any three-dimensional behaviour of the poles caused by the spatial variation of their geometry. However, torsional restraints at one end of the beam were included in the model for two reasons, first to avoid support instability and second to assess any torsional effects.

The global orthogonal system adopted for structural analysis is shown in Figure *5.30*. A unitary load (F) was applied to all the models in *-Z* direction (Figure *5.30*). According to Figure *3.10*, the principal local axes for the cross-sections in models *C & D* were denominated as *1 & 2* for the major and minor axis respectively. The orientation of the physical poles about their axis (X-axis) was measured and recorded before the performance of the test using the scanning reference markers described in Section *3.2.2,* so the same orientation could be digitally modelled. The difference in the percentage of the maximum deflection between Model *A,* and Models *B, C* and *D* was estimated as:

$$\Delta_{\delta} = \frac{uz_A - uz_{B,C,D}}{uz_A} \qquad (5.49)$$

where *uz* is the maximum deflection in the *Z* direction and sub-scripts *A, B, C & D* correspond to the different models.

5.5.2 Results

As part of the analysis of geometric effects in bamboo poles in bending, it was noticed that the geometric variability had an impact during the setting up of the test as described in [92] mainly because this guideline considers the bamboo as a straight hollow cylindrical element. As shown in Figure *5.31* (created using a scanned NURBS-model of pole eM103), the main deviation consisted of the position and alignment of the loads and supports. The standard suggests that wooden saddles should be located as close as possible to the nodes [92]. This suggestion might be based on studies showing that the node offers radial support to the culm and prevent a crushing failure [49]. Not only the variable internodal length in bamboo poles make this

requirement very difficult to comply with, but also a more recent study found that the nodes appear to be the region where the failure originates so that the contribution of the nodes as a reinforcing component is negligible [177]. For these reasons, the load/support points were evenly distributed at the corresponding thirds of the span for all the samples, regardless of the location of the nodes. Additionally, the alignment of supports and loading points in a single vertical plane was not feasible due to the natural out-of-straightness of the poles. As shown in Figure *5.31*, the supports were aligned with a vertical plane that passes through the axis of the transfer beam (*X*-axis), however, the loading points were, in all cases, out of the plane even when the bamboo was let to find its position as suggested by ISO-22157 [92]. Finally, at the beginning of each test, the bamboo changed slightly its position as the load was applied, changing the original recorded orientation of the pole. The results of the experimental test, expressed in a stress-displacement graph, are shown in Figure *5.16*.

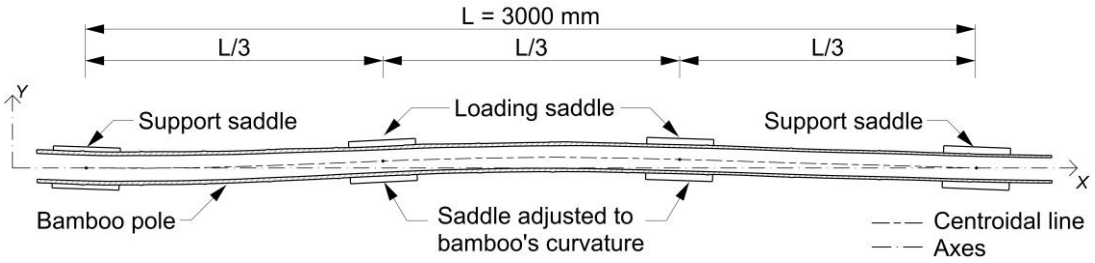

Figure 5.31. Top view of the bending test setup showing misalignment of the saddles in comparison with the bending plane X-Z

The first structural parameter to compare from the FE analysis was the deflection in the *Z* direction for Models *B, C & D* which were normalised with the displacement of the Model *A* according to Eq. *5.49*. The results are shown in Figure *5.32*, where both increment and decrement of the maximum deflection were found with a maximum difference of 14% to the benchmark. The difference found in Model B is attributed to the taper effect previously studied by Nugroho & Bahtiar [76], whereas the difference in Models C/D is related to the combined effect of taper and the irregularity of cross-sections which causes a variation of stiffness depending on the orientation of the principal axis with respect of the direction at which the bending moment is

applied [70]. Nevertheless, the estimations proposed by Bahtiar et al. [70] consider the bamboo as an elliptical shape. In contrast, models *C & D* consider the actual discretised irregular shape, each with different principal axes orientation, increasing the complexity but also the reliability of the model. The effects of the geometric imperfections were also reflected as a shift in the position at which the maximum deflection occurred in comparison with the benchmark model. This shift ranged between 2% to 3% of the total span for the five bamboo poles and occurred towards the direction at which the pole is tapering.

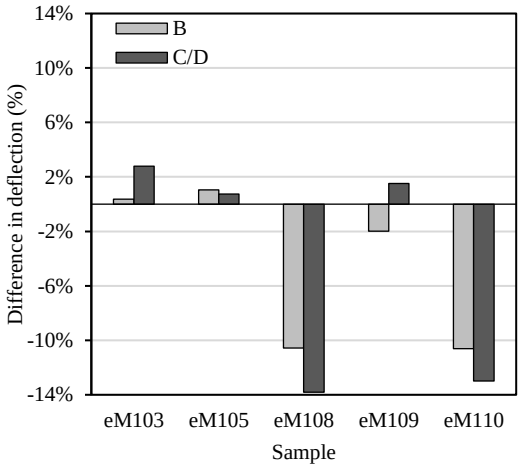

Figure 5.32. Increment (%) of the maximum deflection in the *Z* direction for models *B & C/D* compared to model *A*

By incorporating the spatial deviation of bamboo's axis in Model D, it was expected that out-of-plane deformations and torsional forces appeared in the FE analysis results. For the five bamboo poles studied the magnitude of out-of-plane deformations and torsional effects were not significant in comparison with in-plane effects, however, it proved that modelling bamboo poles using the numerical data can identify and also quantify those effects produced by the organic geometry of the poles which under certain circumstances of a particular pole can become significant.

The tubes with equivalent properties (Models *A & B*) had their principal local axes coinciding with the global set of axes as their cross-section is idealised as a circular tube. Therefore, *A & B* only presented shear forces in their local *-Z* direction (considered minor axis) and bending moment about

their local *Y*-axis (considered major axis). However, for Models *C & D* the orientation angle of the local principal axes, corresponding to the irregular cross-section, did not coincide with the global ones so the forces were decomposed into local, major and minor directions, according to the orientation angle (θ_o) of the principal local axes for each discrete element. Figure *5.33* shows how shear forces (*V*) and bending moments (*M*) of cross-sections extracted from Models *C & D* are decomposed in forces and moments about local major and minor axes, normalised against *V* and *M* of Model *A*. When the direction of the principal major axis for the discrete elements at which shear and moment where measured it was found that their direction with respect of the global *Y*-axis was 21.3°, 6.1°, 0.4°, 73.6° and 32.9° for samples *eM103*, *eM105*, *eM108*, *eM109* and *eM110* respectively.

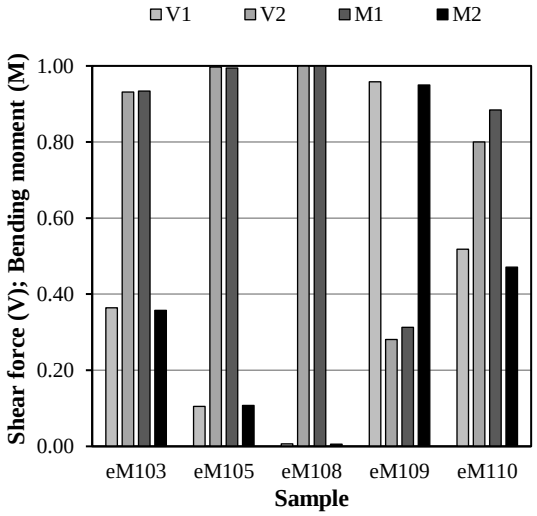

Figure 5.33. Shear (V) and bending moment (M) components (major and minor) of models *C & D* in comparison with normalised value (1.0) for V and M of Model *A*

5.6 Discussion

This chapter presented the development of an analytical model to predict the elastic modulus in bending, and more importantly, the strain and stresses distribution on a bamboo cross-section within the elastic range of the material. The use of a tangent elastic modulus defined between the twenty and sixty per cent of the ultimate load according to [66], was not considered appropriate due to the significant deflections (span/deflection ratio surpassing 150) of the poles already reached at the 20% lower limit of the linear range proposed in

the standard, and instead, an objective cut-off threshold defined by a least-squares regression with a coefficient of determination equal to 0.99 was used (Section *5.2.2*). Although the ISO method is regarded as standard, a least squares regression has been previously used in the literature and is considered to give a more consistent apparent modulus of elasticity (E_b), which is adjusted to the load-displacement behaviour of every tested pole.

The theoretical equivalent modulus of elasticity, E_{eq}, for each of the twenty poles considered in this study, was calculated from Eq. *5.18* based on the compressive strength and volume fraction obtained from the experimental testing of clear bamboo samples. The estimation of the equivalent modulus of elasticity can be limited by the assumption of a constant tensile elastic modulus (E_t), adopted from the literature and indirectly validated through the performance of two control tests. The tensile elastic modulus of fibres, as any other property of bamboo poles, is subjected to variability issues which depend on the species, region, age, among others. For example, [64] found different ranges of tensile elastic modulus of fibres depending on the species and section of the plant. This variation should therefore be measured in the same way the compressive modulus and volume fraction were for each pole, however, the testing procedure to measure tensile properties of fibres is relatively more complex than the elastic compressive strength, posing a significant challenge for this project and therefore it was not included within the scope. The analytic model aims to simplify the procedure to obtain strain and stresses corresponding to a composite material, and therefore the assumption of constant tensile elastic modulus was necessary. Nevertheless, it is encouraged that future research is performed to validate the assumption of tensile elastic modulus here proposed by incorporating tensile tests of clear bamboo samples and also the fibres alone. Besides, the volume fraction was also assumed to be constant across the wall thickness and around the cross-section due to the thin-walled condition of the tubes. The functionally graded characteristic of bamboo poles where volume fraction increases on the wall thickness from the inner to the outer section can be quantified using the same image processing principle, however, the variation around the cross-section

and along the pole would be relatively complex to measure. Therefore, this study was focused on developing a rather simple initial idealisation of a bimodulus material model and validate/calibrate it through experimental tests.

Table *5.1*, together with Figure *5.9* shows a comparison between the measured apparent elastic modulus (E_b) and the equivalent modulus of elasticity (E_{eq}) estimated from the analytical model. A very good agreement was found between the analytical and experimental results, showing an average difference of 4.5%. The discrepancies can be associated with the material assumptions described in the previous paragraph, however, the small average difference suggests that tensile elastic modulus variation and functionally graded condition are not considered significant in the Moso bamboo poles here tested. The main contribution of this section is the prediction of strain and stresses occurring within a cross-section of the pole subjected to bending using an analytical model that assumes the bamboo as a bimodulus material. To the knowledge of the author, a bimidulus analytical model has not been presented before in the literature. The expected shift of neutral axis due to the different elastic modulus, and a relatively linear strain deformation were confirmed during the control bending tests, which in turn, brought confidence to the prediction of direct and shear stresses within the cross-section. It is expected that this model is further validated and adopted in further studies using different species to confirm its suitability to increase the fundamental structural reliability on bamboo structures.

One of the concerning points towards the bending behaviour of bamboo poles was the confirmation of relatively large deformations observed in the samples tested. For example, the limiting value of deflection in timber beams is the total span (L) over 300 [25]. Closed section poles subjected to bending deformed, in average, thirty times more than the limit suggested for timber (*L/10)*, and open section poles, which presented early failure, registered 15 times the limit deflection suggested for timber beams. Service limits for bamboo poles have not been established yet, and timber values are only taken as a reference, however, structural design of bamboo structures would likely be governed by service limits, such as instantaneous deflection, rather

than ultimate strength. Therefore, the experimental results presented in this chapter are an important contribution to improve the overall understanding of the elastic behaviour of bamboo poles and the stresses developed at any cross-section.

The second aim of this chapter was to understand the failure mechanism of bamboo poles in bending. In this study, closed-section poles presented two failure mechanisms: local kink and splitting, both of them originating under the loading saddle and associated with the circumferential tensile stresses exerted by saddles. The composite nature of the pole, with fibres running only along the height of the pole, means that circumferential stresses are only carried by the matrix which is relatively weak when subjected to tensile stresses. This becomes critical in the case of thin-walled Moso bamboo poles (and potentially extends to other species) and therefore the bending capacity was found to be governed by the circumferential tensile strength of the pole. These findings are of high importance to the research community, as well as the industry of bamboo poles, because it means that the bending test as proposed by ISO 22157 [214] is influenced by a different state of stresses derived from the internal structure of the material and the loading condition. Besides, it questions the simplistic bending idealisation commonly assumed for bamboo poles as isotropic cylindrical tubes and turns the attention towards increasing the understanding of this organic and complex material as a natural composite. More studies are therefore needed to include different species and diameter-to-thickness ratios to confirm the findings presented.

As a natural structural element, bamboo poles are susceptible to develop natural surface cracks which change the bending failure mechanism when the crack is oriented towards the top of the compression region. Poles with these characteristics presented a similar behaviour observed in other open profile sections [231]. The observed reduction in ultimate strength and deflection in comparison with closed-section poles is explained by an early local outward buckling failure mechanism of the unsupported ends of the cross-section. This complex effect has not been reported before in bamboo poles, hence, it is encouraged that more tests and numerical models are also developed to

confirm the observations in this work as the buckling failure observed can become critical for the assessment of structural integrity of bamboo elements in bending. Tangential reinforcement of closed-sections had no mechanical or stiffening effect in the pole under a bending load unless the section was cracked, and the crack is located at the centre of the bending span and oriented towards the compression region. In this case, the ultimate strength, maximum deflection and failure mechanism will depend on the spacing between the steel bands. The results and observations of the experimental tests showed that bands can effectively contain the outward buckling deformation between the spacing where the failure occurs. If the spacing is long enough (three diameters in this case) the confinement effect is negligible, and the behaviour and failure are the same to an open-section. With a shorter spacing (one diameter in this case) the outward buckling deformation is contained, and the bamboo ultimately fails with a local buckling between two neighbouring steel bands. Although tangential reinforcement is a common technique against splitting, experimental studies of their effect under bending conditions have not been performed before. This study shows tangential reinforcement only work in certain conditions; however, more experimental and numerical studies are needed to complement this work.

The geometric properties are directly related to the behaviour of a structural element subjected to loads, therefore, irregular variation in the geometry of bamboo poles affects its structural response. As part of the study of bamboo poles in bending, complemented with the digitisation workflow presented in Chapter *3,* a pilot study was carried out to explore the suitability of implementing the numerical database for structural purposes and to assess the structural behaviour, in terms of deformation and resultant forces, of five Moso bamboo structural models incorporating their corresponding geometric imperfections. This pilot study was useful to successfully create structural models of bamboo poles using discrete beam elements, each with their corresponding geometric properties, through a combination of computer-aided design (Rhino3D/Grasshopper), parametric modelling (GeometryGym) and finite element (GSA) software. The results of the FE models showed that

a considerable variation in the total displacement existed between a benchmark model (straight cylindrical tube) and models incorporating the irregular geometry of bamboo in different stages. Due to the relatively large deformations observed within the elastic range of bamboo poles, this variation can have a significant impact not only in the structural reliability of a bamboo structure but also in the estimation of mechanical properties through the performance of experimental tests. This is because the maximum deflection in poles incorporating the real geometric properties registered a shift in the position at which the maximum displacement occurred. This means that the modulus of elasticity can be over or underestimated by measuring the displacement at mid-span, according to [66]. Without exception, all the samples showed that the cross-section is subjected to bi-axial effects due to the irregularity of the cross-section which causes a variation on its local principal direction. This is the main reason why it is important to accurately quantify the geometric properties of bamboo poles and implement them into design and construction procedures.

5.7 Summary

This Chapter presented the development and validation of an analytical model that can predict the elastic bending modulus and the strain and stresses distribution in bamboo poles (Section *5.2*), taking into account the significantly different compressive and tensile elastic moduli of their constituent materials. The experimental parameters required for the use of this bimodulus model are the compressive elastic modulus and average volume fraction of small clear bamboo samples which can be experimentally determined using a low-capacity, table-top testing frame and an entry-level camera. In this way, the bending properties of a bamboo pole could be estimated from the properties acquired through the intensive measurement workflow developed in Chapters *3* and *4*, which together with the results in this Chapter build up a robust geometric, physical and mechanical database for the design, construction and management of bamboo structures.

The failure mechanism of bamboo poles in bending was also investigated. The numerical and experimental tests showed that the

composite nature of bamboo poles plays an important role in the bending behaviour because the failure mechanisms observed during the experimental testing depended more on the transverse mechanical properties of the pole rather than the longitudinal ones. It should be noted that poles failed at a relatively large deformation rate (L/10) which significantly surpasses the serviceability limit proposed for other materials. Results also showed that the length of the loading saddle has a strong influence on the type of failure, which suggests that concentrated loads should be avoided.

A natural characteristic of bamboo poles is the cracking effect due to changes in temperature and humidity within their environment. This work presented the first experimental bending test programme of bamboo poles with open-section simulating a natural crack. Results suggest that when the crack is located within the bending span and oriented towards the compression region, there is a significant change in maximum strength, maximum deflection and failure mechanism when compared to closed-section bamboo poles, however, the apparent modulus of elasticity in bending remains within the same range. For open-sections reinforced with steel bands, the spacing between them affected the capacity as well as the failure mechanism, the closer the spacing the more similar the behaviour would be to a closed-section bamboo pole. In the case of reinforced closed-sections, the bands contained the propagation of the splitting failure, but no improvement on capacity or stiffness was recorded. As a result, it is recommended to reinforce the bamboo using steel bands in critical regions of the pole as a precaution measure, even when the bamboo does not present any cracks as this can potentially change during the structure's life.

The practical implementation of the geometric digitisation workflow was fundamental to analyse the effect that the variable geometry (diameter and thickness taper as well as out-of-straightness) have on the structural behaviour (deformation and resultant forces) of bamboo poles in comparison with the standard idealisation of a perfectly straight cylindrical tube. The digitised data was not just useful to create more realistic structural models of a bamboo pole but also to identify the differences in the structural behaviour

and quantify those effects, therefore, contributing to increasing the structural reliability of bamboo structures.

- Blank -

6 Case study: digitised bamboo poles for the design and construction of a structure

6.1 Overview

The present dissertation began by describing the inherent variability of bamboo poles (Chapter *2*) as the main challenge posed by their organic nature against their formal adoption in the building industry as structural elements. Subsequently, the inherent geometric, physical and mechanical variability of bamboo poles was separately addressed (Chapters *3, 4* and *5*) through the development of reverse engineering methods combined with different digital technologies so that the relevant properties of a stock of bamboo poles could be individually measured and therefore the variability could be simply quantified, opposed to forcibly eliminated. The intensive measurement methods presented in previous chapters can provide fundamental information necessary for the design, construction and management of any structural system.

Bamboo poles are particularly suitable for the construction of lightweight structural systems such as trusses, 3D-grids, arches or membranes [14,151,234]. The lightweight characteristic comes from the low-density and hollow nature of the poles which grant bamboo a relatively high strength-to-weight ratio when compared with conventional construction materials [48]. This characteristic has been exploited to develop bamboo structures that can span medium to long distances including roofs, pavilions and footbridges, among others [14,72,151,152,163]. As a lightweight material, constructability is very practical as sawing, handling and positioning of poles are easily performed during the assembly procedure of a structure. However, one of the main concerns during the design and assembly of bamboo structures is the connectivity between the main structural elements. The hollow cross-section in combination with bamboo's anatomical composition and low transverse capacity [227,235], suggest that the structural system needs to be carefully selected to reduce the concentration of local stresses at the connections while

keeping the integrity of the poles intact (e.g. without drilling and fitting bolts through the pole). Reciprocal frames have been proposed as one of the most suitable structural systems for bamboo poles through its practical implementation, together with the development of bespoke boltless connections [129].

A reciprocal frame (RF) consists of mutually supporting sloping beams placed tangentially in a closed circuit around a central point of symmetry that forms a polygon [236]. The inner end of each beam rests on and is supported by an adjacent beam, while at the outer end, the beams rest on the floor, a circular wall or columns (Figure *6.1*). The minimum number of beams to form a reciprocal frame is three, being this the most rigid RF due to the triangular shape, with no defined maximum. When the outer end of each beam is used to form another reciprocal frame, the resulting structure is known as multi-RF grid or nexorades [237]. Different parameters of the multi-RF grid such as the number of RF units, the length of their RF elements, engagement length and eccentricity, can be manipulated to achieve complex free-form shapes such as domes, cones or doubly-curved surfaces [236]. A multiple RF grid allows to span relatively long distances in comparison with the length of the individual members and can be practically adapted to any free-form shape. In addition, the inner part of the beams that form the RF does not meet in a central point so that connectivity is always limited to only two elements at any point (Figure *6.1*).

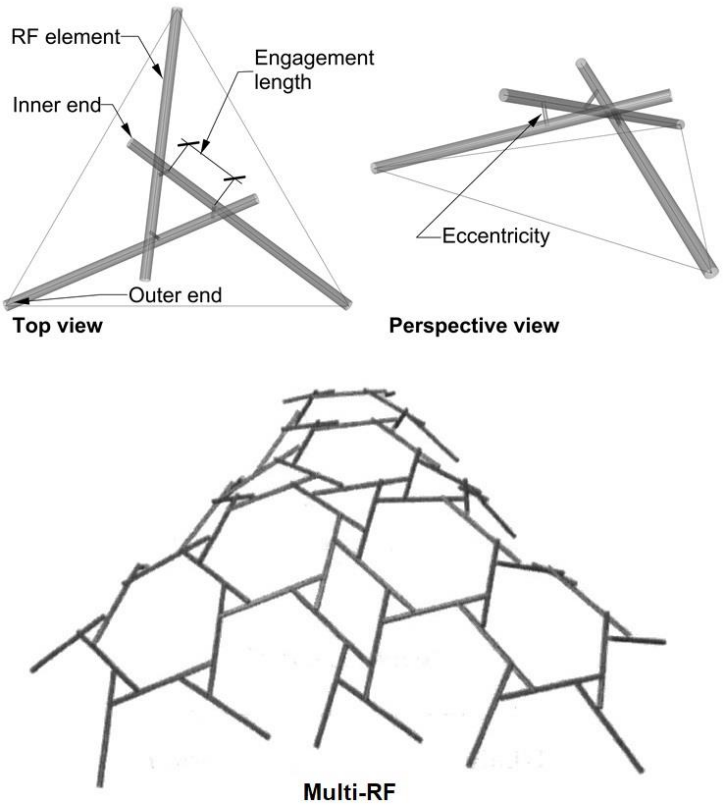

Figure 6.1. Diagram of the reciprocal frame and its main components, as well as an example of a multi-RF [237]

This chapter presents a case study as the practical implementation of the intensive measuring methods developed in previous chapters to integrate them within a digital workflow for the design and construction of a multi-RF structure. The design approach for the multi-RF structure presented in this chapter is based on the bottom-up paradigm (Section *2.8*) that aims to develop structural systems based on the quantified properties of the entire stock of bamboo poles. The digitisation of material properties becomes the back-bone of the design approach which further allows carrying optimisation of material and structural performance. The result of the design procedure is a detailed digital blueprint on which the construction of the multi-RF deeply relies on, being this the main guidance to build the structural prototype. This case study is part of an ongoing research project at UCL focusing on the design, construction and management of bamboo pole structures taking the intensive measuring of material properties as the initial step towards a digital workflow that can provide the fundamental basis to ensure high-quality structures.

6.2 Digitising bamboo poles

The concept of intensively measuring the properties of individual bamboo poles was aimed at quantifying the variability of the material and making the acquired data available within a digital environment so that the data can be used for the design and construction of a bamboo structure. This section describes the digitisation process of a stock of bamboo poles for its subsequent implementation during the design and construction stages of the RF-footbridge.

A combination of 30 Guadua (Guadua angustifolia kunth) and 25 Moso (Phyllostachys pubescens) bamboo poles were defined as the available bamboo stock for the project. The general description of the material is presented in Table *6.1*. The stock of bamboos was kept in a controlled environment of 20°C ± 2°C and relative humidity of 65% ± 5% for at least 14 days before the digitisation procedure. The geometric digitisation workflow was performed according to Section *3.2*. Once the digital geometric data was acquired, the semi-automated robotic fabrication and corresponding testing of clear bamboo samples were performed in line with Sections *4.2.3* and *4.3.1*. Figure *6.2* shows the scanning procedure for Guadua and Moso bamboos, while Figure *6.3* shows the scan-to-fabrication and mechanical testing of clear bamboo samples.

Species	Quantity	Origin	Age	Length	Treatment
Guadua (Guadua angustifolia kunth)	30	Valle del Cauca, Colombia	2 - 5	2.5 - 3.5	Borax/Air dried
Moso (Phyllostachys pubescens)	25	China	4	3 - 4	Air-dried

Table 6.1. General description of the stock of bamboo poles to build a multi-RF structure

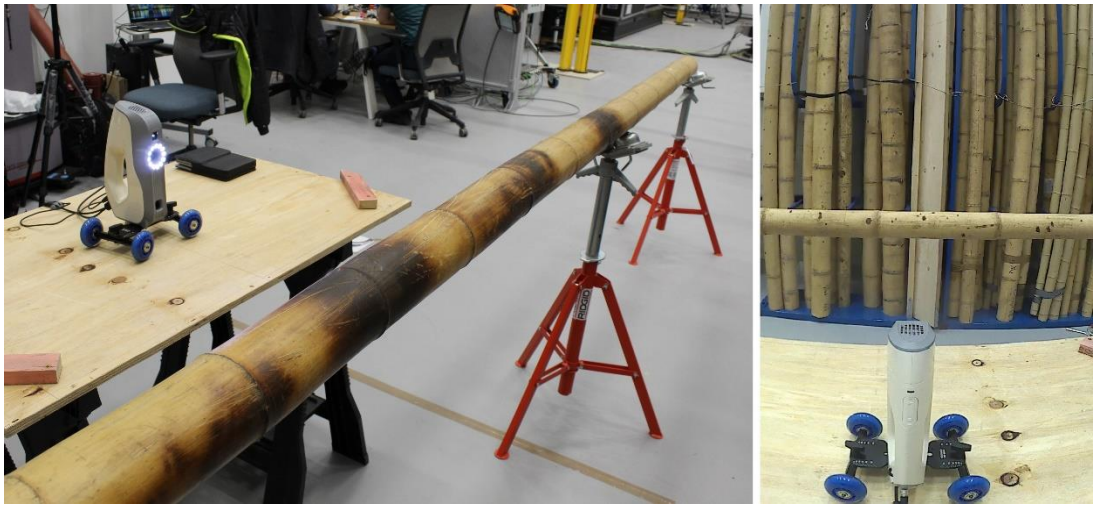

Figure 6.2. Scanning procedure for both Moso (left) and Guadua (right) bamboos

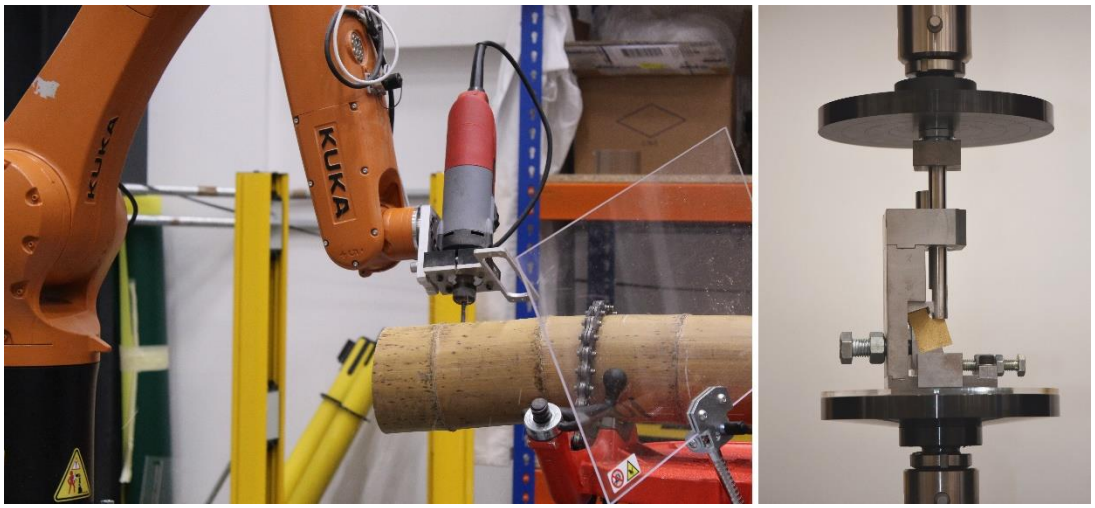

Figure 6.3. Scan-to-fabrication procedure (left) and mechanical testing of clear bamboo samples (right)

The geometric, physical and mechanical properties are summarised in Table *6.2*, expressed as the range, mean and standard deviation for both species. For identification purposes, the sequential numbering adopted for Guadua and Moso included the prefix "*B0"* and "*B1"* respectively. Besides, the detailed description of each bamboo pole's geometric, physical and mechanical properties was stored in a combination of text-based digital files, which becomes the fundamental data for the design and construction of the RF footbridge project (all numerical data is stored as in a similar format as the example shown in Appendix A.1).

Property	Range	Mean	Std. dev.
Guadua			
Diameter (mm)	87 - 146	109	17
Thickness (mm)	6.3 - 19.5	10.9	3.6
Length (mm)	1415 - 2660	2171	276
Out-of-straightness ratio (mm/mm)	66 - 478	212	110
Moisture content (%)	7.9 - 9.6	8.4	0.4
Density (kg/m^3)	581 - 827	720	55
Compressive strength (MPa)	52 - 83	68	6
Elastic modulus (MPa)	13432 -	21679	4574
Shear strength (MPa)	6 - 17	14	2
Moso			
Diameter (mm)	72 - 110	96	9
Thickness (mm)	6.6 - 12.6	10.1	1.4
Length (mm)	2363 - 3459	2900	432
Out-of-straightness ratio (mm/mm)	71 - 653	289	147
Moisture content (%)	7.6 - 8.9	8.3	0.3
Density (kg/m^3)	479 - 741	617	60
Compressive strength (MPa)	36 - 70	56	7
Elastic modulus (MPa)	5637 -	10354	2265
Shear strength (MPa)	11 - 21	17	2

Table 6.2. Summary of the geometric, physical and mechanical properties for each bamboo species.

6.3 Footbridge design

6.3.1 Multi Reciprocal Frame system

The proposed bamboo pole structure consisted of an eight-metre long tubular footbridge whose cross-section's radius was 2.5 m. A hexagonal grid was created on the surface of the tube which defined the general topology of the structure (Figure *6.4*). The hexagonal pattern is the most effective way of dividing a surface into regions of equal area with the least linear elements, optimising material utilisation [238]. Besides, each vertex of the grid has a {6,3} configuration, meaning that the edges of three hexagons meet at one point. This characteristic is an advantage for the creation of three-pole reciprocal frames at the vertices of the hexagonal grid which by its triangular geometry, represents the stiffest form of an RF unit (Figure *6.1*). The dimensions of the hexagonal grid were parametrically adjusted considering the quantity and approximate length of the poles in stock. The three-pole multi-RF was created with a semi-automated script based on [237] through the Rhino 3D [176] parametric plugin Grasshopper [194], using the eccentricity of

the RF system and the engagement length as critical parameters (this bespoke procedure was developed by others within the BIM Bamboo group at UCL). To avoid clashes between the poles, the eccentricity of the system was defined as 150 mm based on the largest diameter found in the bamboo pole stock (Table *6.2*) and is represented in the model as a straight line which is perpendicular to and joins both connecting beams (Figure *6.1*). Considering that the internal angle of the hexagons remains constant (120°), the minimum engagement length to install a connection for a three-pole RF unit is approximately 350 mm, which is further discussed in Section *6.4.1*. The bespoke script allows controlling the final geometric output of the multi-RF system according to the original hexagonal grid, adjusting parametrically the individual engagement length of each RF unit. Figure *6.4* shows a typical RF unit formed at a vertex of the hexagonal grid. Figure *6.5* shows the multi-RF line-based geometry for the entire bamboo pole footbridge, which was composed by a total of 51 RF beam elements. Having a higher number of bamboo poles in stock than the required, gave the possibility of optimising the material selection. Figure *6.4* also shows that the last three outer RF elements of the multi-RF system at each end of the footbridge are free. These free elements required additional vertical support at their outer vertices (as is the case in any RF system). Instead of providing vertical support, these elements were linked back to the structure with additional RF elements (Figure *6.5*).

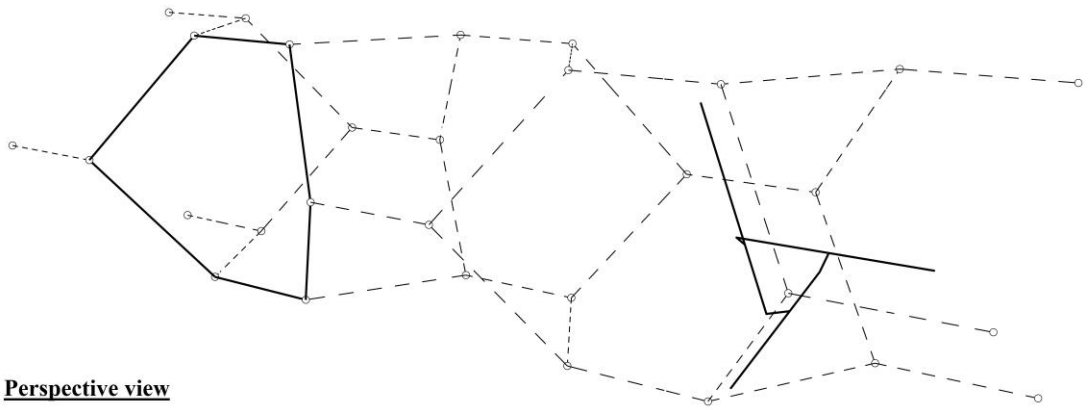

Figure 6.4. Structural topology based on a hexagonal grid (dashed) from which a multi-RF system is defined (line). Bold lines highlight the hexagonal pattern and a three-pole RF formed at a vertex of the grid.

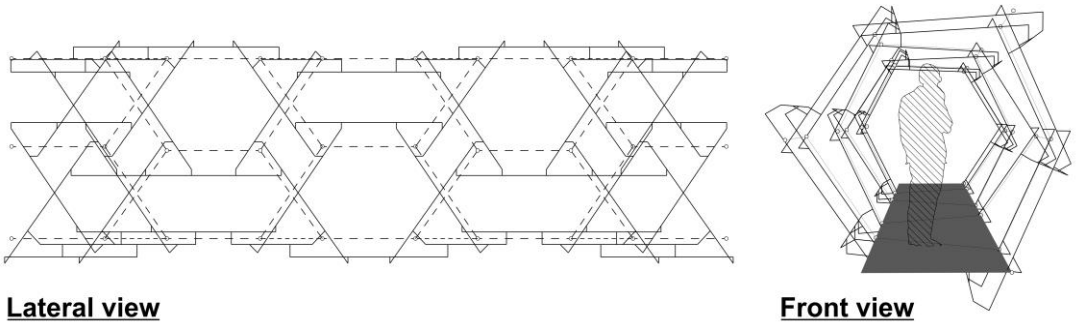

Figure 6.5. Lateral and front view of the structure's topology.

6.3.2 Incorporating bamboo's digital data

Once the line-based geometry of the multi-RF footbridge was defined, the quantified properties measured in Section *6.2* became the backbone of the design workflow. This section describes how a digital database containing the properties of each measured bamboo is created, but more importantly, it shows that the variability of the material properties is used in benefit of the structure by optimising the positioning and orientation of the bamboo elements within the footbridge.

The digital geometry of every bamboo pole is found in each of the NURBS-model, containing the outer and inner surfaces of the pole, the corresponding centroidal line and the reference markers (Figure *3.24*). In addition, the geometric information of the discretised poles (according to Section *3.2.4*), as well as the material properties (physical and mechanical) and general data of the poles (e.g. ID, number, species, age, treatment) are stored in comma-separated value files. The numerical database of the poles can be used in isolation, for example, to analyse the geometric variability or the mechanical properties of the digitised poles, as shown in Sections *3.3* and *4.3.* However, for those cases where the combination of both visual and numerical data is required, for example, the combination of computer-aided design (CAD) with finite element (FE) or computer-aided manufacturing (CAM) software, each geometric object contained in the NURBS-model can be enhanced with text-based attributes describing the geometric, physical, mechanical and general properties [176].

Adding attributes to each object within a NURBS-model of a bamboo pole would conceptually convert the NURBS-model into a building information modelling object [239] containing all relevant information for the design, construction and management of bamboo structures. The bamboo pole as a digital, geometric-enhanced object is an essential concept on which the development of a digital design and construction workflow that allows to store and share data relies on. Figure *6.6* shows a graphical example of a digitised Moso bamboo pole (*B101*) and the data added as attributes to it. Each object (surface, curve or point) will contain different information according to its characteristic. For example, the external surface contains general information (species, felling date or treatment) as well as physical and mechanical properties that apply for the entire pole (moisture content, density, E_c, f_c and f_v). Each discrete curve defining the centroidal axis of the pole contains the end-coordinates (sorted from bottom to top) and corresponding section properties. The points representing the reference markers will contain the coordinates of the point as well as its reference number (sorted from bottom to top). Attributes containing the information as a function of the in-space location of the NURBS-model (e.g. coordinates or local principal axes) are automatically updated within Rhino3D/Grasshopper once the position of the pole is changed.

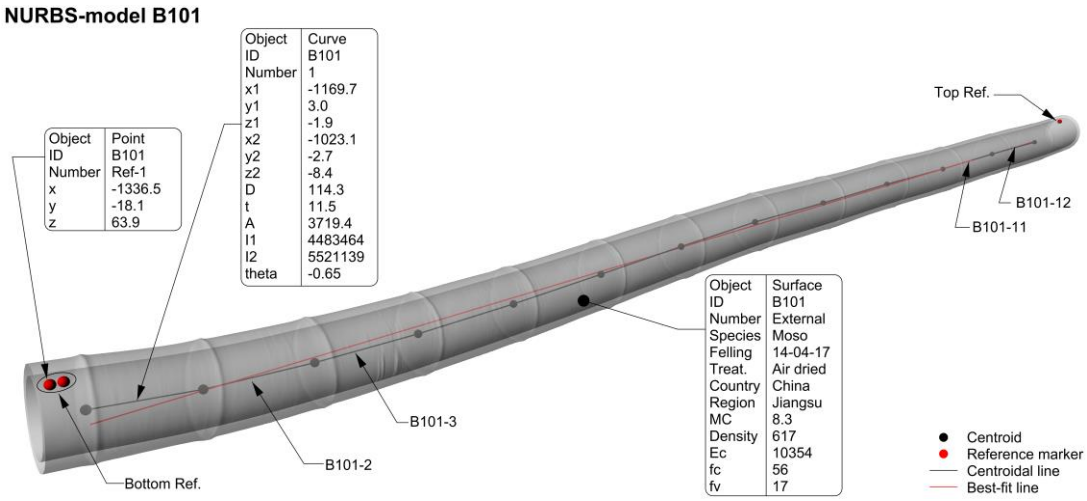

Figure 6.6. Example of a digitised bamboo pole enhanced with data attributes (pole *B101*)

The 55 NURBS-models of bamboo poles were imported into the Grasshopper script where the topology of the RF-footbridge structure was contained. The attributes of each object were added to the NURBS-model and organised in a compatible data structure so that Grasshopper could query the relevant information during the design of the RF-footbridge.

A list of RF element lengths was extracted from the geometric model (Figure *6.5*) and was best-matched with the total length of each NURBS-model, optimising material utilisation and avoiding cut lengths. This simple step showed an improvement of material selection in comparison with traditional bamboo construction where poles are selected on-site, based on empirical experience and without considering any resource management [68].

The geometry of the RF-footbridge shown in Figure *6.5* is made of straight RF elements which are, in principle, incompatible with the non-straight centroidal line of any bamboo pole (Figure *3.23*) as the latter cannot be physically forced to fit a straight line. To match the position of each digital pole with its corresponding RF element, a best-fit line that passes through the centroid of each node of the pole was created (Figure *6.6*). The mid-point and directional axis of each best-fit line were used as a reference to translate and aligned with its corresponding mid-point and axis of each RF element in the footbridge. Then, each pole was oriented with its largest diameter towards the centre of the footbridge span, where maximum stresses are expected to occur. The orientation of each pole was performed by examining its geometric data so that the portion of the pole with the largest diameter was oriented towards the centre of the span regardless of its bottom or top orientation.

In combination with the geometric data, the physical and mechanical properties were subsequently used to perform a preliminary structural analysis through the engineering plugin Karamba3D [240]. The material was assumed as isotropic linear elastic, which properties were assigned using average density and elastic modulus according to its corresponding species, Guadua or Moso (Table *6.2*). The structure was simply supported at the base of each end of the footbridge and a distributed load of 5 kN/m^2 [241] was applied along the walking platform as shown in Figure *6.7*. The eccentricity line joining the

RF elements, which represents the connection, was assumed to transfer all shear forces and bending moments from one pole to the other and modelled as a link-element (relatively high translational and rotational stiffness) [240].

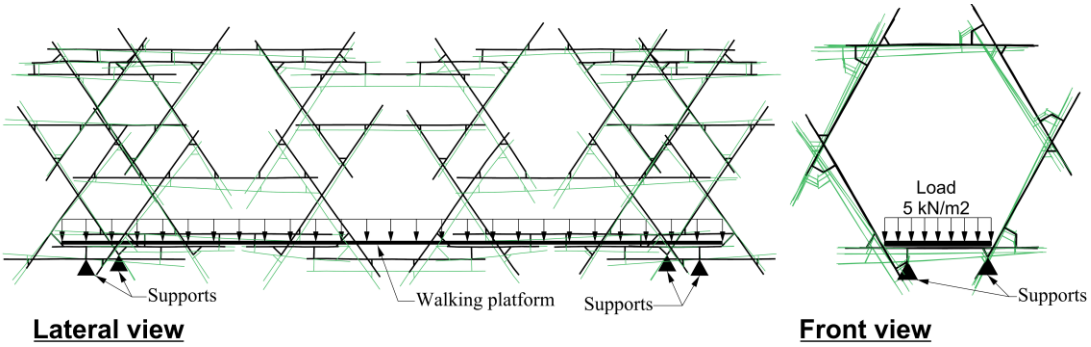

Figure 6.7. Finite element model showing supports and loads (black), together with the deformed structure (green - deformation scaled by 3)

After performing structural analysis, a list containing the elastic energy of deformation for each pole was extracted and sorted from the largest to the smallest value. This list was used to match the poles with a higher diameter with the elements that registered the higher elastic energy while keeping the initial length criteria previously defined. After this iteration, the maximum vertical deformation of the footbridge was reduced by approximately 11%.

A comparison was also made between the analytical model created with variable geometric properties and analytical models built with average and extreme (maximum and minimum) geometric properties (Table *6.2*). For average and extreme values, the bamboo poles were considered as straight, hollow circular tubes. The maximum displacement of the model built with average properties was 7% smaller than the model using variable geometric properties. When applying extreme values, the displacement differed ±50% for the minimum and maximum properties, respectively, when compared to the model built with variable geometric properties. These differences cannot be taken as guidance for other structures or batches of bamboo poles because of the variability, however, it shows how the variability of the geometry can affect the behaviour of a bamboo structure.

Further structural optimisation of the footbridge is possible, for example, by considering the individual bending stiffness of each pole as a parameter or

by modifying the eccentricity and engagement length on each RF unit according to the individual characteristics of the bamboos joining at each vertex of the hexagonal grid; however, further optimisation tasks were out of the scope of the present case study as the focus is oriented to demonstrate the potential of quantifying the individual properties of bamboo poles to implement them in the design and construction of a multi-RF structure. Figure *6.8* shows the final RF-footbridge model with the corresponding identification tags of each bamboo. This model, which contained the geometric, physical and mechanical details of each bamboo pole, was used as the main guidance for the subsequent construction process.

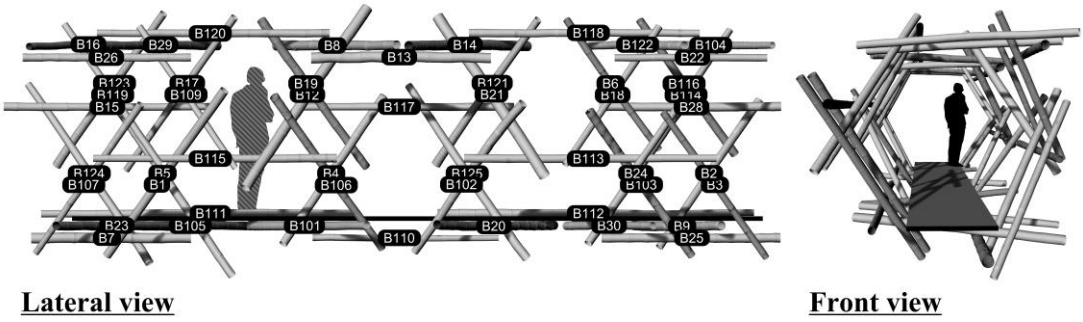

Figure 6.8. Lateral and front view of the multi-RF footbridge including the identification tag for each pole

6.4 Footbridge construction

6.4.1 Connection system

In general, bamboo connections can be divided into traditional and modern. Traditional connections were mostly developed through generations of local workers by transferring their experience and empiric knowledge of bamboo structures [186]. Examples of traditional connections are mortise and tenon or lashed connections, which are low-cost and are commonly made of natural materials (e.g. bamboo pins or palm rope). However, the mechanical capacity and adaptability on different structural systems have proved to be limited [178,186]. Modern connections, on the other hand, are those in which an industrialised material (e.g. steel, aluminium, timber or, concrete) is involved in the transferring of forces from one bamboo to the other. These connections derived from standard timber or steel structures and include bolts, gusset-plates, steel spherical joints, mortar-filled or embedded bamboo,

timber pegs, among others [14,68,72,162,242,243]. The main concern over modern connections is the common use of bolts through the bamboo to transfer all or part of the loads. Evidence has shown that structural failure originates at the location of the bolts, especially when the concentration of stresses acts in the transverse direction of the pole [186]. In addition, the variability of shape and sizes of cross-sections requires labour intensive jointing techniques that only highly qualified workers can perform [187]. The challenge of connecting bamboo elements has been considered an important factor that halts the continuity in the development of bamboo structural systems [186]. This has started to be leveraged by the current advances in technology which have allowed the development of new methods for the design and fabrication of bamboo connections where the shape and functioning of the connection can be customised depending on the characteristics of individual bamboos [129,147,157,244]. These new methods combine different digital technologies (e.g. parametric design, automated fabrication or 3D printing) which are compatible with the general concept of digitising bamboo poles.

For this case study, there were four aspects considered for the selection of an appropriate connection: i) adaptability to the geometric variation of the bamboo poles; ii) avoid damaging the integrity of the poles; iii) relatively rigid connection system to transfer shear forces while restraining local rotation; and iv) simple fabrication. The first aspect is related to the irregular geometric variability of bamboo poles as shown in Section 3.3. For example, the diameter range of the stock of poles for this project goes from 72 to 146 mm (considering both Guadua and Moso). With this wide range of diameters there is a possibility that two connecting bamboo poles are each at the extreme lower and higher diameter ranges, therefore, the connector must adapt to host both. In addition, the irregular cross-section to which the connector is fixed, and the spatial curvature of the pole suggest that prismatic-shaped connections would not work. The second aspect is related to the hollow cross-section and unidirectional reinforcement of the material which suggest that perforating or carving the pole reduces the effective cross-section, increasing

the likeliness of concentration of stresses, besides, bolts through the bamboo pole are considered a cause of splitting [186]. The third aspect is based on the structural behaviour of three-pole bamboo reciprocal frames previously observed [129], suggesting that a rigid connection system is required. Finally, the simplicity of fabrication is required as the focus of this case study is the integration of the intensive measurement procedures to digitise a stock of bamboo poles and subsequently use the acquired information to design and construct a bamboo structure.

Initially, the RF connection system was designed mainly as structural spacers aimed at keeping the required eccentricity on each RF unit. These spacers consisted of short triangular aluminium extrusions connected through M8 threaded bars and tied to each bamboo pole with steel banding. These steel bands helped to avoid the perforation of the poles and tightly adjusted to the bamboo's organic shape. Besides, steel bands can also reduce the structural effect of natural splitting as shown in Section *5.4*. Experimental trials were performed to assess the suitability of this spacer to achieve the geometric requirements of a multi-RF system as shown in Figure *6.9*. Godina [129] explored the general behaviour of this initial connection finding that it provides enough stiffness for the multi-RF structure to achieve the intended topology, to sustain its weight and to maintain the interlocking system of the structure even after failure, however, it was recommended that the connection system between two poles should be composed by four individual connectors.

Figure 6.9. Initial experimental trials of a connection using studding bars, aluminium extrusions and steel bands. Left: detail of the connection; centre: assembled RF unit; right: three RF units jointed.

Further development of the connection for this case study is presented in Figure *6.10a*, showing a diagram of the aluminium connector which consisted of two pairs of 60 mm x 3 mm circular aluminium tubes with a 16

mm studding bar passing through them. To attach the connector to the bamboo pole, two steel bands were passed through a 5 mm thick aluminium plate placed between each pair of tubes and tightly fixed to the pole. The adjustable length of the steel bands covers for a large range of bamboo sizes whereas its flexibility is essential to adapt to the irregular shape of the pole. The centre-to-centre height between the plates was set as 150 mm, which ensures a constant eccentricity for the multi-RF structural system as defined during the design stage. The main difference in this connector is the replacement of the single piece of aluminium extrusion (Figure *6.9*) with a double-tube and plate system. The double-tube provides a double tangent contact point which is aimed at avoiding hard edge contact with the bamboo's surface and thus reduce damage, and in addition, direct contact between the tube profile and the pole was avoided by locating the steel band between the aluminium tube and the pole's surface (Figure *6.10*). The load applied on the pole (represented with green arrows in Figure *6.10b*) is transferred through the steel bands into the mechanically jointed (by the pair of nuts in compression) components of the connection (plate, tubes and the studding bar) and transferred to the opposite end of the connection where the second pole is connected. The local pull-push system between the connection and the bamboo (represented with black arrows in Figure *6.10b*) restrains the relative rotational and translational movement between the parts.

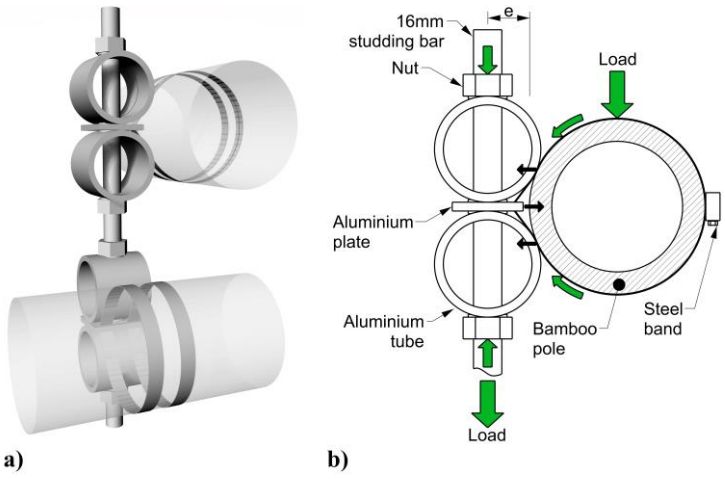

Figure 6.10. 3D diagram of the aluminium connector (a), and cross-section detail showing the load path

An RF system relies on the geometric accuracy at which the overall topology of the structure is built. This means that the location of the connectors is of paramount importance because a slight change in their location would modify the three-dimensional orientation of the RF elements and therefore produce a geometric variation on the position and orientation of subsequent connecting RF units. This is one of the reasons why the digitisation of bamboo poles is fundamental to enable the use of these irregular and organic elements in this structural system. Based on the RF model of the footbridge including the position and orientation of each bamboo pole (Figure *6.8*), a parametric procedure was developed to find the exact location of each connector.

Figure *6.11a* shows an example of two connecting poles, with their corresponding centroidal line and the eccentricity line between them representing the connection. Two planes normal to the eccentricity line are created at each of its ends. The surface of the poles is intersected with the planes, finding four perimetral curves (shown in green in Figure *6.11a*). The curves at the top pole are projected onto the bottom ones and vice versa, finding a total of eight intersection points. Each pair of the bottom and top points are joined with a line (Figures *6.11a* and *6.11b*). These four lines share the same direction than the eccentricity line, joining both centroidal lines of the poles. The four lines are therefore representing the centroidal line of the studding bar of each connector, however, as shown in Figure *6.10*, there is a distance *e* between the surface of the pole and the centroidal line of the studding bar. This distance is a function of the average diameter of the cross-section at the specific connecting point, which for the range found in the stock of poles, *e* varies from 23 mm to 27 mm. For practicality, this distance was assumed constant and equal to 25 mm. To account for *e* in both top and bottom poles, the centroid of the studding bar has to be moved a distance *s*, along the perimetral curves in an outward direction from the intersection, as shown in Figure *6.11c*. As the distance *e* is assumed constant, the distance *s* is the same for both top and bottom poles and is equal to *e* over the tangent of the angle ϕ (Figures *6.11b* and *6.11c*). Figure *6.11c* shows the final position

of the studding bar, which is then used to find the connection points on the surface of each pole.

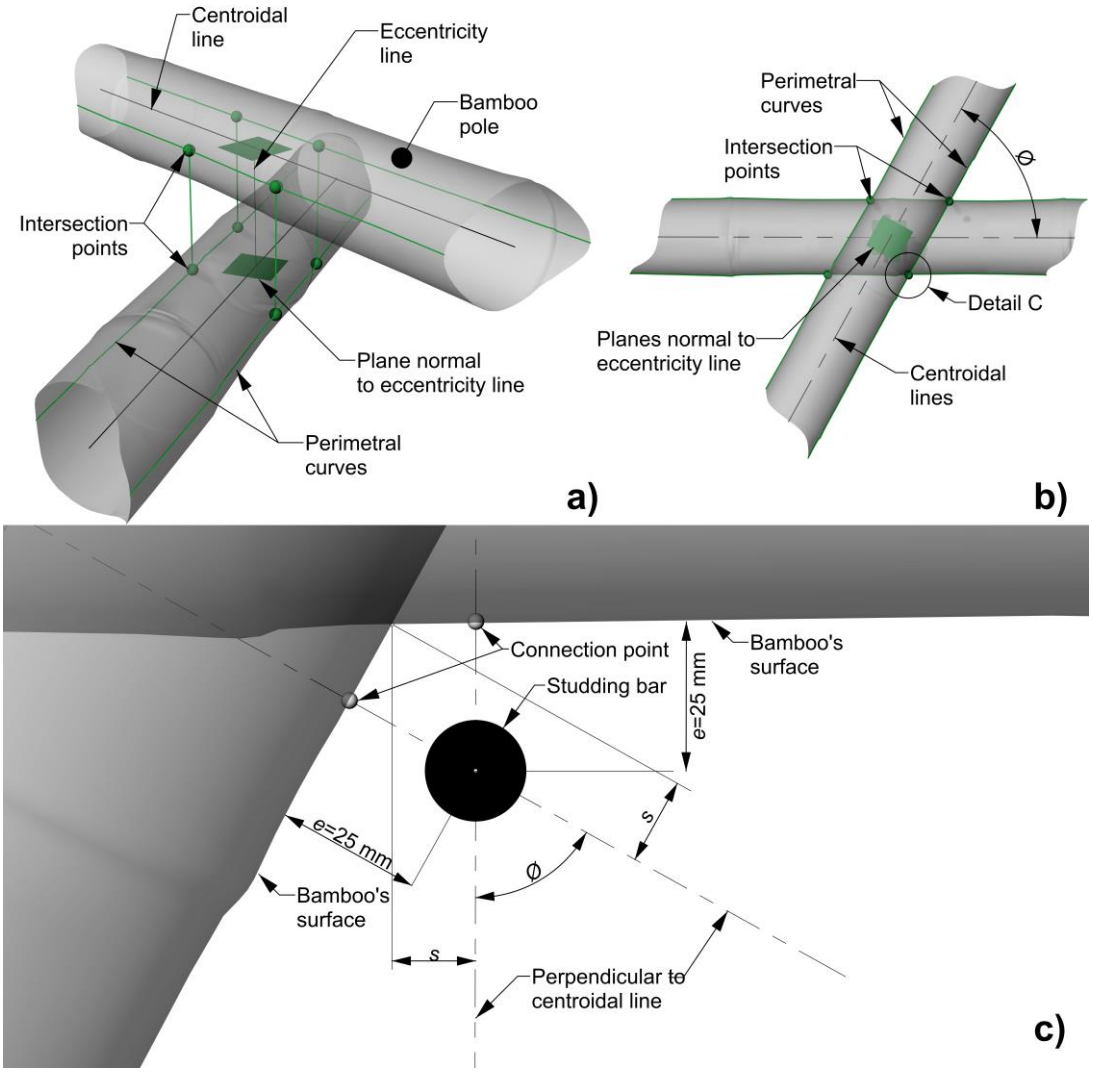

Figure 6.11. Process to find connection points between two poles (a and b), together with the detail of locating the studding bar and final connection points

Figure *6.12a* shows the arrangement of four connectors, together with their corresponding connection points on the surface of the poles. Connector prototypes were subsequently produced and fitted as a trial on two Guadua bamboos as shown in Figure *6.12b*.

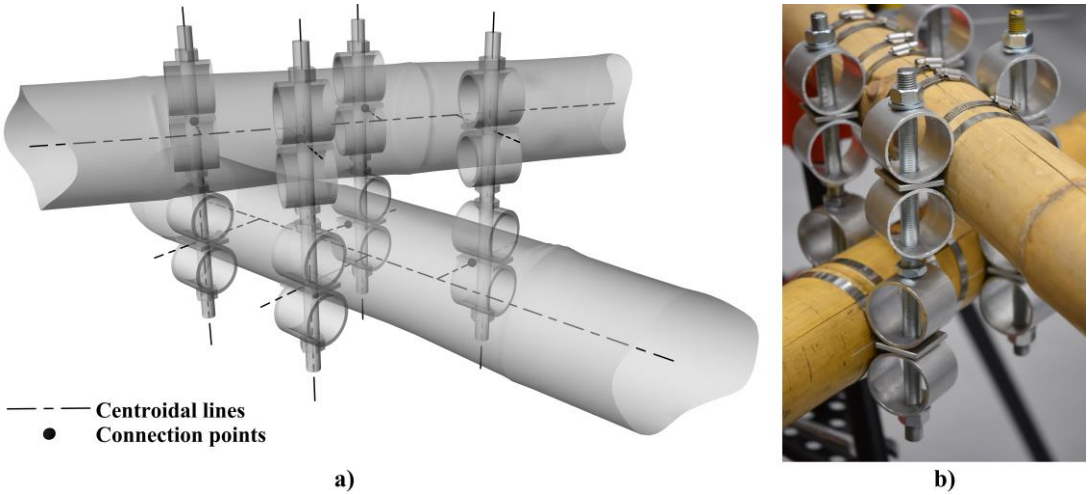

Figure 6.12. Arrangement diagram of four aluminium connectors (a) and its corresponding prototype using two Guadua bamboos (b)

6.4.2 Assembly procedure

The first step of the assembly procedure consisted of translating the location of the connectors found in the digital model to the physical poles. Marking the location of the connector was essential for the multi-RF structure to correctly assemble the irregular bamboo pole elements according to their position and orientation. The marking methodology consisted of intersecting the reference markers at the bottom and top sacrificial internodes of the pole with a longitudinal plane that approximately passes through the centroidal axis of the pole (Figure *6.13*). By intersecting this plane with the outer surface of the digital pole a longitudinal reference curve was found. Subsequently, a cross-section curve is found at the location of each connection point. The intersection of longitudinal and cross-sectional curves allows to correlate the connector's position along (from bottom to top) and around (following the right-hand rule) the pole with respect of the scanned targets as shown in Figure *6.13*. A list of dimensions was automatically created for each bamboo pole and incorporated as attributes to each corresponding digital pole. To perform the physical marking, a three-plane, self-levelling laser was used to project a longitudinal plane on the physical poles, ensuring that bottom and top reference marks were intersected (Figure *6.14a*). A flexible tape was used to measure the longitudinal and circumferential dimensions. Finally, a chalk marker was used to indicate the location of the connector with a cross mark

(Figure *6.14b*). The connection between a pair of bamboo poles only occurs once within the entire multi-RF system, therefore each connection was simply labelled with the name of both connecting poles for identification purposes (e.g. *B123-B015*).

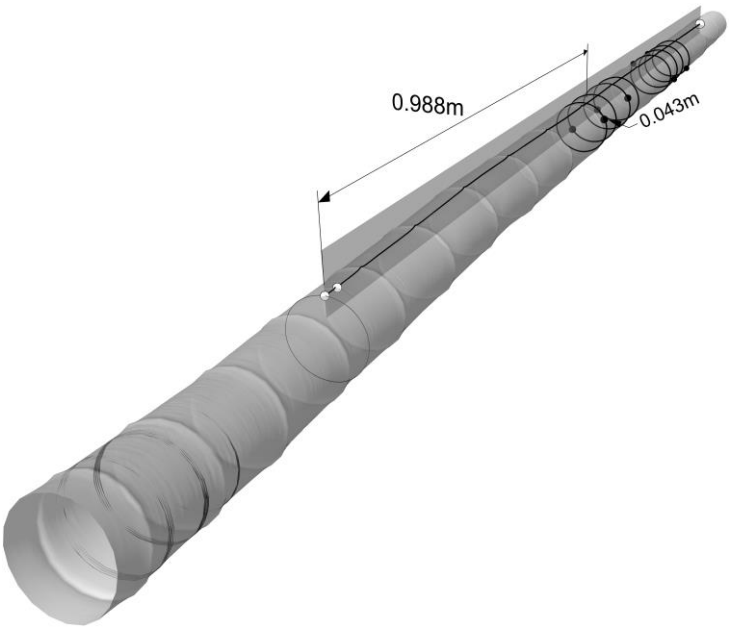

Figure 6.13. Longitudinal and circumferential dimensions that allow positioning each connector point (black dot) with respect to the scanning reference marks (white dots).

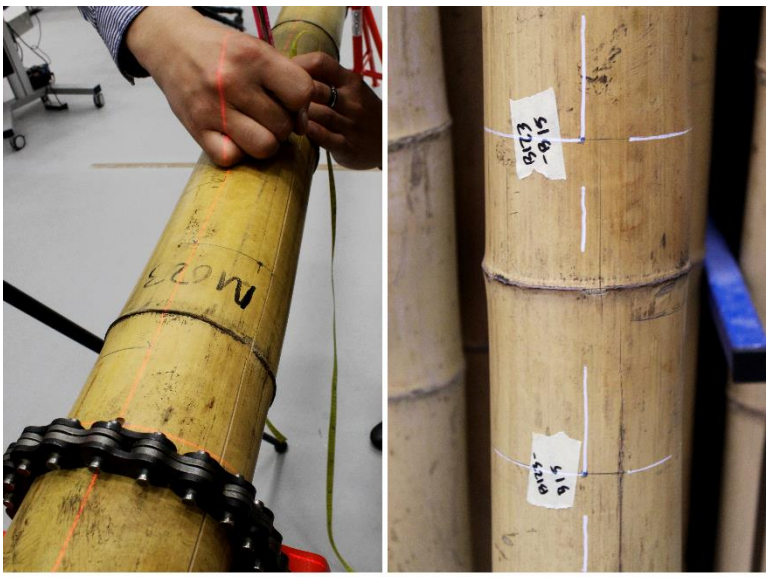

Figure 6.14. Marking connector points on physical bamboo poles (a) and reference cross mark with its respective label for each connector (b)

To evaluate the accuracy at which the connection points were marked, a laser measure device Leica Disto s910 Pro, capable of reading 3D coordinates with an accuracy of up to ±2 mm/10 m, was used to acquire a set of connection points together with the reference marks of three marked bamboo poles prior the assembly of the prototype. The acquired set of points for each pole was matched with their corresponding digital ones using an absolute orientation Matlab function [245] that calculates the optimal transformation matrix which minimises the root mean squared deviation between two paired sets of points. The connection points of three bamboo poles (*B008, B012* and *B118*) resulted in an average spatial deviation of 3 mm. This result showed a good level of accuracy of the marking procedure when compared with the 5 mm tolerance usually adopted for standard timber construction [173], but also by considering the complex and irregular geometry of bamboo poles, the hand marking procedure and the accuracy specification of the laser measure equipment.

The assembly sequence for the footbridge was proposed based on empirical knowledge incorporated into the digital blueprint of the structure to facilitate the construction procedure. The construction of the footbridge prototype was divided into five stages as shown in Figure *6.15*. This case study covered the construction of the first stage of the footbridge as part of an ongoing experimental prototype (Figure *6.15* top). Stage one of the construction sequence corresponds to one-third of the entire footbridge, consisting of 18 bamboo poles. This portion of the structure was self-contained and structurally stable, meaning that it could stand on its base and support its weight. The assembly procedure was performed by joining three to four poles into initial modules that could be then joined together to gradually form the first stage of the footbridge as shown in Figure *6.16*. Modular assembly is considered beneficial in any construction setting as it helps to reduce time and material, but can also allow prefabricating parts of the structure off-site [164,165]. Besides, once the initial modules were assembled, an as-built of each module was performed using the laser measure Leica Disto s910. Physical points on the surface of the module (reference marks and

unused connection points) were acquired and stored. Subsequently, both model and laser coordinates were imported into the absolute orientation function [245] to find the least root mean square deviation. The overall accuracy of the initial modules was 6 mm which is still an acceptable tolerance when compared with tolerances in timber construction [173]. This result confirmed the suitability of using the connection marks as guidance to assemble the footbridge prototype. The assembly of bamboo elements was a relatively simple task, joining two bamboos at a time following the corresponding cross-marks and ensuring the height of each connector was correct while using the digital model as a guide. Figure *6.17* shows the assembled prototype of the footbridge corresponding to the first stage of the construction sequence.

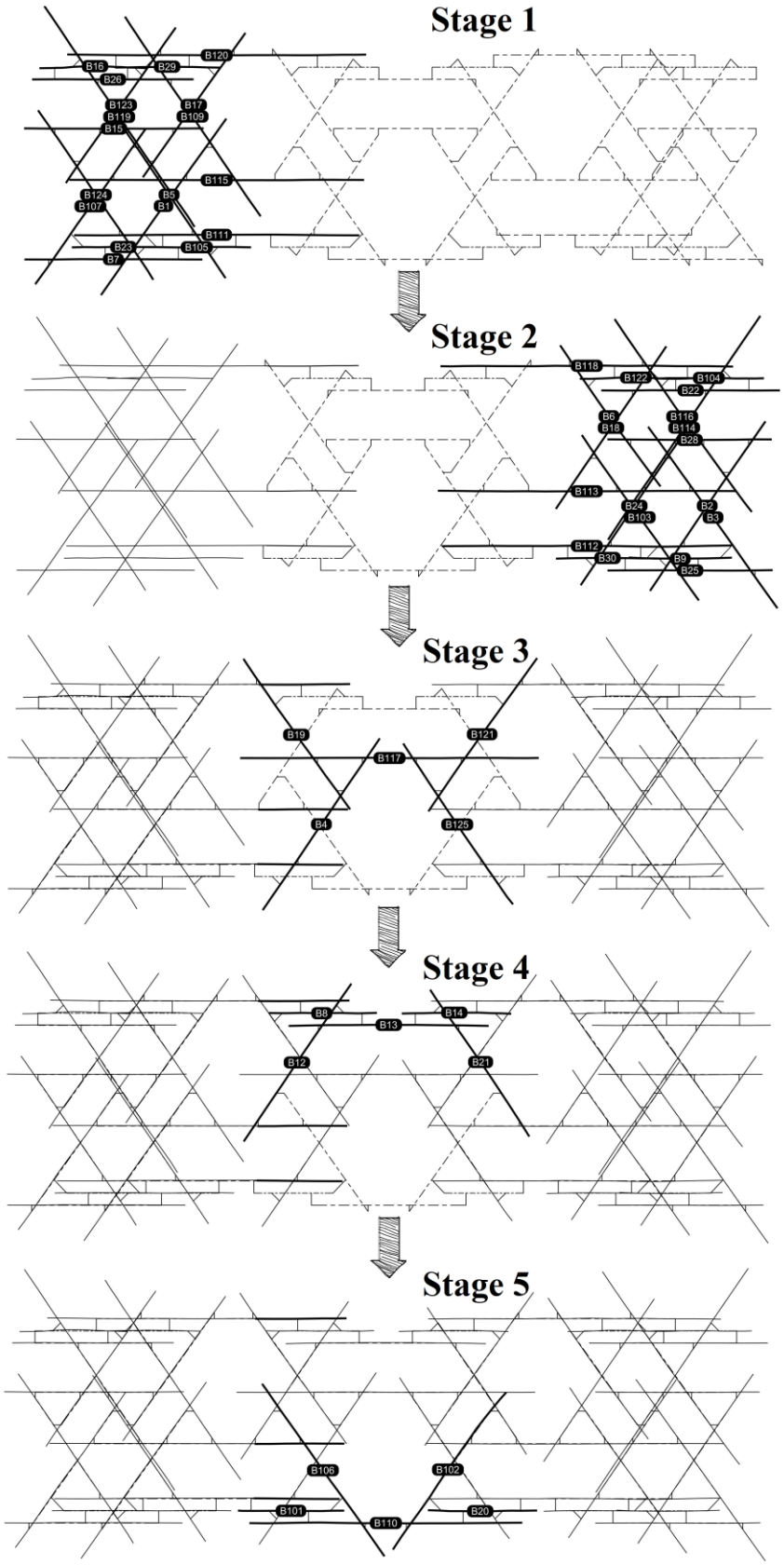

Figure 6.15. Proposed construction sequence for the bamboo pole RF-footbridge

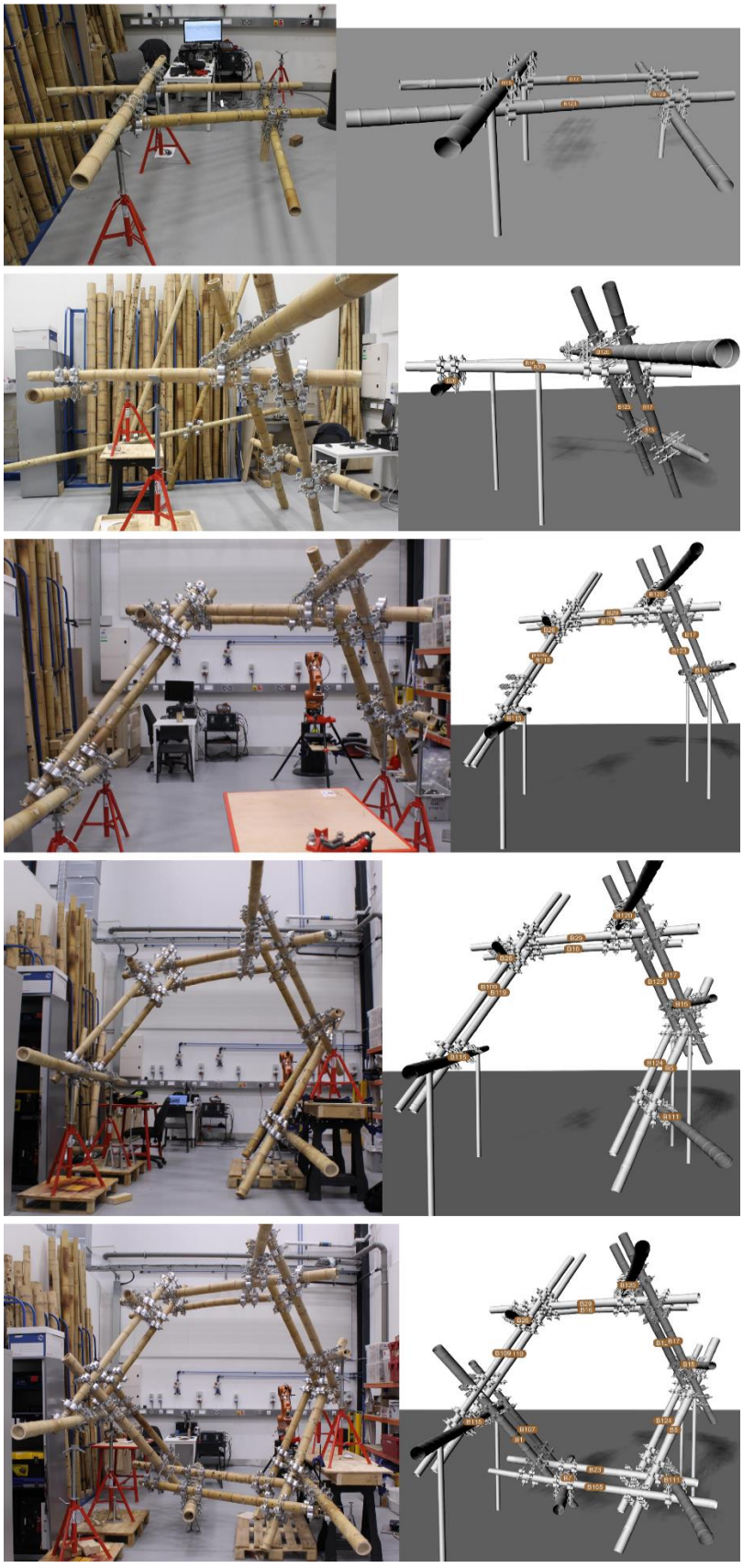

Figure 6.16. Assembly procedure of footbridge prototype corresponding to the first stage

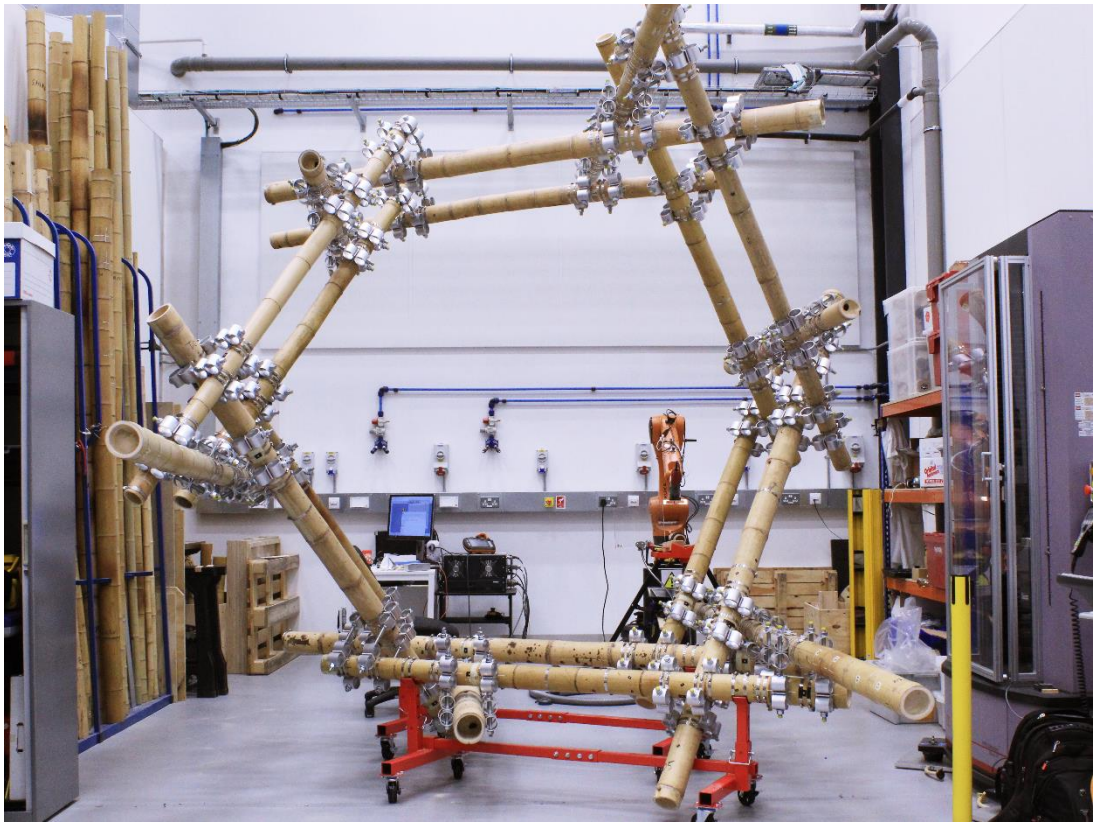

Figure 6.17. Assembled prototype corresponding to stage one

6.5 Discussion

This case study was aimed at integrating the individual digitisation and testing of poles and use the acquired data to design and construct a reciprocal frame footbridge prototype. The workflow allowed to quantify the geometric, physical and mechanical properties of the available stock of poles to build the footbridge. This exercise served as a proof of concept showing that the impact of variability can be mitigated through intensive measurement. The digitisation procedure has therefore potential to be further developed into a semi-industrial, low-energy production chain, where each pole is labelled, measured and stored for its subsequent use in a construction project as shown in this chapter. The case study here presented is part of an ongoing project where the prototype will be further subjected to structural testing, and therefore, the nominal physical and mechanical properties, grouped per species, were adopted. The impact of the variability was manged through the modelling of the individual geometric properties and the subsequent sorting of elements according to their diameter to minimise the maximum deformation.

This simple optimisation process helped to improve the structural behaviour of the multi-RF footbridge. The use of analytical models built with variable, average and extreme geometric values showed a significant difference in the maximum displacement. This interesting result proves the concept that a more refined geometric definition of a bamboo structure can lead to a more reliable behaviour of the structure. To further minimise the effect of variability, the material propertiescan be grouped and sorted according to the physical and mechanical properties measured as presented in Chapter *4*. For this case study, the limitation was the low number of samples, therefore, grouping of properties and the assessment of their effect was not performed.

The acquired geometric data of each pole was fundamental to define design parameters of the reciprocal frame topology. For example, the design approach presented in this case study used the maximum diameter to define a fixed eccentricity for the entire system which facilitated the multi-RF design, however, the eccentricity can be adjusted to a minimum depending on the diameter of poles connecting at a single point, which in turn favours the overall stiffness of the structure [129]. The drawback of the latter approach is that the construction procedure increases in complexity as different eccentricities are needed for the connection of every pair of poles. Nevertheless, what it is stressed in this chapter is that either approach is feasible due to the digital data of bamboo poles available which allows optimising the multi-RF by considering the individual geometric parameters of each pole contained in the stock (i.e. implementing a bottom-up design approach).

The importance of having individual digital models of each bamboo pole was also reflected during the construction procedure. For example, the position of each connector was digitally found on the surface of bamboo poles according to the geometric configuration between each bamboo and connector. These digital connection points were translated into the physical poles using a simple approach validated through a direct comparison between the digital and physical coordinates. The structure was then assembled by following these connection marks. The positioning of connectors was an essential factor to achieve the intended geometry because multi-RF is a space

structural system where the direction of each RF element is unique. Besides, every bamboo pole also has an irregular and unique shape, which means that by varying the orientation of the pole around its axis would be enough to cause a significant variation in the structure's topology. Basic as-built geometry checks showed that the detailed geometric data implemented throughout the design and construction processes helped to achieve a relatively good tolerance level when building the initial modules, which was subsequently translated in achieving the hexagonal geometry of the footbridge prototype.

Combining geometric models of bamboo poles with individual attributes (e.g. geometric, physical, mechanical or general) is a fundamental concept introduced in this case study. This concept was implemented following a geometry-driven approach (e.g. using Rhino3d model), where the relevant attributes of each pole were attached to the digital model, generating unique digitised bamboo elements within a digital stock of poles. Those attributes were subsequently used within the design platform (Grasshopper) to select, position and orient the poles as well as perform a basic structural optimisation procedure. The main challenge ahead for managing the acquired digital data of bamboo poles is to implement a dynamic system that allows the interaction of design, construction and management platforms with the main digital database generated through the intensive measuring methods. This would enable to control other aspects of bamboo structures such as durability, sustainability and maintenance.

7 Conclusion

7.1 Quantification of material properties as a quality assurance for bamboo poles

As an organic resource, variability is an inherent characteristic of bamboo poles and therefore it is part of every aspect involved towards their formal integration into the building industry. To address variability, quantification of the material properties was a concept adopted in this research as an approach to provide quality assurance and added value to each natural bamboo pole as an irregular and unique structural product. This approach is an alternative to standardisation efforts that have tried to simplify the organic complexity of bamboo poles by adopting geometric idealisations and universal characteristic values that so far have failed to fully support the formal incorporation of the material into the architecture, engineering and construction industry.

The geometric digitisation procedure developed and validated in Chapter *3* offers an efficient reverse engineering solution to acquire the 3D geometric information of bamboo poles, in comparison with traditional manual measuring methods, and produces a digital model ready for its implementation in any design platform. Equally important is the numerical geometric description of the bamboo poles which allows the creation of a generic text-database. As part of this research, a geometric database containing 235 bamboo poles was collected and further implemented for the analysis of geometric variability. This analysis confirmed the high variability that exists between bamboos of different species, bamboos of the same species and even within a single pole. Moreover, it also showed that correlation patterns between different basic geometric properties are unlikely, and thus, strengthening the concept of intensive measuring, quantification and creation of digital or numerical records of a stock of poles for its further management through modern design and construction tools.

The quantification of physical and mechanical properties was addressed in Chapter *4* through a scan-to-fabrication approach using a robotic arm equipped with a 3D scanner and a milling spindle that ensures the rapid extraction of clear bamboo samples from an entire stock of bamboo poles, without compromising the integrity of each element. Testing of small clear samples requires simple set-up and machines, making this a suitable process to be adopted within a semi-industrial set-up. The material testing of three species allowed to analyse correlation patterns between physical and mechanical properties and further explore the impact that variability and number of samples cause in the estimation of characteristic values. This exercise showed that direct correlation patterns are highly unlikely in bamboo poles due to their organic nature, but also showed that the acquired data can be used to group the poles according to their specific nominal properties, and thus, significantly reduce the impact that the inherent variability produces in the estimation of characteristic values.

The elastic bending of bamboo poles is an important material property that has been commonly measured by testing full-size samples. To quantify this property, a bimodulus elastic material model was developed in Chapter *5*, aimed at predicting the elastic bending modulus and quantifying the strain and stresses developed at a specific cross-section using the material data obtained through clear bamboo sample testing. The validation of this model through direct comparison with full-size bending tests showed the potential of adopting small samples to predict bending behaviour and so contributes to the intensive quantification of mechanical properties.

The methodologies previously mentioned are the answer of the overall research question of how digital technologies can be implemented to quantify the geometric, physical and mechanical properties of every bamboo pole contained in a stock of poles. The intensive measuring of material properties as a quality control procedure allows for the development of an entire low-energy production chain for this organic material, intended to provide the fundamental basis for the reliability of bamboo structures through the management of digital data.

7.2 Design, construction and management of bamboo structures using digital data

The case study presented in Chapter *6* was a proof of concept showcasing the integration of intensive measuring methodologies through a digital workflow that allowed to design and construct a reciprocal frame structure entirely relying on digital platforms. This case study challenged the *status quo* that bamboo poles are an antonym of modern design and construction tools and went further on implementing a bottom-up design paradigm, adjusting the different parameters that defined the reciprocal frame structure based on the individual properties of each bamboo pole. Although the scope of Chapter *6* was limited to basic geometric and structural optimisation iterations, it proved that once the properties of a stock of poles are quantified, the variability problem shifts towards simpler tasks of how to best manage the data so that the material is used more efficiently within the structure. Material utilisation and structural efficiency are relatively trivial topics when conventional materials, such as concrete, steel or aluminium are involved, but for bamboo poles, it just becomes accessible through the acquisition and use of material data.

A great portion of bamboo structures relies on traditional assembly and construction procedures driven by the empirical knowledge of highly skilled but scarce bamboo builders. The use of a computational model during the construction procedure of the multi-RF structure practically ruled out the need of any previous experience in bamboo construction and instead, general engineering knowledge was employed to produce a connection prototype, plan the assembly sequence through small-scale modules and check geometric tolerances through simple as-built surveying. These construction-related activities are just in their infancy but pave the way on how digital data can ensure the quality of an organic structure and further support the formal utilisation of bamboo poles into the building industry.

7.3 Future work: bamboo structures into the digital era

The current need of the building industry to transit towards more sustainable materials and construction approaches is the main driving force

encouraging the formal integration of bamboo poles as structural elements. However, most of the current design, construction and management platforms using conventional structural elements already live in dynamic digital platforms aimed to improve the coordination of construction projects. Therefore, quantifying properties associated with the structural behaviour of bamboo poles only covers part of the entire data required during the planning, construction and management of a construction project using bamboo poles. For example, the embodied energy of structural elements is an important aspect involved in the sustainable design, and therefore, methodologies to measure this and other parameters can be further developed and integrated into the digital workflow concept that this thesis presents to allow the management of the data within digital platforms.

This work also puts forward the idea that organic materials such as bamboo poles are incompatible with current standardisation processes, instead, standardisation and automation efforts should focus on the intensive measuring processes that will help to quantify the unique characteristics of bamboo poles. A new mainstream involving bamboo pole producers, policymakers, stakeholders and the industry, derives from this fundamental concept which can subsequently ensure the quality of bamboo structures through the development of: i) standard acquisition of material properties; ii) quality control measures during harvesting, treatment and durability methods; iii) transportation guidelines; iv) fabrication and assembly codes; v) maintenance; and vi) decommissioning of the bamboo elements. There is no doubt that significant work is still needed for the development of future bamboo structures, however, the digital era seems to bring the right tools to finally allow bamboo poles to competing against industrial materials.

Bibliography

[1] GABC, Global status report- Towards a zero-emission, efficient and resilient buildings and construction sector, 2018. http://wedocs.unep.org/bitstream/handle/20.500.11822/27140/Global_Status_2018.pdf?sequence=1&isAllowed=y.

[2] J. Allwood, J. Cullen, Sustainable Materials – with Both Eyes Open: Future Buildings, Vehicles, Products and Equipment, UIT Cambridge Ltd, Cambridge, UK, 2011.

[3] UN, World Urbanization Prospects 2018 - Highlights, (2019). https://population.un.org/wup/.

[4] UN, Transforming our world: The 2030 agenda for sustainable development, US, 2015.

[5] P. Van Der Lugt, Booming bamboo, International Network for Bamboo and Rattan, Beijing, China, 2017.

[6] D. Grosser, W. Liese, On the anatomy of Asian bamboos, with special reference to their vascular bundles, Wood Sci. Technol. 5 (1971) 290–312. https://doi.org/10.1007/BF00365061.

[7] W. Liese, Research on bamboo, Wood Sci. Technol. 21 (1987) 189–209.

[8] S. Kaminski, A. Lawrence, D. Trujillo, Structural use of bamboo Part 1 : Introduction to bamboo, Struct. Eng. (2016) 40–43.

[9] I.R. Hunter, Bamboo — solution to problems, J. Bamboo Ratt. 1 (2002) 101–107.

[10] BS EN 336, British adoption of European Standard BS EN 336: 2013. Structural timber - Sizes, permitted deviations, (2013).

[11] M.S. Vorontsova, L.G. Clark, J. Dransfield, R. Govaerts, T. Wilkinson, W.J. Baker, World checklist of bamboos and rattans, International Network for Bamboo and Rattan, Beijing, China, 2016. http://apps.kew.org/wcsp.%0AHow.

[12] M. Lobovikov, S. Paudel, M. Piazza, H. Ren, J. Wu, World bamboo resources. A thematic study prepared in the framework of the Global Forest Resources Assessment 2005, Rome, 2007. http://www.fao.org/3/a-a1243e.pdf (accessed August 18, 2019).

[13] Y. Yang, C. Hui, China ' S Bamboo, (2010) 156. https://doi.org/10.1016/j.carbpol.2013.12.007.

[14] G. Minke, Building with Bamboo, Birkhauser, Basel, Switzerland, 2012.

[15] D. Trujillo, Bamboo structures in Colombia, Struct. Eng. 85 (2007) 25–30. https://doi.org/10.1145/945649.945655.

[16] S.T. Partey, D.A. Sarfo, O. Frith, M. Kwaku, N. V. Thevathasan, Potentials of Bamboo-Based Agroforestry for Sustainable Development in Sub-Saharan Africa: A Review, Agric. Res. 6 (2017) 22–32. https://doi.org/10.1007/s40003-017-0244-z.

[17] D. Opoku, J. Ayarkwa, K. Agyekum, Factors Inhibiting the Use of Bamboo in Building Construction in Ghana: Perceptions of Construction Professionals, Mater. Sci. Appl. 07 (2016) 83–88. https://doi.org/10.4236/msa.2016.72008.

[18] INBAR, An overview 2016: Bamboo and Rattan Products in the International Market, 2016. https://resource.inbar.int/upload/file/1534489167.pdf.

[19] WSA, World steel in figures 2019, Brussels, 2019.

[20] ITTO, Biennial review and assessment of the world timber situation 2015-2016, International Tropical Timber Organization, Yokohama, Japan, 2017. http://www.itto.int/news_releases/id=5195.

[21] S.A. Miller, A. Horvath, P.J.M. Monteiro, Readily implementable techniques can cut annual CO 2 emissions from the production of concrete by over 20%, Environ. Res. Lett. 11 (2016). https://doi.org/10.1088/1748-9326/11/7/074029.

[22] EN 10025, EN 10025-1:2004. Hot rolled products of structural steels, (2004).

[23] EN 206, European Standard EN 206:2013. Concrete — Specification , performance , production and conformity, (2013).

[24] ASTM A6, American Society for Testing and Materials ASTM A6/A6M-14. Standard specification for general requirements for rolled structural steel bars, plates, shapes and sheet piling, (2014). https://doi.org/10.1520/A0006_A0006M-14.

[25] EN 1995-1-1, European Standard EN 1995-1-1: 2004. Eurocode 5: Design of timber structures - Part1-1: General- Common rules and rules for buildings, (2004).

[26] WSA, Steel's contribution to a low carbon future and climate resilent societies, 2019. https://www.worldsteel.org/en/dam/jcr:7ec64bc1-c51c-439b-84b8-94496686b8c6/Position_paper_climate_2019_vfinal.pdf (accessed August 21, 2019).

[27] R.M. Andrew, Global CO 2 emissions from cement production, Earth Syst. Sci. Data. 10 (2018) 195–217. https://doi.org/10.5194/essd-10-195-2018.

[28] ISO 2768-1, World urbanization prospects, the revision: Highlights, New York, 2014.

[29] J. Poker, K. MacDicken, Tropical forest resources: Facts and tables, in: Trop. For. Handb., Springer Berlin Heidelberg, Berlin, Heidelberg, 2016: pp. 3–45. https://doi.org/10.1007/978-3-642-54601-3_7.

[30] INBAR, Bamboo and sustainable consumption: seminar on SDG 12- INBAR, (2017). https://www.inbar.int/bamboo-and-sustainable-comsumption-seminar-on-sdg-12/ (accessed August 22, 2019).

[31] Q.B. Bui, A.C. Grillet, H.D. Tran, A bamboo treatment procedure: Effects on the durability and mechanical performance, Sustain. 9 (2017) 1–11. https://doi.org/10.3390/su9091444.

[32] S. Kaminski, A. Lawrence, D. Trujillo, C. King, Structural use of bamboo Part 2: Durability and preservation, Struct. Enginner. 94 (2016) 38–43. www.thestructuralengineer.org (accessed April 27, 2019).

[33] J. Mena, S. Vera, J.F. Correal, M. Lopez, Assessment of fire reaction and fire resistance of Guadua angustifolia kunth bamboo, Constr. Build. Mater. 27 (2012) 60–65. https://doi.org/10.1016/j.conbuildmat.2011.08.028.

[34] BSI ISO 19624, British adoption for International Standard Organization ISO 19624 : 2018 Bamboo structures — Grading of bamboo culms — Basic principles and procedures, (2018).

[35] B. Sharma, A. Gatoo, M. Bock, H. Mulligan, M. Ramage, Engineered bamboo: State of the art, Proc. Inst. Civ. Eng. Constr. Mater. 168 (2015) 57–67. https://doi.org/10.1680/coma.14.00020.

[36] J.F. Correal, J.S. Echeverry, F. Ramírez, L.E. Yamín, Experimental evaluation of physical and mechanical properties of Glued Laminated Guadua angustifolia Kunth, Constr. Build. Mater. 73 (2014) 105–112. https://doi.org/10.1016/j.conbuildmat.2014.09.056.

[37] H. Li, J. Su, Q. Zhang, A.J. Deeks, D. Hui, Mechanical performance of laminated bamboo column under axial compression, Compos. Part B Eng. 79 (2015) 374–382. https://doi.org/10.1016/j.compositesb.2015.04.027.

[38] H. Li, G. Wu, Q. Zhang, A.J. Deeks, J. Su, Ultimate bending capacity evaluation of laminated bamboo lumber beams, Constr. Build. Mater. 160 (2018) 365–375. https://doi.org/10.1016/j.conbuildmat.2017.11.058.

[39] B. Sharma, A. Gatóo, M. Bock, M. Ramage, Engineered bamboo for structural applications, Constr. Build. Mater. 81 (2015) 66–73. https://doi.org/10.1016/j.conbuildmat.2015.01.077.

[40] E. Zea Escamilla, G. Habert, J. Correal Daza, H. Archilla, J. Echeverry Fernández, D. Trujillo, Industrial or Traditional Bamboo Construction? Comparative Life Cycle Assessment (LCA) of Bamboo-Based Buildings, Sustainability. 10 (2018) 3096. https://doi.org/10.3390/su10093096.

[41] J. Li, Y. Yuan, X. Guan, Assessing the Environmental Impacts of Glued-Laminated Bamboo Based on a Life Cycle Assessment, BioResources. 11 (2016) 1941–1950. https://doi.org/10.15376/biores.11.1.1941-1950.

[42] E. Zea Escamilla, G. Habert, Environmental impacts of bamboo-based construction materials representing global production diversity, J. Clean. Prod. 69 (2014) 117–127. https://doi.org/10.1016/j.jclepro.2014.01.067.

[43] W. Wu, Q. Liu, Z. Zhu, Y. Shen, Managing Bamboo for Carbon Sequestration, Bamboo Stem and Bamboo Shoots, Small-Scale For. 14 (2015) 233–243. https://doi.org/10.1007/s11842-014-9284-4.

[44] S. Brown, Present and potential roles of forests in the global climate change debate, Unasylva. (1996) 3–10. http://www.fao.org/docrep/w0312e/w0312e03.htm#present and potential roles of forests in the global climate change debate.

[45] M. Pervaiz, M.M. Sain, Carbon storage potential in natural fiber composites, Resour. Conserv. Recycl. 39 (2003) 325–340. https://doi.org/10.1016/S0921-3449(02)00173-8.

[46] A. Arrigoni, R. Pelosato, P. Melià, G. Ruggieri, S. Sabbadini, G. Dotelli, Life cycle assessment of natural building materials: the role of carbonation, mixture components and transport in the environmental impacts of hempcrete blocks, J. Clean. Prod. 149 (2017) 1051–1061. https://doi.org/10.1016/j.jclepro.2017.02.161.

[47] P. Van der Lugt, A.A.J.F. Van den Dobbelsteen, J. Janssen, An environmental, economic and practical assessment of bamboo as a building material for supporting structures, Constr. Build. Mater. 20 (2006) 648–656. https://doi.org/10.1016/j.conbuildmat.2005.02.023.

[48] J. Janssen, Designing and Building with Bamboo, 2000.

[49] S. Amada, Y. Ichikawa, T. Munekata, Y. Nagase, H. Shimizu, Fiber texture and mechanical graded structure of bamboo, Compos. Part B Eng. 28 (1997) 13–20. https://doi.org/10.1016/S1359-8368(96)00020-0.

[50] F. Nogata, H. Takahashi, Intelligent functionally graded material: Bamboo, Compos. Eng. 5 (1995) 743–751. https://doi.org/10.1016/0961-9526(95)00037-N.

[51] Wikipedia, Rule of mixtures, (2019). https://en.wikipedia.org/wiki/Rule_of_mixtures (accessed March 9, 2020).

[52] Z.P. Shao, C.H. Fang, G.L. Tian, Mode i interlaminar fracture property of moso bamboo (Phyllostachys pubescens), Wood Sci. Technol. 43 (2009) 527–536. https://doi.org/10.1007/s00226-009-0265-2.

[53] P.G. Dixon, L.J. Gibson, The structure and mechanics of Moso bamboo material, J. R. Soc. Interface. 11 (2014). https://doi.org/10.1098/rsif.2014.0321.

[54] T. Herzog, J. Natterer, R. Schweitzer, M. Volz, W. Winter, Timber construction manual, Birkhäuser Verlag AG, Basel, Switzerland, 2004.

[55] K.T. Wu, The effect of high-temperature drying on the antisplitting properties of makino bamboo culm (Phyllostachys makinoi Hay.), Wood Sci. Technol. 26 (1992) 271–277. https://doi.org/10.1007/BF00200162.

[56] W. Liese, G. Weiner, Ageing of bamboo culms. A review, Wood Sci. Technol. 30 (1996) 77–89.

[57] K.F. Chung, W.K. Yu, Mechanical properties of structural bamboo for bamboo scaffoldings, Eng. Struct. 24 (2002) 429–442. https://doi.org/10.1016/S0141-0296(01)00110-9.

[58] D. Trujillo, S. Jangra, J.M. Gibson, Flexural properties as a basis for bamboo strength grading, Proc. Inst. Civ. Eng. - Struct. Build. 170 (2017) 284–294. https://doi.org/10.1680/jstbu.16.00084.

[59] Nurmadina, N. Nugroho, E.T. Bahtiar, Structural grading of Gigantochloa apus bamboo based on its flexural properties, Constr. Build. Mater. 157 (2017) 1173–1189. https://doi.org/10.1016/j.conbuildmat.2017.09.170.

[60] E.T. Bahtiar, A.P. Imanullah, D. Hermawan, N. Nugroho, Abdurachman, Structural grading of three sympodial bamboo culms (Hitam, Andong, and Tali) subjected to axial compressive load, Eng. Struct. 181 (2019) 233–245. https://doi.org/10.1016/j.engstruct.2018.12.026.

[61] Z.P. Shao, C.H. Fang, S.X. Huang, G.L. Tian, Tensile properties of Moso bamboo (Phyllostachys pubescens) and its components with respect to its fiber-reinforced composite structure, Wood Sci. Technol. 44 (2010) 655–666. https://doi.org/10.1007/s00226-009-0290-1.

[62] K.A. Harries, J. Bumstead, M. Richard, D. Trujillo, Geometric and material effects on

bamboo buckling behaviour, Proc. Inst. Civ. Eng. - Struct. Build. 170 (2017) 236–249. https://doi.org/10.1680/jstbu.16.00018.

[63] X. Zhang, J. Li, Z. Yu, Y. Yu, H. Wang, Compressive failure mechanism and buckling analysis of the graded hierarchical bamboo structure, J. Mater. Sci. 52 (2017) 6999–7007. https://doi.org/10.1007/s10853-017-0933-9.

[64] P. Zakikhani, R. Zahari, M.T. Bin Haji Hameed Sultan, D.L. Abang Abdul Majid, Morphological, Mechanical, and Physical Properties of Four Bamboo Species, BioResources. 12 (2017) 2479–2495. https://doi.org/10.15376/biores.12.2.2479-2495.

[65] MCBI, Ministry of Construction and Building Industry. MCBI: JG/t 199: 2007. Testing methods for the physical and mechanical properties of bamboo materials used in construction industry, (2007) 1–47.

[66] BSI ISO 22157, British adoption for International Standard Organization ISO 22157: 2019 Bamboo structures - Determination of physical and mechanical properties of bamboo culms - Test methods, (2019) 25. https://www.iso.org/standard/65950.html.

[67] ISO 22157-2, International Standard Organization ISO 22157-2. Bamboo-Determination of physical and mechanical properties- Part 2: Laboratory manual, (2004).

[68] J. Moran, Construir con Bambú Manual de construcción, 3rd ed., INBAR, 2015, 2015.

[69] ISO 22156, International Standard Organization ISO 22156. Bamboo - Structural design, (2004).

[70] E.T. Bahtiar, N. Nugroho, S. Surjokusum, L. Karlinasar, Eccentricity Effect on Bamboo's Flexural Properties, J. Biol. Sci. 13 (2013) 82–87. https://doi.org/10.3923/jbs.2013.82.87.

[71] K. Ghavami, L.E. Moreira, The influence of initial imperfections on the buckling of bamboo columns, Asian J. Civ. Eng. (Buillding Housing). 3 (2002) 1–16.

[72] T.S.S. Paraskeva, G. Grigoropoulos, E.G.G. Dimitrakopoulos, Design and experimental verification of easily constructible bamboo footbridges for rural areas, Eng. Struct. 143 (2017) 540–548. https://doi.org/10.1016/j.engstruct.2017.04.044.

[73] EN 13670, European Standard EN 13670:2009. Execution of concrete structures, (2009). http://www.cscses.com/uploads/2016328/20160328110518251825.pdf.

[74] EN 10034, European Standard EN 10034:1993. Structural steel I ad H sections. Tolerances on shape and dimensions, (1993).

[75] M.F. Ashby, L.J. Gibson, U. Wegst, R. Olive, The Mechanical Properties of Natural Materials. I. Material Property Charts, Proc. R. Soc. A Math. Phys. Eng. Sci. 450 (1995) 123–140. https://doi.org/10.1098/rspa.1995.0075.

[76] N. Nugroho, E. Tri Bahtiar, Bamboo taper effect on third point loading bending test, Int. J. Eng. Technol. 5 (2013) 2379–2384.

[77] R. Kappel, C. Mattheck, K. Bethge, I. Tesari, Bamboo as a composite structure and its mechanical failure behaviour, in: Des. Nat. Ii Second Int. Conf. Des. Nat. Comp. Des. Nat. with Sci. Eng., WIT Press, Southampton, UK, 2004: pp. 285–293.

[78] R.A. Sá Ribeiro, M.G. Sá Ribeiro, I.P.A. Miranda, Bending strength and nondestructive evaluation of structural bamboo, Constr. Build. Mater. (2017). https://doi.org/10.1016/j.conbuildmat.2017.04.074.

[79] N. Nugroho, E.T. Bahtiar, Bamboo taper effect on center point bending test, J. Phys. Sci. Appl. 2 (2012) 386–391.

[80] J. Janssen, Bamboo in building structures, Eindhoven University of Technology, 1981.

[81] M. Richard, Assesing the performance of bamboo sturctural components, University of Pittsburgh, 2013.

[82] R. Lorenzo, C. Lee, J.G. Oliva-Salinas, M.J. Ontiveros-Hernandez, BIM Bamboo: a digital design framework for bamboo culms, Proc. Inst. Civ. Eng. - Struct. Build. 170 (2017) 295–302. https://doi.org/10.1680/jstbu.16.00091.

[83] I. Soroka, On compressive strength variation in concrete, Matériaux Constr. 4 (1971) 155–161. https://doi.org/10.1007/BF02479129.

[84] F. Clifton, Strength variability in structural materials, (1969).

[85] L. Simões da Silva, C. Rebelo, D. Nethercot, L. Marques, R. Simões, P.M.M. Vila Real, Statistical evaluation of the lateral–torsional buckling resistance of steel I-beams, Part 2: Variability of steel properties, J. Constr. Steel Res. 65 (2009) 832–849. https://doi.org/10.1016/j.jcsr.2008.07.017.

[86] A. Tsehaye, A.H. Buchanan, J.C.F. Walker, Selecting trees for structural timber, Holz Als Roh- Und Werkst. 58 (2000) 162–167. https://doi.org/10.1007/s001070050407.

[87] S. Thelandersson, H.J. Larsen, Timber engineering, John Wiley & Sons Ltd, Chichester, West Sussex, United Kingdom, 2003.

[88] D.W. Green, J.W. Evans, Evolution of Standardized Procedures for Adjusting Lumber Properties for Change in Moisture Content, 2001.

[89] A.. Teodoro, A preliminary study of the transverse strength of structural bamboos, Agric. Eng. 6 (1925).

[90] J. Espinosa, Bending and compresive strengths of the common phillippine bamboo, Phillippine J. Sci. 41 (1930) 121–135.

[91] G. Kumpe, An experimental bamboo truss, Mil. Eng. 29 (1937) 288–289. https://www.jstor.org/stable/44563953.

[92] ISO 22157-1, International Standard Organization ISO 22157-1. Bamboo-Determination of physical and mechanical properties- Part 1: Requirements, (2004).

[93] T.Y. Lo, H.Z. Cui, P.W.C. Tang, H.C. Leung, Strength analysis of bamboo by microscopic investigation of bamboo fibre, Constr. Build. Mater. 22 (2008) 1532–1535. https://doi.org/10.1016/j.conbuildmat.2007.03.031.

[94] BS EN 1990, British adoption of European Standard BS EN 1990:2002 + A1:2005. Basis of structural design, (2010).

[95] ISO 12122-1, International Standard Organization ISO 12122-1:2014. Timber structures - Determination of characteristic values. Part 1: Basic requirements, (2014).

[96] NSR-10 G, Reglamento Colombiano de Construcción Sismo Resistente. Título G. Estructuras de Madera y Estructuras de Guagua, (2010).

[97] A. Beal, A history of the safety factors, Struct. Eng. 89 (2011) 20–26.

[98] S. Kaminski, A. Lawrence, D. Trujillo, I. Feltham, L.F. Lopez, Structural use of bamboo Part 3 : Design values, Struct. Eng. 94 (2016) 42–45.

[99] A. Bhatti, N.A. Syed, P. John, Reverse Engineering and Its Applications, in: Omi. Technol. Bio-Engineering, Elsevier, 2018: pp. 95–110. https://doi.org/10.1016/B978-0-12-804659-3.00005-1.

[100] W. Wang, Reverse Engineering: Technology of reinvention, CRC Press, London, England, 2010.

[101] G. Sansoni, F. Docchio, Three-dimensional optical measurements and reverse engineering for automotive applications, Robot. Comput. Integr. Manuf. 20 (2004) 359–367. https://doi.org/10.1016/j.rcim.2004.03.001.

[102] L. De Luca, P. Veron, M. Florenzano, Reverse engineering of architectural buildings based on a hybrid modeling approach, Comput. Graph. (2006). https://doi.org/10.1016/j.cag.2006.01.020.

[103] R. Aguilar, M.F. Noel, L.F. Ramos, Integration of reverse engineering and non-linear numerical analysis for the seismic assessment of historical adobe buildings, Autom. Constr. (2019). https://doi.org/10.1016/j.autcon.2018.11.010.

[104] G. Konecny, The international Society for Photogrametry and Remote Sensing - 75 years old or 75 years young, Photogrametric Eng. Remote Sens. 51 (1985) 919–933.

[105] J. Miles, M. Pitts, H. Pagi, G. Earl, New applications of photogrammetry and reflectance transformation imaging to an Easter Island statue, Antiquity. 88 (2014) 596–605. https://doi.org/10.1017/S0003598X00101206.

[106] C. Nicolae, E. Nocerino, F. Menna, F. Remondino, Photogrammetry applied to problematic artefacts, in: Int. Arch. Photogramm. Remote Sens. Spat. Inf. Sci. - ISPRS Arch., Garda, Italy, 2014: pp. 451–456. https://doi.org/10.5194/isprsarchives-XL-5-451-2014.

[107] J. Martinez-Llario, E. Coll, J. Herraez, Three-diemensional scanner software using a

video camera, Adv. Eng. Softw. 37 (2006) 484–489. https://doi.org/10.1016/j.advengsoft.2005.08.003.

[108] N.J. Shih, H.J. Wang, C.Y. Lin, C.Y. Liau, 3D scan for the digital preservation of a historical temple in Taiwan, Adv. Eng. Softw. 38 (2007) 501–512. https://doi.org/10.1016/j.advengsoft.2006.09.014.

[109] W. Bin Yang, M. Bin Chen, Y.N. Yen, An application of digital point cloud to historic architecture in digital archives, Adv. Eng. Softw. 42 (2011) 690–699. https://doi.org/10.1016/j.advengsoft.2011.05.005.

[110] P. Fechteler, P. Eisert, Adaptive color classification for structured light systems, in: 2008 IEEE Comput. Soc. Conf. Comput. Vis. Pattern Recognit. Work., IEEE, 2008: pp. 1–7. https://doi.org/10.1109/CVPRW.2008.4563048.

[111] J.-H. Jeon, I.-D. Jung, J.-H. Kim, H.-Y. Kim, W.-C. Kim, Three-dimensional evaluation of the repeatability of scans of stone models and impressions using a blue LED scanner, Dent. Mater. J. 34 (2015) 686–691. https://doi.org/10.4012/dmj.2014-347.

[112] W. Boehler, A. Marbs, 3D Scanning and Photogrammetry for Heritage Recording : a Comparison, in: 12th Int. Conf. Geoinformatics− Geospatial Inf. Res. Bridg. Pacific Atl., University of Gävle, Sweden, 2004: pp. 291–298.

[113] A. Abdelhafiz, Laser scanner point cloud colouring algorithm applied on real site, Surv. Rev. 45 (2013) 343–351. https://doi.org/10.1179/1752270612Y.0000000031.

[114] L. MacDonald, V. Moitinho de Almeida, M. Hess, Three-dimensional reconstruction of Roman coins from photometric image sets, J. Electron. Imaging. 26 (2017) 011017: 1–20. https://doi.org/10.1117/1.JEI.26.1.011017.

[115] Wikipedia, Point Cloud, (2019). https://en.wikipedia.org/wiki/Point_cloud (accessed January 24, 2019).

[116] Wikipedia, Polygon Mesh, (2019). https://en.wikipedia.org/wiki/Polygon_mesh (accessed January 24, 2019).

[117] R. Garber, BIM Design: Realising the creative potential of building information modelling, John Wiley and Sons, West Sussex, UK, 2014.

[118] C. Thomson, J. Boehm, Automatic Geometry Generation from Point Clouds for BIM, Remote Sens. 7 (2015) 11753–11775. https://doi.org/10.3390/rs70911753.

[119] T. Hinks, H. Carr, L. Truong-Hong, D.F. Laefer, Point Cloud Data Conversion into Solid Models via Point-Based Voxelization, J. Surv. Eng. 139 (2013) 72–83. https://doi.org/10.1061/(ASCE)SU.1943-5428.0000097.

[120] L. Barazzetti, F. Banfi, R. Brumana, G. Gusmeroli, D. Oreni, M. Previtali, F. Roncoroni, G. Schiantarelli, BIM From laser clouds and finite element analysis: combining structural analysis and geometric complexity, ISPRS - Int. Arch. Photogramm. Remote Sens. Spat. Inf. Sci. XL-5/W4 (2015) 345–350. https://doi.org/10.5194/isprsarchives-XL-5-W4-345-2015.

[121] G. Castellazzi, A.M. D'Altri, G. Bitelli, I. Selvaggi, A. Lambertini, From laser scanning to finite element analysis of complex buildings by using a semi-automatic procedure, Sensors (Switzerland). 15 (2015) 18360–18380. https://doi.org/10.3390/s150818360.

[122] B. Conde, A. Villarino, M. Cabaleiro, D. Gonzalez-Aguilera, Geometrical issues on the structural analysis of transmission electricity towers thanks to laser scanning technology and finite element method, Remote Sens. 7 (2015) 11551–11569. https://doi.org/10.3390/rs70911551.

[123] G.E. Farin, NURBS: From projective geometry to practical use, A.K. Peters, Ltd, Natick, MA, USA, 1999.

[124] E. Dimas, D. Briassoulis, 3D geometric modelling based on NURBS: a review, Adv. Eng. Softw. 30 (1999) 741–751. https://doi.org/10.1016/S0965-9978(98)00110-0.

[125] G. Moustakides, D. Briassoulis, E. Psarakis, E. Dimas, 3D image acquisition and NURBS based geometry modelling of natural objects, Adv. Eng. Softw. 31 (2000) 955–969. https://doi.org/10.1016/S0965-9978(00)00060-0.

[126] P. Benko, R.R. Martin, T. Várady, Algorithms for reverse engineering boundary representation models, CAD Comput. Aided Des. 33 (2001) 839–851. https://doi.org/10.1016/S0010-4485(01)00100-2.

[127] R. Bénière, G. Subsol, G. Gesquière, F. Le Breton, W. Puech, A comprehensive process of reverse engineering from 3D meshes to CAD models, CAD Comput. Aided Des. 45 (2013) 1382–1393. https://doi.org/10.1016/j.cad.2013.06.004.

[128] Wikipedia, Boundary Representation, (2019). https://en.wikipedia.org/wiki/Boundary_representation (accessed January 24, 2019).

[129] M. Godina, Design framework for bamboo culms - A study of bamboo reciprocal structures, University College London, 2019.

[130] G. Chryssolouris, D. Mavrikios, N. Papakostas, D. Mourtzis, G. Michalos, K. Georgoulias, Digital manufacturing: History, perspectives, and outlook, Proc. Inst. Mech. Eng. Part B J. Eng. Manuf. 223 (2009) 451–462. https://doi.org/10.1243/09544054JEM1241.

[131] OTA, Computerized Manufacturing Automation: Employment, Education, and the Workplace, Washington, D. C., 1984. https://doi.org/10.1017/S0263574700001491.

[132] Y.A. Hosni, CONTRIBUTION OF CAD-CAM AND REVERSE ENGINEERING TECHNOLOGY TO THE BIOMEDICAL FIELD, in: Curr. Adv. Mech. Des. Prod. VII, Elsevier, 2000: pp. 491–499. https://doi.org/10.1016/B978-008043711-8/50050-7.

[133] L. Lo Russo, G. Caradonna, M. Biancardino, A. De Lillo, G. Troiano, L. Guida, Digital versus conventional workflow for the fabrication of multiunit fixed prostheses: A systematic review and meta-analysis of vertical marginal fit in controlled in vitro studies, J. Prosthet. Dent. 122 (2019) 435–440. https://doi.org/10.1016/j.prosdent.2018.12.001.

[134] M.J. Merchán, P. Merchán, S. Salamanca, E. Pérez, T. Nogales, Digital fabrication of cultural heritage artwork replicas. In the search for resilience and socio-cultural commitment, Digit. Appl. Archaeol. Cult. Herit. 15 (2019). https://doi.org/10.1016/j.daach.2019.e00125.

[135] R. Devlieg, High-Accuracy Robotic Drilling/Milling of 737 Inboard Flaps, SAE Int. J. Aerosp. 4 (2011) 2011-01–2733. https://doi.org/10.4271/2011-01-2733.

[136] M.F. Zaeh, O. Roesch, Improvement of the machining accuracy of milling robots, Prod. Eng. 8 (2014) 737–744. https://doi.org/10.1007/s11740-014-0558-7.

[137] G. Van Ham, K. Denis, J. Vander Sloten, R. Van Audekercke, G. Van Der Perre, J. De Schutter, E. Aertbeliën, S. Demey, J. Bellemans, Machining and accuracy studies for a tibial knee implant using a force- controlled robot, Comput. Aided Surg. 3 (1998) 123–133. https://doi.org/10.1002/(SICI)1097-0150(1998)3:3<123::AID-IGS4>3.0.CO;2-#.

[138] A. Menges, T. Schwinn, O. Krieg, Advancing Wood Architecture. A computational approach, Routledge, New York, USA, 2017.

[139] P. Eversmann, F. Gramazio, M. Kohler, Robotic prefabrication of timber structures: towards automated large-scale spatial assembly, Constr. Robot. 1 (2017) 49–60. https://doi.org/10.1007/s41693-017-0006-2.

[140] Architectural Association, The Wood Chip Barn, Hooke Park, Beaminster, Dorset. Storage barn, 2017.

[141] B. Kolarevic, Digital Fabrication : Manufacturing Architecture in the Information Age, in: Proc. Twenty First Annu. Conf. Assoc. Comput. Des. Archit., 2001: pp. 268–278.

[142] Y. Al-Qaryouti, K. Baber, J.M. Gattas, Computational design and digital fabrication of folded timber sandwich structures, Autom. Constr. (2019). https://doi.org/10.1016/j.autcon.2019.01.008.

[143] J. Willmann, M. Knauss, T. Bonwetsch, A.A. Apolinarska, F. Gramazio, M. Kohler, Robotic timber construction — Expanding additive fabrication to new dimensions, Autom. Constr. 61 (2016) 16–23. https://doi.org/10.1016/j.autcon.2015.09.011.

[144] B. Tepavčević, V. Stojaković, D. Mitov, I. Bajšanski, M. Jovanović, Design to fabrication method of thin shell structures based on a friction-fit connection system, Autom. Constr. (2017). https://doi.org/10.1016/j.autcon.2017.09.003.

[145] J. Monedero, Parametric design: a review and some experiences, Autom. Constr. 9 (2000) 369–377. https://doi.org/10.1016/S0926-5805(99)00020-5.

[146] T.-H. Wang, O. Espinosa Trujillo, W.-S. Chang, B. Deng, Encoding bamboo's nature for freeform structure design, Int. J. Archit. Comput. 15 (2017) 169–182.

https://doi.org/10.1177/1478077117714943.

[147] C.W. Matson, K. Sweet, Simplified for Resilience : A parametric investigation into a bespoke joint system for bamboo, Blucher Des. Proc. 3 (2016) 405–412.

[148] N. Anwar, F.A. Najam, Structures and Structural Design, in: Struct. Cross Sect., Elsevier, Cambridge, UK, 2017: pp. 1–37. https://doi.org/10.1016/B978-0-12-804443-8.00001-4.

[149] L.D. Albano, N.P. Suh, Axiomatic approach to structural design, Res. Eng. Des. 4 (1992) 171–183. https://doi.org/10.1007/BF01607945.

[150] R. Mora, C. Bédard, H. Rivard, A geometric modelling framework for conceptual structural design from early digital architectural models, Adv. Eng. Informatics. 22 (2008) 254–270. https://doi.org/10.1016/j.aei.2007.03.003.

[151] F. Albermani, G.Y. Goh, S.L. Chan, Lightweight bamboo double layer grid system, Eng. Struct. 29 (2007) 1499–1506. https://doi.org/10.1016/j.engstruct.2006.09.003.

[152] M. Seixas, J. Bina, P. Stoffel, J.L. Ripper, L.E. Moreira, K. Ghavami, Active Bending and Tensile Pantographic Bamboo Hybrid Amphitheater Structure, J. Int. Assoc. Shell Spat. Struct. 58 (2017) 239–252. https://doi.org/10.20898/j.iass.2017.193.872.

[153] J. Lienhard, H. Alpermann, C. Gengnagel, J. Knippers, Active bending, a review on structures where bending is used as a self-formation process, Int. J. Sp. Struct. 28 (2013) 187–196. https://doi.org/10.1260/0266-3511.28.3-4.187.

[154] Wikipedia, Top-down and bottom-up design, (2020). https://en.wikipedia.org/wiki/Top-down_and_bottom-up_design (accessed May 3, 2020).

[155] I. Caetano, L. Santos, A. Leitão, Computational design in architecture: Defining parametric, generative, and algorithmic design, Front. Archit. Res. (2020). https://doi.org/10.1016/j.foar.2019.12.008.

[156] J. Frazer, An evolutionary architecture, E. G. Bond Ltd, London, England, 1995.

[157] N. Hang Wu, M. Dimopoulou, H. Hsun Hsieh, C. Chatzakis, Rawbot: A digital system for AR fabrication of bamboo structures through the discrete digitization of bamboo, in: Educ. Res. Comput. Aided Archit. Des. Eur., 2019.

[158] E. Oudot, No Title, Unsplash. (2019). https://unsplash.com/photos/TaEd6ndkRWM.

[159] MVRDV, Porous city lego towers, (2012). https://www.mvrdv.nl/projects/179/porous-city-lego-towers.

[160] M. Bilal, L.O. Oyedele, J. Qadir, K. Munir, S.O. Ajayi, O.O. Akinade, H.A. Owolabi, H.A. Alaka, M. Pasha, Big Data in the construction industry: A review of present status, opportunities, and future trends, Adv. Eng. Informatics. 30 (2016) 500–521. https://doi.org/10.1016/j.aei.2016.07.001.

[161] Y. Dinar, M. Rasel, M. Chowdhury, A. Ashraf, Chronological construction sequence effects on reinforced concrete and steel buildings, Int. J. Eng. Sci. 3 (2014) 52–63.

[162] O. Hidalgo-López, Bamboo the Gift of the Gods, 2003.

[163] K. Crolla, Building indeterminacy modelling – the 'ZCB Bamboo Pavilion' as a case study on nonstandard construction from natural materials, Vis. Eng. 5 (2017) 15. https://doi.org/10.1186/s40327-017-0051-4.

[164] W. Ferdous, Y. Bai, T.D. Ngo, A. Manalo, P. Mendis, New advancements, challenges and opportunities of multi-storey modular buildings – A state-of-the-art review, Eng. Struct. (2019). https://doi.org/10.1016/j.engstruct.2019.01.061.

[165] M. Lawson, R. Ogden, R. Pedreschi, J. Grubb, S. Popo-Ola, Developments in pre-fabricated systems in light steel and modular construction, Struct. Eng. 83 (2005) 28–35.

[166] L. Villegas, R. Morán, J.J. García, Combined culm-slat Guadua bamboo trusses, Eng. Struct. 184 (2019) 495–504. https://doi.org/10.1016/j.engstruct.2019.01.114.

[167] M. Sassu, A. De Falco, L. Giresini, M. Puppio, Structural Solutions for Low-Cost Bamboo Frames: Experimental Tests and Constructive Assessments, Materials (Basel). 9 (2016) 346. https://doi.org/10.3390/ma9050346.

[168] Z. Husri, M.S.A. Rashid, S. Said, R. Kamisan, Bamboo Modular System (BMS) for New Eco Architecture, in: Int. Colloq. Art Des. Educ. Res. (i-CADER 2014), Springer

Singapore, Singapore, 2015: pp. 525–539. https://doi.org/10.1007/978-981-287-332-3_54.

[169] J. Qiu, Q. Wang, Studies on bamboo construction eco-building- Resolved the cup winners “bamboo-framed lives,” Appl. Mech. Mater. 368–370 (2013) 1179–1182. https://doi.org/10.4028/www.scientific.net/AMM.368-370.1179.

[170] D. Fofi, T. Sliwa, Y. Voisin, A comparative survey on invisible structured light, in: J.R. Price, F. Meriaudeau (Eds.), Proc. SPIE Mach. Vis. Appl. Ind. Insp., 2004: p. 90. https://doi.org/10.1117/12.525369.

[171] Artec 3D, (2021). https://www.artec3d.com/ (accessed February 17, 2021).

[172] M.P. Segundo, L. Gomes, O.R.P. Bellon, L. Silva, Automating 3D reconstruction pipeline by surf-based alignment, Proc. - Int. Conf. Image Process. ICIP. (2012) 1761–1764. https://doi.org/10.1109/ICIP.2012.6467221.

[173] R. Lancashire, L. Taylor, Timber frame construction: designing for high performance, 5th Editio, Trada technology Ltd, 2011.

[174] C. Bernal, B. De Agustina, M.M. Marín, A.M. Camacho, Performance evaluation of optical scanner based on blue LED structured light, Procedia Eng. 63 (2013) 591–598. https://doi.org/10.1016/j.proeng.2013.08.261.

[175] Rhino Developer Docs, (2019). https://developer.rhino3d.com/api/RhinoScriptSyntax/ (accessed January 24, 2019).

[176] RMNA, Robert McNeel & Associates- Rhinoceros 3D. Software Version 5.0, (2015).

[177] D. Taylor, B. Kinane, C. Sweeney, D. Sweetnam, P. O’Reilly, K. Duan, The biomechanics of bamboo: investigating the role of the nodes, Wood Sci. Technol. 49 (2015) 345–357. https://doi.org/10.1007/s00226-014-0694-4.

[178] D.L. Jayanetti, P.R. Follet, Bamboo in Construction: An Introduction, 1998.

[179] H. Runne, W. Niemeier, F. Kern, Application of Laser Scanners to Determine the Geometry of Buildings, in: Opt. 3D Meas. Tech. IV, Wien, 2001: pp. 41–48.

[180] S. Kaminski, A. Lawrence, D. Trujillo, I. Feltham, L.F. López, Structural use of bamboo. Part 4: Element design equations, Struct. Eng. 95 (2017) 24–27.

[181] W.K. Yu, K.F. Chung, S.L. Chan, Column buckling of structural bamboo, Eng. Struct. 25 (2003) 755–768. https://doi.org/10.1016/S0141-0296(02)00219-5.

[182] C.J.L. Cunningham, B.L. Weathington, D.J. Pittenger, Correlational Research, in: Underst. Conduct. Res. Heal. Sci., John Wiley and Sons, 2013.

[183] BS 2846-7, British Standard BS 2846-7:1997. Guide to Statistical interpretation of data, (1997).

[184] R.W. Anthony, K.D. Dugan, D.J. Anthony, A Grading Protocol for Structural Lumber and Timber in Historic Structures, 2009.

[185] S.I. Ahmad, M.S. Alam, M.J. Alam, Structural and Life-Cycle Economic Feasibility of Rooftop Low-Height Bamboo Telecom Tower Considering a Case Study from Bangladesh, Pract. Period. Struct. Des. Constr. 25 (2020) 05020007. https://doi.org/10.1061/(ASCE)SC.1943-5576.0000492.

[186] C. Hong, H. Li, R. Lorenzo, G. Wu, I. Corbi, O. Corbi, Z. Xiong, D. Yang and Huizhong Zhang, Review on Connections for Original Bamboo Structures, J. Renew. Mater. 7 (2019) 713–730. https://doi.org/10.32604/jrm.2019.07647.

[187] O.A. Arce-Villalobos, Fundamentals of the design of bamboo structures, Eindhoven University of Technology, 1993.

[188] Occipital, (2019). https://occipital.com/ (accessed January 24, 2019).

[189] S. Subbiah, Science of Machining, in: Handb. Manuf. Eng. Technol., Springer London, London, 2015: pp. 787–810. https://doi.org/10.1007/978-1-4471-4670-4_1.

[190] E. Oberg, J.F. D., H.L. Horton, H.H. Ryffel, Machiner’s handbook, Industrial Press Inc, New York, USA, 2000.

[191] P.D. Rufe, Machining 24.1, Fundam. Manuf. (3rd Ed. (2013). https://app.knovel.com/web/view/swf/show.v/rcid:kpFME00023/cid:kt00BKEKT2/viewerType:pdf/root_slug:fundamentals-manufacturing?cid=kt00BKEKT2&page=1&q=machinise 24.1&b-q=machinise

24.1&sort_on=default&b-subscription=TRUE&b-group-by=true&b-search-type=tech-.
[192] A.K. Gupta, S.K. Arora, J.R. Westcott, Robotics, in: Ind. Autom. Robot., Mercury learning and information LLC, Dulles, Virginia, USA, 2017: pp. 397–439. https://app.knovel.com/hotlink/toc/id:kpIAR00001/industrial-automation/industrial-automation.
[193] Kuka, (2019). https://www.kuka.com/en-gb (accessed January 24, 2019).
[194] Grasshopper, Grasshopper, (2019). https://www.grasshopper3d.com/ (accessed January 24, 2019).
[195] KUKA|prc, Association for Robots in Architecture- KUKA|prc, (2019). https://www.robotsinarchitecture.org/kuka-prc (accessed January 24, 2019).
[196] Kuka Roboter, KR Agilus sixx - Assembly instructions, (2014) 1–89. http://www.wtech.com.tw/public/download/manual/kuka/KUKA KR 6 10_AGILUS.pdf.
[197] Kuka Roboter, Use and programming of industrial robots, (2013).
[198] C. Rattat, CNC Milling for makers, Rocky Nook, San Rafael, USA, 2017. https://learning.oreilly.com/library/view/cnc-milling-for/9781681983042/Text/copyright.xhtml.
[199] Skanect, How can I fully customize the bounding box? - Skanect 3D Scanning Software By Occipital, (2017). https://skanect.occipital.com/question/can-use-custom-bounding-box/ (accessed September 22, 2020).
[200] Rhino.Python, (2019). https://developer.rhino3d.com/guides/rhinopython/ (accessed January 24, 2019).
[201] MathWorks, Matlab and Image Processing Toolbox release 2017b, (2017).
[202] BSI ISO 2768-1, British adoption for the International Standard Organization ISO 22768-1:1993. General tolerances - Part 1: Tolerances for linear and angular dimensions without individual tolerance indications, (1993) 5.
[203] E. Obataya, P. Kitin, H. Yamauchi, Bending characteristics of bamboo (Phyllostachys pubescens) with respect to its fiber-foam composite structure, Wood Sci. Technol. 41 (2007) 385–400. https://doi.org/10.1007/s00226-007-0127-8.
[204] J. Deng, F. Chen, G. Wang, W. Zhang, Variation of Parallel-to-Grain Compression and Shearing, BioResources. 11 (2016) 1784–1795.
[205] N.M. Daud, N.M. Nor, M.A. Yusof, A.A.M. Al Bakhri, A.A. Shaari, The physical and mechanical properties of treated and untreated Gigantochloa Scortechinii bamboo, in: AIP Conf. Proc., 2018: p. 020016. https://doi.org/10.1063/1.5022910.
[206] M. Ota, Studied on the properties of bamboo stem (part 13) on the relation between shearing strength parallel to grain and moisture content of bamboo splint, 1955. https://doi.org/10.15017/14967.
[207] O. Hidalgo-López, Nuevas tecnicas de construccion con bambu, in: Estud. Tec. Univ. Ltda, Universidad Nacional de Colombia, Bogota, Colombia, 1978: pp. 26–137.
[208] Y. Yongqian, X. Hui, L. Chengde, H. Xiaozhen, Influences of carbonization on physical and mechanical properties of moso bamboo strips, J. Bamboo Res. 30 (2011) 23–27.
[209] Y. Akinbade, K.A. Harries, C. V. Flower, I. Nettleship, C. Papadopoulos, S. Platt, Through-culm wall mechanical behaviour of bamboo, Constr. Build. Mater. (2019). https://doi.org/10.1016/j.conbuildmat.2019.04.214.
[210] S. Timoshenko, Strength of materials, D. Van Nostrand Comany Inc, New York, USA, 1930.
[211] F. Tabaddor, Analysis for beams made of bi-modulus elastic orthotropic materials, Fibre Sci. Technol. 9 (1976) 51–62. https://doi.org/10.1016/0015-0568(76)90023-3.
[212] F. Tabaddor, Constitutive equations for bimodulus elastic materials, AIAA J. 10 (1972) 516–518. https://doi.org/10.2514/3.50131.
[213] A.E. Green, J.Z. Mkrtichian, Elastic solids with different moduli in tension and compression, J. Elast. 7 (1977) 369–386. https://doi.org/10.1007/BF00041729.
[214] ISO 22157-1, International Standard Organization ISO 22157-1. Bamboo structures - Determination of physical and mechanical properties of bamboo culms - Test methods, (2019) 25. https://www.iso.org/standard/65950.html.

[215] L. Euler, De curvis elasticis, methodus inveniendi lineas curvas maximi minimive proprietate gaudentes, sive solutio problematis isoperimetrici lattissimo sensu accepti, Marcu-Michaelem Bousquet & Socios, Geneva, 1744.

[216] M.J. Vaessen, J.J.A. Janssen, Analysis of the critical length of culms of bamboo in four-point bending tests, Heron. 42 (1997) 113–124. www.tue.nl/taverne (accessed April 13, 2020).

[217] R.C. Hibbeler, Mechanics of materials, 10th ed., Pearson Education Inc, 2017.

[218] W. Young, R.G. Budynas, Roark's formulas for stress and strain, Seventh Ed, McGRaw-Hill, US, 2002.

[219] L.G. Brazier, On the flexure of thin cylindrical shells and other "thin" sections, Proc. R. Soc. London. Ser. A, Contain. Pap. a Math. Phys. Character. 116 (1927) 104–114. https://doi.org/10.1098/rspa.1927.0125.

[220] E. Reissner, H.J. Weinitschke, Finite pure bending of circular cylindrical tubes, Q. Appl. Math. 20 (1963) 305–319. https://www.jstor.org/stable/43636428.

[221] C.R. Calladine, Theory of Shell Structures, Cambridge University Press, 1983. https://doi.org/10.1017/CBO9780511624278.

[222] K. Schulgasser, A. Witztum, On the strength, stiffness and stability of tubular plant stems and leaves, J. Theor. Biol. 155 (1992) 497–515. https://doi.org/10.1016/S0022-5193(05)80632-0.

[223] U.G.K. Wegst, M.F. Ashby, The structural efficiency of orthotropic stalks, stems and tubes, J. Mater. Sci. 42 (2007) 9005–9014. https://doi.org/10.1007/s10853-007-1936-8.

[224] Y.-S. Huang, F.-L. Hsu, C.-M. Lee, J.-Y. Juang, Failure mechanism of hollow tree trunks due to cross-sectional flattening, R. Soc. Open Sci. 4 (2017) 160972. https://doi.org/10.1098/rsos.160972.

[225] Z. Suo, Delamination Specimens for Orthotropic Materials, J. Appl. Mech. 57 (1990) 627–634. https://doi.org/10.1115/1.2897068.

[226] M. Paschero, M.W. Hyer, Axial buckling of an orthotropic circular cylinder: Application to orthogrid concept, Int. J. Solids Struct. 46 (2009) 2151–2171. https://doi.org/10.1016/j.ijsolstr.2008.08.033.

[227] J.J. Garcia, C. Rangel, K. Ghavami, Experiments with rings to determine the anisotropic elastic constants of bamboo, Constr. Build. Mater. 31 (2012) 52–57. https://doi.org/10.1016/j.conbuildmat.2011.12.089.

[228] E.C.N. Silva, M.C. Walters, G.H. Paulino, Modeling bamboo as a functionally graded material: Lessons for the analysis of affordable materials, J. Mater. Sci. 41 (2006) 6991–7004. https://doi.org/10.1007/s10853-006-0232-3.

[229] L.A. Torres, K. Ghavami, J.J. García, A transversely isotropic law for the determination of the circumferential young's modulus of bamboo with diametric compression tests, Lat. Am. Appl. Res. 37 (2007) 255–260.

[230] R. Moran, K. Webb, K. Harries, J.J. García, Edge bearing tests to assess the influence of radial gradation on the transverse behavior of bamboo, Constr. Build. Mater. 131 (2017) 574–584. https://doi.org/10.1016/j.conbuildmat.2016.11.106.

[231] M.M. Pastor, F. Roure, Open cross-section beams under pure bending. I. Experimental investigations, Thin-Walled Struct. 46 (2008) 476–483. https://doi.org/10.1016/j.tws.2007.10.013.

[232] GeometryGym, (2019). https://geometrygym.wordpress.com/ (accessed January 24, 2019).

[233] GSA: Structural Analysis and Design Software, (2019). https://www.oasys-software.com/products/structural/gsa/ (accessed January 24, 2019).

[234] M. Seixas, J.L.M. Ripper, K. Ghavami, Prefabricated Bamboo Structure and Textile Canvas Pavilions, J. Int. Assoc. Shell Spat. Struct. 57 (2016) 179–188. http://www.ingentaconnect.com/content/iass/jiass/2016/00000057/00000003/art00001.

[235] B. Sharma, K.A. Harries, K. Ghavami, Methods of determining transverse mechanical

properties of full-culm bamboo, Constr. Build. Mater. 38 (2013) 627–637. https://doi.org/10.1016/j.conbuildmat.2012.07.116.

[236] O. Popovic Larsen, Reciprocal Frame Architecture, Elsevier Ltd, Oxford, UK, 2008. https://casaeco.files.wordpress.com/2012/03/reciprocal-frame-architecture.pdf (accessed January 24, 2019).

[237] O. Baverel, Nexorades: A family of interwoven space structures, University of Surrey, 2000.

[238] G.M. Montuori, M. Fadda, G. Perrella, E. Mele, Hexagrid - hexagonal tube structures for tall buildings: patterns, modeling, and design, Struct. Des. Tall Spec. Build. 24 (2015) 912–940. https://doi.org/10.1002/tal.1218.

[239] S. Kubba, Building Information Modeling (BIM), in: Handb. Green Build. Des. Constr., Elsevier, 2017: pp. 227–256. https://doi.org/10.1016/b978-0-12-810433-0.00005-8.

[240] Karamba3D, Karamba3D – parametric engineering, (2020). https://www.karamba3d.com/#projects (accessed July 24, 2020).

[241] EN 1991-2, European Standard EN 1991-2 (2003) - Eurocode 1: Actions on structures - Part 2: Traffic loads on bridges, (2003).

[242] B. Lefevre, R. West, P. O'Reilly, D. Taylor, A new method for joining bamboo culms, Eng. Struct. (2019). https://doi.org/10.1016/j.engstruct.2019.04.003.

[243] R. Moran, J.J. García, Bamboo joints with steel clamps capable of transmitting moment, Constr. Build. Mater. (2019). https://doi.org/10.1016/j.conbuildmat.2019.05.025.

[244] F. Di Paola, A. Mercurio, Design and Digital Fabrication of a Parametric Joint for Bamboo Sustainable Structures, in: 2020: pp. 180–189. https://doi.org/10.1007/978-3-030-20216-3_17.

[245] J. Matt, Absolute Orientation - Horn's method, (2020). https://uk.mathworks.com/matlabcentral/fileexchange/26186-absolute-orientation-horn-s-method (accessed July 14, 2020).

Appendices

A.1 Geometric digitisation results

This section shows an example of the digital outputs (both geometric and numerical) of a relatively short bamboo pole. Figure A.1a shows the polygon-mesh model which in this work was considered as raw data. As shown in the detail (Figure A.1a), this geometric representation is formed by triangular polygons with an average edge length of 0.5 mm (resolution of Artec Eva scanner). Figure A.1b shows the texturised model of the bamboo pole, which can become important for aesthetic or inspection purposes during the quality control procedure (notice the small cracks along the pole). Figure A.1c shows the NURBS-surface model created from the polygon mesh. This model is 98% lighter than the polygon-mesh model (Section *3.2.4*), and therefore, more suitable for digital design purposes. Figure A.1d shows a graphical representation of the numerical data extracted from the NURBS-model. The coordinates (in mm) of the reference markers (green points) are numerically stored as a text file, sorted from the bottom as:

```
1.  Refx, Refy, Refz
2.  -540.127, -48.914, 14.649
3.  -520.014, -48.439, 16.021
4.  679.875, -41.731, 17.556
```

This short pole has three nodes (or diaphragms), which centroid coordinates (in mm) are sorted from the bottom and stored as:

```
1.  x, y, z
2.  -396.232, -0.539, -1.211
3.  -2.511, 1.072, 2.408
4.  396.232, -0.532, -1.196
```

therefore, this bamboo will contain two discrete elements (internodes) and one internode at each end from which clear bamboo samples are extracted. The equivalent and actual cross-section properties extracted at the middle of each internode (Section *3.2.4*) are sorted from the bottom and stored as:

```
1.  D, t, A, Ib, J, I1, I2, Theta1
2.  97.115, 7.982, 2234.998, 2.24E+06, 4.48E+06, 2.44E+06, 2.03E+06, 42.28
3.  95.517, 8.018, 2204.084, 2.13E+06, 4.25E+06, 2.31E+06, 1.94E+06, 5.25
```

This simple numerical data describing bamboo's geometry was used in Sections 3.3 and 5.5 to analyse the geometric variability and their effect on bamboo poles in bending.

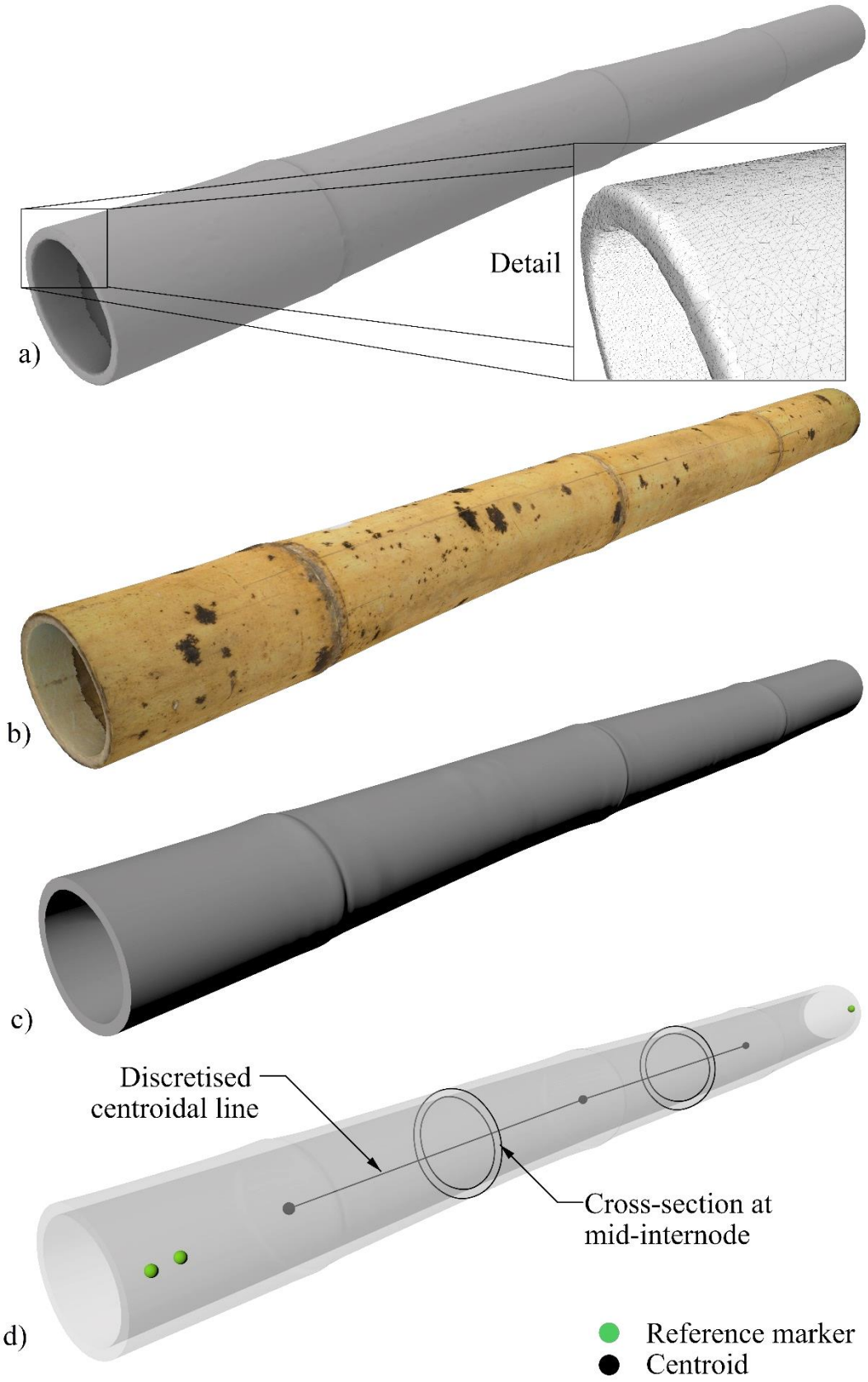

Figure A.1. Geometric digitisation results

A.2 Correlation graphs for basic geometric properties

This section presents the plots regarding the correlation analysis between the different basic geometric properties and their relation to the length of the pole, as outlined in Section *3.3.3.*

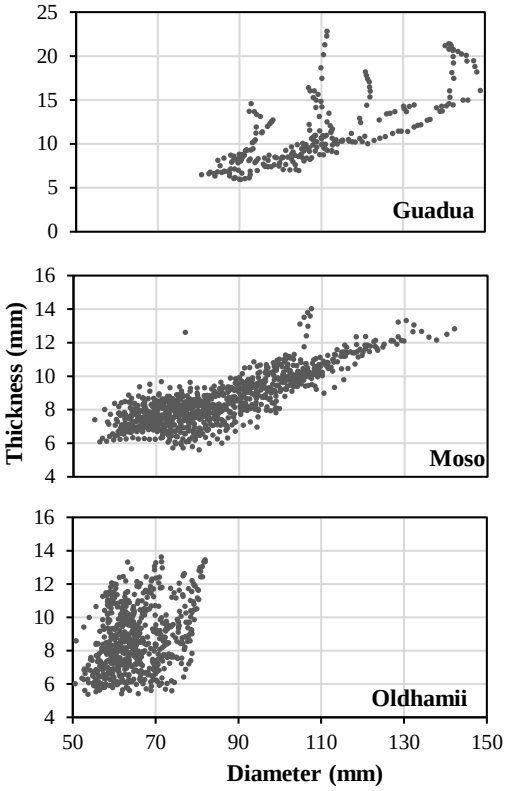

Figure A.2. Thickness to diameter correlation for Guadua, Moso and Oldhamii

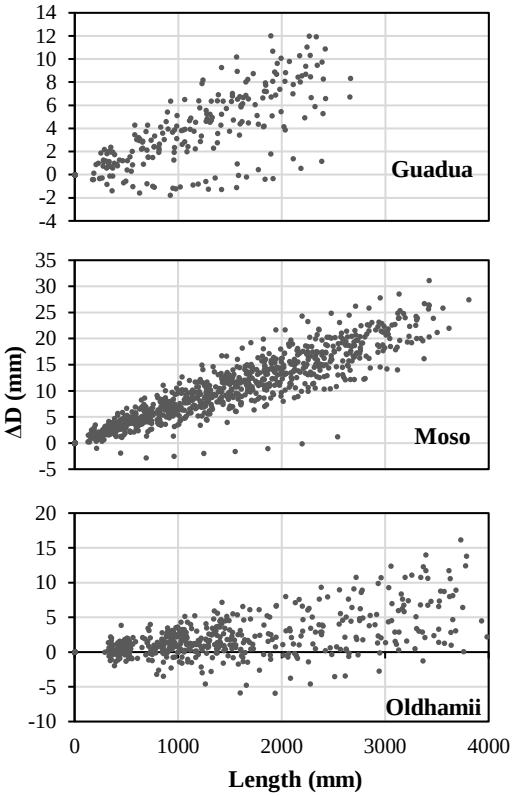

Figure A.3. Increment of diameter (from bottom) to length correlation for Guadua, Moso and Oldhamii

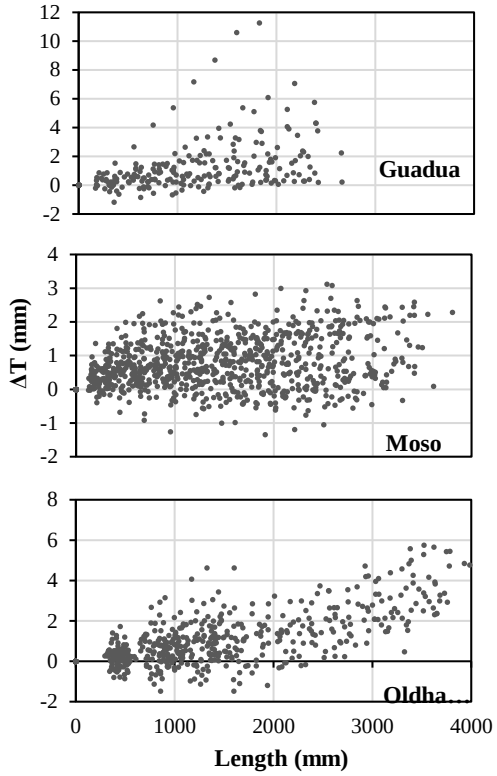

Figure A.4. Increment of the thickness (from bottom) to length correlation for Guadua, Moso and Oldhamii

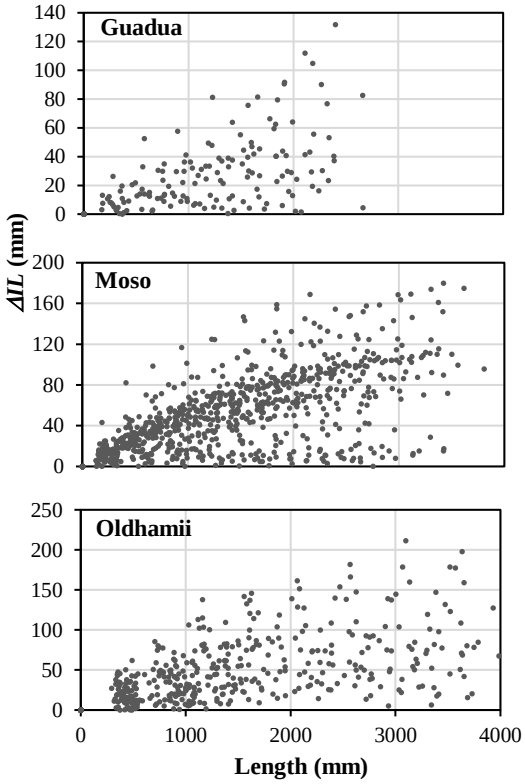

Figure A.5. Increment of internode length (from bottom) to length correlation for Guadua, Moso and Oldhamii

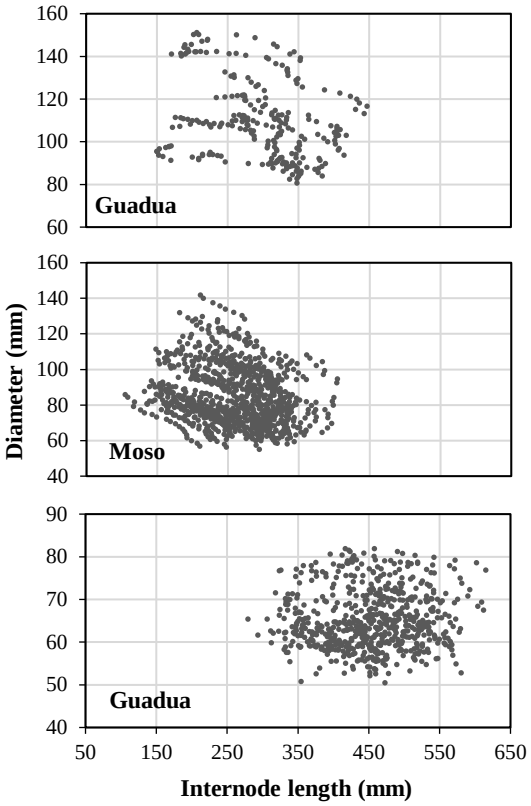

Figure A.6. Diameter to internode length correlation for Guadua, Moso and Oldhamii

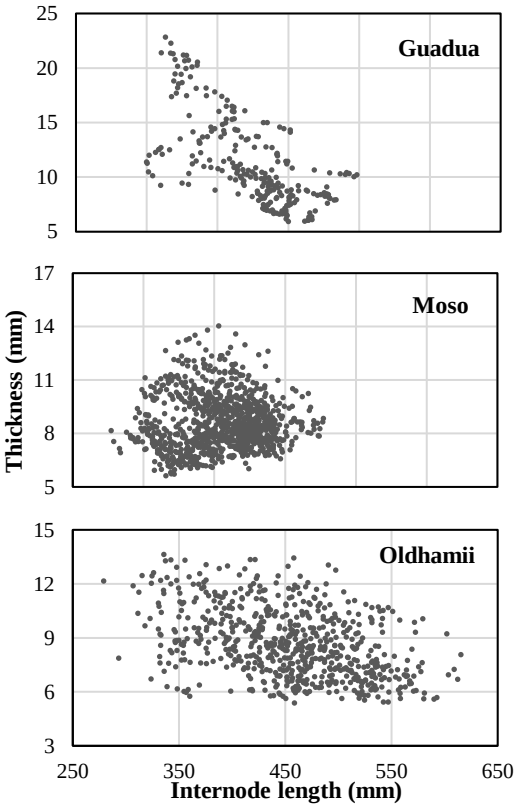

Figure A.7. Thickness to internode length correlation for Guadua, Moso and Oldhamii